UNIVERSITY OF CALIFORNIA
RIVERSIDE

Investigation of Particle and Gaseous Emissions from Conventional and Emerging Vehicle Technologies Operating on Bio-Fuels

A Dissertation submitted in partial satisfaction
of the requirements for the degree of

Doctor of Philosophy

in

Chemical and Environmental Engineering

by

Daniel Zachary Short

August 2014

Dissertation Committee:
Dr. Akua Asa-Awuku, Chairperson
Dr. David Cocker
Dr. Heejung Jung

The Dissertation of Daniel Zachary Short is approved:

Committee Chairperson

University of California, Riverside

Acknowledgments

I would first like to thank and recognize my advisor, Dr. Akua Asa-Awuku, who has played a significant role in my success. You helped guide me through many of my struggles in classroom and laboratory work. Through the many times I felt overwhelmed and confused there was guidance and support. Thank you for believing in me so that I could truly perform to my true potential. Next, I also owe a great deal of gratitude to Dr. George Karavalakis which he has been a true friend and inspiration to me throughout my graduate student years. Countless times you gave me advice on projects, life, and publication ideas through my graduate student years. I will always be grateful for the time spent with you here and we will continue to have a friendship for years to come. Another person I would like to give a considerable amount of thanks is my colleague, Miss Diep Vu. Countlessly, you listened to my speeches, gave me suggestion on basically everything, and worked countless hours with me on projects (including this dissertation work). You have been a true friend and a great colleague.

I would also like to thank Dr. Tom Durbin who gave me support and guidance throughout my dissertation. You helped me tremendously in data analysis and journal writing. I learned a great deal from your abilities and am truly thankful. And remember we are always having fun. Also, I must thank Dr. David Cocker, one of my committee members, who helped guide me to this particular area of research. I thank you for helping me through my struggles and giving advice on instruments that never seem to give the data I

need. You gave valuable and insightful feedback on all of my work which help me enormously through this journey. Thank you!

I would also like to extend a thank you to particular CE-CERT faculty such as Dr. J. Wayne Miller, Dr. Kent Johnson, Dr. Heejung Jung, Kurt Bumiller, Joe Valdez, and Mark Villela. All of you helped me tremendously throughout my PhD, and I greatly appreciate your help and support.

A thank you also goes to my numerous colleagues during my graduate school years whom are Derek, Mary, Chai-Li, Carlos, Vincent, Michael, and Shaokai. At some point all of you listened to me and helped me get to where I am today. I thank you for all of your help and support. In addition, I must thank the numerous students (Tyler, Hans, Carola, Wartini, and Jimmy) that worked in the Laboratory for me or helped out with a project. You gave your time and expertise to my work and I am extremely thankful.

Last but by far not least, I would like to thank my parents who have devoted a tremendous amount of energy, time, and encouragement for me to pursue my dreams. You were beside me when life had a different plan. You challenged me to push my limits and to dream bigger. You allowed me to realize there isn't limits in what you want in life; you just need to go and seize it. Thank you for sticking by me for the wild journey life has brought thus far. I am certain that you will always be by my side and I am forever indebted to what you have invested in me. Thank you!

The text of Chapter 2, part or in full, is a reprint of the material as it appear in the Journal of Aerosol Science and Technology, Volume 48, Issue 7, 2014, Pages 706-714. The text of Chapter 3, part or in full, is a reprint of the material as it appear in the journal Environmental Science and Technology; Components of Particle Emissions from Light-Duty Spark-Ignition Vehicles with Varying Aromatic Content and Octane Rating in Gasoline, Daniel Short, Diep Vu, Georgios Karavalakis, Thomas Durbin, Akua Asa-Awuku; Submitted. The text of Chapter 4, part or in full, is a reprint of the material as it appear in the journal Fuel; Georgios Karavalakis, Daniel Short, Diep Vu, Mark Villela, Akua Asa-Awuku, Thomas Durbin; Evaluating the regulated emissions, air toxics, ultrafine particles, and black carbon from SI-PFI and SI-DI vehicles operating on different ethanol and iso-butanol blends; Pages 410-421, 2014. The text of Chapter 5, part or in full, is a reprint of the material as it appear in the Journal of Aerosol Science; Daniel Short, Diep Vu, Thomas Durbin, Georgios Karavalakis, and Akua Asa-Awuku, Particle Speciation of Emissions from Iso-Butanol and Ethanol Blended Gasoline in Light-Duty Spark-Ignition Vehicles, Submitted. The text of Chapter 6, part or in full, is a reprint of the material as it appear in the Environmental Science and Technology; Georgios Karavalakis, Daniel Short, Diep Vu, Akua Asa-Awuku, Thomas Durbin, The impact of ethanol and iso-butanol blends on gaseous and particulate emissions from two passenger cars equipped with spray-guided and wall-guided direct injection S.I. engines, Submitted. The text of Chapter 6, part or in full, is a reprint of the material as it appear in the Science

of the Total Environment; Particle Composition Emissions from Spray and Wall-Guided GDI and Flex Fuel Vehicles on Various Ethanol and Iso-butanol Gasoline Blends Daniel Short, Diep Vu, Vincent Chen, Carlos Espinoza, Tyler Berte, Georgios Karavalakis, Thomas Durbin, Akua Asa-Awuku; Submitted.

ABSTRACT OF THE DISSERTATION

Investigation of Particle and Gaseous Emissions from Conventional and Emerging Vehicle Technologies and Bio-Fuels

by

Daniel Zachary Short

Doctor of Philosophy, Graduate Program in Chemical and Environmental Engineering
University of California, Riverside, August 2014
Dr. Akua Asa-Awuku, Chairperson

Light-duty vehicles emit gaseous and particle emissions that have the ability to effect climate, human health, and air quality. Vehicle technologies are changing rapidly due to the need to increase fuel efficiency. The use of biofuels (i.e., ethanol and iso-butanol) may increase due to the desire to reduce the use of fossil fuels. The changes in fuels and vehicle technologies may change the resulting emissions and need to be assessed. For instance, the water-soluble and water-insoluble particle composition could have detrimental health effects. This dissertation investigates the emissions of PM and gaseous emissions from current and emerging vehicle technologies.

The first section of the dissertation discusses a novel technique developed to determine the real-time Water-Insoluble Mass (WIM) fractions of vehicle emissions. The technique is then implemented in the following sections to infer the WIM fraction of vehicle emissions. The next section investigated the PM emissions from a number of hybrid, PFI, and GDI vehicle technologies on ranging aromatic concentrations and octane rating. The

next section evaluated the gaseous and particulate emissions from PFI and GDI vehicles on varying concentrations of ethanol and iso-butanol fuels. Ethanol concentration ranged from E10 to E20 and iso-butanol fuels ranged from B16 to B32. The last section of this dissertation examined the gaseous and particle emissions from GDI and FFV technologies from vary concentrations of ethanol and iso-butanol fuels. For the GDI vehicles, ethanol concentration ranging from E10 to E20 and iso-butanol concentrations of B16 to B32 were used. The FFVs used ethanol concentrations were E10, E51, and E83 with an addition iso-butanol blend of B55. PM mass, Particle Size Distributions (PSDs), Particle Number (PN), BC/soot, Water-Soluble Organic Carbon (WSOC), and real-time WIM fractions were measured for the last three sections mentioned. Significant results on particle composition effects from vehicles, fuels, and driving conditions were found. Increasing vehicular speed increased particle hygroscopicity and decreased the WIM fraction. Alcohol concentration decreases the fraction of soot to the total PM mass for the GDI vehicles tested. Generally, increased ethanol concentration decreased the PN and PM mass.

Table of Contents

List of Figures

List of Tables

List of Acronyms

^{O}C	Celsius
µg	Micrograms
APM	Aerosol Particle Mass
BC	Black Carbon
B-CPC	Butanol-Condensation Particle Counter
CARB	California Air Resources Board
CCN	Cloud Condensation Nuclei
CE-CERT	College of Engineering- Center for Environmental Research and Technology
CPC	Condensation Particle Counter
CPCB	Condensation Particle Counter Battery
CVS	Constant Volume Sampler
DMA	Differential Mobility Analyzer
DOP	Di-Octyl Phthalate
EC	Elemental Carbon
EF	Emission Factor
EPA	Environmental Protection Agency
FFV	Flex Fuel Vehicle
FTP	Federal Test Procedure

GDI	Gasoline Direct Injection
L	Liter
LDT	Light- Duty Vehicles
MAAP	Multi- Angle Absorption Photometer
m	Meter
mg	Milligrams
mi	Mile
min	minute
mph	miles per hour
MSS	Micro Soot Sensor
OC	Organic Carbon
OM	Organic Mass
PFI	Port-Fuel Injection
PM	Particulate Matter
PN	Particle Number
PSD	Particle Size Distribution
RFS	Renewable Fuels Standard
RVP	Reid Vapor Pressure
SA	Sulfuric Acid
SCAQMD	South Coast Air Quality Management District
SI	Spark Ignition
SMPS	Scanning Mobility Particle Sizer

UC	Unified Cycle
VERL	Vehicle Emissions Research Laboratory
W-CPC	Water-Condensation Particle Counter
WIM	Water-Insoluble Mass
WIOM	Water-Insoluble Organic Mass
WSOC	Water-Soluble Organic Carbon
WSOM	Water-Soluble Organic Mass

Chapter 1: Introduction

Gaseous and Particulate Matter (PM) emissions are emitted every day from numerous sources such as ships, planes, trucks, passenger vehicles, etc. These emissions can have detrimental effects on human health, air quality, and climate (Nauss et al. 1995, Davidson et al. 2005, Andreae et al. 1997, Baumer et al. 2008, Avol et al. 1979, Twomey et al 1977, and references therein). Common gaseous pollutants, such as CO_2, cause warming effects on the earth's surface from the absorption of solar radiation (IPCC 2007 and references therein). Oxides of nitrogen (NO_x) is another gaseous pollutant that is a precursor for ozone formation (Derwent et al. 2001; Fry et al. 2012). Ozone can effect climate by absorbing solar radiation, and ground level ozone can be harmful to human health leading to numerous deaths every year (Sheffield et al. 2011; Devlin et al. 2012; Dickerson et al. 1997). PM below 2.5μm can be inhaled deep within human lungs and can lead to detrimental human health effects (Yang et al. 2008). In addition, the inhalation of particular particle composition such as Water-Soluble Organic Mass (WSOM) can lead to various pulmonary and cardiovascular diseases (Ramgolam et al. 2009). Black Carbon (BC), like CO_2, is able to absorb solar radiation and is a leading contributor to global warming with CO_2 (Bond et al. 2013; Ramanathan and Carmichael 2008). Light Duty Vehicles (LDVs) emit all of these harmful pollutants, which choosing a vehicle technology and fuel that limits these harmful pollutants is essential.

Gasoline fuels and Light-Duty Vehicle (LDV) technologies are changing rapidly due to efforts to limit the emission effects on climate, regulate emissions that harm human health, reduce the dependence on fossil fuels, and increase vehicle fuel economy.

With increasing concentration of oxygenates in gasoline, such as ethanol, vehicle gaseous and particulate emissions can change. In addition, changes vehicle technologies, such as increase use of Gasoline Direct Injection (GDI), can also effect these emissions. Thousands of LDVs drive on major roadways every day and emitting large amounts of emissions. Communities near these major roadways are particularly vulnerable to these PM and gaseous emissions. In addition, lower income families and minority children live in areas that have two times the traffic density compared to other regions in Southern California (Boarnet et al. 2001). Moreover, Children are 6 times as likely to develop cancer when they reside 250 yards near heavily traveled roadways (Pearson et al. 2000). These individuals become helpless to these health effects. Also, these pollutants have contributed to a noted decrease in home values near major roadways. Home values decrease within ~.25 miles of a major roadway compared to home values that are of a greater distance from the major roadways (Boarnet et al. 2001, Langley et al. 1981). A reduction in the amount of vehicular emissions is crucial to making these areas healthy to inhabit. Which an essential process in emission reductions is measuring the actual emissions from new emerging fuels and vehicle technologies. This is to ensure changes in vehicle and fuel infrastructure maintain or reduce emission levels and update the global aerosol and gaseous emission inventories and models.

1.1 Gasoline Oxygenates and Octane Rating

Oxygenates are commonly added in gasoline to increase octane rating and to reduce crude oil usage. Ethanol is a common oxygenate found in gasoline and is

increasing in concentration every year due to the Renewable Fuels Standard (EPA, 2007). As of 2012, 10% ethanol in gasoline or E10 is found in almost every gasoline station in the United States (EPA, 2013). However, ethanol can be extremely corrosive at large concentrations and due to its lower energy content compared to gasoline can decrease fuel economy (Yan et al. 2013; Karavalakis et al. 2014). In addition, ethanol can increase gasoline's RVP values thus having fuel manufactures adjust gasoline RVP values to comply state and federal regulations (Anderson et al. 2012; Yan et al. 2013).

Iso-butanol is another oxygenate that is showing promise due to its higher energy content and less corrosive compared to ethanol (Morela et al. 2012) . These properties make it more ideal to blend with gasoline. In addition, iso-butanol less corrosive properties allow for its use in existing infrastructure. However, iso-butanol is not economically feasible due to lower yield production. Iso-butanol is produced from the Acetone-Butanol-Ethanol (ABE) method and currently produces lower yields of butanol per bushel of corn compared to current production technologies for ethanol (Jin et al. 2011; Nigam and Singh 2011). Both ethanol and iso-butanol can serve as octane boosters thus increasing the octane rating in gasoline (Anderson et al. 2012).

Aromatic concentration is another octane booster that is commonly found is gasoline (Salvia et al. 2005; Nadim 2001). Average gasoline blends today contain roughly 25% aromatic concentration and is slowly decreasing due to the addition of ethanol. Fuel manufacturers must maintain a constant octane rating. In order to maintain a specific octane rating, aromatic concentration must decrease with increasing ethanol concentration (EPA, 2013). EPA Tier 3 regulations tries to address this concern with

limiting the amount of aromatics and/or increasing the minimum octane rating in the fuel (EPA, 2013).

1.2 Emerging Vehicle Technologies

Port-Fuel Injection (PFI) vehicles have been the conventional vehicle in the U.S. market for the last several decades. PFI vehicle technology mixes gasoline and air together before entering the combustion chamber (Shin et al. 1995). Gasoline Direct Injection (GDI) vehicles have seen increased production over the last few years due to their increased fuel economy compared to PFI vehicles (Zhao et al.. 1999). GDI vehicles inject fuel, separately from air, directly into the combustion chamber (Alkidas 2007). This method increases fuel economy by up to 15% compared to PFI vehicles (Alkidas 2007). The increase in fuel economy helps vehicle manufacturers meet federal fuel economy standards which out major changes to the vehicle infrastructure.

One of the drawbacks to GDI vehicle technology is that it can emit 4 to 5 times more PM compared to PFI vehicles (Liang et al. 2013). The increase in PM emissions is attributed to increased piston bowl fuel wetting preventing the complete combustion of the fuel (Stevens and Steeper 2001). Spray-Guided (SG) GDI vehicles is another emerging vehicle technology that sprays the fuel from the top of the piston cylinder in the combustion chamber (Giglio et al. 2013). This technique allows for significantly reduced PM emissions compared to the WG-GDI vehicle with the expected increased fuel economy from a GDI vehicle (Giglio et al. 2013).

Conventional vehicles have limits on the total amount of ethanol concentration blended with gasoline. There are unknown effects with concentrations of ethanol higher

than E10 in conventional vehicles due to the corrosivity of ethanol and the unknown long-term compliance of these vehicles using higher ethanol fuels (Cadle et al. 2009). Flex Fuel Vehicles (FFVs) incorporate anti-corrosive material in the vehicle allowing for increased concentrations of ethanol in gasoline to be used. These vehicles allow up to E85 to be used and both PFI and GDI engines are manufactured for their use.

1.3. Particle Composition

Particles are formed during combustion through locally fuel rich areas (Kittelson 1998). These particles can have various compositions such as solid carbonaceous material known as soot or BC. Particle diameters below 2.5 μm have the potential for lung deposition, which the probability for lung deposition is higher for diameters below 100nm (Yang et al. 2008, Nauss et al. 1995). Lung deposition of particles has been shown to have negative effects on human health (Yang et al. 2008). In addition, organic material known as Organic Carbon (OC) can be formed, and can either be water-soluble or insoluble. Water-Soluble Organic Carbon (WSOC) can be harmful to human health and effect Cloud Condensation Nuclei (CCN) activity. Various cardiovascular and pulmonary diseases have been found to be associated with the inhalation of WSOC. Long term exposure to WSOC has been linked to induce DNA damage when inhaled. Specifically, Reactive Oxygen Species (ROS) activity, known to cause damage to cellular macromolecules, has been measured and correlated with WSOC emissions (Verma et al. 2012; Shafer et al. 2010).

The characterization of the hydrophobic and hydrophilic properties of PM is important to determine the impacts on not only human health but also climate change

(IPCC, 2007; Andreae and Rosenfeld, 2008). Cloud formation is achieved from water vapor condensing onto aerosols. These aerosols are known as cloud condensation nuclei (CCN). Emissions have water-insoluble matter that can affect these water-uptake properties which will alter cloud formation. This will have an effect on climate patterns and global warming (IPCC, 2007; Squires, 1958). In addition, CCN activity can be affected by the amount of WSOC in the atmosphere. Everns et al. (2005) shows that WSOC concentration can affect the droplet concentration in the atmosphere. Determining the amount to water-insoluble and water-soluble matter from engine exhaust is important to find the level of impact vehicles have on climate patterns.

This dissertation work aims to increase the scientific knowledge on particle and gaseous emissions from emerging and conventional vehicle technology using various biofuels. It is largely unknown the real-time particle water-solubility from conventional vehicles driving on various driving conditions. In addition, WSOM emissions from GDI and FFV technologies are largely unknown. Oxygenate concentration in gasoline has been increasing in the U.S., which defining the emissions from high oxygenated fuels becomes crucial. As oxygenate concentration increases, aromatic concentration has decreased in gasoline. These are all factors in this dissertation that will be investigated to determine emissions effects.

1.4. Outline of Dissertation

Chapter 2 discusses a real-time method developed to determine the water-insoluble mass fractions of particle emissions. The method was first implemented on a near-roadway study located 15 m from the I-710 freeway in Long Beach, CA. BC

concentrations were correlated to the water-insoluble mass fraction to find the BC contribution to the water-insoluble mass.

Chapter 3 outlines the particle speciation of emissions from GDI and PFI vehicles running on varying aromatic concentrations and octane rating. These vehicles were run on the Unified Cycle (UC) and three steady-state speeds of 70, 50, and 30 MPH. Particle speciation includes WSOM, particle surface tension, Real-Time Water-Insoluble particle emissions, and BC emissions. This chapter determines the effects aromatic content and octane rating in emerging and conventional vehicle particle composition emissions.

Chapter 4 investigates the criteria pollutants, Particle Number (PN), PM mass, and Particle Size Distributions (PSDs) of 5 vehicles tested over the Federal Test Procedure (FTP) and UC. These 5 vehicles include 3 Port Fuel Injection (PFI) and 2 Gasoline Direct Injection (GDI) vehicles. The vehicles were run on a range of ethanol and iso-butanol concentrations. Little information exists on measurements of particle emissions from iso-butanol blended fuels.

Chapter 5 discusses the particle composition emissions from conventional and emerging light-duty vehicles. The vehicle technologies included 3 PFI and 2 GDI vehicles over both the FTP and UC. In addition, the vehicles were driven at 3 steady-state speeds of 70, 50, and 30 MPH to see particle composition effects from vehicle speed. Vehicles used various blends of ethanol and iso-butanol in gasoline. Black Carbon, Water-Soluble Organic Carbon, and Real-Time Water-Insoluble Particle Emissions were measured and the determination of their contributions to the total PM mass were investigated.

Chapter 6 analyzes the criteria pollutants, PN, PM Mass, and PSDs of 4 vehicles on ranging ethanol and iso-butanol blends. The vehicle technologies tested include: SG-GDI, WG-GDI, PFI- FFV, and GDI-FFV. The SG-GDI and WG-GDI vehicles were run on ethanol blends ranging from E10 to E20 and iso-butanol blends of B16 to B32. The FFVs were run on ethanol blends ranging from E10 to E83 and an iso-butanol blend of B55. Vehicles were driven over the FTP and UC. This chapter shows the effects on higher ethanol blends on particulate and criteria emissions as well as emission differences between WG-GDI and SG-GDI vehicles.

Chapter 7 investigates the particle speciation of emissions from 4 different vehicle technologies. Two of these vehicles include a PFI-FFV and GDI-FFV which used ethanol blends of E10 to E83 and an iso-butanol blend of B55. The other two vehicles include a SG-GDI and WG-GDI running on ethanol blend of E10, E15, and E20 and iso-butanol blends of B16, B24, and B32. Soot, WSOM, Real-Time Water-Insoluble particle emissions, and Organic Carbon/ Elemental Carbon fractions were measured. PFI and GDI FFV technologies showed changes in particle composition in relation to the total mass and differences in SG-GDI and WG-GDI vehicles with particle composition were also shown.

Chapter 8 concluded the findings of this dissertation

1.5. Literature Cited

Alkidas, A.C. 2007. Combustion Advancements in Gasoline Engines, Energy Conversion and Management, 48(11), 2751-2761.

Anderson J.E., DiCicco D.M., Ginder J.M., Kramer U., Leone T.G., Raney-Pablo H.E., Wallington T.J. 2012. High octane number ethanol-gasoline blends: Quantifying the potential benefits in the United States. Fuel, 97:585-594.

Andreae, M. O. and Crutzen, P. J. 1997. Atmospheric aerosols: biogeochemical sources and role in atmospheric chemistry. Science, 276, 1052–1058

Andreae, M.O., Rosenfeld, D. 2008, Aerosol-cloud-precipitation interactions. Part 1. The nature and sources of cloud-active aerosols, Earth Science Reviews, 89, 13-41

Avol, E. L., Jones, M. P., Bailey, R. M., Chang, N. M. N., Kleinman, M. T., Linn, W. S., Bell, K. A., and Hackney, J. D. 1979. Controlled exposures of human volunteers to sulfate aerosols - Health-effects and aerosol characterization. Am. Rev. Respir. Dis., 120: 319-327

Baumer, D., Vogel, B., Versick, S., Rinke, R., Mohler, O., and Schnaiter, M. 2008. Relationship of visibility, aerosol optical thickness and aerosol size distribution in an ageing air mass over South-West Germany. Atmospheric Environment, 42, 989–998

Boarnet, M. and Chalermpong, S. 2001. New highways, house prices, and Urban development: A case study of toll roads in orange county, Ca, Housing Policy Debate,12, 3

Bond, T.C., Doherty, S.J., Fahey, D.W., Forster, P.M., Berntsen, T., DeAngelo, B.J., Flanner, M.G., Ghan, S., Karcher, B., Koch, D., Kinne, S., Kondo, Y., Quinn, P.K., Sarofim, M.C., Schultz, M., Venkataraman, C., Zhang, H., Zhang, S., Bellouin, N., Guittikunda, S.K., Hopke, P.K., Jacobson, M.Z., Kaiser, J.W, Klimont, Z., Lohmann, U., Schwarz, J.P., Shindell, D., Storelvmo, T., Warren, S.G., Zender, C.S. 2013. Bounding the Role of Black Carbon in the Climate System: A Scientific Assessment, Jounral of Geophysical Research: Atmospheres, 118, 5380-5552

Cadle , S.H., Ayala, A., Black, K., Graze, R.R., Koupal, J., Minassian, F., Murray, H.B., Natarajan, M., Tennant, C.J., Lawson, D.R. 2009. Real World Vehicle Emissions: A Summary of the 18th Coordinating Research Council On-Road Vehicle Emissions Workshop, Journal of Air and Waste Management Association, 59, 130-138.

Davidson, C. I., Phalen, R. F. and Solomon, S. 2005. Airborne particulate matter and human health: A review. Aerosol Sci. Tech. 39: 737-749

Derwent, R.G., Collins, W.J., Johnson, C.E., Stevenson, D.S. 2001. Transient Behavior of Tropospheric Ozone Precursors in a Global 3-D CTM and Their Indirect Greenhouse Effects, Climate Change, 49, 463-487.

Devlin, R.B., Duncan, K.E., Jerdim, M., Schmitt, M.T., Rappold, A.G., Diaz-Sanchez, D. 2012. Controlled Exposure of Healthy Young Volunteers to Ozone Causes Cardiovascular Effects, Circulation, DOI: 10.1161/CIRCULATIONAHA.112

Dickerson, R.R., Kondragruta, S., Stenchikov, G., Civerolo, K.L., Doddridge, B.G., Holben, B.N., 1997. The Impact of Aerosols on Solar Ultraviolet Radiation and Photochemical Smog, Science, 278, 827-830.

Ervens, B., Feingold G., Kreidenweis, S.M., 2005. Influence of water-soluble organic carbon on cloud drop number concentration, Journal of Geophysical Research, 110, D18211

Forster, P., Ramanswamy, V. (IPCC, 2007). Climate Change 2007: The Physical Science Basis — Contribution of Working Group I to the Fourth Assessment Report of the Intergovernmental Panel on Climate Change, Cambridge Univ. Press, Cambridge UK, New York USA.

Fry, M.M., Naik, V., West, J.J., Schwarzkopf, M.D., Fiore, A.M., Collins, W.J., Dentener, F.J., Shindell, D.T., Atherton, C., Bergmann, D., Duncan, B.N., Hess, P., MacKenzie, I.A., Mermer, E., Schultz, M.G, Szopa, S., Wild, O., Zeng, G. 2012. The Influence of Ozone Precursor Emissions From Four World Regions on Tropospheric Composition and Radiative Climate Forcing, Journal of Geophysical Research, 117, D07306.

Giglio V, Fiengo G, di Gaeta A, Palladino A. 2013. Common rail system for GDI engines. Springer Briefs in Control, Automation and Robotic

Jin, C., Yao, M., Liu, H., Lee, C.F., Ji, J. 2011. Progress in the Production and Application of n-Butanol as a Biofuel, Renewable and Sustainable Energy Reviews, 15, 4080-4106

Karavalakis, G., Short, D., Vu, D., Villela, M. Jung, H., Asa-Awuku, A., Durbin, T. 2014. Regulated Emissions, Air Toxics, and Particle Emissions from SI-DI Light-Duty Vehicles Operating on Different Iso-Butanol and Ethanol Blends, SAE Int. Journal of Fuels and Lubrricants, 7(1)

Kittelson, D.B., 1998. Engines and Nanoparticles: A Review, Aerosol Science and Technology, 29(5-6), 575-588

Langley, C. John Jr. 1981. Highways and Property Values: The Washington Beltway Revisited. Transportation Research Record, 812, 16–20.

Liang, B., Ge, Y., Tan, J., Han, X., Gao, L., Hao, L., Ye, W., Dai, P., 2013. Comparison of PM Emissions From a Gasoline Direct Injected (GDI) vehicle and a Port Fuel Injected (PFI) vehicles measured by Electrical Low Pressure Impactor (ELPI) With Two Fuels: Gasoline and M15 Methanol Gasoline, Journal of Aerosol Science, 57, 22-31.

Morela, S.S., Tornatore, C., Marchitto, L., Valentino, G., Corcione, F.E. 2012. Expertimental Invesitigation of Butanol-Gasoline Blends Effects on the Combustion Process in a SI Engine, 3, 6

Nadim F.; Zack, P.; Hoag, G.; Liu, S. United States Experience with Gasoline Additives. Energy Policy. 2001. 29(1), 1-5

Nauss, K. 1995. Diesel Exhaust: A Critical Analysis of Emissions, Exposure, and Health Effects; Health Effects Institute

Nigam, P. S., Signh, A. 2011. Production of Liquid Biofuels from Renewable Resources, Progress in Energy and Combustion Science, 37, 52-68

Pearson, R. L., Wachtel, H., & Ebi, K. L. 2000. Distance-weighted traffic density in proximity to a home is a risk factor for leukemia and other childhood cancers. Journal of the Air Waste Management Association, 50, 175–180.

Ramanathan, V., Carmichael, G. 2008, Global and Regional Climate Changes Due to Black Carbon, Nature Geoscience, 1, 221-227.

Ramgolam, K., Favez, O., Cachier, H., Gaudichet, A., Marano, F., Martinon, L., and Baeza-Squiban, A. 2009. Size-partitioning of an urban aerosol to identify particle determinants involved in the proinflammatory response induced in airway epithelial cells, Particle and Fibre Toxicology, 2009, 6,10

Twomey, S. 1977. The influence of pollution on the shortwave albedo of clouds. J. Atmos. Sci. 34: 1146-1152

Silva, R.; Cataluna, R.; Weber de Menezes, E.; Samios, D.; Piatnicki, C.M.S. Effect of Additives On the Antiknock Properties and Reid Vapor Pressure of Gasoline. Fuel. 2005, 84(7-8), 951-959

Shafer, M. M.; Perkins, D. A.; Antkiewicz, D. S.; Stone, E. A.; Quraishi, T. A.; Schauer, J. J., Reactive oxygen species activity and chemical speciation of size-fractionated atmospheric particulate matter from Lahore, Pakistan: an important role for transition metals, Journal of Environmental Monitoring, 2010, 12, 3, 704-715.

Sheffield, P.E., Knowlton, K., Carr, J.L., Kinney, P.L. 2011. Modeling of Regional Climate Change Effects on Ground-Level Ozone and Childhood Asthma, American Journal of Preventive Medicine, 41,3, 251-257.

Shin, Y., Min, K., and Cheng, W., "Visualization of Mixture Preparation in a Port-Fuel Injection Engine During Engine Warm-up," SAE Technical Paper 952481, 1995, doi:10.4271/952481.

Squires, P. 1958. The microstructure and colloidal stability of warm clouds. 1. The relation between structure and stability. Tellus 10-256-261

Stevens E, Steeper R. Piston wetting in an optical DISI Engine: fuel films, poolfires, and soot generation. 2001. SAE Int J Engines, 110:1287-1294.

U.S. Environmental Protection Agency. 2007. Fuels and Fuel Additives, Renewable Fuel Standard; http://www.epa.gov/otaq/fuels/renewablefuels

U.S. Environmental Protection Agency. 2013. Draft Regulation Impact Analysis: Tier 3 Motor Vehicle Emission and Fuel Standards, Assessment and Standards Division; http://www.epa.gov/otaq/documents/tier3/420d13002.pdf

Yan X., Inderwildi O.R., King D.A., Boies A.M. 2013. Effects of ethanol on vehicle energy efficiency and implications on ethanol life-cycle greenhouse gas analysis. Environmental Science Technology, 47, 5535-5544.

Yang, W., Peters, J., Williams, R. 2008. Inhaled Nanoparticles-A Current Review, International Journal of Pharmaceuticals, 356, 239-247

Verma, V, Rico-Martinez, R., Kotra, N., King, L., Liu, J., Snell, T.W., Weber, R.J., 2012. Contributions of Water-Soluble and Insoluble Components and Their Hydrophobic/Hydrophilic Subtractions to the Reactive Oxygen Species-Generating Potential of Fine Aerosol Particles, Environmental Science and Technology, 46, 11384-11392

Zhao F., Lai, M.-C., and Harrington D.L. 1999. Automotive spark-ignited direct-injection gasoline engines. Progress in Energy and Combustion Science, 25, 437-562.

Chapter 2: A Unique Online Method to Infer Water-Insoluble Mass Fractions

2.1. Introduction

The mass, size, and water-insoluble chemical composition of particulate matter with aerodynamic diameter equal to or less than 2.5μm ($PM_{2.5}$) significantly affects air quality, climate, and human health (Avol et al. 1979; Charleston et al. 1992; Davidson et al. 2005). Carbonaceous materials, such as Black Carbon (BC), can contribute to water-insoluble $PM_{2.5}$ and their subsequent effects on health and climate. BC is formed from the incomplete combustion of fossil fuels and biomass (Novakov et al. 2000) and can have a peak mode below 100 nm in diameter (Rose et al. 2006). BC is defined as light absorbing material formed by the incomplete combustion of fossil fuels and biomass. BC is emitted from both anthropogenic and natural sources. Thus the BC combustion species is operationally defined by the method of detection. Here, BC is quantified by the ability of a material to absorb energy at a 670 nm wavelength. BC aerosol is often considered water-insoluble when freshly emitted but can add water-soluble materials in surface oxidation and condensation reactions during its atmospheric lifetime (Cooke et al. 1996; Koehler et al. 2009; McMeeking et al. 2011; Snider et al. 2010). Hence as a BC particle ages, the particle can modify its overall water-insoluble fraction, hygroscopic properties, and reduce the critical water-vapor saturation required to initiate heterogeneous nucleation (Zhang et al. 2008). BC has garnered recent attention due to its complex and transient role in the atmosphere (e.g., but not limited to Ramanathan et al. 2008; Liggio et al. 2012; McMeeking et al. 2011). Freshly emitted BC can absorb radiation and heat the

surrounding air (Conant et al. 2002; Chung and Seinfeld 2005; IPCC 2007). However as additional water-soluble (or non-refractory materials) condense on the surface, the particle can directly reflect sunlight and have a cooling effect that can reduce temperatures at the earth's surface (Bond et al. 2004). The real-time contribution of BC to the water-insoluble mass is important for our intrinsic understanding of ambient particles and must be quantified. In this study, we present and test a unique method to estimate BC contributions to the inferred water-insoluble mass from real-time particle counts.

Real-time particle concentrations can be measured using a condensation particle counter (CPC). One of the earliest particle concentration counters was introduced by Aitken et al. 1890-1891 and counted condensed particles with a magnifying glass. The first CPC that used Kelvin-effect measurement principles to size particles was developed in 1935 (Junge 1935) and is now the most-widely used method. In the 1970's the saturation tube, growth tube, and optical particle techniques were implemented to improve aerosol counting measurements (Rosen et al. 1974; Bricard et al. 1976). One of the first commercial CPCs was developed in 1980 by TSI, Inc. (Agarnal and Sem 1980) and uses the same measurement principles as the CPCs used in this study.

The lower limit of particle detection for CPCs is defined by the 50% particle activation efficiency or ε_{50}. The ε_{50} of a CPC is calculated by plotting the ratio of particles counted by two distinct counting devices at varying diameters. For commercial CPC calibration, counts are compared with data from an Aerosol Electrometer (an instrument that counts particles based on net charge). Above the ε_{50} diameter, larger

particles will likely activate, form droplets, and be detected. Hence, there are fewer statistical counting errors above ε_{50}.

Modern butanol-based CPCs (B-CPC) can detect aerosols with a lower size limit of 3 nm (Stolzenburg and McMurry 1991). Yet stored butanol is flammable and the exhaust from the CPC can be toxic if not properly vented. To address these safety concerns, a commercial continuous-flow water-based CPC (W-CPC) was introduced to the market in 2003 (Hering et al. 2005). The reported ε_{50} for ambient particles away from major roadway particle sources is 4.7 nm for the TSI 3785 W-CPC (Liu et al. 2006). A newer version of the W-CPC (TSI Model 3786) has ε_{50} = 2.4 nm for ambient particles. Hermann et al. 2007 reported a ε_{50} = 7.6 nm for the TSI 3785 Model W-CPC and ε_{50} = 7.8 nm for the TSI Model 3772 B-CPC for silver particles. The reported W-CPC ε_{50} diameter was comparable to the B-CPC counting efficiency for silver particles. However, adjustments in the temperature gradients between the saturation and growth tubes within the CPC can alter the ε_{50} diameter. An increased difference in temperature between the saturation and growth tubes in the W-CPC can also decrease ε_{50} diameters (Petaja et al. 2006). Petaja et al. (2006) reports that the ε_{50} of silver particles ranged from 4 to 14 nm with a temperature difference of 55^{o}C to 15^{o}C, respectively.

There are few studies that directly compare the differences between the B-CPC and W-CPCs. Previous studies discuss the discrepancies that exist. Franklin et al. (2010) showed a correlation between 1% of measured geometric mean diameter of the W-CPC TSI Model 3786 and the B-CPC TSI Model 3025 for low sulfur diesel particle diameters

above 10 nm. Biswas et al. (2005) and Herring et al. (2005) have shown sensitivity toward particle counting abilities of the W-CPC for particles that range below 30 nm for ambient particle measurements. Mordas et al. (2008) concluded that the efficiency of the W-CPC (TSI 3786) was dependent on the chemical composition of the particle but provided little or no chemical information. Kulmala et al. (2007) presented a method that used four CPCs consisting of an ultrafine W-CPC, ultrafine B-CPC, W-CPC, and B-CPC called a condensation particle counter battery (CPCB). The CPCB is used to infer chemical composition information of newly formed particles between diameters of 2 to 20nm. Kulmala et al. (2007) CPCB study aligns the ε_{50} diameter (ε_{50}=11nm) for both the W-CPC and B-CPC. In CPCB operation, a hygroscopic particle lowers the ε_{50} diameter; the W-CPC will measure a larger particle concentration than the B-CPC. A study with the CPCB in the Boreal Forest finds new particle formation compositions have a strong affinity for water (Riipinen et al. 2009) and therefore the comparison of CPCs can determine the hygroscopicity of a particle up to 20nm. A similar exploitation between the butanol and water based instruments but different method is explored in our study to understand the effects of chemical composition on the lower detection efficiency.

In this study we quantify the particle hygroscopicity parameter with simultaneous particle detection in butanol and water-based CPCs. The developed theory, derived from classical thermodynamics of droplet formation, estimates the water-insoluble mass in particle compositions. A late model W-CPC, with smaller instrument temperature gradient, was used to exploit the theoretical differences in particle counting measurements that can be used to infer the water-insoluble mass. The method was

calibrated with known simple organic and inorganic aerosol compositions, and the experimental set-up (Section 2.1) was applied to a field study. The differences in the two CPC instruments provide quantitative and real-time information on the water-insoluble component found in near-road aerosol sources.

2.2. Theory and Analysis

2.2.1. Water-Insoluble Mass Estimates Method

The method described here uses a W-CPC and B-CPC with two separate electrostatic classifiers and Differential Mobility Analyzers (DMAs). When operated in scanning mode to rapidly size and count electrical mobility particle distributions, the unit is often referred to as a scanning mobility particle sizer (SMPS). Two SMPS units were used for this analysis; one with a B-CPC and the other with a W-CPC. Each unit consists of a TSI 3080 Electrostatic Classifier with a TSI 3081 DMA and CPC. The experimental setup is shown in Fig. A-1. The SMPS samples a polydispersed flow of particles and charges particles with a Krypton-85 radioactive source. An equilibrium charge distribution was applied to particles entering the DMA. Then the electrical mobility of the particles size selects particles into a monodisperse flow (Wang et al. 1990). The dry monodispersed particles then flow into the CPC; the concentration of size-selected particles was measured. The SMPS was connected to either a B-CPC (TSI Model 3772) or a W-CPC (TSI Model 3785). Both CPCs were synchronized and verified to be scanning on the same universal time. Because CPCs were not connected to the same electrostatic classifier during the field study, the ε_{50} values were averaged over a 10 minute period.

This ensured both CPCs were counting the same particles during the averaging period. Each electrostatic classifier has a scan time of 2.25 minutes with a sheath flow rate of 10 L/minute. A total of four scans were performed for each 10 minute average; four ε_{50} were calculated for each averaged value. We report differences in CPC particle counts below 250 nm by taking the ratio of particle concentrations from the water and butanol based counting instruments. For our analysis, it was assumed that the B-CPC counts all particles measured in the DMA selected size range. The differences in CPC particle counts were used to estimate the water-insoluble mass (Section 2.3). Discrepancies between the W-CPC and B-CPC, especially those between the minimal detectable size (10nm and 40nm) were attributed to particle solute properties. Unlike the CPCB, our method size selects each particle. In addition, the CPCs were not calibrated to have the same ε_{50}. Thus the method presented here can determine the particle hygroscopicity parameters for much larger particle diameters (up to 40 nm, given the TSI 3785 set-point water-vapor saturation). The 40nm limit is estimated from the thermodynamic models discussed in the next section.

2.2.2. Droplet Growth in CPCs

In CPCs, dry particles are exposed to a high relative humidity, or saturated vapor of the working fluid. Saturation, S, is the ratio of partial pressure (P_v) to the saturation vapor pressure (P_{sat}) of the working fluid. After the particles exposure to saturated conditions, the B-CPC employs a cooled growth tube to condense the working fluid vapor on the particle surface, which initiates wet droplet growth. For butanol-based instruments, it is

assumed that activation depends on the Kelvin effect and the maximum *S* encountered along the particle trajectory through the condenser (Stoltzenberg and McMurry 1991).

The process to form wet particles in the W-CPC is different. The initial saturation area in the W-CPC is cool; the W-CPC uses a cold growth tube to produce the saturated working fluid vapor followed by a wetted/warm-walled condenser to grow wet particles (Hering et al. 2005). When the particle passes through the condenser, the mass transfer of water vapor is faster than the thermal transfer of heat to the aerosol flow. Lower molecular weight water vapor molecules diffuse more quickly, from the wetted/warm wall, to the particle surface than air and water molecules condense in the saturated environment. Dry particles are wetted, activated and grow to sizes detected by the optical counter.

Here, we present the robust theory of chemical effects for droplet formation and then explain the simplifications and assumptions used from the original theory for our analysis. The heterogeneous condensation of water vapor into the particulate phase can be predicted with Köhler Theory (Köhler 1936).

$$S = \frac{P_v}{P_{sat}(T)} = a_b \, exp\left(\frac{4M_b\sigma_b}{\rho_b RTD}\right) \qquad (1)$$

where R is the universal gas constant, T is the temperature at activation, D is the wet droplet diameter, ρ_b is the density of the bulk fluid condensing onto the particle (water or butanol), M_b is the molecular weight of the bulk fluid, and σ_b is the surface tension at the droplet vapor/liquid interface. a_b is the activity of the bulk fluid. Köhler theory is the combination of the Kelvin effect that increases vapor pressure and the dissolved solute

effect that decreases vapor pressure at the droplet surface. When solute effects are negligible, a_b = 1. Equation 1 reduces to the Kelvin term. Thus a maximum critical saturation, S_c, exists for which a minimum layer of water is required to form a droplet. S_c is greater than one and critical supersaturation, s_c, (S_c -1) is commonly used in its place. For dry particles greater than 40 nm exposed to water or butanol s_c > 2%, the Kelvin term dominates and the dry particle will experience uncontrollable droplet growth. Assuming the Kelvin effect is ideal and governed by the fluid properties, changes in particle activation for a given fluid are thus controlled by the dissolved solute properties and the activity of the droplet solution. The water activity, a_w, is approximated by Raoult's Law where a_w is equivalent to the mole fraction of water in droplet solution. Rearrangement of Eq. 1 yields (Seinfeld and Pandis 2006);

$$\ln s_c = \left(\frac{4A^3}{27B}\right)^{1/2}, \quad A = \frac{4M_b\sigma_b}{\rho_b RT} \quad \text{and} \quad B = \frac{6n_s M_b}{\pi\rho_b} \qquad (2)$$

where n_s is the moles of solute and v is the ion dissociation of the particle in water. For a spherical solute particle, n_s is related to the dry particle diameter, d_s, the density of the particle, ρ_s and the molecular weight of the particle, M_s such that s_c and d_s are related as follows:

$$\ln {s_c}^2 = \frac{4A^3\rho_b M_s}{27v\rho_s M_b {d_s}^3} \qquad (3)$$

For an instrument with s_c, d_s is equal to the theoretical ε_{50} diameter. Köhler Theory requires explicit chemical information of each solute species present. For unknown and

rapidly changing particle composition, the full Köhler Theory is complex. The theory can be simplified to predict the activation behavior of soluble and insoluble particle mixtures.

2.3 Water-Insoluble Mass Fraction Estimates

Traditional Köhler theory can be rewritten in terms of a single solute parameter called κ- Köhler theory. a_w is parameterized as follows (Petters and Kreidenweis 2007):

$$\frac{1}{a_w} = 1 + \kappa \frac{V_s}{V_w} \qquad (4)$$

where V_s is the Volume of the solute, V_w is the volume of water, and κ is the hygroscopicity parameter. For multicomponent system at equilibrium the Zdanovskii, Stokes, and Robinson (ZSR) assumption is applied. A simple mixing rule is derived for which

$$\kappa = \sum \varepsilon_i \kappa_i \qquad (5)$$

where ε_i is the component volume fraction of species and κ_i is the hygroscopicity parameter of that component.

The parameter κ characterizes the effects of solute composition for droplet activation. κ-values can range from 0 to 1; where 0 is less hygroscopic but wettable and 1 is a very hygroscopic solute. The κ value is calculated from direct measurements of d_s (or ε_{50}) measurements at a fixed instrument s_c as follows:

$$\kappa = \frac{4A^3}{27 {d_s}^3 \ln(s_c)^2} \qquad (6)$$

κ- Köhler theory (Eq. 6) is similar to Eq. 3 but assumes the σ_b properties of the droplet are that of the pure fluid. Changes in measured κ values suggest chemical changes in solute composition (Petters and Kreidenweis 2007). The changes in composition can be approximated with a two-component model of low hygroscopic and highly hygroscopic solute material. In this study, we choose sulfuric acid (SA) and dioctyl phthalate (DOP) as a proxy two-component mixture. SA has been measured in vehicular diesel exhaust, and is believed to be a key nucleation gas component in engine new particle formation (Tobias et al. 2001; Arnold et al. 2006; Arnold et al. 2012). SA is highly hygroscopic and has a κ_{sa}=0.9 (Petters and Kreidenweis 2007). Motor vehicle particulate composition (up to 95%) is dominated by unburned lubricating oil and fuel spectral signatures (Schauer et al. 1999; Tobias et al. 2001; Sakurai et al. 2003). DOP has been previously used as a proxy for hydrophobic but wettable aerosol from vehicular exhaust (e.g., Asa-Awuku et al. 2009). DOP is a diester of phtlaic acid with $\kappa_{DOP} \approx .01$.

The two-component mixtures were applied for two reasons 1) the simple model must comprise of materials that may be found near major roadway sources and 2) each component must have distinct water-affinities, preferably approaching realistic limits of the single parameter, κ-hygroscopicity. By assuming a unit particle density and a two-component mixture, we infer the water-insoluble mass fraction, χ with Eq. 7.

$$\kappa_{am} = \kappa_{sa}(1-\chi) + \kappa_{DOP}(\chi) \qquad (7)$$

where, κ_{am} is the hygroscopicity of ambient unknown composition (Eq. 6. and Sect. 2.3). κ_{am} is also an indication of the hygroscopic fraction (assuming ideal Kelvin with a two

component hygroscopic and a low hygroscopic core with κ =1 and 0, respectively). Equation 7 is a modified approximation accounting for likely hygroscopic and a low hygroscopic, but wettable, components found in vehicular exhaust. Equation 7 is a form of Eq. 5, where the water-insoluble volume fraction, χ, relates specifically to DOP and κ_i is the κ of either SA or DOP. κ_{am} is derived from measurements using Eq. 6, where only the χ term is unknown. The SA and DOP two-component model (Eq. 7) provides conservative estimates of χ within 15% uncertainty. 15% uncertainty is derived from the variability of κ_{am} in section 3.2. The uncertainty includes 10% error in particle counting from CPC instrumentation. In follow-up work, Petters and Kreidenweis (2008) and Petters and Kreidenweis (2013) discussed the limitations of partially soluble species and surfactant partitioning in κ-Köhler theory. As with traditional Köhler theory, chemical speciation is required to account for the non-ideal solubility and surfactant tension effects in the extension of κ- Köhler theory. In this study, we utilize the single parameter first posed in Petters and Kreidenweis (2007) that assumes a complete soluble and insoluble species exists to provide fast measurements of particle hygroscopicity. If the size distribution is assumed to be internally mixed (a uniform composition is applied to each size), we can estimate the mass of water-insoluble material as χ multiplied by the particle volume distribution and unit density.

2.2.2.2. External Mixing State Effects

In complex aerosol, there are multiple chemical species that can inhibit droplet activation. These chemical species may be indicative of an external mixture of two distinct soluble populations at different sizes. These populations will produce two separate ε_{50} diameters, which will also produce multiple κ_{am}. The weighted average of multiple κ_{am} represents the varying chemical composition. The corresponding water-insoluble mass fractions, χ, can be averaged to provide an overall water-insoluble mass fraction. Each corresponding water- insoluble mass fraction is solved with Eqs. 6 and 7. Once an overall water-insoluble mass fraction is calculated, Eqs. 6 and 7 are rearranged to solve for an overall κ_{am} and overall ε_{50}.

2.2.3. Method Calibration and Analysis

The water-insoluble mass estimate method was calibrated with atomized ammonium sulfate, sodium chloride, and DOP. For calibration, the atomized aerosol is dried and size selected with the TSI Model 3081 DMA. The monodisperse stream was split and the W-CPC and B-CPC sample at a rate of 1 LPM, respectively. For a given particle diameter, the ratio of W-CPC counts was divided by B-CPC counts. The data selected for each scan of the size distribution is similar to a cloud condensation nuclei (CCN) activation curve; the ratio of activated water droplets to total particles versus particle diameter is plotted. This economical method is similar to the use of a CCN counter with a s_c =2% to retrieve κ values for the measured particles. A sigmoidal equation was fit to the data to find the diameter corresponding to a ratio of 0.5. Fig. A-2

shows the curve for both ammonium sulfate, sodium chloride and DOP. The ratio of 0.5 is the ε_{50} that is assumed to be the minimum diameter for droplet activation and subsequently used to calculate κ. Again, κ was calculated in Eq. 5 with the only unknown parameter, ε_{50}. This same method for calculating κ was also used to calculate the ambient hygroscopicity near roadway (κ_{am}), obtained from during the field study. The ε_{50} measured for calibration ammonium sulfate aerosol was 16.9 nm, as shown in Fig. A-2. A 16.9 nm critical diameter is used in in Eq. 6 to calculate the single hygroscopicity parameter, κ. κ for the calibration is 0.62 within ± 0.1 of published and theoretical values for the CCN activation of ammonium sulfate (Petters and Kreidenweis 2007). The calibration procedure was repeated with DOP. For DOP κ < 0.00804 and ε_{50} =71.3 nm; consistent with wettable but low hygroscopic material (Fig. A-2). In addition, the calibration procedure was repeated for sodium chloride. κ =1.38 and ε_{50} =12.9 nm for NaCl. The measured κ for sodium chloride is ± 0.1 to the literature value of 1.28 (Petters and Kreidenweis 2007). Each of the calibration solution ε_{50} measurements were measured with the same instrument critical supersaturation (s_c) at 2%. It was assumed that the presence of multiple charged particles is negligible for our data. The calibration data agrees well with literature values thus supporting this assumption. The experimental analysis was applied to ambient aerosol measurement to infer real-time water-insoluble mass estimations. Thus in addition to the field measurement, the proposed experimental method was also tested with known aerosol in controlled settings.

2.2.4. BC Measurement and Analysis

BC mass concentration was measured with a multi-angle absorption photometer (MAAP). The MAAP is a filter-based measurement that uses one light source at 670 nm to produce photons directed toward an accumulation of particles on Teflocarbon filter paper (Petzold et al. 2004). The back scattering of these photons was then measured by four photodetectors located at 45 degree intervals. As particles accumulate on the filter paper, the light transmitted back or above the filter paper correlates to the concentration of BC. A photodetector below the filter paper determines the upper limit of detection. The upper limit occurs when < 10% of light emitted is transmitted through the filter paper. Once this is achieved, clean filter paper is moved on to the detection area for continuous online black carbon measurements. Calibrating the instrument requires a known amount of BC that is aerosolized and then analyzed with the MAAP. Aquadag © aqueous solution is atomized and then dried. The Aquadag © BC mass concentration is simultaneously measured with an Aerosol Particle Mass (APM, Kanomax model 3600) Analyzer (Schwarz et al. 2006) and the MAAP. After calibration, The MAAP BC concentrations agree to within ± 11% of APM measurements.

2.2.5. Field Study Location

The Interstate Highway 710 (I-710) is a major truck route in Southern California. Approximately 20% of the I-710 total traffic flow is comprised of heavy-duty trucks. Measurements were taken 15 meters east (and mostly downwind) of the I-710, on the

southbound side of the freeway near the intersection with Long Beach Blvd. on May 10th (weekday) and 14th, 2011(weekend). There were no other significant sources of particles other than the highway traffic emissions. Data were provided for the days which simultaneous sizing and counting instrumentation is available. All instruments were housed inside one of SCAQMDs air conditioned monitoring trailers. Five minute average traffic information (i.e. total and heavy duty diesel traffic flows) on the north and southbound I-710 lanes were retrieved from Caltrans website (http://pems.dot.ca.gov). Meteorological instrumentation recorded wind direction and velocity data (Fig. A-3).

2.3. Results and Discussion

2.3.1. Black Carbon and Particle Number Concentration

Fewer than 200 trucks and ~ 1000 cars per 5 minute traversed the I-710 highway on the weekday and weekend. The concentration of cars and trucks (Fig. A-4) showed small variations for both days. However significantly less vehicles travelled on the highway during the weekend. On both days, wind and particle instrument measurements increase in magnitude/direction in the late afternoon (14:00 and 16:00 PDT, pacific daylight time). A significant change in wind direction from downwind to upwind of the freeway occurs for both the BC and total particle concentrations (Fig. 2-1a). Downwind aerosol measurements are considered to be when freeway aerosols were flowing in the opposite direction of the sampling inlet. Whereas, upwind aerosol measurements are defined as when the freeway aerosols were flowing in the direction of the sampling port

inlet. Data showing the total particle concentration measured with a W-CPC (TSI Model 3781) was only available for the weekday measurements during the campaign. The BC concentration for both days (Fig. 2-1), reached a maximum 10 minute average concentration of 3 μg m^{-3} and 1 μg m^{-3} at 14:00 and 16:00 PDT for the weekday and weekend measurements, respectively. The measurements were averaged every 10 minutes with a lower detection limit of 0.1 μg m^{-3}. BC concentrations on the weekend are lower compared to the weekday concentrations. Lower BC concentrations are likely due to fewer weekend heavy-duty vehicle traffic (Fig. A-4.)

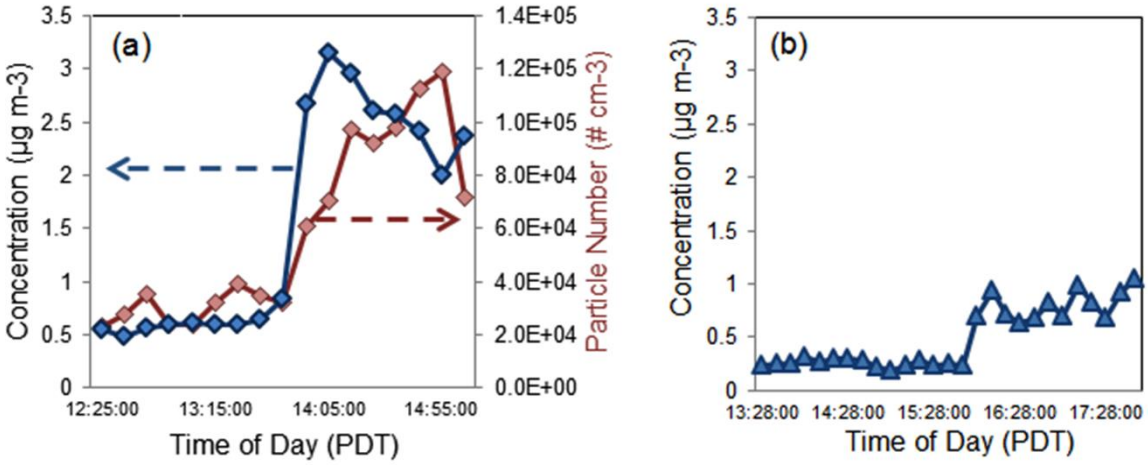

Fig. 2- 1. Ten minute averaged black carbon (BC) and particle number (PN) concentrations from water-based (W-CPC) particle concentrations on the weekday (a) and only averaged BC concentrations on the weekend (b).

2.3.2. Particle Size Distribution

The particle counts of both the W-CPC and B-CPC instruments were compared to infer solute properties. A ten minute average was applied to the particles counts for each particle diameter of each instrument. Ten minute averages account for size distribution

number and variability of four size distribution scans (2.25 minutes each) taken with the SMPS. A ratio of the W-CPC to B-CPC particle count averaged data was calculated. Again, ε_{50} is calculated from the ratio of W-CPC and B-CPC particle counts which was used to calculate κ_{am} (Eq. 5). We note that there were occurrences in our data set, especially above the 200 nm regime, where the W-CPC recorded greater particle counts than the B-CPC. For these occurrences at high instrument s_c, particle size (surface area) is more important for droplet activation than solute composition. Thus we focus our comparison on the discrepancies near or below 40 nm.

Fig. 2-2 shows the relationship between two CPCs for the weekday and weekend. There were fewer particle counts in the W-CPC data compared to the B-CPC data. The instruments agree above the 30 nm particle diameter range.

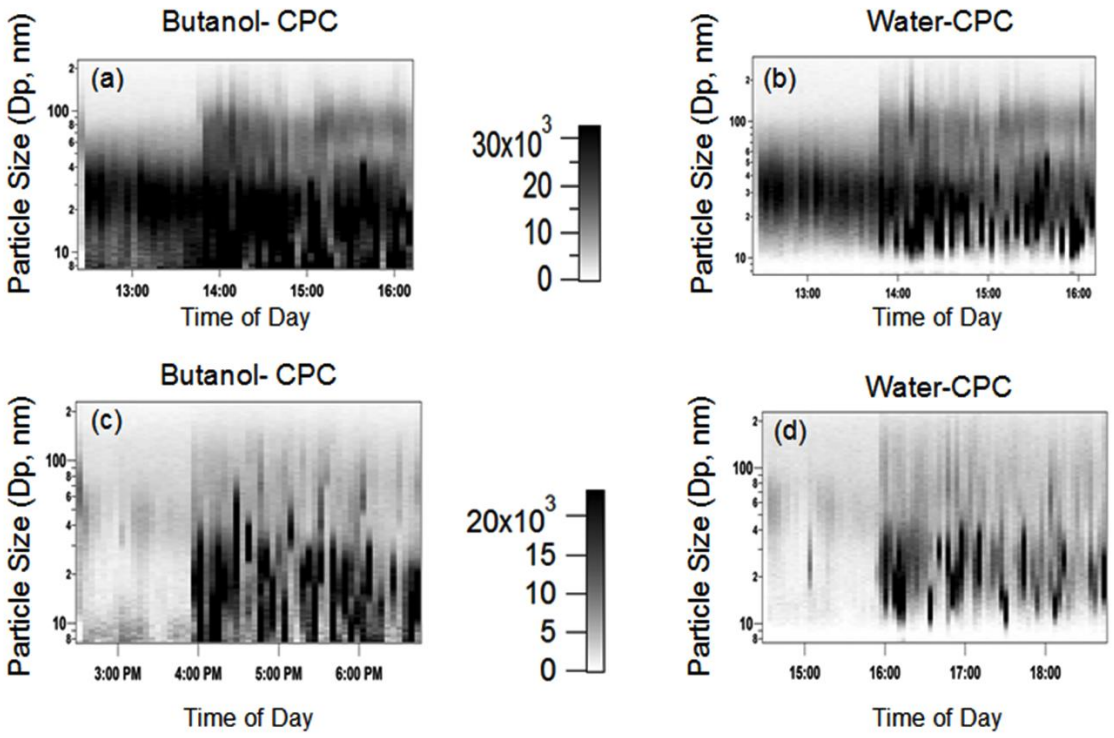

Fig. 2- 2. The weekday particle size and number distributions measured with a (a) B-CPC and (b) W-CPC. The weekend particle size and number distributions measured with a (c) B-CPC and (d) W-CPC. The scale between the figures shows particle number concentration (# cm^{-3}).

Fig. 2-2a and 2-2b show a large increase in particle counts after 14:00 hrs. The increase in particle number concentration correlated to the change in sampling wind direction (downwind to upwind, Fig. 2-1). Lower particle number concentrations persist during the weekend. The weekday and weekend diurnal profiles are similar. Fewer particles were measured during the weekend. The B-CPC size distributions had a majority of weekend particle counts below the 40 nm range (Fig. 2-2c). The W-CPC size distribution (Fig. 2-2d) show fewer particles below the 30nm range (similar to the

comparison of weekday measurements Fig. 3-2a-b). Both Figs. 2-2c and 2-2d show an increase in particle concentration at 16:00 hours, which is due to the change in wind direction.

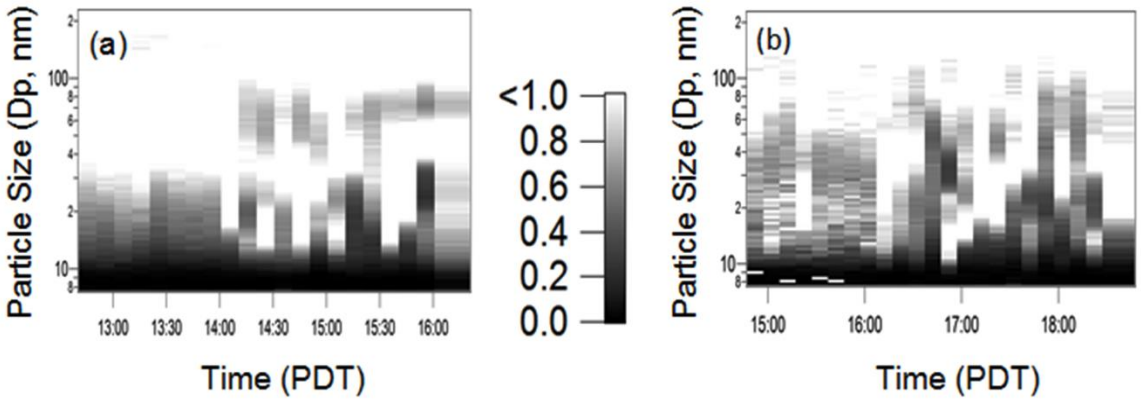

Fig. 2- 3. The comparison of water to butanol particle concentration counts (ratio from 0 to 1) for the (a) weekday and (b) weekend measurements.

The ratio of particle number concentrations measured by B-CPC and W-CPC is shown in Fig 2-3. Before changes in wind direction on the weekday (Fig. 2-3a), the W-CPC measured fewer than 50% of the particles below 30nm measured by the B-CPC. Hence a gradual change in the activation ratio occurs as particles increase in size (observed via the changing color gradient in Fig. 2-3). Before the change in wind direction on the weekend (Fig. 2-3b.), the W-CPC measures 50% of the particles at a range of sizes below 100nm. However, the CPC count ratio was more variable on the weekend than on the weekday (Fig. 2-3). The diameter for which the W-CPC measures 50% or more of the total particles occurs at sizes above and below 30 nm for the upwind weekend measurements.

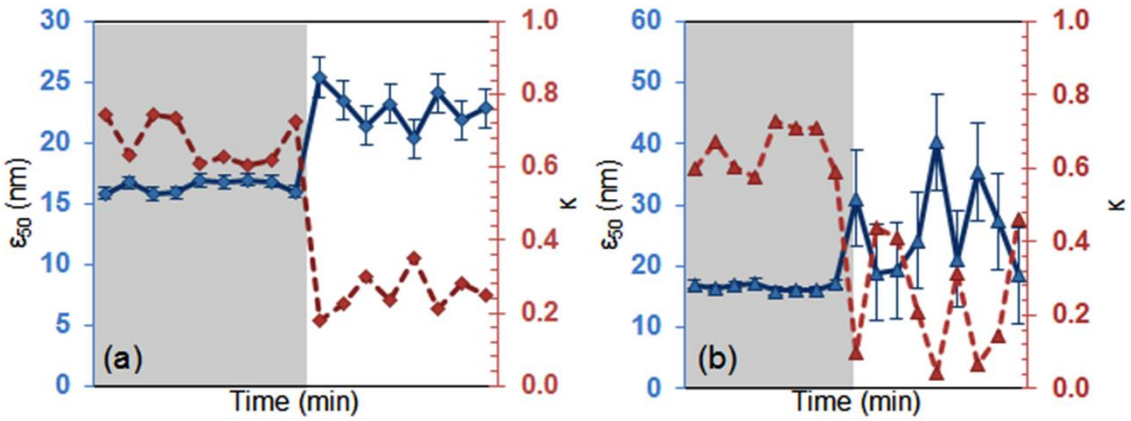

Fig. 2- 4. Changing κ (dashed line) and ε50 (solid line) for both weekday and weekend data sets. The shaded region represents the time before the wind change.

Fig. 2-4 shows the aerosol ε_{50} and calculated κ_{am} values for sampling downwind and upwind of the freeway. As ε_{50} increases, κ_{am} decreases. A sample activation plot is shown in Fig. A-5 for the weekday and weekend, which is used to determine ε_{50}. Multiple ε_{50} values were shown from upwind of the freeway aerosol. The average ε_{50} was used to calculate κ_{am} values for multiple ε_{50} (Section 2.3.1). The weekend has more of these multiple ε_{50} which accounts for the variation in ε_{50} (Fig. A-5). The overall hygroscopicity parameter decreases ($\Delta\ \kappa_{am} \sim 0.35$) for upwind aerosols on both days. Despite changes in traffic patterns and overall particle concentrations, κ_{am} was greater than 0.6 (very hygroscopic) in the morning hours and then becomes less than 0.2 (slightly hygroscopic). Though there were significantly more particles emitted during the weekday (Fig. 2-2.), the composition of particles on the weekday and weekends were similar. The changes in particle soluble composition were dominated by changing wind direction aerosol sampling rather than traffic volume.

2.3.3. Inferred Water-Insoluble Mass

Fig. 2-5 correlates the inferred water-insoluble mass and BC mass concentration. The water-insoluble mass was estimated from the particle volume distributions and κ_{am} (Fig. 2-4). The total particle mass was estimated using the aerosol size distributions measured from the B-CPC particle number, assuming a density of 1 g/cm^3. 1 g/cm^3 was used as an estimate for the density of the particles sampled since density information was not measured. Turpin and Lim (2001) determined the density of the Los Angeles Basin aerosol was about 1.2 g/cm^3. The difference in prescribed and literature roadway source aerosol density is within 25%.The weekday data points correlate to a slope of 1 to 1; whereas the weekend data points correlated to the 2 to1 line (Fig. 2-5.). The majority of these points were within 25% of the slopes (dotted lines in Fig. 2-5). During the weekday BC mass concentrations are equivalent to the estimated particle water-insoluble mass (Fig. 2-5a). This was determined from the data correlating with the 1 to 1 line. On the weekend, the BC concentration and the estimated water-insoluble mass data were within 25% of the 2 to1 slope; suggesting the estimated water-insoluble mass increases more rapidly than the BC mass concentrations.

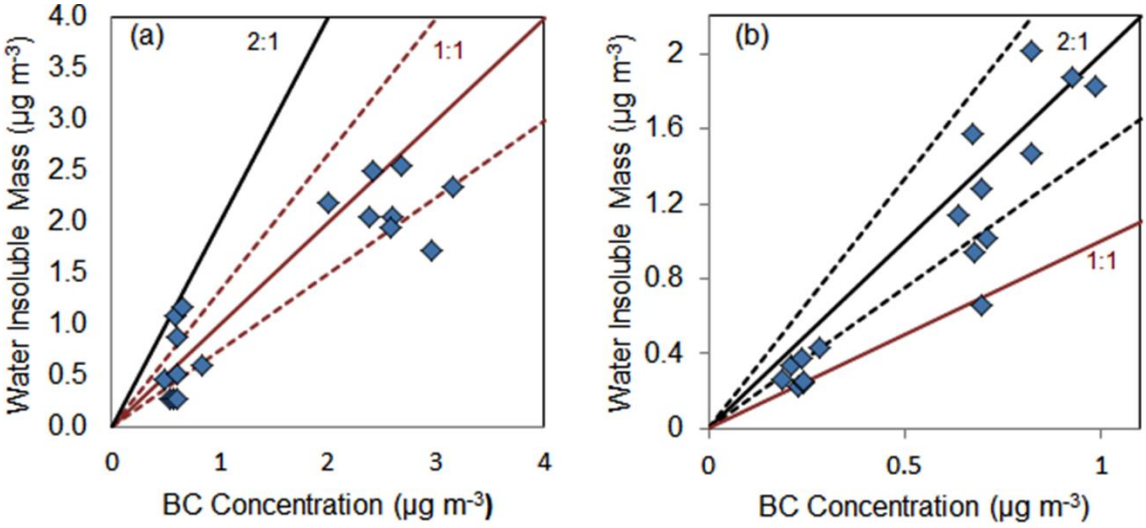

Fig. 2- 5. Black Carbon Concentration versus inferred water insoluble mass from the weekday (a) and weekend (b) measurements. The solid line shows the rate of increase; either 1:1 for the weekday and 2:1 for weekend. Dashed lines represent 25% deviation from (a) 1:1 or (b) 2:1 solid lines.

Both slopes in Fig. 2-5 were positive and thus BC mass concentrations contribute to the estimated water-insoluble mass. We note that BC may not be the only water-insoluble component from roadway emissions. The weekend data shows a larger amount of the estimated water-insoluble mass compared to the BC mass concentration (data points correlate with the 2 to 1 line) indicating that BC is not the only water-insoluble composition. There may be other particulate compositions (i.e, lubrication oil) that can contribute to the water-insoluble mass estimates that may not absorb light at a 670 nm wavelength. Conversely our data shows that the weekday measurements of BC material may be entirely water-insoluble; the contribution of BC was the main source of water-insoluble mass for the weekday. The unknown water-insoluble compositions contribute less than 25% uncertainty to the correlation of the water-insoluble mass estimates and BC

mass concentrations for the weekday. Additionally, changes in unit particle density could contribute to the 25% deviations. Nonetheless, the data shows that the presence of BC (and other water-insoluble materials) affect counting efficiencies of the W-CPC.

2.4. Summary

The aerosol solute composition affects the counting efficiency of W-CPC and B-CPCs. Published work confirms discrepancies exist between the two CPC instruments and can be used to infer water-affinities (Kulmala et al. 2007; Riipinen at al. 2009). In this study, two SMPS systems measured differences in particle size and number distributions with two CPCs of different working fluids. The method was used to capture quick changes in solute hygroscopicity and gain quantitative insight into the ephemeral nature of near road-way sources. Initial calibration measurements confirm that the discrepancies in CPC readings can be attributed to the estimated water-insoluble mass and are consistent with classical thermodynamic theory. The method presented here is different than those already published, and is able to determine particle hygroscopicity up to a 40nm particle diameter (instead of 10nm with the method described in Kulmala et al. (2007)). The method can find critical activation diameters that are translated into a single hygroscopicity parameter, κ. The assumption that particles are a two-component mixture of highly hygroscopic and low hygroscopic compositions works well for internally mixed aerosols. In our near roadway field study the sampled air mass particle number, composition, and estimated water-insoluble mass varied with traffic patterns and wind

direction. Sampling downwind to upwind of the freeway aerosol had the greatest influence on measurements; particles from the freeway that were directly adverted to the sampling port inlet during peak traffic hours were less hygroscopic than those measured earlier in the day. The fresh vehicular emissions contained higher concentrations of BC and water-insoluble material that were less likely to nucleate in the W-CPC. The particle number concentrations that contained water-insoluble material affected the counting efficiency of the instrumentation. On the weekend, the increase in the water-insoluble mass estimates was about two times the contribution of the BC. This suggests that other species (e.g., aerosol that do not absorb at 670nm wavelengths) were present and water-insoluble. Thus other water-insoluble species from near-roadway sources may affect the efficiency of water-based condensational particle counting instrumentation. Additional chemical composition measurements (not available during this field study) can provide further insight into the total particle composition. The coupling of CPCs with different working fluids can provide fast and real-time evidence of changes in hygroscopic composition. A conservative estimate of the water-insoluble mass fraction from traffic-related aerosols can be inferred using a two-component mixture of wettable hydrophobic material and highly hygroscopic solute.

2.5. Acknowledgements

The authors would like to thank the U.S Environmental Protection Agency for funding this work, made possible by EPA grant number 83504001. Its contents are solely the responsibility of the grantee and do not necessarily represent the official views of the EPA. Further, the EPA does not endorse the purchase of any commercial products or

services mentioned in the publication. In addition, the authors would also like to thank Dr. Wayne Miller for his support in facilitating collaborations on the project. The South Coast Air Quality Management District (SCAQMD) is also acknowledged for their support in the use of facilities and additional expertise for the study.

2.6. Literature Cited

Agarwal, J. K., Sem, G. J. (1980). Continuous Flow, Single-Particle-Counting Condensation Nucleus Counter, Journal of Aerosol Science, 11: 343–357.

Aitken, J. (1890-1891). On a Simple Pocket Dust-Counter, Proceedings of the Royal Society of Edinburgh, 18: 39–53.

Arnold F., Pirjola, L., Aufmhoff, H., Schuck, T., Lähde T., Heikkilä J. (2006). First Gaseous Sulfuric Acid Measurements in Automobile Exhaust: Implications for Volatile Nanoparticle Formation. Atmospheric Environment, 40: 7097-7105.

Arnold F., Pirjola L., Rönkkö T., Reichl U., Schlager H., Lähde T., Heikkilä J., Keskinen J. (2012). First online measurements of sulfuric acid gas in modern heavy-duty diesel engine exhaust: implications for nanoparticle formation, Environmental Science and Technology, 46: 11227-11234.

Asa-Awuku, A., Miracolo, M.A., Kroll, J.H., Robinson, A.L., Donahue, N.M. (2009). Mixing and Phase Partitioning of Primary and Secondary Organic Aerosols. Geophysical Research Letters, 15: L15827

Avol, E. L., Jones, M. P., Bailey, R. M., Chang, N. M. N., Kleinman, M. T., Linn, W. S., Bell, K. A., Hackney, J. D. (1979). Controlled exposures of human volunteers to sulfate aerosols - Health-effects and aerosol characterization, American Review of Respiratory Disease, 120: 319-327.

Akhter, M.S., Chughtai, A.R. and Smith, D.M., (1985). The structure of hexane soot I. Spectroscopic studies. Applied Spectroscopy. 39: 143-153.

Biswas, S., Fine, P. M., Geller, M. D., Hering, S. V., Sioutas, C. (2005). Performance Evaluation of a Recently Developed Water-Based Condensation Particle Counter, *Aerosol Science and Technology*, 39: 419–427.

Bond, T. C., Streets, D.G., Yarber, K.F., Nelson, S.M., Woo, J., Klimont, Z. (2004). A technology-based global inventory of black and organic carbon emissions from combustion, Journal of Geophysical Research, 109: D14203.

Bricard, J., Delattre, P., Madelaine, G., Pourprix, M. (1976). Detection of Ultra-Fine Particles by Means of a Continuous Flux Condensation Nuclei Counter. In Fine Particles: Aerosol Generation, Measurement, Sampling, and Analysis, edited by B.Y.H. Liu, Academic Press, NewYork, 565–580.

Charlson, R. J., Schwartz, S.E., Hales, J.M., Cess, R.D., Coakley, J.A., Hansen, J.E., Hofmann, D.J. (1992). Climate forcing by anthropogenic aerosol, Science, 255: 423-430.

Conant, W. C., Nenes, A., Seinfeld, J.H. (2002). Black carbon radiative heating effects on cloud microphysics and implications for the aerosol indirect effect 1. Extended Köhler theory, *Journal Geophysical Research, 107*: 4604.

Cooke W.F., Wilson J.N. (1996). A global black carbon aerosol model. Journal of Geophysical Research, 101: 19395–19409.

Chung, S. H., Seinfeld, J. H. (2005). Climate response of direct radiative forcing of anthropogenic black carbon. Journal of Geophysical Research, 110: D11102.

Davidson, C. I., Phalen, R. F., Solomon, S. (2005). Airborne particulate matter and human health: A review. Aerosol of Science and Technology, 39: 737-749.

Forster, P., Ramanswamy, V. (2007). Climate Change 2007: The Physical Science Basis — Contribution of Working Group I to the Fourth Assessment Report of the Intergovernmental Panel on Climate Change, Cambridge Univ. Press, Cambridge UK, New York USA.

Franklin, L.M., Bika, A.S., Watts, W.F., Kittelson, D.B. (2010). Comparison of Water and Butanol Based CPCs for Examining Diesel Combustion Aerosols, Aerosol Science and Technology, 44: 629-638.

Hering, S. V., Stolzenburg, M. R. (2005). A Method for Particle Size Amplification by Water Condensation in a Laminar, Thermally Diffusive Flow. Aerosol Science and Technology, 39: 428–436.

Hering, S. V., Stolzenburg, M. R., Quant, F. R., O'Berreit, D. R., Keady, P. B. (2005). A Laminar-Flow, Water-Based Condensation Particle Counter (WCPC). Aerosol Science and Technology, 39: 659–672.

Hermann, M., Wehner, B., Bischof, O., Han, H., Krinke, T., Liu, W., Zerrath,A., Wiedensohler, A. (2007). Particle counting efficiencies of new TSI condensation particle counters, Journal of Aerosol Science, 38: 674-682.

Junge, C. (1935). Neuere Untersuchungen an der Grossen Atmosph¨arischen Kondensationskerne, Meteorologische Zeitschrift, 52: 467 –470.

Köhler, H. (1936). The nucleus in and the growth of hygroscopic droplets, Transaction of the Faraday Society, 32: 1152–1161.

Koehler, K. A., DeMott, P. J., Kreidenweis, S. M., Popovicheva, O., Petters, M. D., Carrico, C. M., Kireeva, E., Khokhlova, T., Shonija, N. (2009). Cloud condensation nuclei and ice nucleation activity of hydrophobic and hydrophilic soot particles, Atmospheric Chemistry and Physics, 11: 7906–7920.

Kulmala, M., Mordas, G., Petäjä, T., Grönholm, T., Aalto, P.P., Vehkamäki, H., Hienola, A., Herrmann, E., SipiläM., Riipinen, I., Manninen, H., Hämeri, K., Stratmann, F., Bilde, M., Winkler, P.M., Birmili, W., Wagner, P.E. (2007). The condensation particle counter battery (CPCB): A new tool to investigate the activation properties of nanoparticles, Journal of Aerosol Science, 38:289-304

Liggio, J., Gordon, M., Smallwood, G., Li, S., Stroud, C., Staebler, R., Lu, G., Lee, P., Taylor, B., Brook, J.R. (2012). Are Emissions of Black Carbon from Gasoline Vehicles Underestimated? Insights from Near and On-Road Measurements, Environmental Science and Technology, 46: 4819-4828.

Liu, W., Kaufman, S., Osmondson, B., Sem, G. (2006). Water-Based Condensation Particle Counters for Environmental Monitoring of Ultrafine Particles, Journal Air & Waste Management, 56: 444-445.

McMeeking, G.R., Good, N., Petters, M.D., McFiggans, G., Coe, H. (2011). Influences on the fraction of hydrophobic and hydrophilic black carbon in the atmosphere, Atmospheric Chemistry and Physics, 11: 5099–5112.

Moosmuller, H., Chakrabarty, R.K., Arnott, W.P. (2009). Aerosol light absorption and its measurement: A review, Journal of Quantitative Spectroscopy & Radiative Transfer, 110: 844–878.

Mordas, G., Manninen, H.E., Petäjä, T., Aalto, P.P., Hämeri, K., Kulmala ,M. (2008). On Operation of the Ultra-Fine Water-Based CPC TSI 3786 and Comparison with Other TSI Models (TSI 3776, TSI 3772, TSI 3025, TSI 3010, TSI 3007), Aerosol Science and Technology, 42: 152-158.

Nel, A. E., Diaz-Sanchez, D., Ng, D., Hiura, T., Saxon, A. (1998). Enhancement of Allergic Inflammation by the Interaction between Diesel Exhaust Particles and the Immune system, Journal of Allergy Clinical Immunology, 102: 539.

Novakov, T., Andreae, M.O., Gabriel, R., Kirchstetter, T.W., Mayol-Bracero, O.L., Ramanathan, V. (2000). *Origin of carbonaceous aerosols over the tropical Indian Ocean: Biomass burning or fossil fuels?,* Geophysical Research Letters, 27: 4061-4064.

Petaja, T., Mordas, G., Manninen, H., Aalto, P., Hameri, K., Kulmala, M. (2007). Detection Efficiency of a Water Based TSI Condensation Particle Counter 3785, Aerosol Science and Technology, 40: 1090-1097.

Petters, M.D., Kreidenweis, S.M. (2007). A single parameter representation of hygroscopic growth and cloud condensation nucleus activity. Atmospheric Chemistry and Physics, 7: 1961–1971.

Petters, M.D., Kreidenweis, S.M. (2007b). A single parameter representation of hygroscopic growth and cloud condensation nucleus activity- Part 2:Including Solubility. Atmospheric Chemistry and Physics, 8: 6273-6279.

Petters, M. D. and S. M. Kreidenweis (2013), A single parameter representation of hygroscopic growth and cloud condensation nucleus activity - Part 3: Including surfactant partitioning, Atmos Chem Phys, 13(2), 1081-1091, doi:10.5194/acp-13-1081-2013.

Petzold, A., Schönlinner, M. (2004). The Multi-angle absorption photometer – A new method for the measurement of aerosol light absorption and atmospheric black carbon. Journal of Aerosol Science, 35: 421-441.

Pope, C. A., Dockery, D. W. (2006). Health effects of fine particulate air pollution: Lines that connect, Journal of Air & Waste Management, 56: 709-742.

Ramanathan, V., and Carmichael, G. (2008) Global and regional climate changes due to black carbon, Nature Geoscience , 1: 221 – 227.

Riipinen, I., Manninen, H.E., Yli-Juuti, T., Sipilä, M., Ehn, M., Junninen, H., Petäjä, T., Kulmala, M. (2009). Applying the condensation particle counter battery (CPCB) to study the water-affinity of freshly-formed 2-9nm particle in boreal forest, Atmospheric Chemistry and Physics, 9:3317-3330

Rose, D., Wehner, B., Ketzel, M., Engler, C., Voigtl¨ander, J., Tuch, T., Wiedensohler, A. (2006). Atmospheric number size distributions of soot particles and estimation of emission factors, Atmospheric Chemistry and Physics, 6: 1021–1031.

Rosen, J. M., Pinnick, R. G., Hall, R. (1974). Recent Measurements of Condensation Nuclei in the Stratosphere, Proceedings 3rd Conference Climatic Impact Assessment Program DOT-TCSOST-74-15, Department of Transportation, Washington, D.C.

Sakurai, H., Tobias,*H.J,* Park,*K.,* Zarling, D., Docherty, *D.B.,* Kittelson, *S.*, McMurry, *P.H.,* Ziemann, P.J. (2003). On-line measurements of diesel nanoparticle composition and volatility, Atmospheric Environment, 37*:* 1199–1210.

Seinfeld J. H. and Pandis, S.N., 2006. Atmospheric Chemistry and Physics: From Air Pollution to Climate Change, Wiley.

Stolzenburg, M. R., McMurry, P. H. (1991). An Ultrafine Aerosol Condensation Nucleus Counter. Aerosol Science and Technology, 14: 48–65.

Schauer, J. J., Kleeman, M. J., Cass, G.R., Simoneit, B.E.T. (1999). Measurement of Emissions from Air Pollution Sources. 2. C1 through C30 Organic Compounds from Medium Diesel Trucks. Environmental Science and Technology, 33(10): 1578-1587.

Schwarz, J. P., Gao, R. S., Fahey, D. W., Thomson, D. S., Watts, L. A., Wilson, J. C., Reeves, J. M., Darbeheshti, M., Baumgardner, D. G., Kok, G. L., Chung, S. H., Schulz, M.; Hendricks, J., Lauer, A., Kärcher, B., Slowik, J. G., Rosenlof, K. H., Thompson, T. L., Langford, A. O., Loewenstein, M., Aikin, K. C. (2006). Single-particle measurements of midlatitude black carbon and light-scattering aerosols from the boundary layer to the lower stratosphere. Journal of Geophysical Research, 111, D16207.

Snider J.R., Wex, H., Rose, D., Kristensson, A., Stratmann, F., Hennig, T., Henning, S., Kiselev, A., Bilde, M., Burkhart, M., Dusek, U., Frank, G.P., Kiendler-Scharr, A., Mentel, T. F., Petters, M.D., and Põschl, U. 2010. Intercomparison of Cloud Condensation Nuclei and Hygroscopic Fraction Measurements: Coated Soot Particle Investigated During the LACIS Experiment in November(LExNo), Journal of Geophysical Research, 115, D11205.

Tobias, H.J., Beving, D.E., Ziemann, P.J., Sakurai, H., Zuk, M., McMurry, P.H., Zarling, D., Waytulonis, R., Kittelson, D.B. (2001). Chemical Analysis of Diesel Engine Nanoparticles using a Nano-DMA/thermal Desorption Particle Beam Mass Spectrometer. Environmental Science and Technology, 35

Turpin, B. J., and Lim, H. J. (2001). Species Contributions to PM2.5 Mass Concentrations: Revisiting Common Assumptions for Estimating Organic Mass, Aerosol Science Technology, 35: 602–610

Venkatachari, P., Zhou, L., Hopke, P.K., Schwab, J.J., Demerjian, K.L., Weimer, S., Hogrefe, O., Felton, D., Rattigan, O. (2006). An Intercomparison of Measurement Methods for Carbonaceous Aerosol in the Ambient Air in New York City, Aerosol Science and Technology, 40: 788-795.

Wang, S. C., Flagan, R. C. (1990). Scanning Electrical Mobility Spectrometer. Aerosol Science and Technology, 13: 230–240.

Zhang, R. Y., Khalizov, A. F., Pagels, J., Zhang, D., Xue, H., McMurry, P. H. (2008). Variability in morphology, hygroscopicity, and optical properties of soot aerosols during atmospheric processing, Proceeding of the National Academy of Sciences, 105: 10291–10296.

Chapter 3: Components of Particle Emissions from Light- Duty Spark-Ignition Vehicles with Varying Aromatic Content and Octane Rating in Gasoline

3.1. Introduction

Gasoline manufactured in the U.S. contains several components (e.g., oxygenates and aromatic compounds) that are used to modify gasoline octane rating. An example component, Tetraethyl lead (TEL), was used to increase the octane rating of the fuel, thus allowing for better combustion within the engine (Nadim et al. 2001). However, TEL proved to be detrimental to air quality and was banned from all consumer fuels (Nadim et al. 2001). Other additives were found to replace TEL and provide the octane rating needed for gasoline (Nadim et al. 2001). These additives include oxygenates, such as ethanol, and aromatic hydrocarbons (Nadim et al. 2001; Silva et al. 2005; Perry et al. 1995). Regulations of these additives in the U.S. are enforced by state and federal governments. For example, the California Air Resources Board (CARB) limits the amount of aromatic hydrocarbons to be 35% by volume in gasoline (CARB 2010) . The federal baseline of aromatic hydrocarbons for conventional gasoline in the U.S. is ~29% for summer and winter blends (Weaver et al. 2010). Gasoline blends of 10% ethanol are found in most gas stations across the United States (RFS 2007). However, due to the increased ethanol concentration in fuels over the last decade, the amount of aromatics in fuels has decreased to not exceed the minimum octane rating (EPA 2013). If this trend continues, aromatic concentrations could be considerably lower if E15 fuels become the standard in the U.S.

The most common light-duty vehicle (LDV) engine in production is the Port-Fuel Injection (PFI) engine (Zhao et al. 1999). PFI technology mixes air and gasoline before entering the combustion chamber. Hybrid vehicles use a variation of PFI engine technology and an electric motor. Both engines alternate as the primary running engine to decrease fuel usage and increase the rate of energy storage in the form of lithium ion batteries. Gasoline direct injection (GDI) engines have increased in manufacturing and are predicted to dominate the U.S. market in the future (Zhao et al. 1999; Graham 2005). GDI technology injects gasoline and air in the combustion chamber separately (Zhao et al. 1999). Previous studies have concluded GDI engines increase PM emissions compared to PFI engine on E10 blended gasoline (Liang et al. 2013).

Vehicular particle emissions can cause adverse health effects. PM composition, such as water-soluble, can pose a health risk to humans (Ramagolam et al. 2009; Gutierrez-Castillo et al. 2006; Valavandidis et al. 2008; Squires 1958 and references therein). Water-soluble PM has been linked to pulmonary and cardiovascular diseases, and long- term exposure is shown to cause human DNA damage (Ramagolam et al. 2009l Gutierrez-Castillo et al. 2006). Water-soluble and water-insoluble organic materials and metals have been linked with the cellular production of reactive oxygenated species (ROS) (Geller et al. 2006; Verma et al. 2010; Biswas et al. 2009). Furthermore, hygroscopic particles can grow to droplet sizes when inhaled and enhance PM deposition rates (Longest et al. 2010).

To our knowledge, there is a lack of research for particle composition and number emissions from combustion with varying aromatic concentration and octane rating. A

companion paper to this report will be published with criteria pollutant and air toxic emissions associated with this study. The primary focus of this work is to determine particle hygroscopicity and composition effects from current light duty vehicle (LDV) inventory and possible fuel blends. In particular, the effect of decreased oxygenated and aromatic components in the combustion of alternative fuels of advanced vehicle technologies and their subsequent impact for particulate matter (PM) emitted from vehicles will also be explored. The study will discuss changes in these emissions from fuels, differences in engine technologies, and operating conditions. PM mass and PN are noted to be much larger for the GDI vehicles compared to the PFI vehicles, as is shown in the Supplemental Materials. Data presented show vehicle speed effects on BC emissions rates and water-insoluble particle composition from varying aromatic fuels and octane rating. Fuel properties and vehicle technology can impact emissions. This will work will also show that vehicle speed also plays an important role in the particle composition emissions.

3.2. Experimental Methods

3.2.1. Testing Procedure

Vehicles were tested at the Vehicle Emissions Research Laboratory (VERL) located at the College of Engineeing- Center for Environmental Research and Tehcnology (CE-CERT). VERL is equipped with a Burke E. Porter light-duty chassis dynamometer and a constant volume sampler (CVS) that creates uniform dilution of the

emissions from the tailpipe for each vehicle. Vehicles were tested over 3 California Unified Cycles (UC). Additional information about the transient cycle procedure can be found in the Appendix B.1. After the cycle, the vehicles were driven at three steady-state speeds (70, 50, and 30 MPH).

3.2.2. Test Vehicles and Fuels

Seven vehicles were tested, which include five passenger cars and two light duty trucks. The vehicle engine configurations include 5 wall-guided GDI technology vehicles, one hybrid vehicle with a PFI configuration, and one conventional PFI vehicle. The vehicle test matrix includes 5 passenger cars: 2012 Chevrolet Impala, 2012 Mazda 3, 2012 Kia Optima, 2012 Honda Civic Hybrid, and a 2012 Nissan Altima. The majority of these vehicles were GDI technology except the Nissan Altima, which was a conventional PFI, and a Honda Civic Hybrid, which was a hybrid vehicle with a PFI configuration. In addition, two light-duty trucks were also tested, a 2012 Ford-F150 and a 2012 GMC Terrain. Both light-duty trucks had GDI technologies. All vehicles were certified to meet the Federal Tier 2, Bin 2 exhaust emission standards or the California LEV-II, SULEV exhaust emissions standards. The vehicles were Tier-3 like, which Tier-3 regulations have yet to be implemented. The Ford F-150 was equipped with a 3.5L V-6 Ecoboost engine. The Ford F-150 was certified to meet the Tier 2 Bin 4 emission certification.

Four fuels with varying aromatic content were used in this study. All fuels were blended with nominal aromatic content of 15%, 25%, and 35% by volume. In addition,

the fourth fuel has higher octane number but the same aromatic content as the third fuel (35% Aromatics by volume). These aromatic fuels were blended to be within 0.5 vol% of the specific aromatic target. Sulfur content was maintained at appromimately 27ppm. All fuels are blended with ~10 vol% ethanol (E10). The lubrication oil used was 5W-20 and non-synthetic. Additional fuel properties are listed in Appendix Table B-1.

3.2.3. Online Particle Water-Insolubility

For the experiment setup, a water-condensation particle counter (W-CPC) (TSI Model 3785) and butanol- CPC (B-CPC) (TSI Model 3772) were used with an electrostatic classifier (TSI Model 3080). Scanning mobility particle sizer (SMPS) is used to determine the size and number of particles (Wang et al. 1990). The characterization of the size distribution is important, as heterogeneous particle nucleation is a function of particle size. The electrostatic classifier selects a particle diameter between 10 to 289 nm. The dry particles then exit the classifier and the stream is split into both the B-CPC and the W-CPC. A particle scan from 10 to 280 nm takes approximately 135 seconds, thus about 17 scans were completed during a UC. Significant differences between these instruments were shown for particles below 40 nm (Short et al. 2014). The difference is due to the particle hygroscopicity properties or κ. As the surface area of the particle decreases, the particles solubility properties have an increasing effect on the probability of droplet activation (Short et al. 2014).

Appendix Fig. B-3 shows the real-time plot of the ratio of water to butanol particle counts for a given SMPS scan. The plot shows a sigmoidal distribution from 0 to

1. When the distribution reaches a ratio of 0.5 then 50% of the total particle, for any particular diameter, are forming droplets within the W-CPC. The diameter of the particles that reach this 50% threshold is known as the critical diameter or d_s. This operates under the assumption that the B-CPC provides total particle number. The diameter, d_s, that corresponds to this 0.5 ratio is used to calculate the Water-Insoluble Mass (WIM) fraction. The WIM fraction is the total fraction of particles that exhibit water-insoluble properties of particles with diameters below 40nm. The method is calibrated with aerosolized ammonium sulfate. The d_s for ammonium sulfate was 20.5 nm at the W-CPC instrument critical supersaturation and is consistent with predicted results published in (Petters and Kreidenweis 2007). To find an cumulative overall WIM fraction over a driving cycle, the total W-CPC to B-CPC ratio was found. The ratio was calculated by the sum of each total particle number for every particle diameter selected by the electrostatic classifier. A plot of the ratio was used to determine an overall d_s for that particular vehicle and fuel. Appendix B.2 and Short et al (2014) gives a more detailed description of the method to determine the WIM fraction from d_s.

3.2.4. Water-Soluble Organic Mass Fraction and Surface Tension Measurement

Teflon filter samples were taken during each UC test. Hence, the WSOC and surface tension measurements are representative of the cumulative aerosol composition. Each filters was placed in a vial and sonicated for 90 minutes with Millipore © DI water (18mΩ, < 100ppb). Once sonicated, large non-dissolved particles were removed using a

Whatman© 25mm syringe filter. The sample was then diluted into ratios of 1:1, 1:3, and 1:5. Each vial contains 30mL of sample. The surface tension, σ_b, for each samples was measured with a pendant drop tensiometer (Attension Theta 200). The tensiometer is an optical unit that uses the Young-Laplace equation to compute the droplet surface tension. 100 images were captured for each droplet. The water-soluble organic carbon (WSOC) concentrations of these samples were measured using a GE Seivers 900 Total Organic Carbon (TOC) analyzer. The instrument takes two measurements per sample of total dissolved organic carbon and inorganic carbon. The total dissolved organic carbon concentration, in ppm or mg/L, was then multiplied by the amount of water added (60 mL). The WSOC concentration was then multiplied by the ratio of the average organic molecular weight per carbon weight, 1.2, to account for all water-soluble organic noncarbonaceous components (Turpin and Lim 2001). This term is defined as the Water Soluble Organic Mass (WSOM). The WSOM mass was divided by the total mass of PM on the filter to determine the water-soluble organic mass fraction.

3.2.5. Online Black Carbon Measurement

A Multi-Angle Absorption Photometer (MAAP) (Thermo Scientific Model 5012) measures BC concentrations. The MAAP applies a light source at ~670 nm on a flat layer of aerosol accumulated on Teflocarbon filter paper. Four optical detectors, above the filter paper, then determine the backscattering of light from the aerosol. The scattering is correlated with the concentration of black carbon. Calibration of the instrument can be done using 2 different procedures. The thermometer, pressure sensor, and sample flow rate are calibrated first. The calibration is also verified by aerosolizing Aquadag© BC

solution and simultaneous measuring the solution with an aerosol particle mass (APM, Kanomax Model 3600) Analyzer and the MAAP (Schwarz et al. 2006). Both methods were used in this study. The calibrations used in this test resulted within ± 12% agreement with the APM measurements.

3.3. Results and Discussion

3.3.1. Water-Soluble Organic Mass

This section discusses the WSOM results from the method described in Section 2.4. Results are shown for six vehicles (except the Nissan Altima) and all four fuels over the UC in Fig. 3-1a. In general, there were consistent fuel trends of increasing WSOM emission factors with increasing aromatics for most vehicles with an average WSOM emission factor (EF) of 1.34 mg mi^{-1}. The GMC Terrain showed the highest WSOM EF value from all 6 vehicles, which was 4.97 mg mi^{-1} for the 15% aromatic fuel. The WSOM EF for the Honda Civic Hybrid increased by 37% from 0.29 mg mi^{-1} to 0.39 mg mi^{-1} for the 15% aromatic fuel compared to the 35% aromatic fuel. The Kia Optima showed a 46% increase in the WSOM emission factor from 1.19 mg mi^{-1} for the 15% aromatic fuel to 1.73 mg mi^{-1} for the 35% aromatic fuel. The Ford F-150 had a WSOM EF increase of 42% from the 15% aromatic fuel to the 35% aromatic fuel. All three of these vehicles did not show a change in the WSOM EFs with an increase in the fuel octane rating. The Chevrolet Impala showed a 123% increase in the WSOM emission factor from the 15% to the 35% aromatic fuel. The increased octane rating fuel decreased the WSOM emission factor 47% to 1.1 mg mi^{-1} for the Chevrolet Impala. For the Mazda 3, the

WSOM emission factor did not show an effect from the different aromatic contents or octane ratings with an average WSOM EF of 0.91 mg mi^{-1}.

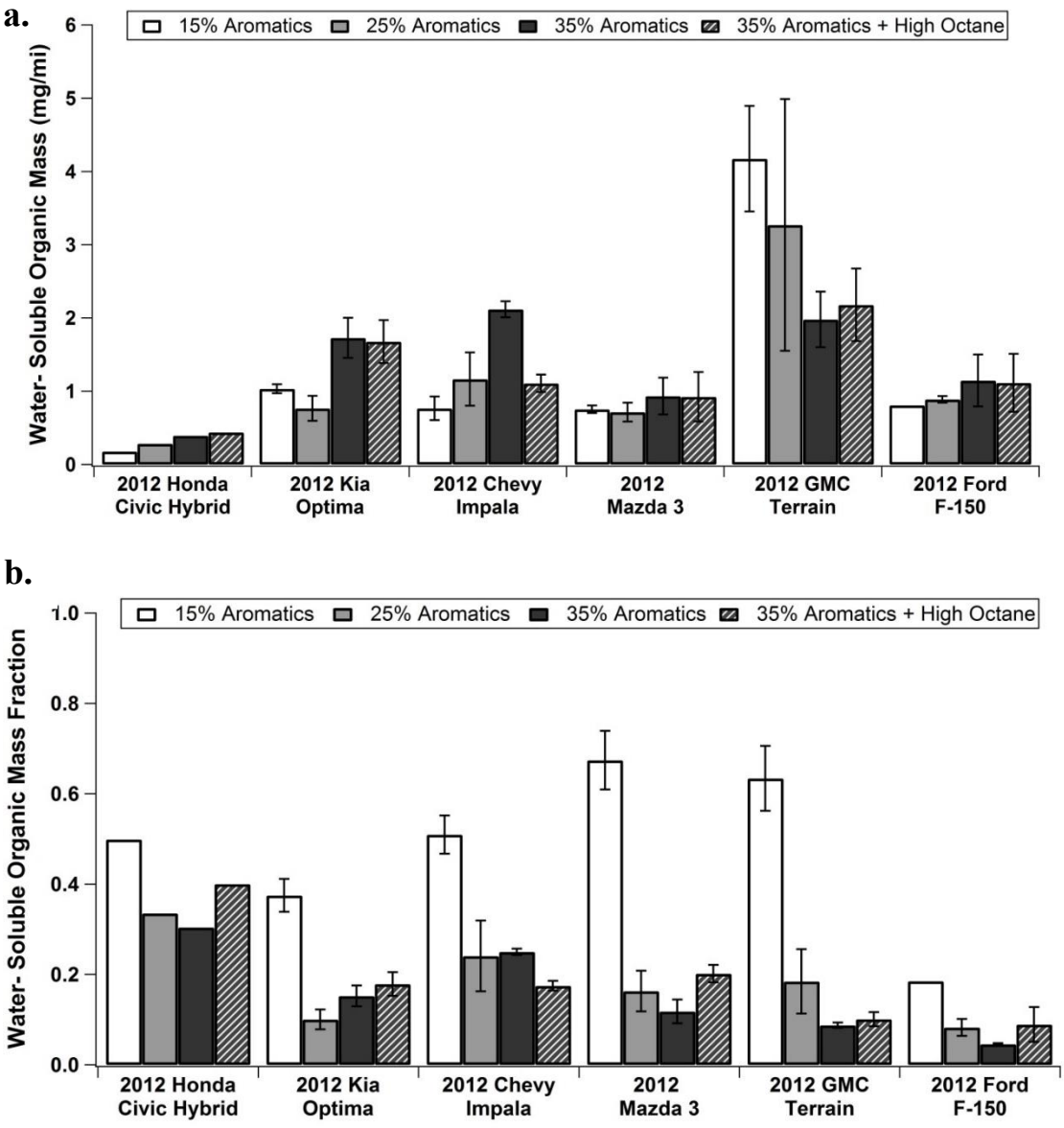

Fig. 3- 1. The WSOM Emission Factor (a.) and the WSOM/PM mass Fraction (b.) over the UC cycle for six vehicles tested.

In Fig. 1b, the WSOM/PM mass fractions are shown for the six vehicles tested over the UC cycle. The 15% aromatic fuel has a consistently larger WSOM/PM mass fraction compared to the other fuels tested, ranging from 0.2 to 0.65. The other fuels range from 0.05 to 0.4 for the 15% aromatic fuel. The majority of the PM emissions are WSOM for the Chevrolet Impala, Mazda 3 and the GMC Terrain. The Ford F-150 shows the lowest WSOM/PM mass fractions of all the vehicles. The Honda Civic Hybrid has a large fraction of WSOM for all fuels. The highest aromatic content fuels and the high octane rating fuel showed WSOM (~0.15) emission factors similar to those reported in a previous study for a PFI vehicle (Chueng et al. 2009).

3.3.2. Paraffin and Isoparaffin compound effects on WSOM/PM mass emissions

The WSOM/PM Mass emissions were above 0.4 wt% for the 15% Aromatic fuel and very low for the other fuels. This trend was correlated with several fuel compounds and a correlation was found between WSOM/PM Mass fraction and the wt% of Iso-paraffins and the dominate iso-parrafin compound (2,2,4 trimethylpentane or iso-octane), Table 1. The sum of the Iso-paraffins and C8 iso-paraffins and iso-octane had the largest amounts in the 15% aromatic fuel and dropped 50% for the 25% aromatic fuel. WSOC/PM mass also showed a 50% decrease in the fraction between the 15% and 25% aromatic fuels. The iso-paraffin amounts and WSOM/PM Mass fractions for the other three fuels were relatively low and remained low (<10%wt and <0.2).

	Total Paraffins (wt%)	Total Isoparaffins (wt%)	C8 Isoparaffins (wt%)	2,2,4-Trimethylpentane (wt%)	Honda Civic Hybrid (WSOM/PM)	Kia Optima (WSOM/PM)	Chevrolet Impala (WSOM/PM)	Mazda 3 (WSOM/PM)	GMC Terrain (WSOM/PM)	Ford F150 (WSOM/PM)
15% Aromatics	9.21	40.69	20.54	13.70	0.498	0.375	0.509	0.674	0.634	0.185
25% Aromatics	12.93	26.39	10.87	6.55	0.335	0.100	0.241	0.163	0.184	0.083
35% Aromatics	13.17	20.2	3.62	2.49	0.304	0.152	0.250	0.118	0.087	0.046
35% Aromatics with High Octane	12.08	23.87	10.9	9.31	0.4	0.178	0.175	0.202	0.101	0.089

Table 3- 1. Paraffin and Isoparaffin compounds in all fuels with WSOC/PM Mass fraction emissions for six vehicles tested

Studies have shown that the oxidation of paraffins is possible with a TWC (Yung Fang 1980; Canvani and Trifiro 1999). In addition, Yung-Fang et al. (1980) showed that a increased number of carbon chains also increase oxidation rates at high temperatures (200-500^{o}C). In addition, Curran et al. (2002) proposed mechanisms of iso-octane oxidation from which other carbon chain free radicals may form. Thus, the TWC could be potentially oxidizing these particular isoparaffins, making the particles more soluble. The spectated organic composition is unavailable. However, it is possible that the oxidation of C8 iso-paraffins would cause an increase in WSOM when an increased C8 iso-paraffin concentration exists in the fuel.

Potential effects on human health from the inhalation of WSOM can be caused by an increase in paraffin and iso-paraffin concentrations. The results have shown that a 50% increase in paraffin and iso-paraffin concentrations increased the amount of WSOM

emitted by as much as 50%. This could have a potentially more significant impact on human health from vehicular emissions. In addition, communities near roadways with large concentrations of vehicular traffic could be especially vulnerable from these increased emissions. Increases in hygroscopic and WSOM emissions can have an impact on Cloud Condensation Nuclei (CCN) activity (Ervens et al. 2005; Ekman et al. 2007). Increases in CCN will impact climate by reflecting sunlight back into space, thus causing a cooling effect on the earth's surface (Pierce and Adams 2009). More effectively quantifying vehicle EFs of WSOM and other water-soluble material could be crucial to obtaining a better radiative budget.

3.3.3. Water- Insoluble Mass Fraction by Phase

Fig. 3-2 shows the results of the WIM faction for each individual phase of the UC. Collectively, the results suggest that particle emissions during phase 2 dictate the water-insolubility of the particles overall. Phase 2 is more transient in nature with higher average vehicle speed and load than cold-start and hot-start phases. The WIM fraction changes with respect to vehicle speed. In Fig. 3-2c, the Kia Optima results are shown. The results from the Kia Optima show a more significant decrease in the WIM fraction between phases 1 and 2. Phase 1 and 3 PM emissions were largely water-insoluble, but phase 2 particle emissions were more soluble particle emissions. The WIM fraction for the 15% aromatic fuel decreased by 94% from phase 1 to phase 2, ranging from 0.05 to 0.9. Fig. 3-2a shows the results from the Chevrolet Impala and Fig. 3-2b shows the results from the Nissan Altima. These vehicles were selected because their water-insoluble particle emissions were similar to and representative of other vehicles in the

fleet. For example, the Nissan Altima had similar water-insoluble particle emissions compared to the Honda Civic Hybrid and the Chevrolet Impala had water-insoluble particle emissions similar to those for the Mazda 3 and Ford F-150. In Fig. 3-2a for the Chevrolet Impala, the WIM fraction for the 25% aromatic fuel decreased by 20% between phases 1 and 2. For the same fuel, the WIM fraction decreased by 35% for the Nissan Altima (Fig. 3-2b), ranging from 0.59 to 0.91. The results from these two graphs show that phase 1 and 3 have higher WIM fractions compared to Phase 2. The results for the GMC Terrain, Mazda 3, Honda Civic Hybrid, and Ford F-150 are shown in Appendix Fig. B-4.

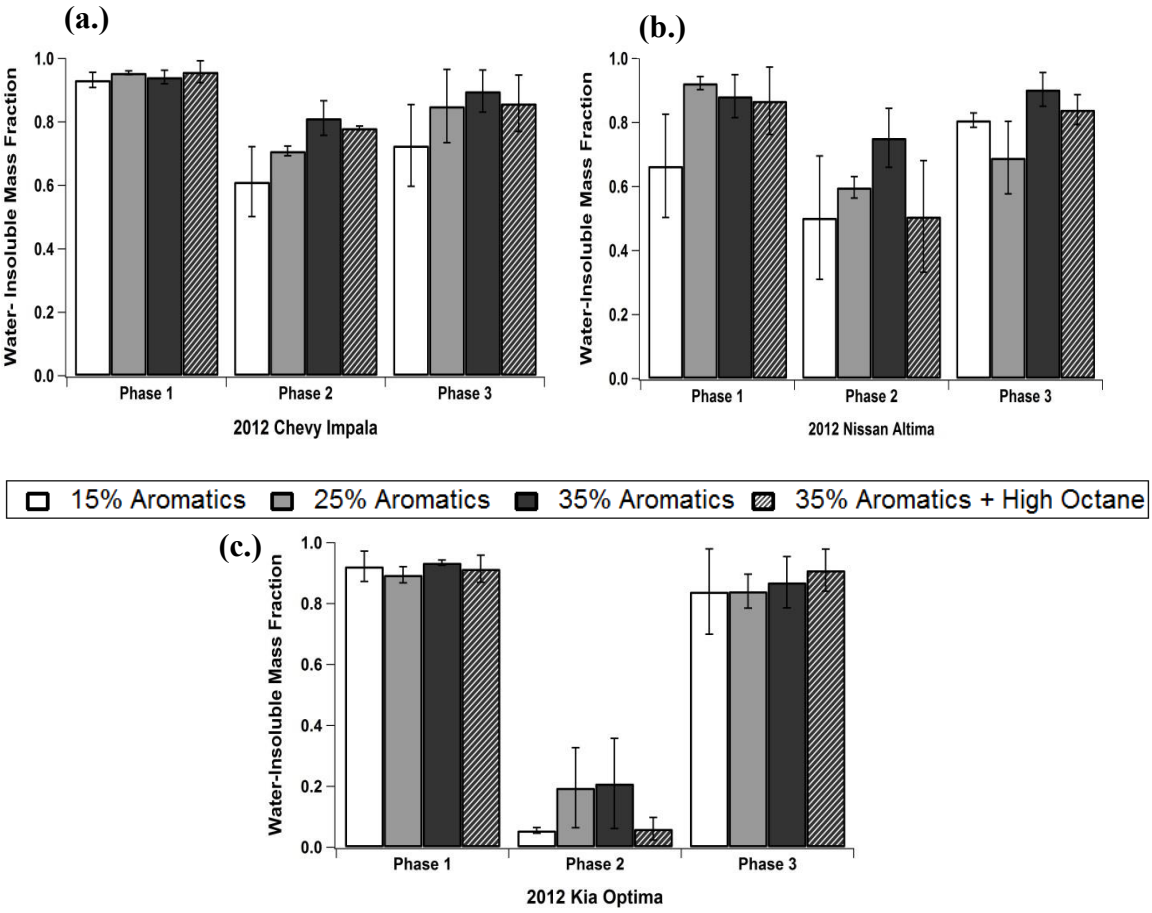

Fig. 3- 2 Water-insoluble mass faction by Phase for the Chevy Impala (a.), Nissan Altima (b.), and the Kia Optima (c.) computed over the entire UC cycle

3.3.4. Cumulative Water-Insoluble Mass Fraction

As shown in Fig. 3-3, the majority of the cumulative emissions for the vehicles were water-insoluble. The Honda Civic Hybrid, Nissan Altima, Chevy Impala, and Mazda 3 do not show any particular fuel trends, with WIM fractions ~0.9. The Kia Optima, GMC Terrain, and Ford F-150 show increasing WIM fractions with increasing aromatic content. The WIM fractions for the Kia Optima increased by 23% between the 25% and 35% aromatic fuels, ranging from 0.59 to 0.76. In addition, the Kia Optima showed that the highest octane rating fuel produced the lowest WIM fraction (0.54) of all

four fuels. The other two vehicles showed an increase between the 15% and 35% aromatic content fuel of 189% for the GMC Terrain and 17% for the Ford F150. For the GMC Terrain, the higher octane rating fuel showed an equivalent WIM fraction with the 25% aromatic content fuel (WIM fraction of 0.51). The Ford F150 showed a 6% decrease in the WIM fraction from the 35% aromatic fuel to the high octane rating fuel.

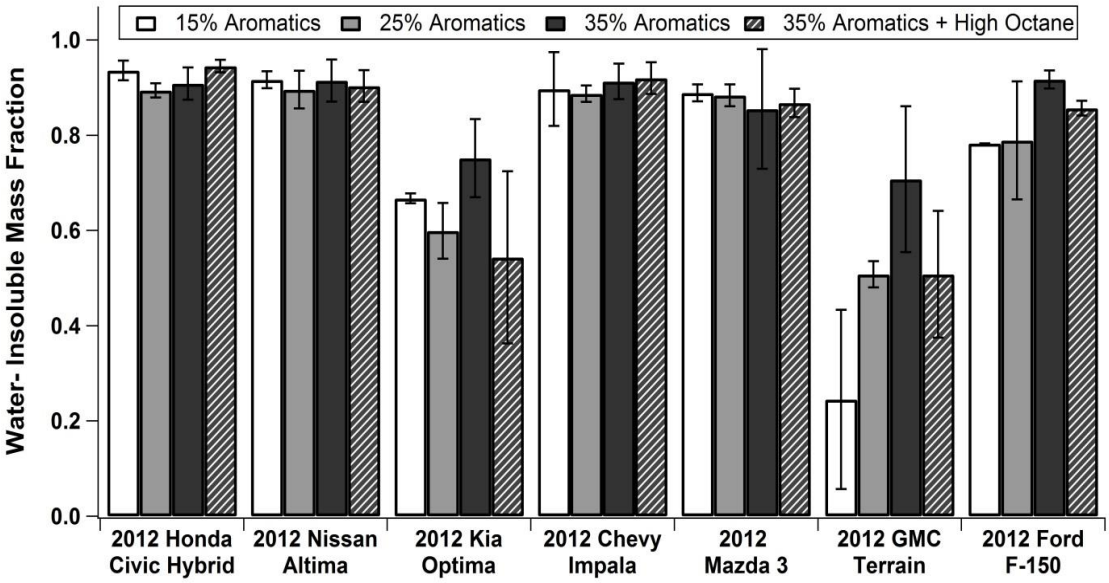

Fig. 3- 3 Water-insoluble mass faction calculated over the UC cycle

3.3.5. Particle Hygroscopicity and BC Concentration during Vehicle Steady-State Speeds

The vehicles were driven at 3 different steady-state speeds of 70, 50, 30 mph. To better understand particle water-insolubility during steady-state speeds the hygroscopicity term, κ, is reported. Particle hygroscopcity was determined through Equation 3 in in Appendix B.2. As stated in the experimental section, as κ approaches 1, the particles are

less water-insoluble; as κ approaches 0, particles are more water-insoluble. The results for the particle hygroscopicity values and BC concentrations for each steady-state condition are shown in Fig. 3-4 for the Chevy Impala, Nissan Altima, and Kia Optima. These vehicles were chosen because of the similar WIM fraction results described in Cumulative Water-Insoluble Mass Fraction section. The other vehicle steady-state results are shown in Fig. B-5. Some fuels during the 70 mph steady-state speed had κ values higher than 1, showing the particles were highly hygroscopic. A common vehicular emission component, sulfuric acid, has a κ value of 0.9, which means that other highly hygroscopic components could be present in the emissions. Although the specific highly hygroscopic component cannot be determined in this study due to the limitations of the instruments used. The majority of particle emissions at 70 mph tend to be less hydrophobic and water-insoluble than sulfuric acid.

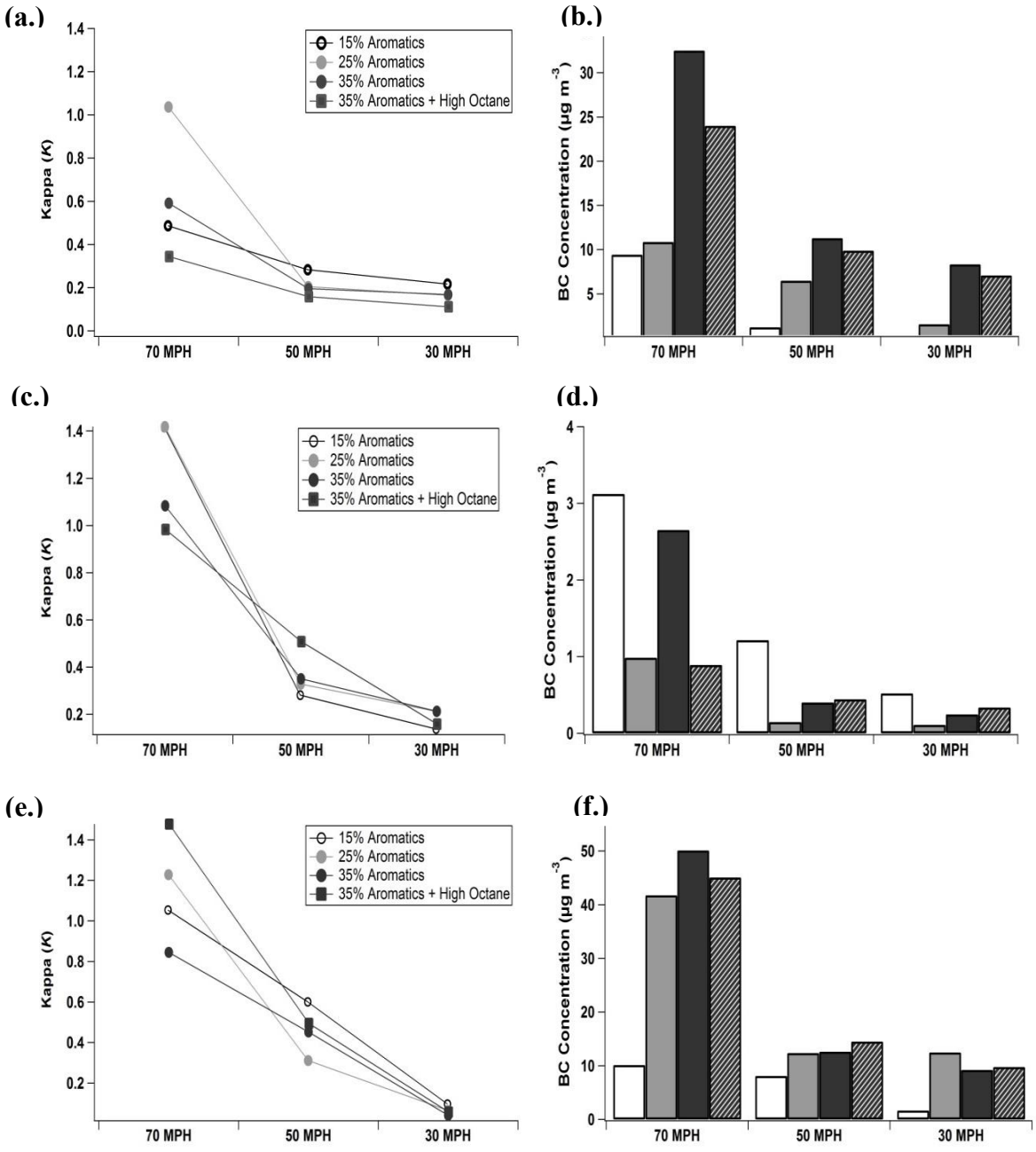

Fig. 3- 4 κ values for the Chevy Impala (a.), Nissan Altima (c.), and Kia Optima (e.) and BC concentration for the Chevy Impala (b.), Nissan Altima (d.), and the Kia Optima (f.) for steady-state vehicle speeds of 70, 50, 30 MPH

The κ values for the Chevrolet Impala, Nissan Altima, and Kia Optima, over the steady-state cycles are shown in Fig. 3-4a, 3-4c, and 3-4e, respectively. All vehicles show decreasing particle hygroscopicity with decreasing vehicle speed. For the Chevrolet Impala, the largest κ value was 1.05 for the 70 mph speed. The Nissan Altima showed the largest hygroscopicity reduction between the 70 and 50 mph speeds of 73% and the largest κ value for the 70 mph speed of 1.41. The Kia Optima showed some of the highest κ decreases of all the vehicles in this study with a 91% decrease in the κ values from the 70 to 30 mph speeds for the 35% aromatic fuel with the high octane rating. In addition, the Kia Optima showed a different effect from that of the mph other vehicles, with large decreases in particle hygroscopicity between the 50 to 30 MPH speeds.

BC concentrations are shown in Fig. 3-4b, 3-4d, and 3-4f. The majority of the trends for all three vehicles show that BC concentration decreases with vehicle speed. This trend was also consistent with particle hygroscopicity. The Chevrolet Impala BC concentration from 70 to 30 mph decreases from 9.445 to 0.340 $\mu g\ m^{-3}$. In addition, BC fuel trends shown during the UC were also seen for the Chevrolet Impala BC concentrations during steady state speeds. The BC steady-state fuel trends were not similar to the BC EFs over the UC for the Nissan Altima, which increasing aromatic concentration did not increase the BC concentrations over the steady-state speeds. The BC steady-state concentrations for the Kia Optima followed a relatively similar pattern to those for the UC, where increasing aromatics increased BC emissions.

High vehicle speeds were shown to cause increases in particle hygroscopicity and lower particle water-insolubility. Phase 2 of the UC cycle contains higher vehicle speeds and accelerations than the other 2 phases in the cycle. Fig. 3-2 shows that the Kia Optima and GMC Terrain emit lower WIM fractions during phase 2 of the UC because of the higher vehicle speeds. In addition, the cumulative overall WIM, Fig. 3-3, are low for the Kia Optima and GMC Terrain compared to the other GDI vehicles. In addition, steady state vehicle conditions, Fig. 3-4, showed that higher vehicle speeds produce more hygroscopic particles ($\kappa > 1$) compared to lower vehicle speeds ($\kappa < 0.1$). Thus, vehicle speed directly effects particle hygroscopcity. The cumulative WIM fractions reflect emissions at lower vehicle speeds in phase 1 rather than phase 2 because the majority of particle emissions were emitted.

3.3.5. BC Emission Rate

It is assumed that all BC emissions from these vehicles is water-insoluble. The BC emissions were compared to the WIM fractions by dividing the BC EFs by the total PM mass, shown in the next section. This will be used to determine the BC contribution to the cumulative WIM fraction. Fig. 3-5a shows the BC EFs for all seven vehicles driven over the UC. Increasing aromatic content increases BC EFs. Increased octane rating in fuel reduces the BC EFs for the GDI vehicles. In addition, the GDI vehicles emit more BC and exhibit larger differences in BC with increasing aromatic content compared to the PFI vehicles. The BC EFs for the GDI vehicles ranged from 255 $\mu g\ mi^{-1}$ to 2385 $\mu g\ mi^{-1}$. BC emissions for the Kia Optima increased by 190%, the Chevrolet Impala increased by 138%, Mazda 3 increased by 356%, the GMC Terrain increased by 334%, and the Ford

F150 increased by 155% from the 15% to 35% aromatic fuels. The GMC Terrain had the largest range of BC EFs between the 15% and 35% aromatic fuels, from 549.7 μg mi^{-1} to 2385.4 μg mi^{-1}, respectively. The Honda Civic Hybrid showed a BC EF increase of 107%, ranging from 136 μg mi^{-1} to 282 μg mi^{-1}, between the 15% to 35% aromatic fuels. BC EF for the Nissan Altima increased by 175%, ranging from 83 μg mi^{-1} to 228 μg mi^{-1}, between the 15% to 35% aromatic content fuel.

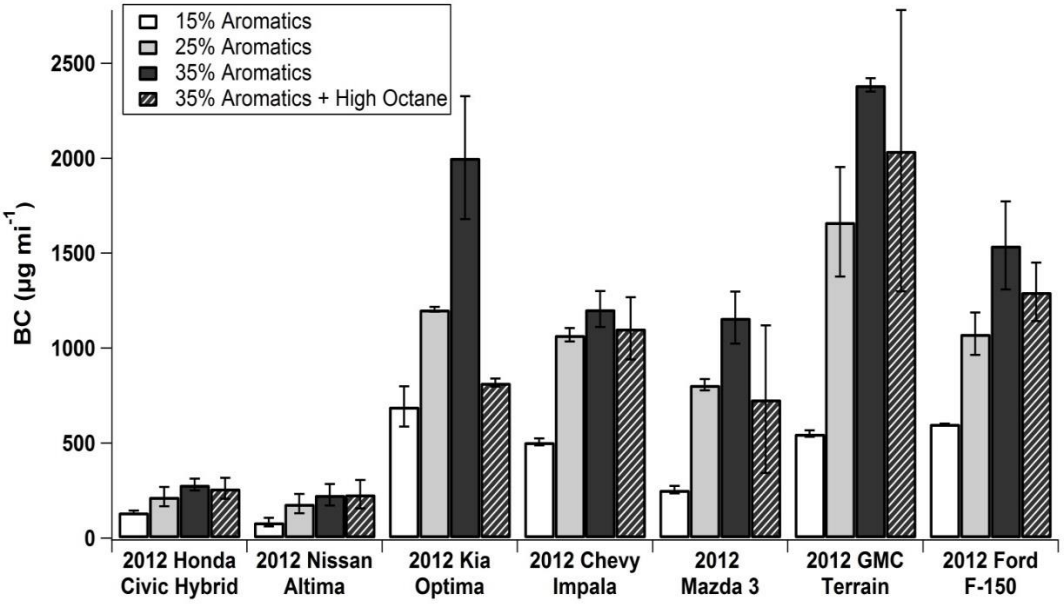

b.

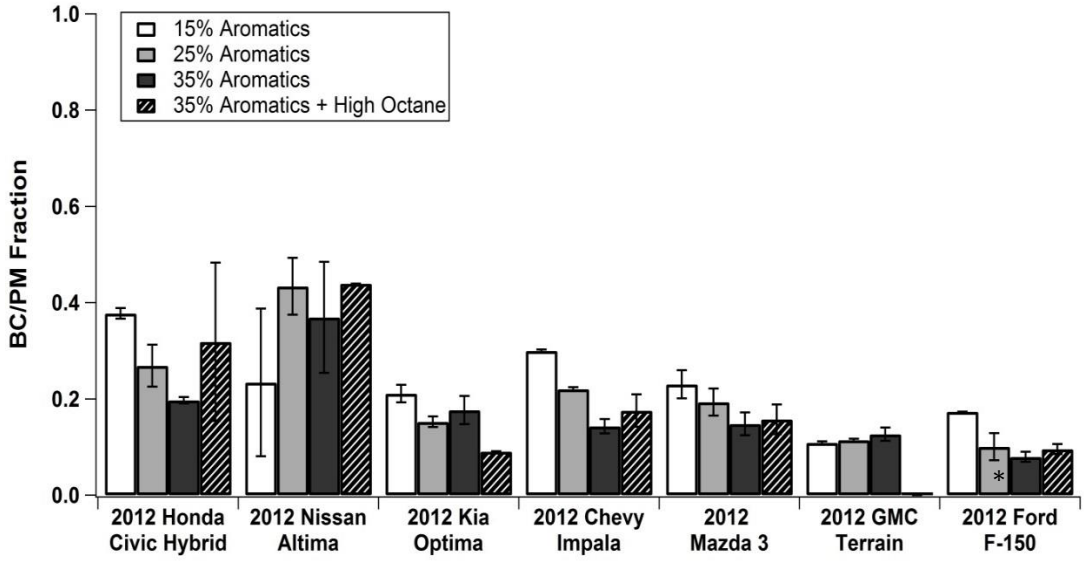

Fig. 3- 5 The BC Emission Factor (a.) and BC/PM Mass Fraction (b.) for all seven vehicles and all fuels driven on the Unified Cycle (*Unavailable data values)

Increased octane rating in fuel reduces the BC EFs for the GDI vehicles. There was no effect from the increase in octane rating for the Nissan Altima or Honda Civic Hybrid with a BC EF of 230.19 μg m^{-3} and 260.7 μg mi^{-1}, respectively. The increase in octane rating at the 35% aromatic composition had a varying, but definitive, effect for the 5 GDI vehicles. With the 35% aromatic with high octane fuel, the Kia Optima has a BC emission factor of 817.7 μg mi^{-1}, similar to the 15% aromatic content BC concentration. The higher octane number fuel was similar to the 25% and 35% aromatic content fuel for the Chevrolet Impala vehicle at 1103.1 μg mi^{-1}. The Mazda 3 had a BC EF, of 730 μg mi^{-1}, also similar to the 25% aromatic and 35% aromatic BC EF. The BC emissions factor for the 35% aromatic fuel with high octane was 2038.5 μg m^{-3} for the GMC Terrain and

1295.6 μg mi^{-1} for the Ford F-150. These values were both similar to the 25% and 35% aromatic content BC emissions for their respective vehicles.

3.3.6. BC/PM Mass Fraction

The fraction of BC to PM mass is shown in Fig. 3-5b for all seven vehicles. PM Mass emission factors are shown in Appendix Fig. B-6. It should be noted that due to a lack of PM mass measurements for the GMC Terrain on the 35% aromatic with high octane number fuel there are not any BC to PM mass fractions reported. The fractions were averaged for each trial where both PM and BC emission factors were available. The Honda Civic Hybrid and Nissan Altima vehicles showed larger BC and PM fractions compared to the GDI vehicles. The impact of increasing aromatic content and octane rating was less consistent for the BC to PM fraction than with the BC emission rate. The BC to PM ratios for the Honda Civic Hybrid, Chevrolet Impala, Mazda 3, and the Ford F-150 vehicles decreased with increasing aromatic content from 15% to 35%. Interestingly, the Honda Civic Hybrid was the only vehicle of this set which was not a GDI vehicle. The Ford F-150 had the largest BC to PM mass fraction decrease, of about 54% between the 15% and 35% aromatic fuels, which was similar to the decrease for the Chevy Impala (53%) and the Honda Civic Hybrid (48%) vehicles, with the Mazda 3 vehicle having the smallest decrease of about 36%. The Nissan Altima, Kia Optima, and GMC Terrain vehicles had statistically similar BC and PM fractions with increasing aromatic content in gasoline. The higher octane rating fuel had similar BC to PM mass fractions to the 35% aromatic content with lower octane rating fuel for the Honda Civic Hybrid, Nissan Altima, Chevy Impala, Mazda 3, and Ford F-150, which were 0.32, 0.44, 0.18, 0.16, and

0.10, respectively. The Kia Optima vehicle showed a significant decrease of 49% in the BC to PM mass fraction for the higher octane number fuel. Overall, the ratios of BC to PM mass were considerably low compared to the overall WIM fractions shown in Fig. 3. Over half of all PM emissions are composed of material other than the measured BC in this study. This study is the first to determine the BC EFs, over the UC, from the optical techniques implemented with the MAAP. Other studies have shown measurements of BC using a photoacoustic technique, where the BC contribution to the total PM mass is much larger (~80%) [34-36]. However, this studies BC measurements contribute additional information into the complex properties and measurement of BC.

Large increases in BC emissions could have a profound effect on climate patterns if aromatic level fuels were to become more heavily produced. However, increased octane rating in fuels has the potential to reduce BC emissions with the higher aromatic fuels. BC is a short lived climate forcer in the atmosphere that has the ability to absorb radiative light, thus causing a warming effect. If increased production of wall-guided GDI vehicles are to be heavily produced as predicted, then there could be a large change in climate patterns due to the increased amounts of BC. The results showed that GDI vehicles are 5 to 6 times higher emitters of BC compared to the PFI and Hybrid vehicles. In addition, the higher aromatic fuels increased the amounts of BC EFs. The 35% aromatic fuel increased the BC EF by as much as 350% from the 15% aromatic fuel. However, BC was reduced with the higher octane rating fuel. If the trend of decreasing aromatics in fuels continues and higher octane rating fuels become more common (due to

higher ethanol blends) than reductions in BC from the higher PM emitting GDI vehicles could be shown.

In the next decade, higher ethanol concentrations in gasoline will become more common due to the Renewable Fuels Standard (RFS). Decreasing aromatic concentration in gasoline may also become common due to increased ethanol concentration. The results show that decreasing aromatic concentration also decreases PM mass and more importantly BC from the high emitting GDI vehicles. High ethanol concentrated gasoline may be a better alternative fuel in the market in terms of decreased BC emissions. As ethanol concentrations are increased in the U.S., the higher octane fuel would effectively decrease BC emissions from the high PM emitting GDI vehicles thus helping to minimize BC impacts on the atmosphere.

3.4. Acknowledgments

The authors would like to thank Mark Villela and Kurt Bumiller for their technical support on this study. In addition, the authors thank Tyler Berte, Hans Phang, Chun Liang, and Wartini Ng for their help on the offline measurement analysis. This work was supported by the University of California Transportation Center and the U.S. Environmental Protection Agency (EPA). Specifically, funding for BC measurements were made possible by EPA grant number 83504001. Its contents are solely the responsibility of the grantee and do not necessarily represent the official views of the EPA. Further, the EPA does not endorse the purchase of any commercial products or services mentioned in the publication.

3.5. Literature Cited

Biswas S.; Verma, V.; Schauer, J.J.; Sioutas, C., Chemical Speciation of PM Emissions From Heavy-Duty Diesel Vehicles Equipped With Diesel Particulate Filter (DPF) and Selective Catalytic Reduction (SCR) Retrofits. Atmospheric Environment. 2009, 43, 1917-1925

Canvani, F.; Trifirò, F. Selective oxidation of light alkanes:interation between the catalyst and the gas phase on different classes of catalytic materials. Catalysis Today. 1999, 51(3-4), 561-580; DOI: 10.1016/S0920-5861(99)00041-3

Chueng, K.L.; Polidori, A.; Ntziachristos, L.; Tzamkiozis, T.; Samaras, Z.; Cassee, F. R.; Gerlofs, M.; and Siouras, C. Chemical Characteristics and Oxidative Potential of Particulate Matter Emissions from Gasoline, Diesel, and Biodiesel Cars. Environ. Sci. and Tech.. 2009, 43, 6334-6340

Curran, H.J.; Gaffuri, P.; Pitz, W.J., Westbrook, C.K. A comprehensive modeling study of iso-octane oxidation. Combustion and Flame. 2002. 129(3), 253-280

Ekman, A. M. L.; Engstrom, A.; Wang, C. The effect of aerosol composition and concentration on the development and anvil properties of a continental deep convective cloud. 2007, Q. J. R. Meteorol. Soc., 133, 1439-1452.

EPA. Draft Regulatory Impact Analysis: Tier 3 Motor Vehicle Emission and Fuel Standards. U.S. Environmental Protection Agency. 2013. EPA-420-D-13-002

Ervens, B.;Feingold G.; Kreidenweis, S.M. Influence of water-soluble organic carbon on cloud drop number concentration, Journal of Geophysical Research. 2005, 110, D18211

Geller, M. D.; Ntziachristos L.; Mamakos, A.; Samaras, Z.; Schmitz, D.A.; Fraines, J.R.; Sioutas, C. Physicochemical and redox characteristics of particulate matter (PM) emitted from gasoline and diesel passenger cars. Atmospheric Environment. 2006, 40(36), 6988-7004.

Graham, L. Chemical Characterization of Emissions From Advance Technology Light-Duty Vehicles, Atmospheric Environment, 2005, 39(13), 2385-2398

Gutiérrez-Castillo, M.; Roubicek, D. A.; Cebrián-Garcia, M. E.; De Vizcaya-Ruiz, A.; Sordo-Cedeòo, M.; Ostrosky-Wegman, P. Effect of chemical composition on the induction of DNA damage by urban airborne particulate matter. Environmental and Molecular Mutagenesis. 2006, 47, 199–211.

Hering, S. V.; Stolzenburg, M. R. A Method for Particle Size Amplification by Water Condensation in a Laminar, Thermally Diffusive Flow. Aerosol Science and Technology. 2005, 39, 428–436.

Liang, B.; Ge, Y.; Tan, J.; Han, X.; Gao, L.; Hao, L.; Ye, W.; Dai, P. Comparison of PM Emissions From a Gasoline Direct Injected (GDI) vehicle and a Port Fuel Injected (PFI) vehicles measured by Electrical Low Pressure Impactor (ELPI) With Two Fuels: Gasoline and M15 Methanol Gasoline. J. of Aerosol Sci. 2013, 57, 22-31.

Lighty, J.S.; Veranth, J.M.; Sarofim, A.F. Combustion Aerosols: Factors Governing Their Size and Composition and Implications to Human Health, J. of the Air and Waste Manag. Assoc., 2000, 50(9) 1565-1618

Longest, P.W.; McLeskey, J.T.; Hindle, M. Characterization of Nanoaerosol Size Change During Enhanced Condensational Growth. Aerosol Science and Technology. 2010, 44(6), 473-483

Nadim F.; Zack, P.; Hoag, G.; Liu, S. United States Experience with Gasoline Additives. Energy Policy. 2001. 29(1), 1-5

Perry, R.; Gee, I.L. Vehicle Emissions In Relation to Fuel Composition. The Science of the Total Environment. 1995, 169, 149-156

Petters, M.D.; Kreidenweis, S.M. A single parameter representation of hygroscopic growth and cloud condensation nucleus activity. Atmospheric Chemistry and Physics. 2007, 7, 1961–1971.

Pierce, J.R.; Adams, P.J. Uncertainty in global CCN concentrations from the uncertain aerosol nucleation and primary emissions rates, 2009, Atmos. Chem. Phys., 9, 1339-1356

Ramgolam, K.; Favez, O.; Cachier, H.; Gaudichet, A.; Marano, F.; Martinon, L.; and Baeza-Squiban, A. Size-partitioning of an urban aerosol to identify particle determinants involved in the proinflammatory response induced in airway epithelial cells. Particle and Fibre Toxicology. 2009, 6(10)

Schwarz, J. P.; Gao, R. S.; Fahey, D. W.; Thomson, D. S.; Watts, L. A.; Wilson, J. C.; Reeves, J. M.; Darbeheshti, M.; Baumgardner, D. G.; Kok, G. L.; Chung, S. H.; Schulz, M.; Hendricks, J.; Lauer, A.; Kärcher, B.; Slowik, J. G.; Rosenlof, K. H.; Thompson, T. L.; Langford, A. O.; Loewenstein, M.; Aikin, K. C. Single-particle measurements of midlatitude black carbon and light-scattering aerosols from the

boundary layer to the lower stratosphere. Journal of Geophysical Research. 2006, 111, D16207

Short, D.; Giordano, M.; Zhu, Y.; Fine. P.; Polidori, A.; Asa-Awuku, A. A Unique On-line method to infer black carbon contributions to water-insoluble contributions. Aerosol Science and Technology. 2014, DOI:10.1080/02786826.2014.916778

Silva, R.; Cataluna, R.; Weber de Menezes, E.; Samios, D.; Piatnicki, C.M.S. Effect of Additives On the Antiknock Properties and Reid Vapor Pressure of Gasoline. Fuel. 2005, 84(7-8), 951-959

Squires. P. The microstructure and colloidal stability of warm clouds. Tellus. 1958, 10(2), 256-261; DOI: 10.1111/j.2153-3490.1958.tb02011.x

The California Reformulated Gasoline Regulations, California Air Resources Board (CARB), Title 13, California Code of Regulations, Section 2261(b)

Turpin, B.J.; Lim, H.. Species Contributions to PM 2.5 Mass Concentrations: Revisiting Common Assumptions for Estimating Organic Mass. Aerosol Science and Technology. 2001, 35(1) 602-610

U.S. Environmental Protection Agency. Fuels and fuel additives, renewable fuel standard <http://www.epa.gov/otaq/fuels/renewablefuels>

Valavandidis, A.; Fiotakis, K.; Vlachogianni, T. Airborne Particulate Matter and Human Health: Toxicological Assessment and Importance of Size and Composition of Particles for Oxidative Damage and Carcinogenic Mechanisms. Journal of Environmental Science and Health, Part C. 2008, 26(4), 339-362

Verma, V.; Shafer, M.M.; Schauer, J.J.; Sioutas, C. Contribution of Transistion Metals In the Reactive Oxygen Species Activity of PM Emissions From Retrofitted Heavy-Duty Vehicles. Atmospheric Environment. 2010, 44(39), 5165-5173

Wang, S. C., Flagan, R. C. 1990. Scanning Electrical Mobility Spectrometer. Aerosol Science and Technology, 13: 230–240

Weaver, J.; Exum, L.; Prieto, L.; 2010. Gasoline Composition Regulations Affecting LUST Sites, EPA Report, EPA 600/R-10/001

Yung-Fang Y.Y. Ocidation of alkanes over noble metal catalysts. Ind. Eng. Chem. Prod. Res. Dev. 1980, 19, 293-298

Zhao F.; Lai M. C.; Harrington D. L. Automotive Spark-Ignited Direct-Injection Gasoline Engines, Progress in Energy and Combustion Science, 1999, 25(5), 437-562

Chapter 4: Criteria and Particle Emissions from Port Fuel Injection and Gasoline Direct Injection Vehicles on Ethanol and Iso-Butanol Blended Fuels

4.1. Introduction

Globally the on-road transportation sector contributes significantly to air pollution and climate change. One of the challenges for the automotive manufacturers is to decrease pollutant emissions meeting strict fuel economy and carbon dioxide (CO_2) emissions requirements. One possible solution is the use of oxygenated biofuels. Biofuels have been the subject of significant political and scientific attention, owing to concerns about climate change, global energy security, and the decline of world oil resources that is aggravated by the continuous increase of the demand for fossil fuels. Among the different oxygenated biofuels being used globally today, ethanol is the most widely employed, although geographically its usage is somewhat restricted to U.S. and Brazil. In 2010, the United States (U.S.) Environmental Protection Agency (EPA) implemented the Renewable Fuel Standard (RFS) Program Final Rule, which mandates the use of 36 billion gallons of renewable fuels to be blended into transportation fuel by 2022, with ethanol expected to make up the majority of this requirement (RFS, 2007).

Another pathway that could help reach the congressionally mandated biofuel volumes is the use of bio-butanol. Butanol or butyl alcohol also has potential as a biofuel for use in internal combustion (IC) engines Szwaja and Naber (2010) and Merola et al. (2013). Analogous to ethanol, butanol can be produced both by petrochemical and fermentative processes. Biomass-derived butanol can be produced by alcoholic fermentation of

biomass and agricultural feedstocks, such as corn, wheat, sugar beet, sugarcane, and cassava Xue et al. (2013). Butanol is a higher-chain alcohol with a four-carbon structure. It exists as different isomers based on the location of the hydroxyl (OH) group and carbon chain structure. Butanol offers a number of advantages over ethanol for transportation use. Butanol is less corrosive than ethanol, has a higher energy content than ethanol, and more closely resembles gasoline. In comparison to ethanol, butanol has higher tolerance to water contamination, potentially allowing its use of the existing distribution pipelines, whereas ethanol must be transported via rail or truck (Jin et al. 2011). Butanol also has an increased octane number compared to gasoline, but lower than ethanol. Butanol's heat of vaporization is less compared to ethanol, which would provide cold-start benefits for engines running with butanol blended fuels compared with ethanol blends with gasoline (Cooney et al. 2009).

In addition to the alternative fuels diversity in the fuel pool, the automotive manufacturers have taken efforts in improving the overall efficiency of gasoline powered passenger cars, which is directly connected to meeting more stringent carbon dioxide (CO_2) emissions limits. To reach CO_2 targets, different strategies have been studied, including engine downsizing and higher boost pressures in combination with direct gasoline injection. Gasoline Direct Injection (GDI) engines can offer up to 25% improvement in fuel economy compared with port-fuel injected (PFI) engines (Zhao et al. 1999). This is mainly achieved through reductions in pumping and heat losses when operated unthrottled at low-mid loads. GDI fueling for gasoline engines significantly improves engine power, which allows the engine displacement volume to be reduced for

a given application, even while the engine performance improves (Alkidas 2007). The penetration of GDI vehicles in the U.S. market is rapidly increasing. It is foreseen that this category of vehicles will dominate the gasoline market, eventually replacing the conventional and less efficient PFI vehicles. It is interesting to note that in the U.S., half of all light-duty vehicle certifications for the 2012 model year included gasoline DI engines, reaching approximately 24% of the market, up from virtually 0% in 2007. This trend is expected to dramatically increase, with a projection of 48% and 93%, respectively, of all new vehicles having GDI engine by 2016 and 2025 (MECA, 2013).

One of the drawbacks of GDI engines is the increase in particulate emissions in comparison to PFI engines, due to combustion in fuel rich regions in the cylinder. Aakko and Nylund (2003) found that particle mass emissions for a GDI vehicle were an order of magnitude higher than for a PFI vehicle for the European 70/220/EEC driving cycle. Szybist et al. (2011) reported that particle number emissions with GDI fueling increased by 1–2 orders of magnitude compared to PFI fueling. There are also a plethora of studies examining the effects of ethanol on gaseous and particle emissions from PFI and GDI vehicles. Studies of older vehicles have generally shown reductions in total hydrocarbons (THC), non-methane hydrocarbon (NMHC), and carbon monoxide (CO) emissions with ethanol blends, while nitrogen oxide (NO_x) emissions have either shown no significant changes or increases with increasing ethanol blends (Knoll et al. 2009; Durbin et al. 2007; Graham et al. 2008). Karavalakis et al. (2012) found that THC, NMHC, and CO emissions were lower with ethanol blends, while NO_x emissions showed some increases with increasing ethanol content in gasoline. These trends were more consistent for the

older vehicles in the study. They also found higher acetaldehyde and some higher formaldehyde emissions with the ethanol blends, whereas the toxic compounds of benzene and 1,3-butadiene were lower. A recent study by Bielaczyc et al. (2013) showed small reductions in THC, CO, and NO_x emissions from SI-PFI vehicles with higher ethanol blends over the New European Driving Cycle (NEDC). They also found that the addition of ethanol caused a decrease in the number of particles and a significant reduction in particulate matter (PM) mass emissions. Maricq et al. (2012) showed small benefits in PM mass and particle number emissions as the ethanol level in gasoline increased from 0% to 20% when testing a GDI turbocharged vehicle with two engine calibrations. They also found higher reductions in both PM mass and particle number emissions with ethanol contents >30%. Finally, Storey et al. (2010) reported that NO_x emissions decreased with increased ethanol concentration, while some increases were seen in THC emissions when they tested a turbocharged GDI vehicle over the Federal Test Procedure (FTP) cycle and the more aggressive US06 cycle. They also showed reduced PM mass and particle number emissions with ethanol blends.

Butanol has not been studied as extensively as ethanol. An earlier study found that butanol blends resulted in lower CO_2, CO, and NO_x emissions compared to gasoline (Gautam et al. 2000). Dernotte et al. (2010) assessed different butanol–gasoline blends at different engine loads, spark timings, and equivalence ratios in a SI-PFI engine. They found some THC reductions with butanol, while no significant differences were seen in NO_x emissions. Schulz and Clark (2011) carried out a study comparing various ethanol blends and a 16% butanol blend using six modern technology vehicles over the FTP

cycle. They found a limited number of statistically significant differences between the fuels tested, however, a decreasing trend in CO and formaldehyde emissions was observed with the butanol blend compared to gasoline. With respect to GDI engines, Wallner and Frazee (2010) found that NO_x, CO, and THC emissions were lower with increasing butanol content in gasoline, while some increases were seen for formaldehyde and acetaldehyde emissions when they utilized n-butanol and iso-butanol as blending agents with gasoline. In a similar study, the same authors showed lower volumetric fuel consumption and lower NO_x emissions for butanol compared to ethanol blends (Wallner et al. 2009).

The purpose of this investigation is to elucidate the effects of fuel type and blend concentration for ethanol and iso-butanol on the exhaust emissions from five modern technology light-duty gasoline vehicles fitted with PFI and GDI stoichiometric engines. Testing was conducted over the FTP and the Unified Cycle (UC) that include effects of both cold-start and transient operation. The study utilized a total of seven alcohol blends, including 10%, 15%, and 20% ethanol blends and 16%, 24%, and 32% butanol blends, and an alcohol mixture consisting of 20% ethanol and 16% butanol.

4.2. Experimental

4.2.1. Test fuels and vehicles

A total of seven fuels were employed in this study. The fuel test matrix included an E10 fuel (10% ethanol and 90% gasoline), which served as the baseline fuel for this study, and two more ethanol blends, namely E15 and E20. For this study, iso-butanol was

blended with gasoline at proportions of 16% (Bu16), 24% (Bu24), and 32% (Bu32) by volume, which is the equivalent of E10, E15, and E20, respectively, based on the oxygen content. In addition, an alcohol mixture consisting of 20% ethanol and 16% iso-butanol (E10/Bu8) was used. This mixed alcohol formulation was equivalent to E15 based on the oxygen content. All fuels were custom blended to match the oxygen contents, maintain the Reid vapor pressure (RVP) within certain limits (6.4–7.2 psi), and match the fuel volatility properties, except the E10/Bu8 fuel that was a 50/50 splash blend of the E20 and Bu16 fuels. The main physicochemical properties of the test fuels are given in Appendix Table C-1.

This study utilized five light-duty gasoline vehicles of different designs (passenger cars and trucks). The vehicles included a 2007 model year (MY) Honda Civic equipped with a PFI engine, a 2007 MY Dodge Ram equipped with a PFI engine, a 2012 MY Toyota Camry equipped with a PFI engine, a 2012 MY Kia Optima equipped with a GDI engine, and a 2012 MY Chevrolet Impala equipped with a GDI engine. The Honda Civic, Dodge Ram, Toyota Camry, Kia Optima, and Chevrolet Impala had 29,000, 52,400, 13,500, 11,824 and 25,372 miles, respectively, at the start of the test campaign. The technical specifications of the test vehicles are given in Appendix Table C-2. It should be noted that not every vehicle was tested on all fuels. Only the Toyota Camry and the Kia Optima were tested on the E10/Bu8 mixture.

4.2.2. Driving cycles and measurement protocol

Each vehicle was tested on each fuel over three Federal Test Procedure (FTP) and three Unified Cycle (UC) tests. The 6 tests on a particular fuel were conducted sequentially once the vehicle was changed to operate on that fuel, and the fuel was not changed to another fuel during this time. A fuel change with multiple drain and fills was conducted between the testing on each fuel to condition the vehicle and ensure no carryover effects. Detailed information on the driving cycles employed in this study and the testing protocol are provided in Appendix Section C-2.

4.2.3. Emissions testing and analysis

All tests were conducted in CE-CERT's Vehicle Emissions Research Laboratory (VERL), which is equipped with a Burke E. Porter 48-inch single-roll electric dynamometer. A schematic on the experimental setup and sampling system on a chassis dynamometer is provided in Appendix Fig. C-2. A Pierburg Positive Displacement Pump–Constant Volume Sampling (PDP–CVS) system was used to obtain certification-quality emissions measurements. For all tests, standard bag measurements were obtained for THC, CO, NO_x, non-methane hydrocarbons (NMHC), and CO_2. NMHC was determined from the combined results from the THC analyzer and a separate CH_4 analyzer. Bag measurements were made with a Pierburg AMA-4000 bench.

PM measurements were made on both a mass and number basis. PM mass samples were collected cumulatively over the entire FTP and UC cycles, with one sample collected for

each test. Total PM mass determinations were collected using 47 mm Teflon® filters and measured with a 1065-compliant microbalance in a temperature and humidity controlled clean chamber. Particle number measurements were made with a TSI model 3772 condensation particle counter (CPC) for the Honda Civic and Dodge Ram and a TSI model 3776 CPC for the Toyota Camry, Kia Optima, and Chevrolet Impala. The TSI 3772 was replaced by the TSI 3776, since it has a lower cut point, 2.5 nm compared to 10 nm for the TSI 3722, and also a low coincidence error, which is below 300,000 particles per second.

4.3. Results and discussion

The figures for each emissions component show the results for each vehicle tested on the alcohol blends over the FTP and UC cycles based on the average of all tests conducted on that particular fuel blend. The error bars represent the standard deviation for the average of each fuel. Statistical comparisons between fuels for a given vehicle were made using a 2-tailed, 2-sample, equal variance *t*-test. For the purpose of this discussion, results are considered to be statistically significant for $p \leqslant 0.05$.

4.3.1. Regulated emissions

THC emissions for all vehicle/fuel combinations over the FTP and UC test cycles are shown in Fig. 4-1a. In general, THC emissions were found at low levels for all five vehicles for both test cycles, ranging from 0.005 to 0.12 g/mile for the FTP and 0.005 to 0.09 g/mile for the UC. Higher THC emissions were observed for the older model PFI

fueled Honda Civic and Dodge Ram vehicles compared to the newer vehicles. Overall, the largest portion of THC emissions was emitted during the first 200–300 s of the FTP and UC cycles (bag 1) when the engine was cold, ranging from 0.014 to 0.675 g/mile for the FTP and 0.043 to 1.135 g/mile for the UC. The higher cold-start THC emissions can be attributed to the catalyst being below its light-off temperature during the cold-start phase and incomplete combustion products from the fuel enrichment during start up. For the GDI vehicles, it was hypothesized that an important source of THC emissions would be fuel impingement on combustion chamber surfaces. It is therefore reasonable to assume that a portion of THC emissions might be derived from unburned fuel fractions during the initial stages of the cold-start portions of the FTP and UC.

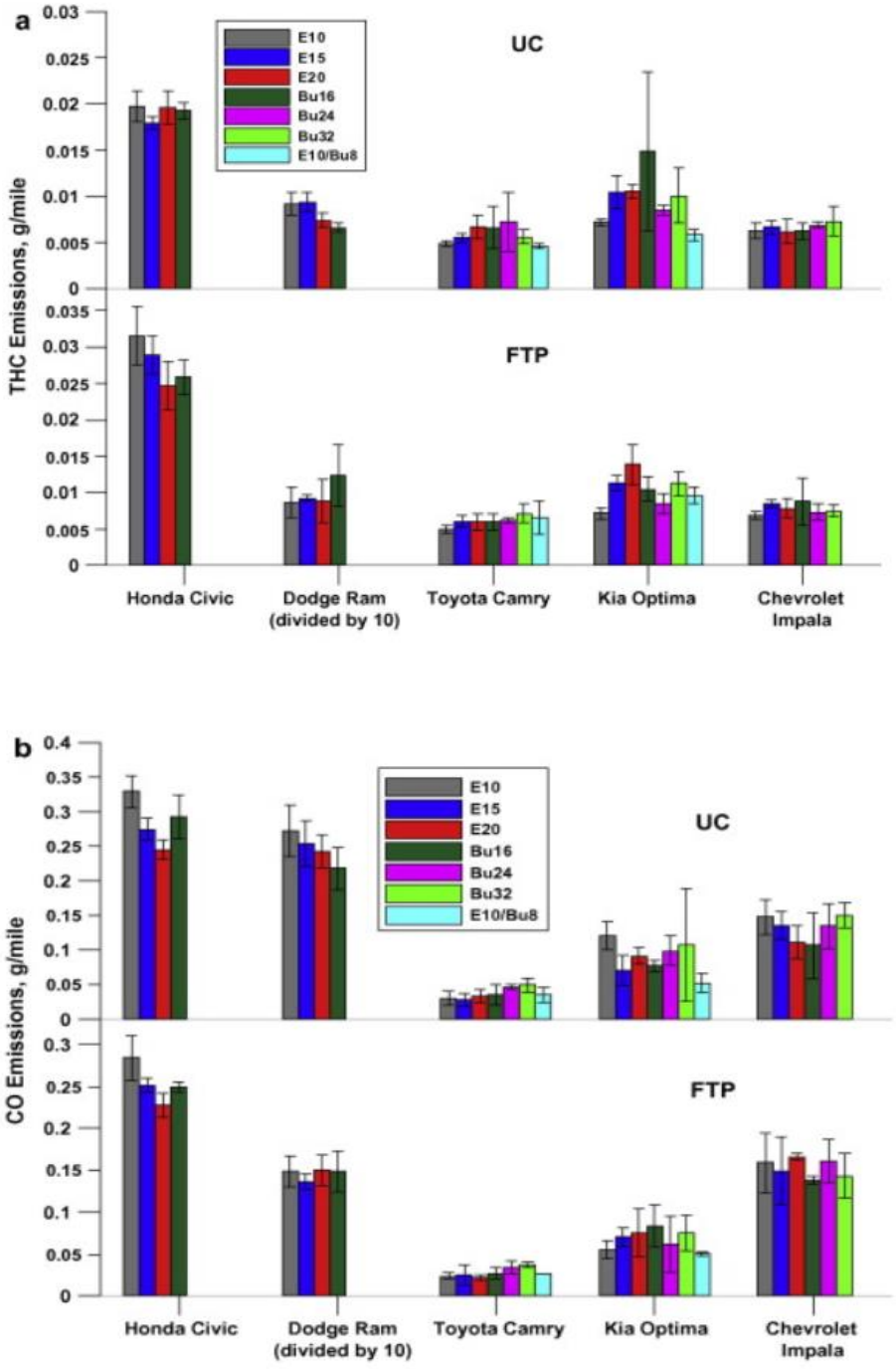

Fig. 4- 1. THC (top panel, a) and CO (bottom panel, b) emissions for all vehicle/fuel combinations over the FTP and UC test cycles

Fuel effects showed mixed results for different vehicles and cycles. For the PFI vehicles, the E20 and Bu16 blends showed lower THC emissions for the Honda Civic on the FTP and for the Dodge Ram over the UC, but showed higher THC emissions for the Toyota Camry over the UC. The GDI Kia Optima showed some of the strongest trends, with the E15, E20, Bu16, and E10/Bu8 showing higher THC emissions than E10, but the higher butanol blends were either lower or comparable to the Bu16 fuel. The Chevrolet Impala showed very limited fuel differences, with most fuel pairs showing no statistically significant differences.

Trends of decreasing THC emissions with increasing alcohol concentration have generally been seen in previous studies utilizing test cell engines or larger fleets of older technology vehicles (Knoll et al. 2009; Karavalakis et al. 2012; Schulz et al. 2011; Gu et al. 2012). This phenomenon has been widely attributed to the presence of oxygen content in the fuel, which leans the air–fuel ratio and promotes oxidation during combustion and over the catalyst. On the other hand, some increases in THC emissions with ethanol and butanol fuels have been observed in previous studies conducted with test cell engines and light-duty vehicles (Durbin et al. 2007;Dernotte et al. 2010). The present study did not show strong fuel trends over the fleet of vehicles tested. In particular, while specific vehicle/cycle combinations may have shown differences between fuels, these differences were generally not consistent for both cycles on a particular vehicle, or for more than one of the vehicles. The lack of strong trends indicates advancements in catalyst technology and air/fuel ratio control are reducing the impact of fuel differences on exhaust emissions. Overall, there is not a strong trend of higher or lower THC emissions for the butanol

blends in comparison with the ethanol blends with the equivalent oxygen content. Previous studies have suggested that iso-butanol could produce lower THC emissions due to the lower latent heat of vaporization of iso-butanol compared to ethanol (Wallner et al. 2009).

Fig. 4-1b presents the influence of ethanol and iso-butanol addition on CO emissions for both cycles. The higher alcohol fuels showed lower CO emissions for the Honda Civic on both cycles and for the higher emitting Dodge Ram over the UC. This is consistent with previous studies that have shown reductions in CO with increasing alcohol content due to improved oxidation of the CO as a result of the oxygen content in the fuel (Karavalakis et al. 2012; Schifter et al. 2001). For the Honda Civic, a statistically significant decrease of 20% for E20 relative to E10 was seen over the FTP, while statistically significant decreases of 17% and 26% for E15 and E20, respectively, relative to E10 were seen over the UC. For the Toyota Camry, CO emissions trended higher with the higher butanol blends, with Bu32 showing a 54% increase in CO emissions compared to E10 at a statistically significant level. For the FTP, the GDI vehicles showed no statistically significant differences between the fuels tested. For the UC, the Kia Optima showed some decreases at a statistically significant level in CO emissions with the higher ethanol and butanol blends compared to E10. The Chevrolet Impala showed lower emissions for E20 and Bu16, but not at a statistically significant level. The statistically significant decreases in CO emissions for the Kia Optima were 41%, 36%, and 56% for E15, Bu16, and E10/Bu8, respectively.

CO production is primarily controlled by the air–fuel ratio in the cylinder. Mixtures richer than stoichiometric produce high CO emissions, whereas mixtures at stoichiometric and leaner produce little CO emissions. For the test fleet as a whole, there were not strong fuel effects on CO emissions, with the exception of some trends of lower CO emissions for higher alcohol blends for the 2007 MY vehicles. This was due to the fact that the test engines utilized stoichiometric combustion and tightly controlled the global equivalence ratio close to 1.0, producing little CO emissions and relatively minor changes in air–fuel ratio throughout testing. The 2007 MY vehicles appear to be more sensitive to small changes in air–fuel ratio, as they produced less CO for the higher alcohol fuel formulations. Analogous to THC emissions, the cold-start portion of the FTP and UC dominated CO emissions for all test vehicles. Comparing the 2012 MY vehicles, the PFI Toyota Camry had relatively low concentrations of CO during the cold-start phase. The relatively low CO suggests that the combustion was not rich. For the GDI vehicles, cold-start CO emissions were found to be significantly higher compared to hot-running and hot-start emissions, and considerably higher than those of the Toyota Camry. This result suggests that the combustion was richer for the GDI engines during the first 200–300 s of the test cycles. For the 2007 MY PFI vehicles, the CO emissions during cold-start had much high concentrations, while the bags 2 and 3 CO emissions were comparable to those of the newer vehicles. This result implies that these engines run close to stoichiometric and slightly rich through the entire FTP and UC tests.

NO_x emissions as a function of fuel type are shown in Fig. 4-2. The NO_x emissions for the Honda Civic, Toyota Camry, and the two GDI vehicles were about an order of

magnitude lower than those for the Dodge Ram. For the Honda Civic, there was a tendency towards higher NO_x emissions over both test cycles for the E15, E20, and Bu16 blends relative to E10. For the FTP, statistically significant increases of 36% and 31%, respectively, for E20 and Bu16 were seen, while for the UC a 54% statistically significant increase in NO_x was observed for E15 relative to E10. For the Dodge Ram, some decreases in NO_x emissions were seen for both cycles, however, these differences were not statistically significant. For the Toyota Camry, lower NO_x emissions were seen for the E15 fuel for the FTP and the Bu24 and Bu32 fuels for both the FTP and UC, but these reductions relative to E10 were only statistically significant for Bu24 (22%) and Bu32 (22%) blends over the UC. For the GDI vehicles, NO_x emissions were found to be higher for the Chevrolet Impala than the Kia Optima for the FTP, which trends with the lower THC emissions for the Chevrolet Impala. For the Kia Optima, NO_x emissions did not show any significant differences between the fuels over the FTP, whereas some higher NO_x emissions were seen for E20 (26%) and E10/Bu8 (33%) at a statistically significant level over the UC. For the Chevrolet Impala, the only statistically significant increase in NO_x emissions compared to E10 was seen for Bu32 (29%) blend over the FTP.

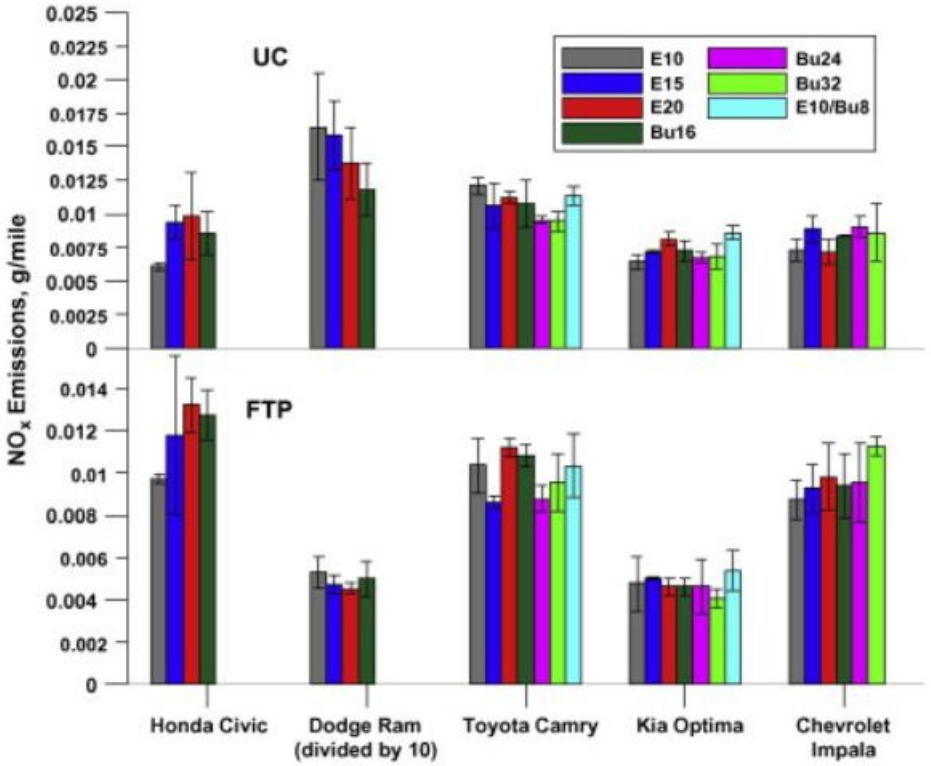

Fig. 4- 2. NO_x emissions for all vehicle/fuel combinations over the FTP (bottom panel) and UC (top panel) test cycles

NO_x emissions can vary with air–fuel ratio/oxygen content or other combustion factors such as in-cylinder temperatures and the residence time/duration for combustion (Masum et al. 2013). Previous studies have shown that NO_x emissions can increase with low, intermediate, and higher ethanol blends, although this trend is not consistent between studies, and is stronger in older vehicles or vehicles with less sophisticated control of air–fuel ratio (Knoll et al. 2009; Karavalakis et al. 2012; Masum et al. 2013). Other studies have shown reductions in NO_x emissions with higher ethanol blends may be due to the higher latent heat of vaporization of ethanol and it's subsequently lower flame temperature, leading to an increase in-cylinder cooling and lower process temperatures,

and thus, lower NO_x emissions (Koc et al. 2009). Previous investigations have also shown that NO_x emissions can decrease with the addition of butanol (Wallner et al. 2009; Merola et al. 2012). Under the present test conditions, there were no consistent fuel trends with oxygenate content, suggesting that individual fuel differences for different vehicles could be related to factors that were unique to the different test vehicles, including test-to-test variability.

Fig. 4-3a shows the effect of alcohol type and concentration on the CO_2 emissions for the test vehicles over the FTP and UC. CO_2 emissions showed some specific differences between different fuels for different vehicles, but no consistent trends over all testing conditions. From a theoretical standpoint, it might be expected that CO_2 emissions would trend with either the carbon/hydrogen ratio or carbon/energy content in the fuel. Carbon/hydrogen ratio decreases in the following order E10–Bu16, E15–Bu24–E10/Bu8, and E20–Bu32, as shown in Appendix Table C-1. Overall, there are not universal trends relating to either of these metrics, but in the cases where fuel differences are seen for the different vehicles, they tend to track better with the decreasing carbon/hydrogen ratio. Reductions in CO_2 emissions at a statistically significant level for the lower carbon/hydrogen ratio fuels were seen for the Dodge Ram over the FTP, but not for the UC, and the Toyota Camry for both the FTP and UC cycles, but not for the butanol blends. Interestingly, the Honda Civic over the UC did show a trend of lower CO_2 emissions for the E15 and E20 blends relative to the E10 fuel, but higher CO_2 emissions relative to the Bu16 fuel. The GDI vehicles exhibited lower CO_2 emissions for the higher ethanol blends with some differences being statistically significant for the Kia Optima.

For the Chevrolet Impala, CO_2 emissions were about the same between the fuels over both test cycles, with some weak trends towards lower CO_2 emissions for the higher ethanol and butanol blends relative to E10.

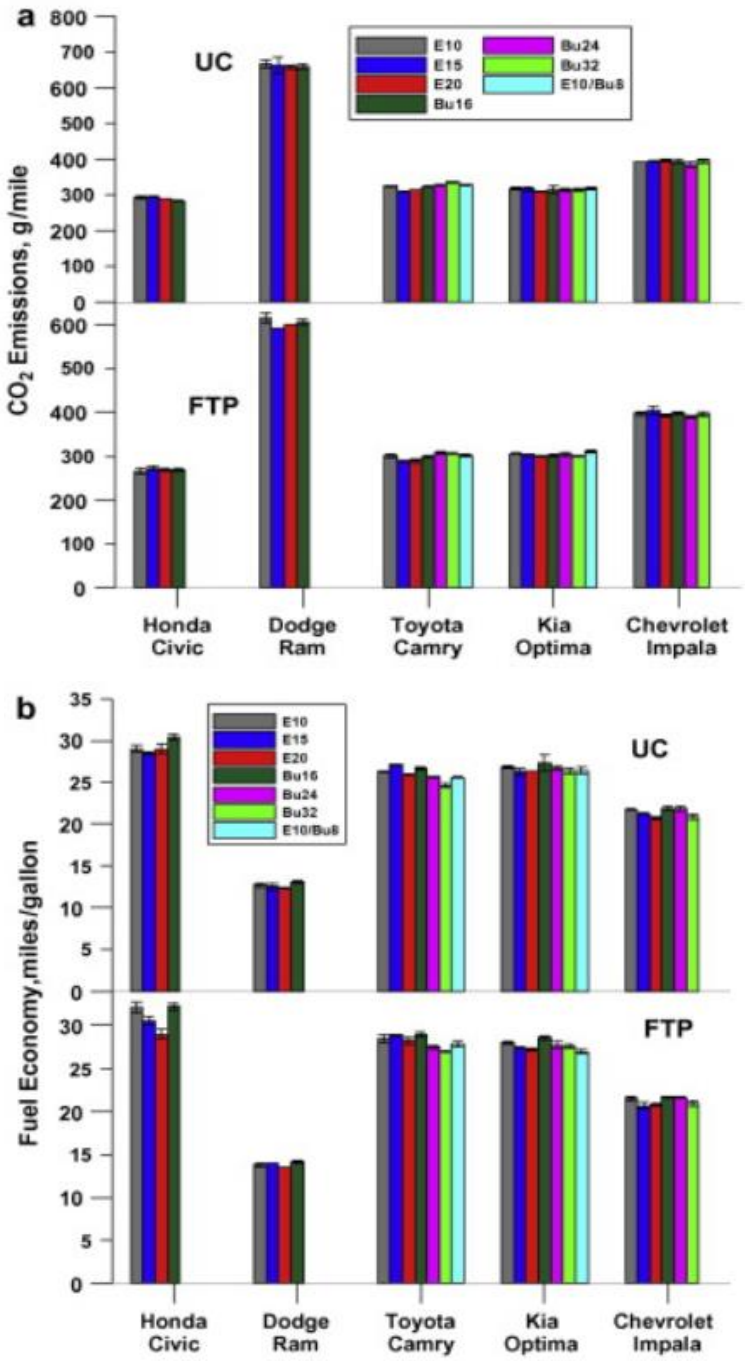

Fig. 4- 3. CO_2 (top panel, a) emissions and fuel economy based on the carbon balance method (bottom panel, b) for all vehicle/fuel combinations over the FTP and UC test cycles.

Fuel economy results for the test vehicles are presented in Fig. 4-3b. For this study, fuel economy was calculated based on the carbon balance method and the unique properties for each different test fuel and not according to the standard EPA equation. The carbon balance equation more directly accounts for the differences in energy content between different fuels, which are somewhat normalized out in the standard EPA equation. Overall, the results revealed that as the alcohol concentration increased the fuel economy decreased by 2–5% for the FTP and 1–6% for the UC, which is approximately proportionally to the decrease in energy content of the blend. This trend was consistent for all vehicles, with the higher ethanol blends and butanol blends showing lower fuel economy than E10 and Bu16, respectively, while the E10/Bu8 blend had about the same fuel economy as the E15 blend for the SI-SIDI vehicles and a slightly lower fuel economy for the Toyota Camry.

4.3.2. PM mass, particle number, and black carbon emissions

The cumulative PM mass emissions are shown in Fig. 4-4a. Note that PM mass was only collected for the GDI vehicles and for most of the fuels for the Toyota Camry. PM mass emission results for the GDI vehicles showed reductions with the fuels with the highest oxygen levels for a number of the vehicle/cycle combinations, but not necessarily the blends with the intermediate oxygen levels. Other properties, such as fuel volatility, can also play a role in PM emissions, which is sometimes more important than the presence of oxygen in the fuel. However, in the current study most physicochemical properties of the test fuels were kept constant with relatively narrow ranges. Thus, the oxygen content should be the primary contributing factor for lowering PM emissions.

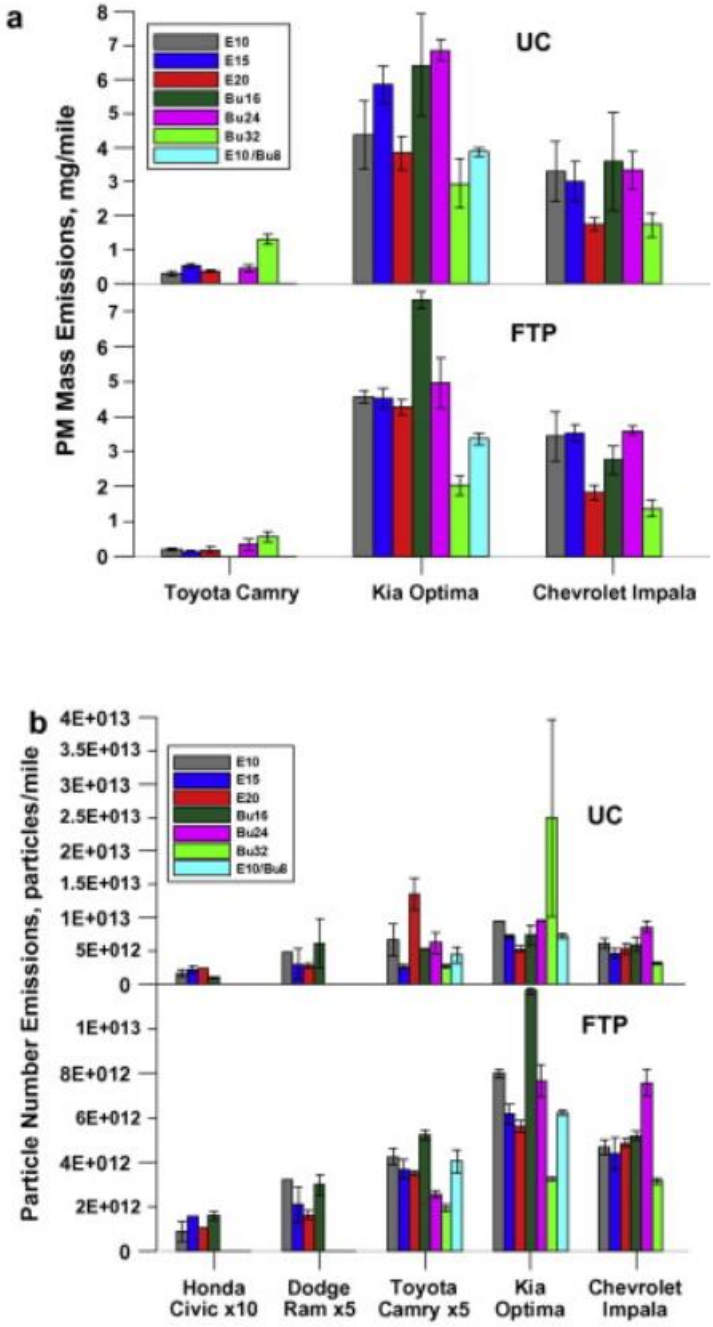

Fig. 4- 4. PM mass emissions for the Toyota Camry and the GDI vehicles over the FTP and UC test cycles (top panel, a) and total particle number emissions for all vehicle/fuel combinations over the FTP and UC test cycles (bottom panel, b).

For the Chevrolet Impala, the PM mass results showed some trends with the oxygen content in the fuel, with the E20 and Bu32 fuels showing the lowest PM mass levels over both cycles. For the butanol blends for the Chevrolet Impala, PM benefits were seen for the higher butanol fuels relative to Bu16 over the UC and for Bu32 compared to both Bu16 and Bu24 over the FTP. For the Kia Optima, the E20 and Bu32 fuels showed the lowest PM mass emissions for both the FTP and UC cycles. For the Kia Optima, the Bu32 fuel showed the lowest PM mass emissions, while the Bu16 showed the highest emissions over the FTP. Over the UC for the Kia Optima, the fuel trends were less consistent, with the E15, Bu16, and Bu24 fuels showed the highest emissions, while the Bu32 fuel was slightly lower than the remaining fuels. For the Toyota Camry, the use of higher ethanol blends produced discordant results with both decreases in PM emissions over the FTP and increases over the UC. While the reductions in PM emissions for the FTP were not statistically significant, the use of E15 led to a statistically significant 74% increase in PM emissions relative to E10 over the UC. For both test cycles, the use of higher butanol blends resulted in increases in PM emissions compared to ethanol blends, although data on Bu16 and E10/Bu8 is missing to draw a more complete picture of how the ethanol and butanol blends compare. The Bu32 blend showed dramatic increases in PM emissions relative to E10 at a statistically significant level on the order of 183% and 336% for the FTP and UC, respectively.

PM mass results ranged from 0.15 to 7.3 mg/mile for the FTP and 0.30 to 6.87 for the UC, averaging 0.28 and 0.59 mg/mile for the Toyota Camry, 4.40 and 4.88 mg/mile for the Kia Optima, and at 2.75 and 2.78 mg/mile for the Chevrolet Impala for the FTP and

UC, respectively. This study showed considerably higher PM mass emissions from the GDI vehicles compared to the PFI vehicle. High PM emissions for the GDI fueled vehicles are expected and have been reported in previous studies (Storey et al. 2012; Maricq et al. 2013). Our results are also in agreement with a more recent study of PFI vehicles of model year 2005 and newer, which show PM mass rates of <1 mg/mile over the FTP (Zhang et al. 2010). Elevated PM mass emissions from GDI vehicles can be ascribed to insufficient homogeneous mixture and subsequent fuel evaporation, wall wetting, and a less efficient mixing of air and fuel compared to PFI vehicles, where the fuel is injected and vaporized into the intake ports (Piock et al. 2011; He et al. 2012). In addition, the higher PM emissions from the GDI vehicles were predominantly released from the cold-start phase where cold piston and cylinder surfaces exacerbate liquid fuel impingement and reduce evaporation from surfaces, which produces soot when the fuel ignites (Maricq et al. 2013). It should be noted that while this study employed relatively modern GDI vehicles, these vehicles did not have sufficient control of PM emissions meet the future California LEV III and Tier 3 standards for PM mass emissions to be implemented in 2017 (3 mg/mile), and in particular the even more stringent LEV III PM mass standards for 2025 (1 mg/mile).

The total particle number emissions are displayed in Fig. 4-4b. For the GDI vehicles, particle number emissions corroborate the PM mass trends, with the Kia Optima generally showing higher particle number emissions than the Chevrolet Impala. Both GDI vehicles exhibited significantly higher particle number counts compared to their PFI counterparts. This can be ascribed to the better mixture preparation of PFI engines in

relation to GDI engines and the likelihood of fuel impingement onto the piston for the GDI engines. This may result in liquid fuel that is not totally vaporized at the start of combustion. As a consequence, local fuel-rich combustion or even pool fires can occur near the piston, generating high particle emissions (Whelan et al. 2010; He et al. 2010). Overall, the more aggressive driving conditions for the UC increased particle number counts for all vehicle/fuel combinations compared to the FTP.

For the FTP, the use of E15 and E20 reduced particle number emissions compared to E10, with some exceptions. For the UC, the use of E15 and E20 blends showed mixed results with some particle number benefits for the Dodge Ram and the Kia Optima. For the Kia Optima, the blends of E15 and E20 exhibited statistically significant decreases in particle number emissions of 23% and 30%, respectively, compared to E10. Particle number for E15 and E20 benefits were also seen over the UC, however, no statistical comparisons can be made due to the fact that only a single test was available for E10 for the UC. For the Chevrolet Impala, particle number emissions for E10, E15, and E20 were not significantly different for both cycles. For the butanol blends, particle number comparisons were complicated for some vehicles and some butanol blends. For the 2007 PFI vehicles, the use of Bu16 increased particle number emissions compared to E15 and E20 for both cycles, except for the Honda Civic over the UC. For the Toyota Camry, particle number emissions for Bu16 remained roughly the same as those of E10 for both cycles, while lower particle number emissions were observed for the higher butanol blends compared to Bu16 with these reductions over the FTP being statistically significant. For both cycles, the E10/Bu8 blend was at about the same levels as the E15.

Analogous to ethanol blends, the Kia Optima showed statistically significant decreases in particle number emissions for the FTP were also seen for Bu24 (34%) and Bu32 (72%) blends relative to Bu16. The alcohol mixture (E10/Bu8) showed a statistically significant reduction in particle number emissions from both E10 (22%) and Bu16 (47%) blends, respectively. For the UC, however, a different picture was observed for the butanol blends. The higher butanol blends resulted in increases in particle number emissions compared to Bu16 with Bu32 showing a sharp increase of 236% at a statistically significant level. For the butanol blends for the Chevrolet Impala, there was 46% and 44% increase in particle number emissions for Bu24 relative to Bu16 at a statistically significant level over the FTP and UC, respectively. Statistically significant decreases of 39% and 47%, respectively, for the FTP and UC for Bu32 compared to Bu16 were also observed.

Particle number results reported here generally decreased with the addition of ethanol and iso-butanol, implying that the presence of oxygen in the fuel was the main contributing factor for the particle number decrease by suppressing soot formation. In addition to the oxygen content, particles are also strongly related to the aromatic hydrocarbons content in the fuel (Gu et al. 2012). The addition of higher blends of ethanol and iso-butanol in gasoline decreased the fraction of aromatic hydrocarbons and therefore their propensity of forming soot. This is consistent with the findings of Wallner and Frazee (2009), which showed that the reduction in the availability of carbon in ethanol combustion decreases the potential for benzene and soot formation as the ethanol blend ratio increases. The iso-butanol blends had higher particle number emissions compared to their corresponding

ethanol blends in some cases, but not in others, although the Bu32 blend emitted the lowest particle number emissions for most vehicle/fuel combinations. Previous studies have suggested that during GDI combustion branched butanols can produce intermediate products, such as propene and butene, leading to the formation of more benzene and soot (McEnally and Pfefferle 2005). The results of this study indicate that, in some cases, the degree of branching (iso-butanol versus ethanol) may have a stronger impact on soot formation than the oxygen content, since the butanol blends had equivalent oxygen contents to their corresponding ethanol blends. In addition to fuel structure, the higher viscosity of butanol blends relative to ethanol blends could have also influenced particle number emissions by altering the fuel spray characteristics (Aleiferis and Romunde 2013).

The cold-start phase for both test cycles contributes strongly to the overall particle number emissions, as the engine and catalyst are not yet at operating temperature and therefore particles consisting of volatile residues cannot be effectively oxidized. It is interesting to note that most of the particle emissions occur towards the beginning of the FTP and UC, with roughly 60–90% of the particle emissions occurring in the first 200–300 s. More specifically, for the Honda Civic, fuel average particle number counts for cold-start, hot-running emissions, and hot-start were 3.46×10^{11}, 9.14×10^{10}, and 4.62×10^{10} #/mile for the FTP and 9.52×10^{11}, 1.42×10^{11}, and 9.67×10^{10} #/mile for the UC, respectively. For the Dodge Ram, fuel average particle number counts were 1.48×10^{12}, 2.52×10^{11}, and 2.40×10^{11} #/mile for the FTP and 2.59×10^{12}, 6.77×10^{11}, and 3.01×10^{11}, #/mile for the UC, respectively. For the Toyota Camry fuel average

particle number counts were 1.75×10^{11}, 2.58×10^{10}, and 3.26×10^{10} #/mile for the FTP and 1.58×10^{12}, 1.19×10^{11}, and 3.10×10^{10} #/mile for the UC, respectively. For the Kia Optima, fuel average particle number counts were 1.95×10^{13}, 3.82×10^{12}, and 2.64×10^{12} #/mile for the FTP and 4.44×10^{13}, 8.72×10^{12}, and 3.57×10^{12} #/mile for the UC, respectively. Finally, for the Chevrolet Impala, fuel average particle number counts were 1.91×10^{13}, 1.39×10^{12}, and 9.40×10^{11} #/mile for the FTP and 4.60×10^{13}, 3.50×10^{12}, and 1.09×10^{12} #/mile for the UC, respectively. The cold-start emissions for the UC are substantially higher compared to those of the FTP, because the cold-start phase for the FTP is about ~200 s longer than that for the UC, and hence includes some driving after the initial spike in cold-start emissions has ended. For the UC, hot-running particle emissions were also systematically lower than those for the hot-start due to the driving schedule being less aggressive than in the hot-running phase and that there is a much lower tendency to overfuel in the hot-start compared with the cold-start. For the cold-start for the GDI vehicles, fuel accumulation onto the cold piston and cylinder surfaces can contribute to the sharp increases in particle number emissions. Hot-running and hot-start particle emissions for the FTP did not show significant differences as opposed to those of the UC. The significant reduction in particle number emissions after the cold-start can be attributed to the higher intake air temperatures, fuel temperatures, and piston surface temperatures, which promote fuel vaporization and thus better fuel–air mixing, coupled with the higher efficiency of the TWC once it has reached its light-off temperature (He et al. 2010).

4.4. Conclusions

There is a growing need to evaluate the potential impacts of new fuels on the exhaust emissions for modern technology vehicles, and ultimately their effect on regional and global air quality, as the deployment of ethanol and potentially butanol fuels continues to expand in the gasoline pool along with more widespread penetration of direct injection gasoline vehicles. In this study, seven alcohol formulations including ethanol blends, iso-butanol blends and an alcohol mixture were tested on five different light-duty vehicles. Testing was performed on three PFI vehicles and two wall-guided GDI vehicles over the FTP and UC test cycles using a light-duty chassis dynamometer.

For THC, CO, and NO_x emissions, the results did not show strong fuel trends. Although some fuel differences were identified, these differences were generally not consistent for both cycles on a particular vehicle, or for more than one of the vehicles. The lack of strong trends indicates advancements in catalyst technology and air/fuel ratio control are reducing the impact of fuel differences on exhaust emissions. Our results also indicated that THC, CO, and NO_x emissions were predominantly obtained during the cold-start phase, when the catalyst was temporarily cold and inactive. CO_2 emissions showed reductions in some cases for the higher alcohol blends, while fuel economy based on the carbon balance method showed decreases with increasing alcohol concentration in the fuel. PM mass was substantially lower for the PFI vehicles compared to the GDI vehicles. PM mass emission results for the GDI vehicles showed reductions with the fuels with the highest oxygen levels for a number of the vehicle/cycle combinations, but not necessarily

the blends with the intermediate oxygen levels. Analogous to PM mass, particle number emissions were significantly lower for the PFI-fueled vehicles compared to the GFDI vehicles. In general, particle number emissions showed reductions with increasing ethanol and butanol concentration in the fuel, with these differences being statistically significant for some fuels and some vehicles but not for others.

4.5. Acknowledgements

This study was supported by the California Energy Commission (CEC) under contract 500-09-051. D. Short was supported under University of California Transportation Center (UCTC) and D. Vu was supported under U.S. Environmental Protection Agency (EPA) STAR Fellowship Assistance Agreement no. FP-91751101. Black Carbon Measurements were made possible by EPA grant number 83504001. The contents are solely the responsibility of the grantee and do not necessarily represent the official views of the EPA. Further, the EPA does not endorse the purchase of any commercial products or services mentioned in the publication. The authors thank Mr. Kurt Bumiller, Kevin Castillo, Michelle Ta, and Danny Gomez of the University of California, Riverside for their contribution in conducting the emissions testing for this program.

4.6. References

Aakko P, Nylund NO. 2003. Particle emissions at moderate and cold temperatures using different fuels. SAE Technical Paper 2003-01-3285.

Aleiferis, P.F., Romunde, Z.R. van, 2013. An analysis of spray development with iso-octane, n-pentane, gasoline, ethanol, and n-butanol from multi-hole injector hot fuel conditions, Fuel, 105, 143-168.

Alkidas AC. 2007. Combustion advacements in gasoline engines. Energy Conversion and Management, 48:2751-2761.

Bielaczyc P, Woodburn J, Klimkiewicz D, Pajdowski P, Szczotka A. 2013. An examination of the effect of ethanol-gasoline blends' physicochemical properties on emissions from a light-duty spark ignition engine. Fuel Processing Technology, 107:50-63.

Cooney C, Wallner T, McConnell S, Gillen JC, Abell C, Miers SA, Naber JD. 2009. Effects of blending gasoline with ethanol and butanol on engine efficiency and emissions using a direct-injection, spark-ignition engine. Proceedings of the ASME Internal Combustion Engine Division 2009 Spring Technical Conference, ICES2009-76155, May 6-9, 2009, Milwaukee, Wisconsin, USA.

Dernotte J, Mounaim-Rousselle C, Halter F, Seers P. 2010. Evaluation of butanol-gasoline blends in a port fuel-injection, spark-ignition engine. Oil & Gas Science and Technology-Rev. IFP, 65:345-351.

Durbin TD, Miller JW, Younglove T, Huai T, Kathalena Cocker. 2007. Effects of Fuel Ethanol Content and Volatility on Regulated and Unregulated Exhaust Emissions

for the Latest Technology Gasoline Vehicles," Environ Sci Technol, 41:4059-4064.

Gautam M, Martin DW, Carder D. 2000. Emissions characteristics of higher alcohol/gasoline blends. Proc Instn Mech Engrs, Part A: Journal of Power and Energy, 214:165-182.

Graham LA, Belisle SL, Baas CL. 2008. Emissions from light duty gasoline vehicles operating on low blend ethanol gasoline and E85. Atmospheric Environment, 42:4498-4516.

Gu X, Huang Z, Cai J, Wu X. 2012. Emissions characteristics of a spark-ignition engine fuelled with gasoline-n-butanol blends in combination with EGR. Fuel, 93:611-617.

He X, Ireland JC, Zigler BT, Ratcliff MA, Knoll KE, Alleman TL, Tester JT. 2010. The impacts of mid-level biofuel content in gasoline on SIDI engine-out and tailpipe particulate matter emissions. SAE Technical Paper 2010-01-2125.

He X, Ratcliff MA, Zigler BT. 2012. Effects of gasoline direct injection engine operating parameters on particle number emissions. Energy and Fuels, 26:2014-2027.

Jin C, Yao M, Liu H, Lee CFF, Ji J. 2011. Progress in the production and application of n-butanol as a biofuel. Renewable and Sustainable Energy Reviews, 15:4080-4106.

Karavalakis G, Durbin TD, Shrivastava M, Zheng Z, Villela M, Jung H. 2012. Impacts of ethanol fuel level on emissions of regulated and unregulated pollutants from a fleet of gasoline light-duty vehicles. Fuel, 93:549-558.

Knoll K, West B, Huff S, Thomas J. 2009. Effects of mid-level ethanol blends on conventional vehicle emissions. SAE Technical Paper 2009-01-2723.

Koc M, Sekmen Y, Topgul T, Yucesu HS 2009. The effects of ethanol-unleaded gasoline blends on engine performance and exhaust emissions in a spark-ignition engine. Renewable Energy, 34:2101-2106.

Liu FJ, Liu P, Zhu Z, Wei YJ, Liu SH. 2012. Regulated and unregulated emissions from a spark-ignition engine fuelled with low-blend ethanol-gasoline mixtures. Proc Instn Mech Engrs, Part D: Journal of Automobile Engineering, 226:517-528.

Masum BM, Masjuki HH, Kalam MA, Rizwanul Fattah IM, Palash SM, Abedin MJ 2013. Effect of ethanol-gasoline blend on NOx emission in SI engine. Renewable and Sustainable Energy Reviews, 24:209-222.

Maricq MM, Szente JJ, Jahr K. 2012. The impact of ethanol fuel blends on PM emissions from a light-duty GDI vehicle. Aerosol Science and Technology, 46:576-583.

Maricq MM, Szente JJ, Adams J, Tennison P, Rumpsa T. 2013. Influence of mileage accumulation on the particle mass and number emissions of two gasoline direct injection vehicles. Environ. Sci. Technol., 47:11890-11896.

McEnally C, Pfefferle L. 2013. Fuel decomposition and hydrocarbon growth processes for oxygenated hydrocarbons: butyl alcohols. Proc Combust Inst., 30:1363-1370

Merola SS, Valentino G, Tornatore C, Marchitto L. 2013. In-cylinder spectroscopic measurements of knocking combustion in a SI engine fuelled with butanol-gasoline blend. Energy, 62:150-161.

Merola SS, Tornatore C, Marchitto L, Valentino G, Corcione FE. 2012. Experimental investigations of butanol-gasoline blends on the combustion process in a SI engine. International Journal of Energy and Environmental Engineering, 3:1-14.

Piock W, Hoffmann G, Berndorfer A, Salemi P, Fusshoeller B. 2011.Strategies towards meeting future particulate matter emission requirements in homogeneous gasoline direct injection engines. SAE Technical Paper 2011-01-1212.

Schifter I, Diaz L, Rodriguez R, Salazar L. 2011. Oxygenated transportation fuels. Evaluation of properties and emission performance in light-duty vehicles in Mexico. Fuel, 90:779-788.

Schulz M. Clark S. 2011. Vehicle emissions and fuel economy effects of 16% butanol and various ethanol blended fuels (E10, E20, and E85). Journal of ASTM International, 8:1-19.

Storey JM, Barone T, Norman K, Lewis S. 2010. Ethanol blend effects on direct injection spark-ignition gasoline vehicle particulate matter emissions. SAE Int. J. Fuels Lubr., 3:650-659.

Storey J, Barone T, Thomas J, Huff S. 2012. Exhaust Particle Characterization for Lean and Stoichiometric DI Vehicles Operating on Ethanol-Gasoline Blends. SAE Technical Paper 2012-01-0437.

Szwaja S, Naber JD. 2010. Combustion of n-butanol in a spark-ignition IC engine. Fuel, 89:1573-1582.

Szybist JP, Youngquist AD, Barone TL, Storey JM, Moore WR, Foster M, Confer K. 2011. Ethanol blends and engine operating strategy effects on light-duty spark ignition engine particle emissions. Energy and Fuels, 25:4977-4985.

Ultrafine particulate matter and the benefits of reducing particle numbers in the United States. A report to the Manufacturers of Emission Controls Association (MECA). Prepared by Gladstein, Neandross & Associates. July 2013; http://www.meca.org/resources/MECA_UFP_White_Paper_0713_Final.pdf

U.S. Environmental Protection Agency. Fuels and Fuel Additives, Renewable Fuel Standard; http://www.epa.gov/otaq/fuels/renewablefuels

Wallner T, Frazee R. 2010. Study of regulated and non-regulated emissions from combustion of gasoline, alcohol fuels and their blends in a DI-SI engine. SAE Technical Paper 2010-01-1571.

Wallner T, Miers SA, McConnell S 2009. A comparison of ethanol and butanol as oxygenates using a direct-injection, spark-ignition engine. Journal of Engineering for Gas Turbines and Power, 131:1-9.

Whelan I, Samuel S, Timoney D, Hassaneen A. 2010. Characteristics of nano-scale particulates from gasoline turbo-intercooled direct-injection engine. SAE Technical Paper 2010-01-2197.

Xue C, Zhao XQ, Liu CG, Chen LJ, Bai FW. 2013. Prospective and development of butanol as an advanced biofuel. Biotechnology Advances, 31:1575-1584.

Zhang S, McMahon W, Toutoundjian H, Cruz M, Frodin B. 2010. Particulate mass and number emissions from light-duty low emission gasoline vehicles. SAE Technical Paper 2010-01-0795.

Zhao F, Lai MC, Harrington D. 1999. Automotive spark-ignited direct-injection gasoline engines. Prog. Energy Combust. Sci., 25:437–562.

Chapter 5: Particle Speciation of Light-Duty PFI and GDI vehicles on Mid-Level Ethanol and Iso-Butanol Gasoline Blends

5.1. Introduction

Port-fuel injection (PFI) vehicles have represented the vast majority of the U.S. light-duty vehicle (LDV) market for several decades. Gasoline direct injection (GDI) vehicles have recently garnered attention due to their increased fuel economy and reduced carbon dioxide (CO_2) emissions. These vehicles are predicted to dominate the U.S. market in the next few years (Graham, 2005; Zhao et al., 1999). For PFI systems, the fuel is injected into the intake ports outside the combustion chamber during the intake stroke as the air moves into the combustion chamber. GDI engines, on the other hand, use an injection system similar to that used in diesel engines, but at a much lower pressure (Alkidas et al. 2007). For the GDI engines, the fuel is injected directly into the combustion chamber during the intake stroke, which provides higher thermodynamic efficiency and lower greenhouse gas emissions. The drawback is that direct injection of fuel can lead to liquid fuel wetting on the piston bowl and cylinder surfaces and fuel-rich zones during combustion, which will likely result in higher emissions of particulate matter (PM) (Stevens and Steeper 2001; Piock et al. 2011). A number of studies have shown that GDI vehicles produce higher PM and particle number (PN) emissions compared to their PFI counterparts (Liang et al., 2013; Aakko et al., 2003; Ristimaki et al., 2005; Mamakos et al. 2013; Szybist et al., 2011; and references therein). PM can affect regional air quality, human health, and climate (IPCC, 2007; Nauss et al., 1995; Davidson et al., 2005; Andreae et al., 1997; Baumer et al., 2008; Avol et al., 1979;

Twomey et al., 1977; and references therein). Particles below 2.5 μm, ($PM_{2.5}$) can be inhaled deep within the lungs and can be deposited in the nose and subsequently access the brain (Nauss et al. 1995; Yang et al. 2009; Oberdorster et al., 2001; Oberdorster et al., 2004). Long-term exposure to $PM_{2.5}$ has been linked to cardiovascular and pulmonary diseases (Pope et al., 2004; Mills et al., 2009). Hence, the number and size distributions of ultrafine particles from modern GDI and PFI vehicular emissions need to be characterized.

Particle chemical composition is also important. $PM_{2.5}$ that contains water-soluble material has the ability to form droplets. Particles that promote water vapor condensation and form droplets are termed Cloud Condensation Nuclei (CCN). By behaving as CCN, inhaled hygroscopic particles can grow to droplet sizes and enhance harmful PM deposition rates (Longest et al., 2010). In addition to affecting health, CCN emissions of water-soluble particles affect climate by altering cloud droplet formation and cloud properties (Ervens et al., 2005).Water-soluble PM can be toxic when inhaled (Ramgolam et al., 2009; Guetterez-Castillo et al., 2006; Valavanidis et al., 2008; Squire, 1958 and references therein), and water-soluble particles have the ability to induce DNA damage (Guetterrez-Castillo et al., 2006). Water-soluble matter can cause pro-inflammatory response, thus promoting pulmonary and cardiovascular diseases (Ramgolan et al., 2009). Furthermore, water-soluble and water-insoluble organic materials (WSOC and WIOC) and metals from vehicular emissions are highly correlated with the cellular production of reactive oxygenated species (ROS) linked to toxicity and detrimental health effects (Cheung et al., 2009; Geller et al., 2006; Verma et al., 2010; Biswas et al., 2009).

Limited studies have characterized the water-insoluble/soluble composition of gasoline vehicle emissions. Cheung et al. (2009) reported water-soluble organic mass (WSOM) and water-insoluble organic mass (WIOC) emissions from a PFI vehicle fueled with gasoline. The WSOC and WIOC were each found to compose ~20%, respectively, of the total PM mass. Small amounts of elemental carbon (EC) were also emitted in their study (Cheung et al., 2009). To the best of our knowledge, little to no studies have characterized the water-insoluble/soluble composition from light-duty PFI and GDI vehicles with different alcohol fuel formulations. The addition of oxygenated fuels, such as ethanol and iso-butanol, can alter the resulting particle chemical composition and hygroscopicity. Thus, the potential influence of emissions of gasoline blends with different alcohols is not completely understood, especially with respect to regional air quality, health, and climate.

Black carbon (BC) is another important component of the vehicular PM composition. Black carbonaceous materials (i.e., soot or EC) are considered a significant source of insoluble material. Limited studies have investigated the contribution of BC to particle emissions from light-duty vehicles, especially as a function of different fuel compositions (Forestieri et al., 2013). Dutcher et al. (2011) found a decreasing trend of BC concentrations using an aetholometer with increasing ethanol content in gasoline in a PFI engine on an engine dynamometer. Giechaskiel et al. (2010) reported a ~90% increase in BC concentrations with increased vehicle speed from 50 to 140 km/h.

The objectives of this study are to evaluate the emissions of gasoline PFI and DI vehicles over a range of ethanol and iso-butanol blends with an emphasis on characterizing

particle hygroscopcity. Five vehicles were tested on seven fuels over the Federal Test Procedure (FTP), the Unified Cycle (UC), and at steady-state speeds. This study investigates how factors, such as fuel type and driving cycle influence particle hygroscopicity, BC, WSOC, surface tension, and water-insoluble fractions.

5.2. Testing Facility and Experimental Set-up

5.2.1. Test Vehicles, Fuels, and Driving Cycles

Three light-duty PFI vehicles and two GDI vehicles were tested for this study. The PFI vehicles tested were a 2007 Honda Civic, 2007 Dodge Ram, and 2012 Toyota Camry. The GDI vehicles tested include the 2012 Kia Optima and 2012 Chevrolet Impala. Vehicle specifications can be found in Karavalakis et al. 2014.

A total of seven fuels were employed in this study, including ethanol and iso-butanol blends. Each vehicle was tested on E10 (10% ethanol and 90% gasoline), E15, and E20 blends. In addition to the ethanol blends, iso-butanol blends were used including B16 (16% iso-butanol and 84% gasoline), B24, and B32. The butanol blends of B16, B24, and B32 were the oxygenated equivalent of E10, E15, and E20, respectively. An alcohol mixture comprising of 10% ethanol and 8% iso-butanol (E10/B8) was also used in this study. It should be noted that only the Toyota Camry and the Kia Optima were tested on the E10/B8 fuel blend. The fuels were custom made to maintain Reid Vapor Pressure (RVP), oxygen content, and fuel volatility and other properties. The main fuel properties can be found elsewhere (Karavalakis et al., 2014) and in Appendix Table C-1.

Each vehicle was tested on each fuel over three FTPs and three UC tests, speed versus time plots for each cycle are shown in Appendix Fig. C-1. The 6 tests on a particular fuel were conducted sequentially once the vehicle was changed to operate on that fuel, and the fuel was not changed to another fuel during this time. A fuel change with multiple drain and fills was conducted between the testing on each fuel to condition the vehicle and ensure no carryover effects. Detailed information on the driving cycles employed in this study and the testing protocol can be found elsewhere (Karavalakis et al., 2013). After transient operation, the vehicles were driven at steady-state speeds of 30, 50, and 70 mph for each fuel. Thus, the steady-state emissions characterized the emissions from a "hot" catalyst. Due to operational constraints, not all fuels were tested at the steady-state speeds but all available data are presented.

The three steady-state speeds were driven for a duration of 30 minutes with 10 minutes for each steady state speed. The steady-state tests were performed after an FTP or UC test, the Three-Way Catalyst (TWC) and engine are both warm. Each vehicle was driven at 70 mph before the initial start of the test. The emission measurements would begin when the total particle concentration was steady without any large variation. The vehicles would be driven in the sequence of 70, 50, and 30 mph.

5.2.2. Emission Testing and Analysis

All tests were conducted in CE-CERT's Vehicle Emissions Research Laboratory (VERL), which is equipped with a Burke E. Porter 48-inch single-roll electric dynamometer. Gaseous and PM emissions were measured during each cycle and while the vehicle was operated at steady-state speeds. Appendix Fig. C-2 shows the

experimental set-up with flow rates of the various particle and gaseous instruments used for this study. A Pierburg AMA-4000 bench was used for gaseous emissions. Total particle number (PN) was measured with a TSI-3776 condensation particle counter (CPC). Results from both the PN and criteria pollutants from this study are provided in a separate journal article (Karavalakis et al., 2014).

BC concentrations were measured with a Multi-Angle Absorption Photometer (MAAP). The MAAP concentrates aerosol onto a Teflocarbon filter paper where a light with a 670nm wavelength emits photons toward the aerosol concentrated area (Petzold et al., 2004). The backscattering of photons was used to infer the mass of BC. The MAAP was calibrated with two techniques. In the first technique, the temperature sensors and air flow rates were verified to be within 5% error of environmental conditions. For the second method, BC from a solutions of Aquadag© was aerosolized and the mass concentration was simultaneously measured with an Aerosol Particle Mass (APM, Kanomax Model 3600) Analyzer and the MAAP (Schwarz et al. 2006). The Aquadag calibration showed the MAAP measurements were within ±11% of APM measurements.

Online particle hygroscopicity and soluble-fraction properties were estimated using a technique published in (Short et al., 2014). Briefly described here, the technique exploits discrepancies in particle size distributions measurements from a Water-based Condensation Particle Counter (W-CPC, TSI Model 3785) and Butanol-based CPC (B-CPC, TSI Model 3772). The two CPCs were connected in parallel with an electrostatic classifier (TSI Model 3080). The electrostatic classifier charges the particles with a Kyrpton-85 radiation source, size selects the dry polydisperse flow with a differential

mobility analyzer (DMA, TSI Model 3081L) and generates a mono-disperse stream (Wang et al., 1990). The monodisperse particles were then counted by both CPCs.

The differences in the CPC particle counts below 250 nm are calculated by taking the ratio between the W-CPC and B-CPC instruments. The discrepancies between the two instruments, usually below 40 nm are attributed to the particle hygroscopicity (Short et al. 2014). The experimental method was calibrated through the aerosolization of ammonium sulfate. The corresponding theoretical equivalent diameter for activation, d_s, measured for ammonium sulfate was 20.5 nm, corresponds to a κ value that is equivalent to the known theoretical κ value for ammonium sulfate published in Petters and Kreindenweis (2007). The determination of κ is described in Section 5.3.5. The term d_s is a particular particle diameter at which 50% of all particles were counted within the W-CPC. This was determined from the ratio of W-CPC to B-CPC particle counts. In this study, the Kelvin term, governed by the bulk fluid surface tension, was verified to have little to no effect on the water droplet activation properties.

The water-insoluble mass (WIM) fraction calculations were estimated for all three vehicles over the entire cycle and for each phase within the cycle. The overall cycle WIM fraction was calculated in a further step. Instead of comparing the CPC discrepancies from each 135 second SMPS scan, each diameter particle count was summed over the entire cycle. Thus, giving an overall cycle d_s to provide an overall cycle κ_{am}.

5.2.3. Emission Factor

BC concentrations were reported in this study in units of μg mi^{-1}, or the emission factor (EF) of BC. The average BC concentration (μg m^{-3}), measured from the CVS, was multiplied for each phase by the total volume of air through the CVS during each cycle phase (m^{-3}). The total BC mass for each phase is expressed in μg. The EF of BC was calculated as follows:

$$EF(BC) = 0.43\frac{BC_1+BC_2}{x_1+x_2} + 0.57\frac{BC_2+BC_3}{x_2+x_3} \qquad (1)$$

The numerator in these fractions includes terms for the total BC mass for each phase. For example, the total BC mass for phase 1 is BC_1. The denominator, x, is the total mileage traveled for each phase. For example, x_1, includes terms for the total mileage for phase 1. The constant values 0.43 and 0.57 are weighing factors used to proportion the different phases of the cycle during vehicle certification.

5.2.4. Water-Soluble Organic Carbon and Surface Tension Measurements

Teflon filter samples were taken for each transient cycle test. Hence, the WSOC and surface tension measurements were representative of the cumulative aerosol composition over the FTP and UC. Filters were placed in vials and sonicated for 90 minutes with 60 mL of Millipore© DI water (18 mΩ, < 100ppb). Once sonicated, large non-dissolved particles were removed using a Whatman© 25mm syringe filter. For the

WSOC analysis, the sample was then diluted into ratios of 1:1, 1:3, and 1:5, with each vial containing 30 mL of sample. The surface tension, σ_b, for each sample was measured with a pendant drop tensiometer (Attension Theta 200). The tensiometer is an optical unit that uses the Young-Laplace equation to compute the droplet surface tension. For each droplet, 100 images were captured. The WSOC concentrations of these samples were measured using a GE Seivers 900 Total Organic Carbon (TOC) analyzer. Once the WSOC concentration was determined, the water-soluble organic mass (WSOM) can be found by multiplying the WSOC concentration by the volume of the initial water soluble and the constant 1.2. The constant 1.2 (derived from Turpin and Lim (2001)) is an estimate of the average organic molecular weight per carbon weight. WSOM was reported as an emission factor in units of mg mi^{-1}. The WSOM emission factor was not calculated based on emissions per phase as in the BC emission factor. This emission factor was calculated using the filter loading parameters and divided by the total mileage for each cycle. The WSOM value was divided by the total PM mass to compute the WSOM fraction.

5.2.5. Water-Insoluble Mass Fraction Analysis

Rapid droplet growth in CPCs is possible when the saturation value, *S*, the ratio of the partial pressure (P_v) to the saturation pressure (P_{sat}) is greater than 1. Köhler's theory (Köhler, 1936) predicts the heterogeneous condensation of a bulk fluid vapor with a value *S* into the droplet phase (Eq. 2).

$$S = \frac{P_v}{P_{sat(T)}} = a_b \, exp\left(\frac{4M_b\sigma_b}{\rho_b RTD}\right) \qquad (2)$$

where R is the universal gas constant, T is the temperature at activation, D is the wet droplet diameter, ρ_b is the density of the bulk fluid condensing onto the particle (water or butanol), M_b is the molecular weight of the bulk fluid, σ_b is the surface tension at the droplet vapor/liquid interface, and a_b is the activity of solute in the bulk fluid. A critical supersaturation, s_c (equal to critical saturation, S_c-1), exists for which a minimum layer of condensed water on a particle is required to form a droplet. If s_c>2% for both water and butanol CPCs; then uncontrollable particle growth will occur for particles above 40nm. When σ_b is ideal and that of the fluid, changes in particle activation for a given bulk fluid are controlled by the dissolved solute properties and the activity of the droplet solution.

The fluid activity, a_b, for the water droplet can be approximated by Raoult's Law. The rearrangement of Eq. 2 yields

$$\ln s_c = \left(\frac{4A^3}{27B}\right)^{1/2}, \quad A = \frac{4M_b\sigma_b}{\rho_b RT} \quad \text{and} \quad B = \frac{6n_s M_b}{\pi\rho_b} \tag{3}$$

where n_s is the moles of solute and v is the ion dissociation of the particle in water. For a spherical solute particle, n_s is related to the dry particle diameter, d_s, the density of the particle, ρ_s and the molecular weight of the particle, M_s such that s_c and d_s are related as follows.

$$\ln {s_c}^2 = \frac{4A^3\rho_b M_s}{27v\rho_s M_b {d_s}^3} \tag{4}$$

At a given s_c, d_s is the theoretical critical diameter for activation, and the smallest diameter required for a fluid to condense on the particle surface. The d_s value is obtained by finding the 50% efficiency of the ratio of W-CPC to B-CPC counts. It is an indication

of the particle hygroscopicity that can be represented by a single solute parameter, κ (Petters and Kreindenweis, 2007). κ characterizes the effects of solute composition for droplet activation, and is calculated from fixed CPC s_c and from direct measurements of d_s giving eq. 5.

$$\kappa = \frac{4A^3}{27 {d_s}^3 \ln(s_c)^2} \qquad (5)$$

κ can range from 0 to 1, which 0 is water insoluble and 1 is very water-soluble. Eq. 4 is similar to Eq. 3 but Eq. 4 assumes the σ_b properties are that of a pure fluid. The κ values in Eq. 4 determine particle hygroscopicity. Assuming the particle is comprised of a completely water-soluble or water-insoluble compound, κ-hygroscopicity can be directly used to estimate a particles water-insoluble contribution (Petters and Kreindenweis, 2007). Water-insoluble composition changes can be approximated using a two-component model of a soluble and insoluble solute material. For our model, sulfuric acid (κ_{sa} =.9) and dioctyl phthalate (κ_{DOP} =.03) are used. Sulfuric acid has been measured in vehicular diesel exhaust and is believed to contribute to new particle formation through nucleation. Dioctyl phthalate (DOP) has been studied as a proxy for water-insoluble particle material from vehicular exhaust. With these model components, Eq. 6 estimates the water-insoluble mass fraction, χ.

$$\kappa_{am} = \kappa_{sa}(1 - \chi) + \kappa_{DOP}(\chi) \qquad (6)$$

κ_{am} is the measured hygroscopicity of the unknown composition. The WIM fractions are within 15% error uncertainty of chemical compositions (Short et al 2014).

5.3. Results

5.3.1. Significant PN, PM mass, and Particle Size Distribution Vehicle Trends

Results for measurements of the particle hygroscopicity and BC concentrations for each steady-state speed, the WIM fractions by each cycle phase and for the overall cycle, WSOM EFs and WSOM/PM Mass fractions, and BC EFs and BC/PM mass fractions are provided in this section. Karavalakis et al. (2014) reported additional information on the PM mass and PN emissions from these five vehicles previously. As this background information provides some basis for understanding the results in the current study, these results are briefly summarized here. The PM mass emissions ranged from 0.1 to 1.45 mg/mi for the PFI vehicles and from 1.8 to 7.23 mg/mi for the GDI vehicles, while the PN emissions for the PFI vehicles ranged from $4.9x10^{10}$ #/mi to $6.3x10^{11}$ #/mi, and for the GDI vehicles ranged from $4.1x10^{12}$ #/mi to $2.4x10^{13}$ #/mi. Thus, the GDI vehicles had 5 times more PN and PM mass emissions compared to the PFI vehicles. Particle size distributions (PSDs) were measured for only the PFI vehicles in Karavalakis et al. 2013. The size distributions show that the majority of the particles are in the nucleation mode (Karavalakis et al. 2013). Although PSDs were not measured for the GDI vehicles, Storey et al. 2010 has shown that the mode diameter is approximately ~50 nm, or in the accumulation mode size range under steady-state driving conditions.

5.3.2 Steady- State BC and Hygroscopicity

The hygroscopicity estimates for sub-40 nm particles for all test vehicles during the steady-state conditions of 30, 50, and 70 MPH are shown in Fig. 5-1 for the PFI vehicles and 5-2 for the GDI vehicles. The data shows that hygroscopicity increases with increasing vehicle speed. The higher κ_{am} is equivalent to lower amounts of water-insoluble PM. At 70 mph, all vehicles had the highest kappa or hygroscopicity values. The GDI vehicles and the Toyota Camry had κ_{am} values above 1.5 at 70 mph, which were higher than those for the Dodge Ram and Honda Civic. It is important to note that most of the κ_{am} values at the 70 mph and 50 mph speeds for these fuels and vehicles are larger than the reported κ for sulfuric acid (i.e., $\kappa_{am} > 0.9$), a common soluble vehicular emission. Hence, using a simple two component model of sulfuric acid and DOP does not fully capture the WIM fraction of the aerosol. In fact, the estimated WIM fractions are actually negative, so these values are not shown. This indicates that the particles are very hygroscopic and can be considered fully wettable and water-soluble. It should be noted that $\kappa_{am} > 1$ corresponds to an activation diameter below 10 nm, since particle sizes below 10 nm fall below from the lower detection limit of the SMPS, it is difficult to accurately characterize differences in κ_{am} values > 1. Hence, particles at both 50 and 70 mph are likely both similar in nature to sulfuric acid or sulfate, which have κ_{am} values just below 1. Furthermore, surfactant effects (though negligible in the measured filters, which were not collected at steady-state speeds) could play a role at higher speeds. As these surfactants could be condensing onto the particle surface thus changing the perceived hygroscopicity. This is further described in Section 5.4.3. Most particle emissions at 30

MPH were water-insoluble. At 30 MPH, all five vehicles have κ_{am} values that are significantly lower than their respective 70 MPH κ_{am} values. Decreasing vehicle speed decreased the hygroscopicity of PM from all tested vehicles.

BC concentrations are also shown to be higher with increased vehicle speeds for each of the test vehicles, Fig. 5-1 and 5-2. The GDI vehicles and the Toyota Camry showed larger BC decreases with decreasing vehicle speed than the Dodge Ram and Honda Civic. The Dodge Ram on the E10 fuel had a 16% decrease in BC concentration compared to a 93% decrease for the Toyota Camry between the 70 MPH to 30 MPH steady-state speeds. In addition, the Kia Optima and Chevrolet Impala had a 75% and 71% decrease, respectively, in BC concentration from the 70 MPH to 30 MPH speeds for the E10 fuel.

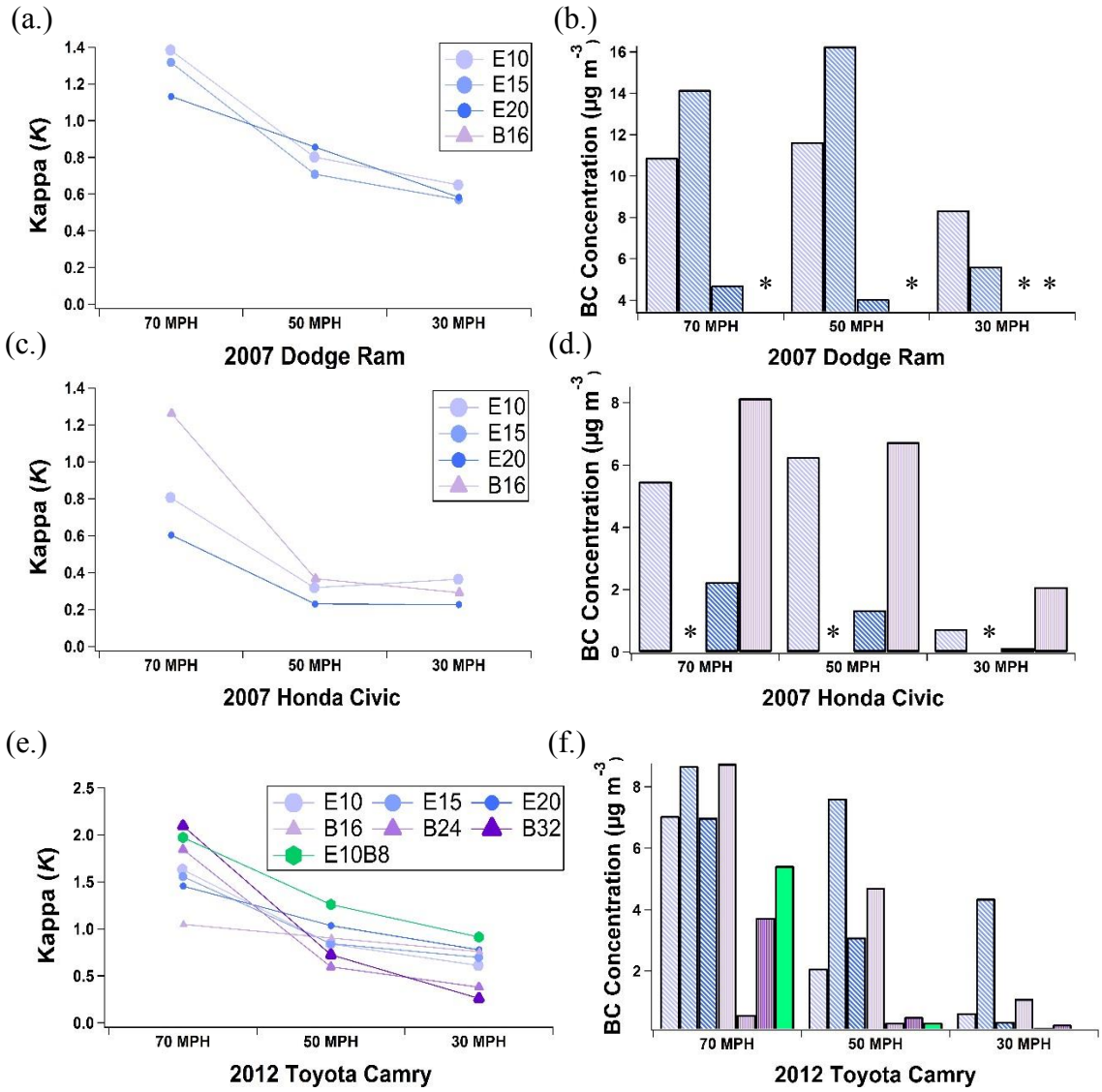

Fig. 5- 1. The particle hygroscopicity parameter (κ) and BC concentrations for 3 steady-state speeds of 70, 50, and 30 MPH for the 2007 Honda Civic {κ (a.) and BC (b.)}, 2007 Dodge Ram {κ (c.) and BC (d.)}, and 2012 Toyota Camry {κ (e.) and BC (f.)} * Denotes data unavailable

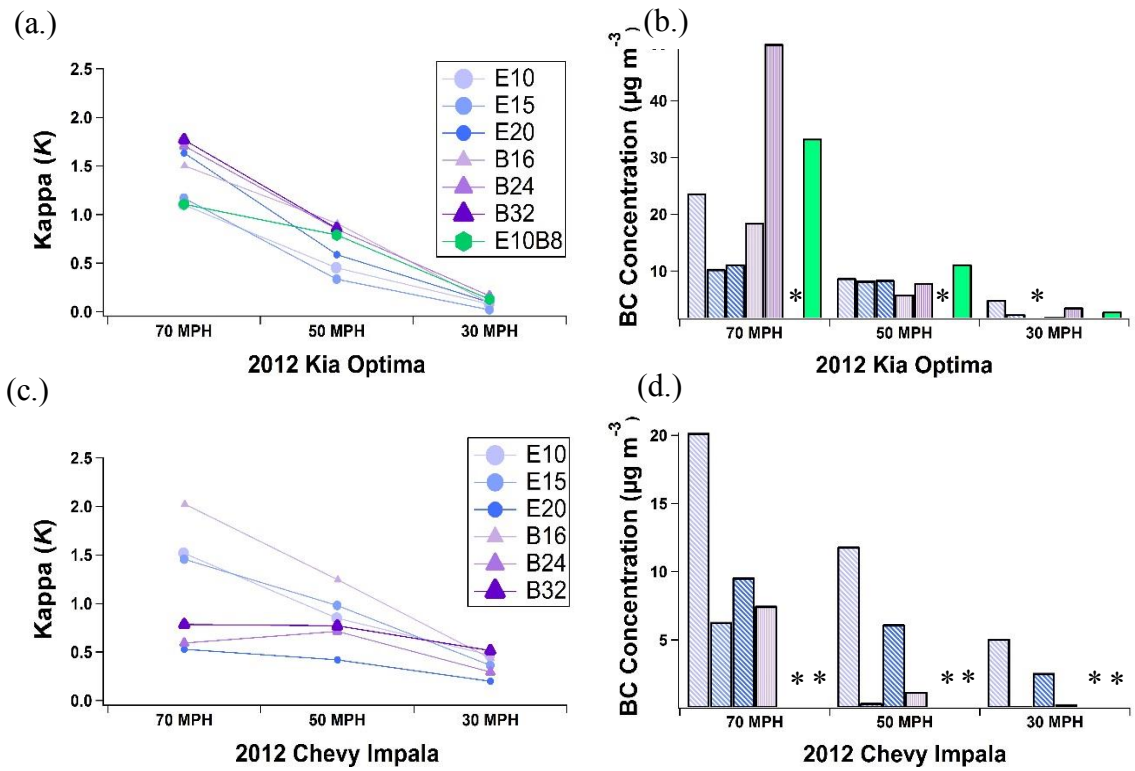

Fig. 5- 2. The particle hygroscopicity parameter (κ) and BC concentrations for 3 steady-state speeds of 70, 50, and 30 MPH for the 2012 Kia Optima {κ (a.) and BC (b.)}, and 2012 Chevy Impala {κ (c.) and BC (d.)}. * Denotes data unavailable

5.3.3 Water-Insoluble Mass Fraction

Fig. 5-2 and Fig. 5-3 show the WIM fractions of each cycle phase and the cumulative WIM fractions, respectively, for all five vehicles. High WIM fractions indicate that particles emitted over the FTP cycle were mostly water-insoluble for all five vehicles. However, the UC shows different trends for the WIM fractions by phase. For the UC cold-start and hot-start phases for all vehicles, WIM emissions fractions remain similar to those for the FTP. The Honda Civic, Dodge Ram, and Kia Optima, on the other hand, all show WIM fractions for the hot-running phase of the UC that decrease

compared to the cold-start and hot-start phases. Higher vehicles speeds occur during the hot-running phase of the UC. These decreases were consistent with the results for the hygroscopicity measurements during steady-state conditions. In particular, driving conditions with the highest speeds (i.e. the hot-running phase of the UC) and the 70 MPH steady-state speed show the lowest WIM fractions. A better understanding of particle solubility emission trends can be obtained by investigating the offline WSOM emission trends, as discussed below is Section 5.4.4. Over the FTP, the Toyota Camry exhibited lower WIM fractions compared to the other four vehicles. It should be noted that this vehicle, also had the lowest PM mass emission rates and the most prominent nucleation mode peak (Karavalakis et al. 2013).

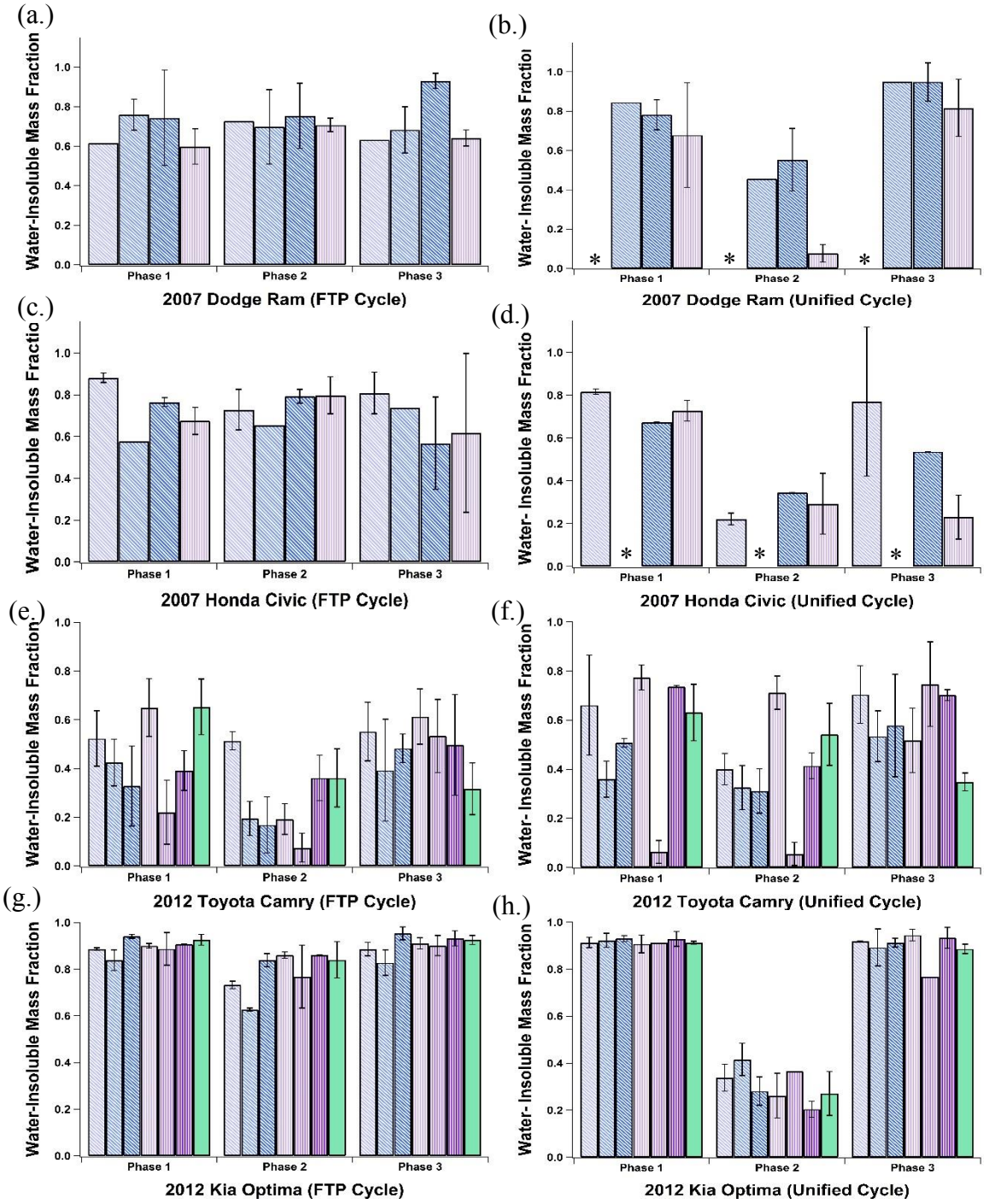

Fig. 5- 3 Estimated water-insoluble mass fraction by phase of both the FTP and Unified Cycles for the 2007 Honda Civic {FTP(a.) and Unified (b.)}, 2007 Dodge Ram {FTP (c.) and Unified (d.)}, 2012 Toyota Camry {FTP (e.) and Unified (f.)}, 2012 Kia Optima {FTP (g.) and Unified (h.)}, and 2012 Chevy Impala {FTP (i.) and Unified (j.)}. * Denotes data unavailable

The decrease in the WIM fraction between the cold-start and hot-running phases can be quantified for specific test fuels for different vehicles. When comparing the E10 fuel for the Honda Civic over the UC, a 70% decrease in the WIM fraction is shown from the cold-start to hot-running phase. For the E15 fuel on the Dodge Ram over the UC, a 44% decrease of the WIM fraction was shown from the cold-start to hot-running phase. The Kia Optima had the most consistent decrease in the WIM fraction over the UC for all fuels. For the E10 fuel, a 62% decrease in the WIM fraction was shown from the cold-start to hot-running phase over the UC.

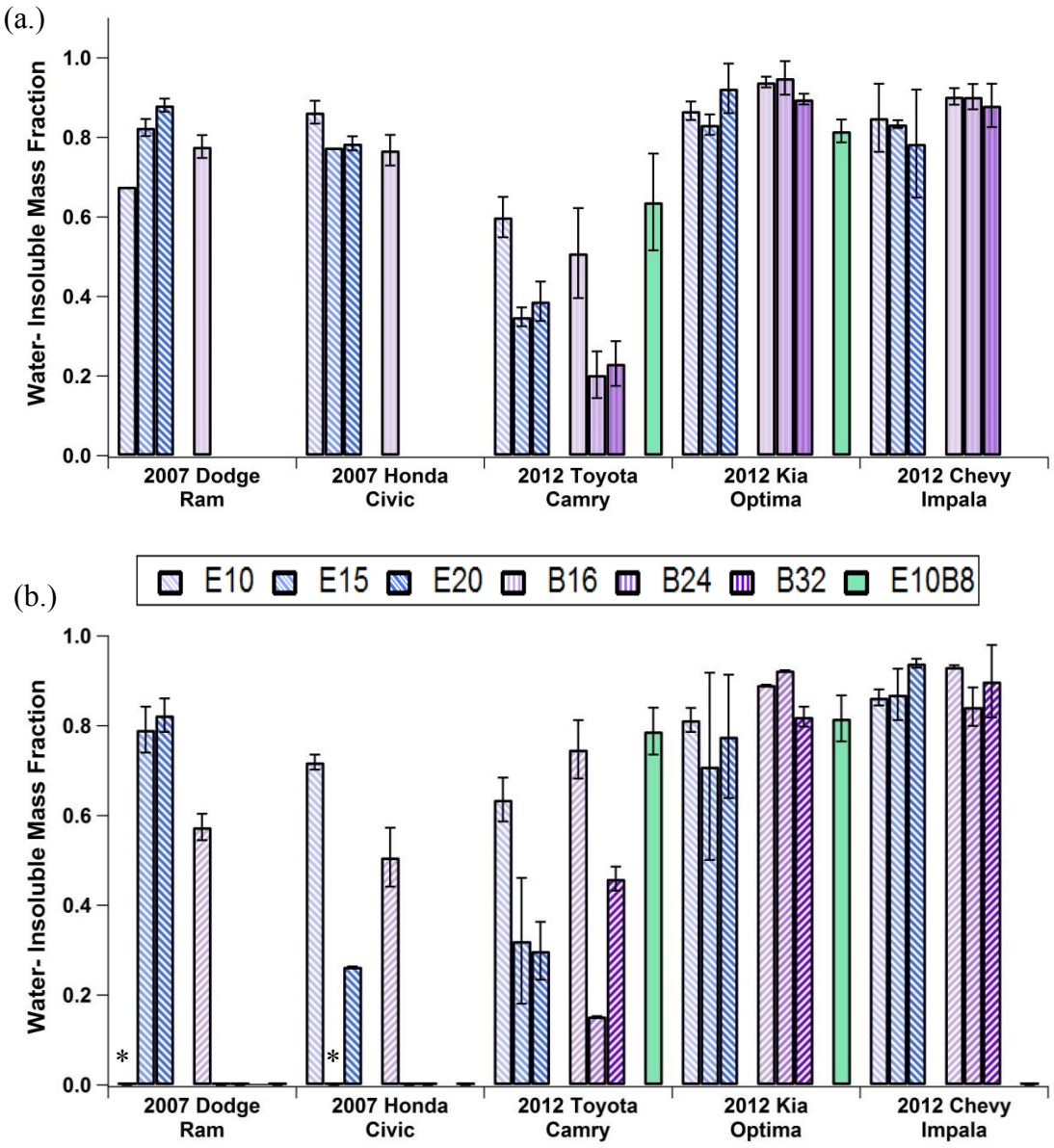

Fig. 5- 4. Estimated water-insoluble mass fraction over the entire FTP (a.) and UC Cycles (b.) * Denotes data unavailable

Cumulative PM emissions, over both the FTP and UC, were mostly water-insoluble as shown in Fig. 5-3. Both GDI vehicles over the FTP cycle have cumulative WIM fractions of ~0.9. The Honda Civic and Dodge Ram also have cumulative WIM

fractions over the FTP cycle of ~0.8. However, the Toyota Camry has lower cumulative WIM fractions compared to the other four vehicles. Similar trends were shown over the UC even though a decrease in the WIM fraction is seen for phase 2 of the UC. This was due to the cumulative WIM fractions being dominated by the cold-start phase of the cycle, as a significant majority of the particles are emitted in the cold-start phase. For both cycles, lower vehicle speeds (speed below 55 mph) are found during the cold-start phase. The cumulative WIM fractions show that the lower vehicle speeds during parts of the cycle where most of the particle are emitted produce higher water-insoluble particle emissions.

Fuel differences also changed the cumulative WIM fractions for some vehicles and fuels. The Toyota Camry was the only vehicle that had a consistent fuel trend over both cycles. Over the FTP cycle, the Toyota Camry showed a 53% decrease in the WIM fraction with increasing ethanol concentration from E10 to E20. The Toyota Camry, with increasing ethanol and iso-butanol fuel concentrations over the UC, also showed decreasing WIM fractions of 53% and 40%, respectively. The Honda Civic and the Dodge Ram both showed fuel effects over the UC. The Honda Civic had a 61% decrease in the WIM fraction from the E10 to the E20 fuel on the UC. The E10/B8 fuel was comparable to both the E10 and B16 gasoline blends for the Toyota Camry and Kia Optima, with a WIM fraction of 0.6. Comparing E10 to the B16 fuel blend over all five vehicles, B16 had a higher WIM fraction for the Toyota Camry and Kia Optima. For both GDI vehicles, the WIM fractions were similar when comparing fuels over both cycles.

Potential correlations between the WIM fractions and fuel properties can be examined for the Toyota Camry. Mono-aromatic compound concentration decreases with increasing alcohol concentration for both the ethanol and iso-butanol fuel blends, as shown in Table 5-1. The WIM fraction for the Toyota Camry also decreases with increasing alcohol concentration. Most mono-aromatic compounds (Toluene, Benzene, m-Xylene, etc.) are considered to be water-insoluble and highly volatile. When plotting the mono-aromatic concentration against the WIM fraction, a R^2 value of 0.70 is shown. Mono-aromatics don't make up all the water-insoluble particles below 40 nm measured in the cumulative WIM fractions for the Toyota Camry. Other water-insoluble components (i.e., BC and inorganic material) could also contribute to the WIM fraction. Thus explaining the low R^2 value shown for the correlation. This correlation only works with the Toyota Camry cumulative WIM fraction, as more sub-40 nm particles make up the total particle mass for this vehicle compared to the GDI vehicles. The GDI vehicles have a particle mode diameter much larger at ~50 nm according to Storey et al. 2010 so the mode diameter is above the detection limit of the WIM fraction measurement.

	E10	E15	E20	B16	B24	B32	E10/B8
Mono-Aromatics (wt %)	26.23	20.91	18.31	25.47	20.69	19.80	26.75
FTP (WIM Fractions)	0.5086	0.2310	0.2030	0.5990	0.3484	0.3875	0.6372
UC (WIM Fractions)	0.7469	0.1531	0.4592	0.6353	0.3208	0.2987	0.7878

Table 5- 1. Table of Mono-Aromatic concentrations in fuels tested with the averaged cumulative WIM Fractions over the FTP and UC for the Toyota Camry

The correlation in high vehicle speeds and increasing particle water-solubility cannot be explained with certainty. However, one particular phenomenon could help determine the cause of the trend. A possible hypothesis is that some water-insoluble particles are being coated with a more water soluble layer. Cruz and Pandis (1998) verified the reverse case, that a coating of DOP around a water-soluble component, such as ammonium sulfate, decreased the activation diameter, d_s. thus, affecting measured particle κ- hygroscopcity. Although DOP is very water-insoluble, it shows that it is possible to affect the perceived hygroscopicity of a particle by condensing different soluble material onto a particle. Our results may indicate that the condensing material is more soluble than the water-insoluble core. Iso-paraffin compounds have been shown to be able to break a part and oxidize (Yung-Fang 1980; Curan et al. 2002). These now oxidized compounds could be water-soluble material and condensing onto the particles emitted. The measured hygroscopicity of the particle is dictated by the composition on the surface of the particle rather than the particle core. Thus for our measurements, the composition of the particle surface decreased the actual particle hygroscopicity from highly water-insoluble to more water-soluble. Our results cannot definitively determine the composition of coatings that might be condensing on insoluble cores. Single particle chemical analysis was not collected here, but might provide additional information on possible soluble inorganic compounds. The bulk chemical composition information provides little information about particle morphology.

5.3.4. Water-Soluble Organic Mass Emission Factors and Surface Tension Analysis

The WSOM EFs are shown for both the Kia Optima and Chevrolet Impala over both cycles in Fig. 5-4 (a-b). In addition, the WSOM/PM mass fraction results are shown in Fig. 5-4 (c-d). These vehicles were selected for the WSOM analysis because they have the highest overall PM mass emissions. Note that the WSOM value is representative of the entire PM mass, whereas the WIM fractions in Section 5.5.3 only represent the mass. The WSOM EF can be compared to the total PM mass to understand the amount of soluble organic mass emitted over each cycle. The Chevrolet Impala had much higher WSOM/PM mass fractions compared to the Kia Optima. The WSOM/PM mass fractions for the FTP and UC ranged from 20% to 60%, respectively, over the Chevrolet Impala. The Kia Optima show fractions of ~20% of the total PM emissions for the FTP and UC.

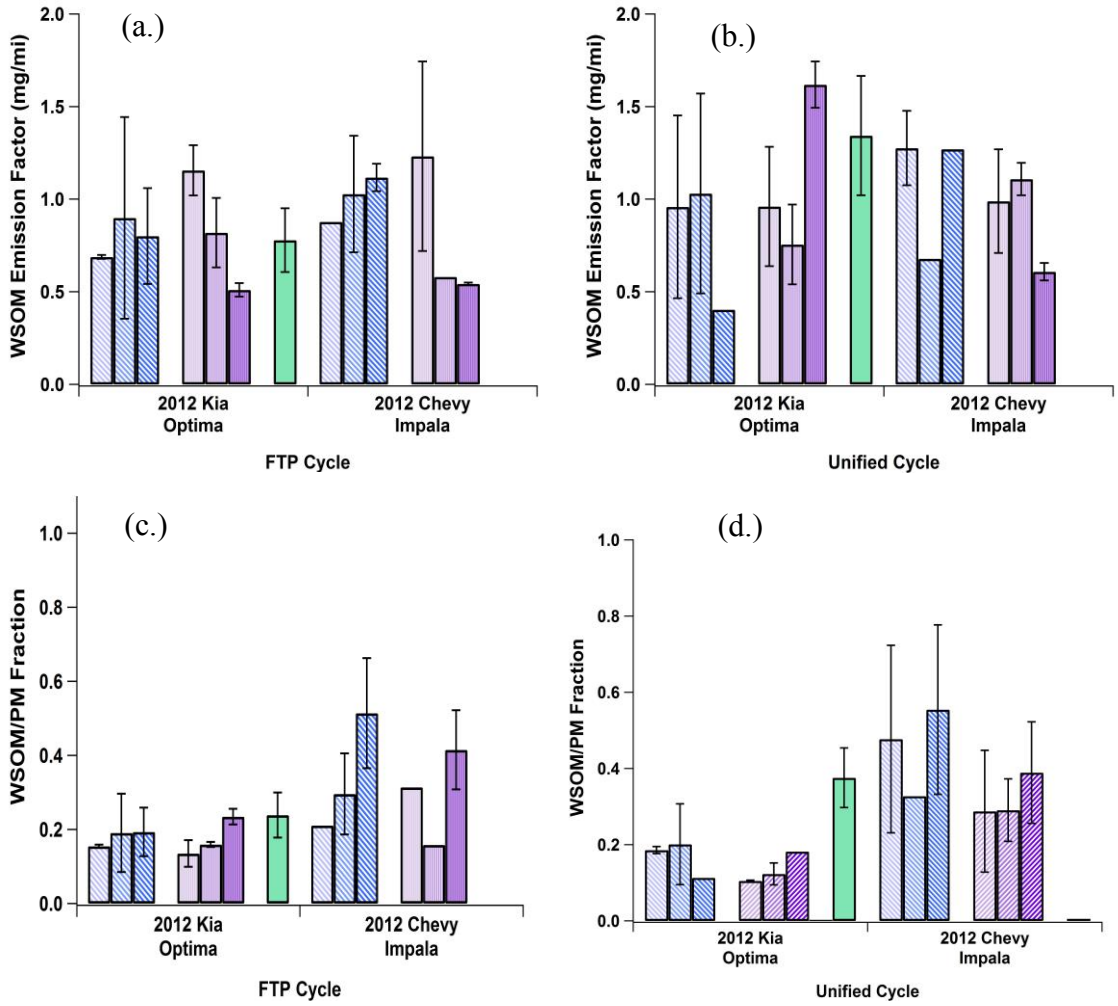

Fig. 5- 5. The Water-Soluble Organic Mass (WSOM) emission factors over the FTP (a.) and UC (b.) and WSOM/PM fractions over the FTP (c.) and UC (d.) for both the Kia Optima and Chevrolet Impala

Both the WSOM EFs and WSOM/PM mass fractions showed different fuel trends for both GDI vehicles. Generally, increasing iso-butanol concentration decreased the WSOM EF for both the vehicles and cycles, but the ethanol fuels did not show consistent trends. Over the FTP cycle, the Kia Optima and Chevrolet Impala exhibit a ~60% decrease in the WSOM emissions with increasing iso-butanol concentration. Over the

UC, the Kia Optima WSOM EF increased ~60% with increasing iso-butanol concentrations, but the WSOM EF decreased ~40% over the same fuels for the Chevrolet Impala. The Chevrolet Impala showed a ~ 21% increase in the WSOM emissions with increasing ethanol concentration. The fuel trends were slightly different for the WSOM/PM mass fractions. The Chevrolet Impala showed different trends in the WSOM/ PM mass fractions, while the Kia Optima shows WSOM/PM mass fractions there were consistently ~20% of the total PM emissions for the FTP and UC. For the Chevrolet Impala over the FTP, the WSOM/PM mass fraction increased 180% with increasing ethanol concentration from the E10 to E20 fuel, while the iso-butanol fuel blends show a ~40% WSOM fraction with a slight increase with increasing alcohol content.

For the Chevrolet Impala, the WSOM/PM mass results were not consistent with our WIM fractions measured in Sections 5.4.3, which showed relatively high levels of WIM. This lack of correlation is due to the PSDs. The PSDs for the Chevrolet Impala are in the accumulation mode, which makes most of the PN above the 40 nm threshold of the WIM fraction. Although part of the total amount of PN is below 40 nm, other water-insoluble material was above 40 nm making the WIM fraction not consistent with the WSOM/PM mass fraction. These results were relatively consistent with WSOM measurements from a Euro 3 compliant Toyota Corolla tested in Cheung et al. (2009), where ~20% of PM emissions were found to be WSOM.

Surface Tension was also measured for the same samples extracted for the WSOM analysis. The majority of these fuels and the vehicles have a surface tension that closely resembles the surface tension of water. The surface tension of water at 23°C and 1

atm is 72 mN/m. As a basis of comparison, the surface tension results are at a maximum with the E10 fuel on the Honda Civic at 73.55 mN/m and are around 71 mN/m for the Toyota Camry. The Kia Optima and Chevrolet Impala both have surface tension results on average of 72.95 mN/m ± 1.04 mN/m. As all the surface tension measurements are similar to the surface tension of water, this suggests that the assumption of pure water used in the kappa calculation (Section 2.5) is valid.

5.3.5. Black Carbon Emission Factors

BC also contributes to the particle mass. Fig. 5-5 shows the BC EFs for the FTP and UC for all five vehicles. The BC EFs showed significant differences from vehicle to vehicle, but were similar for the FTP and UC for any given vehicle. The GDI vehicles had the highest BC EFs of all five vehicles over both cycles, and show about 5 times the amount of BC compared to the PFI vehicles. This is comparable to the differences in total PM mass and PN between the GDI and PFI vehicles, as discussed in Section 5.4.1. The Kia Optima has slightly higher BC EFs overall (~800 μg mi^{-1}) compared to the Chevrolet Impala (~550 μg mi^{-1}) over the FTP cycle. Over the FTP cycle for the PFI vehicles, the Dodge Ram has the highest BC EF of the PFI vehicles over both cycles followed by the Honda Civic and the Toyota Camry, respectively. The Toyota Camry was the only vehicle that showed clear fuel trends over both cycles. Increasing ethanol and iso-butanol concentration over both cycles decreased BC EFs by 17% and 51%, respectively.

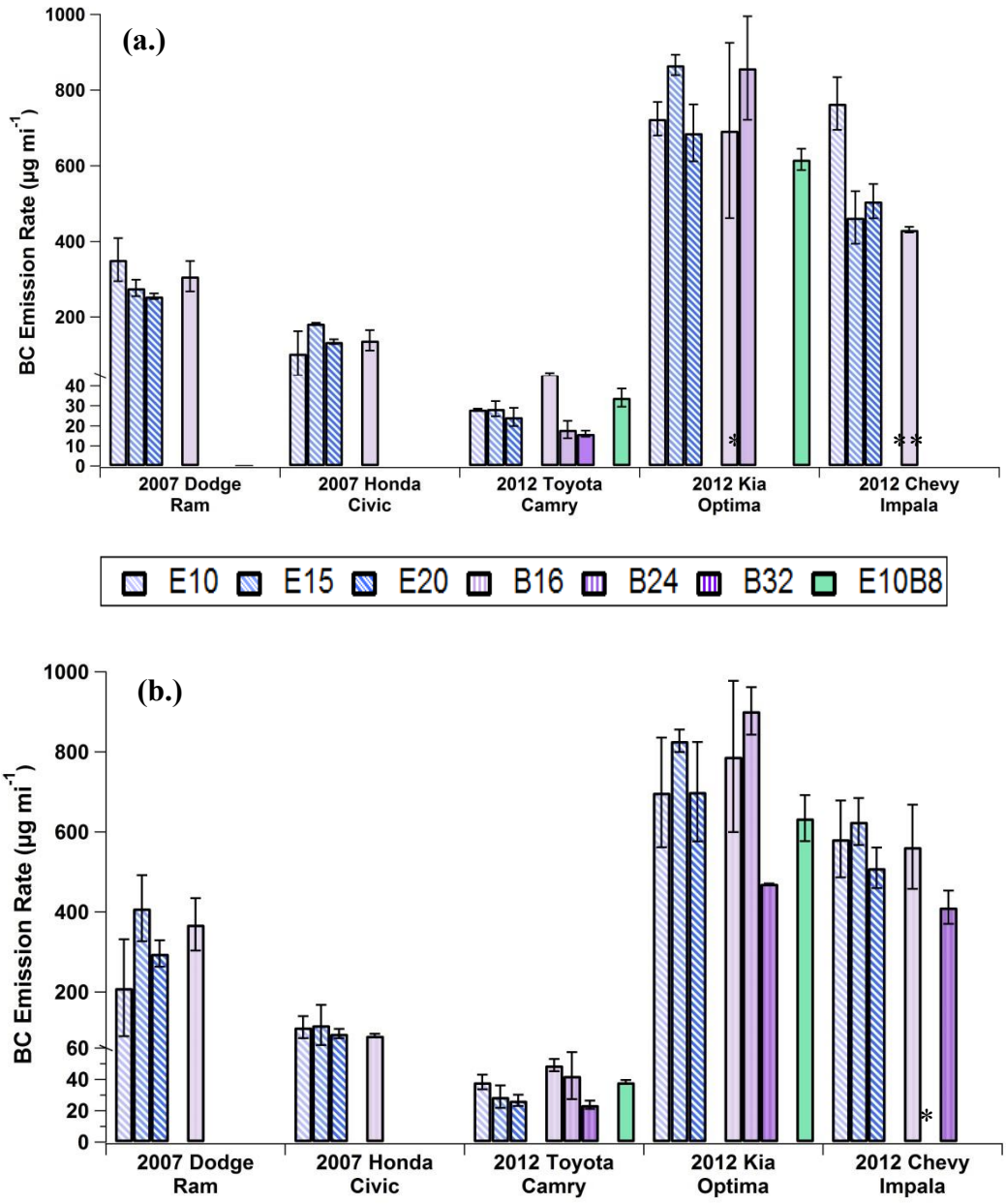

Fig. 5- 6. Black Carbon emission factors over the entire (a) FTP and (b) UC cycles
* Denotes data unavailable

Fig. 5-6 shows the BC/PM mass fractions for the Toyota Camry, Kia Optima, and Chevrolet Impala for both the FTP and UC. Despite differences in the FTP and UC driving cycles, the testing regime did not affect the fraction of BC to PM emitted. For the

majority of the vehicles, cycles, and fuels, the BC/PM mass fraction ranged from 0.1 to 0.3, or BC was ~20% of the total PM. Over the FTP cycle, all three vehicles show consistent BC/PM mass fractions at ~0.20, with the exception of the Toyota Camry showing a low BC/PM mass fraction of ~0.05 for the iso-butanol fuels. For the UC, the Kia Optima BC/PM mass fractions remained at 0.20, similar to the FTP. The Chevrolet Impala showed a clear fuel trend over the UC of increased BC/PM mass fractions from 0.20 for the E10 fuel to 0.30 for the E20 fuel blend with a similar increase was also shown for the iso-butanol fuel blends. The Toyota Camry showed BC/PM mass fractions of ~0.02 to ~0.13 over the UC, with lower mass fractions seen for the higher ethanol and iso-butanol blends.

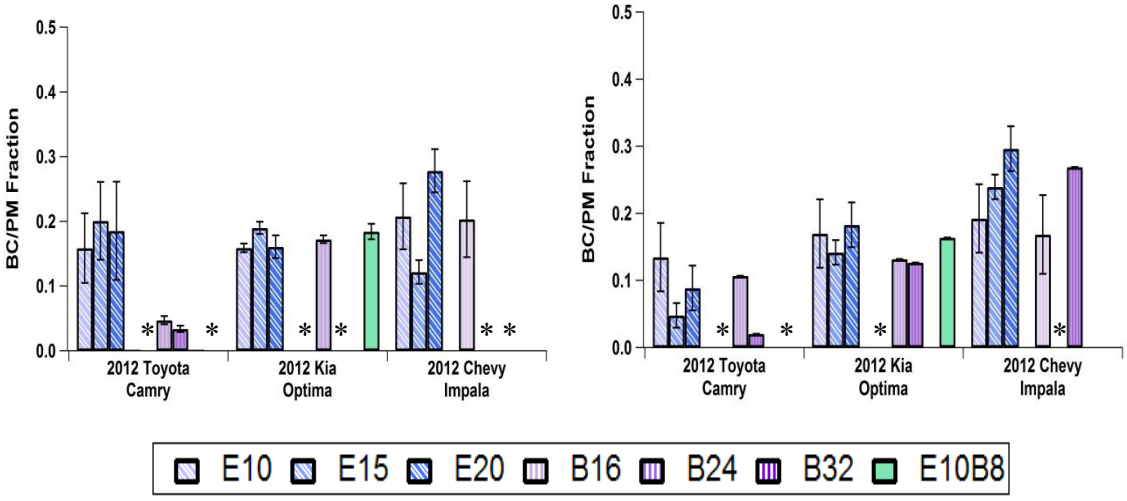

Fig. 5- 7 BC PM fraction over the FTP (a.) and Unified (b.) cycles

* Denotes data available

The total PM mass is roughly 5 times the amount of BC emitted. It should be noted that the BC equivalent concentrations were based on optical methods from the MAAP. Other BC and soot-like measurements may use different wavelengths, measurement techniques, or may measure elemental carbon (EC) from filter media, as opposed to real-time methods (Slowik et al. 2007). In general, previous studies have shown that GDI PM is dominated by 80% to 90% soot/EC emissions (Maricq et al., 2013; Storey et al. 2014; Khalek et al. 2009; and references therein). Other BC measurement techniques (i.e., photoacoustic) have been shown to give a higher soot material mass compared to the MAAP (Slowik et al. 2007). Our measurement found BC or soot material to be lower at ~20% (0.20 BC/PM Mass fraction) of the total PM mass for GDI vehicles, and suggests that further work on EC and BC methods of measurements is needed. For the Toyota Camry (PFI), assuming BC has similar properties to EC, the results were consistent with Cheung at al. (2009), which found elemental carbon (EC) emissions represented a minor fraction of the total PM (roughly 5%).

5.4. Conclusions

This study concluded that high steady-state speeds produce large fractions of sub-40 nm hygroscopic particles for both PFI and GDI vehicles. This was seen for both the higher steady-state speeds and for the higher speeds and more aggressive phase 2 of the UC for the Dodge Ram, Honda, Civic, and Kia Optima. As the steady-state speed decreases from 70 to 30 mph, the emitted particles become less hygroscopic and more water-insoluble for particle diameters below 40 nm. The particle emissions from the

lower speed portions of the transient cycles were mostly non-hygroscopic and behaved like water-insoluble particles. The cold-start phase, during of which the engine is cold and the TWC is below its light-off temperature, produced non-hygroscopic particles. The lower speed hot start phases and the hot running transient phase of the FTP all showed more water-insoluble particles. The enhancement of water-soluble particles has the ability to induce DNA damage, cause pro-inflammatory response, and can promote pulmonary and cardiovascular disease (Ramgolan et al., 2009; Guetterrez-Castillo et al., 2006). Thus, in addition to average daily driving emissions, the spatial regions in which high speed and low speed vehicle operation occurs must be studied; the particle composition on high speed highways maybe significantly different than local residential driving. The difference in results could have important implications for ambient health studies. Future work that correlates the high vehicle speeds and low water-insoluble emitted particles is needed to determine the cause of this phenomena. However, this study provides evidence that particle composition changes exist with vehicle speed and should warrant further investigation.

This study showed that particle composition differences exist between different vehicle technologies and fuels. Overall, roughly 30% of the PM mass consists of WSOM. The Kia Optima showed ~20% of the PM mass was WSOM and the Chevrolet Impala had ~40% WSOM. The total PM mass was roughly 5 times higher than the BC mass for the Toyota Camry and both GDI vehicles with BC making up ~10-30% of the PM mass. No significant trends were shown between the BC EFs and the ethanol and iso-butanol

fuel blends. The WSOM mass makes up roughly 20-60% of the total PM mass for the fuels and two GDI vehicles tested.

5.5. Acknowledgements

The authors would like to thank Tyler Berte, Hans Phang, Chun Liang, and Wartini Ng for their contributions to this work. In addition, the authors thank Kurt Bumiller and Mark Villela for their technical support of the dynamometer test cell. This study was substantially supported by the California Energy Commission Grant Number 500-09-051. Also, D.S. would like to acknowledge the funding support from the University of California Transportation Center (UCTC) Graduate Fellowship. Funding for BC measurements were made possible by the U.S. Environmental Protection Agency (EPA) grant number 83504001. Its contents are solely the responsibility of the grantee and do not necessarily represent the official views of the EPA. Further, the EPA does not endorse the purchase of any commercial products or services mentioned in the publication.

5.6. References

Aakko, P. and Nylund, N.O. 2003. Particle emissions at moderate and cold temperatures using different fuels. SAE Technical Paper 2003-01-3285.

Alkidas AC. 2007. Combustion advacements in gasoline engines. Energy Conversion and Management, 48, 2751-2761.

Andreae, M. O. and Crutzen, P. J. 1997. Atmospheric aerosols: biogeochemical sources and role in atmospheric chemistry. Science, 276:1052–1058

Andreae, M.O., Rosenfeld, D. 2008, Aerosol-cloud-precipitation interactions. Part 1. The nature and sources of cloud-active aerosols, Earth Science Reviews, 89, 13-41

Avol, E. L., Jones, M. P., Bailey, R. M., Chang, N. M. N., Kleinman, M. T., Linn, W. S., Bell, K. A., and Hackney, J. D. 1979. Controlled exposures of human volunteers to sulfate aerosols - Health-effects and aerosol characterization. Am. Rev. Respir. Dis., 120: 319-327

Baumer, D., Vogel, B., Versick, S., Rinke, R., Mohler, O., and Schnaiter, M. 2008. Relationship of visibility, aerosol optical thickness and aerosol size distribution in an ageing air mass over South-West Germany. Atmos. Environ., 42: 989–998: Sierra Research, Inc., Contract No. A932-185, Sacramento, California

Biswas S., Verma, V., Schauer, J.J., Sioutas, C., 2009. Chemical Speciation of PM Emissions From Heavy-Duty Diesel Vehicles Equipped With Diesel Particulate Filter (DPF) and Selective Catalytic Reduction (SCR) Retrofits. Atmospheric Environment, 43, 1917-1925

Cheung, K.L., Polidori, A., Ntziachristos, L., Tzamkiozis, T., Samaras, Z., Cassee, F. R., Gerlofs, M., and Siouras, C. 2009. Chemical Characteristics and Oxidative Potential of Particulate Matter Emissions from Gasoline, Diesel, and Biodiesel Cars, Environmental Science and Technology, 43, 6334-6340

Curran, H.J.; Gaffuri, P.; Pitz, W.J., Westbrook, C.K. A comprehensive modeling study of iso-octane oxidation. Combustion and Flame. 2002. 129(3), 253-280

Dutcher, D.D., Stolzenburg, M.R., Thompson, S.L., Madrano, J.M., Gross, D.S., Kittelson, D.B., McMurry, P.H., 2011. Emissions From Ethanol-Gasoline Blends: A Single Particle Perspective, Atmosphere, 2,2, 182-200.

Ervens, B., Feingold G., and Kreidenweis, S.M., 2005. Influence of water-soluble organic carbon on cloud drop number concentration, Journal of Geophysical Research,110, D18211

Forestieri, S.D., Collier, S., Kuwayama, T., Zhang, Q., Kleeman, M.J., Cappa. C.D. 2013. Real-time black carbon emission factor measurements from light duty vehicles. Environ. Sci. Technol, 47:13104-13112

Geller, Michael D., Ntziachristos L., Mamakos, A., Samaras, Z., Schmitz, D.A., Fraines, J.R., Sioutas, C., 2006. Physicochemical and redox characteristics of particulate matter (PM) emitted from gasoline and diesel passenger cars. Atmospheric Environment, 40,36, 6988-7004.

Giechaskiel, B., Chirico, R., DeCarlo, P.F., Clairotte, M., Adam, T., Martini, G., Heringa, M.F., Richter, R., Prevot, A.S.H., Baltensperger, U., Astorga, C., 2010.

Evaluation of the Particle Measurement Programme (PMP) Protocol to Remove the Vehicles' Exhaust Aerosol Volatile Phase, Science of the Total Environment, 408, 5106-5116

Graham, L. 2005. Chemical Characterization of Emissions From Advance Technology Light- Duty Vehicles, Atmospheric Environment, 39, 13, 2385-2398

Gutiérrez-Castillo, M, Roubicek, D A, Cebrián-Garcia, M E, De Vizcaya-Ruiz, A, Sordo-Cedeòo, M and Ostrosky-Wegman, P. 2006. Effect of chemical composition on the induction of DNA damage by urban airborne particulate matter. Environmental and Molecular Mutagenesis, 47: 199–211.

IPCC, 2007. Climate Change 2007: The Physical Science Basis. Summary for PolicyMakers.

Karavalakis, G., Short, D., Vu, D., Villela, M., Asa-Awuku, A., Durbin, T. 2014. Evaluating the Regulated Emissions, Air Toxics, Ultrafine Particles, and Black Carbon from SI-PFI and SI-DI Vehicles Operating on Different Ethanol and Iso-butanol Blends, Fuel, 128, 410-421

Karavalakis, G., Short, D., Vu, D., Villela, M., Asa-Awuku, A., Durbin, T. 2013. Criteria Emissions, Particle Number Emissions, Size Distributions, and Black Carbon Measurements from PFI Gasoline Vehicles Fuelled with Different Ethanol and Butanol Blends, SAE Technical Paper, 2013-01-1147

Khalek I.A., Bougher T., Jetter J.J. 2010. Particle emissions from a 2009 gasoline direct injection engine using different commercially available fuels. SAE Int. J. Fuels Lubr., 3(2):623-637.

Köhler, H. 1936. The nucleus in and the growth of hygroscopic droplets. Transactions of the Faraday Society, 32, 1152–1161.

Mills, N.L., Donaldson, K., Hadoke, P.W., Boon, N.A., MacNee, W., Cassee., F.R., Sandstom, T., Blomberg, A., Newby, D.E. 2009. Nature Clinical Practice Cardiovascular Medicine, 6, 1, 36-44.

Liang, B., Ge, Y., Tan, J., Han, X., Gao, L., Hao, L., Ye, W., Dai, P., 2013. Comparison of PM Emissions From a Gasoline Direct Injected (GDI) vehicle and a Port Fuel Injected (PFI) vehicles measured by Electrical Low Pressure Impactor (ELPI) With Two Fuels: Gasoline and M15 Methanol Gasoline, Journal of Aerosol Science, 57, 22-31.

Longest, P.W., McLeskey, J.T., Hindle, M. 2010. Characterization of Nanoaerosol Size Change During Enhanced Condensational Growth, Aerosol Science and Technology, 44, 6, 473-483

Nauss, K. 1995. Diesel Exhaust: A Critical Analysis of Emissions, Exposure, and Health Effects; Health Effects Institute

Mamakos A., Martini G., Marotta A., Manfretti U. Assessment of different technical options in reducing particle emissions from gasoline direct injection vehicles. Journal of Aerosol Science 2013, 63:115-125.

Maricq, M.M., Szente, J.J., Adams, J., Tennison, P., Tumpsa, T. 2013. Influence of mileage accumulation on the paticle mass and number emissions of two gasoline

direct injection vehicles, Environmental Science and Technology, 47(20), 11890-11896, DOI: 10.1021/es402686z

Oberdorster, G. 2001. Pulmonary Effects of Inhaled Ultrafine Particles, International Archives of Occupational and Environmental Health, 74, 1, 1-8

Piock W, Hoffmann G, Berndorfer A, Salemi P, Fusshoeller B. 2011. Strategies towards meeting future particulate matter emission requirements in homogeneous gasoline direct injection engines. SAE Int. J. Engines, 4, 1455-1468.

Pope, C.A., Burnett, R.T., Thuston, G.D., Thun, M.J., Calle, E.E., Krewski, D., Godleski, J.J. 2004. Cardiovascular Mortality and Long-Term Exposure to Particulate Air Pollution- Epidemiological Evidence of General Pathophysiological Pathways of Disease, Circulation, 109, 1, 71-77

Petters, M. D. and Kreidenweis, S. M. 2007. A single parameter representation of hygroscopic growth and cloud condensation nucleus activity. Atmos. Chem. Phys., 7, 1961–1971.

Petzold, A. and Schönlinner, M. 2004.The Multi-angle absorption photometer – A new method for the measurement of aerosol light absorption and atmospheric black carbon. Journal of Aerosol Science, 35, 421-441

Pocket Guide to Ethanol 2013, Renewable Fuels Association (RFI), January 2013

Ristimaki, J., Keskinen, J., Virtanen, A., Maricq, M., Aakko, P. 2005. Cold temperature PM emissions measurement: Method evaluation and application to light duty vehicles, Environmental Science Technology, 39: 9424-9430.

Ramgolam, K., Favez, O., Cachier, H., Gaudichet, A., Marano, F., Martinon, L., and Baeza-Squiban, A. 2009. Size-partitioning of an urban aerosol to identify particle determinants involved in the proinflammatory response induced in airway epithelial cells, *Particle and Fibre Toxicology* 2009, 6:10

Oberdorster, G.,Sharp, Z.,Atudorei, V., Elder, A.,Gelein R.,Kreyling, W., Cox, C., 2004. Translocation of inhaled ultrafine particles to the brain. Inhalation Toxicology 16, 437–445

Schwarz, J. P.; Gao, R. S.; Fahey, D. W.; Thomson, D. S.; Watts, L. A.; Wilson, J. C.; Reeves, J. M.; Darbeheshti, M.; Baumgardner, D. G.; Kok, G. L.; Chung, S. H.; Schulz, M.; Hendricks, J.; Lauer, A.; Kärcher, B.; Slowik, J. G.; Rosenlof, K. H.; Thompson, T. L.; Langford, A. O.; Loewenstein, M.; Aikin, K. C. Single-particle measurements of midlatitude black carbon and light-scattering aerosols from the boundary layer to the lower stratosphere. Journal of Geophysical Research, 111, D16207, 2006.

Short, D. , Giordano, M., Zhu, Y., Fine. P., Polidori, A., Asa-Awuku, A., 2014. A Unique On-line method to infer black carbon contributions to water-insoluble contributions, Aerosol Science and Technology

Slowik, J.G., Cross, E.S., Han, J.-H., Davidovits, P., Onasch, T.B., Jayne, JT., Williams, L.R., Canagaratna, M.R., Worsnop, D.R., Chakrabarty, R.K., Moosmuller, H., Arnott, W.P., Schwarz, J.P., Gao, R.-S., Fahey, D.W., Kok, G.L., Petzold, A., 2007. An Inter-Comparison of Instruments Measuring Black Carbon Content of Soot Particles, Aerosol Science and Technology, 41, 3, 295-314

Sorjamaa, R., Svenningsson B., Raatikaimen, T., Henning, S., Bilde, M., Laaksonen, A., 2004. The Role of Surfactants in Khler Theory Reconsidered, Atmospheric Chemistry and Physics, 4, 2107-2117

Stevens E, Steeper R. 2001. Piston wetting in an optical DISI Engine: fuel films, poolfires, and soot generation. SAE Int J Engines,110:1287-1294.

Storey J.M., Barone, T., Norman, K., Lewis, S., 2010. Ethanol Blend Effects on Direct Injection Spark-Ignition Gasoline Vehicle Particulate Matter Emissions, SAE Technical Paper, 2010-01-2129.

Storey JM, Lewis S, Szybist J, Thomas J, Barone T, Eibl M, Nafziger E, Kaul B. 2014. Novel characterization of GDI engine exhaust for gasoline and mid-level gasoline-alcohol blends. SAE Technical Paper 2014-01-1606.

Szybist JP, Youngquist AD, Barone TL, Storey JM, Moore WR, Foster M, Confer K. 2011. Ethanol blends and engine operating strategy effects on light-duty spark ignition engine particle emissions. Energy and Fuels, 25:4977-4985.

Turpin, B.J., Lim, H., 2001. Species Contributions to PM 2.5 Mass Concentrations: Revisiting Common Assumptions for Estimating Organic Mass, Aerosol Science and Technology, 35, 1, 602-610

Twomey, S. 1977. The influence of pollution on the shortwave albedo of clouds. J. Atmos. Sci. 34: 1146-1152

Yang, W., Peters, J., Williams, R. 2008. Inhaled Nanoparticles-A Current Review, International Journal of Pharmaceuticals, 356, 239-247

Yung-Fang Y.Y. Ocxdation of alkanes over noble metal catalysts. Ind. Eng. Chem. Prod. Res. Dev. 1980, 19, 293-298

Valavandidis, A., Fiotakis, K., and Vlachogianni, T. 2008. Airborne Particulate Matter and Human Health: Toxicological Assessment and Importance of Size and Composition of Particles for Oxidative Damage and Carcinogenic Mechanisms, Journal of Environmental Science and Health, Part C, 26;4:339-362

Verma, V., Shafer, M.M., Schauer, J.J., Sioutas, C., 2010. Contribution of Transistion Metals In the Reactive Oxygen Species Activity of PM Emissions From Retrofitted Heavy-Duty Vehicles, Atmospheric Environment, 44, 39, 5165-5173

Wang, S. C., Flagan, R. C. 1990. Scanning Electrical Mobility Spectrometer. Aerosol Science and Technology, 13: 230–240

Zhao, F., Lai, M.C., Harrington, D.L. 2006, Automotive Spark- Ignition Direct- Injection Gasoline Engines, Progress in Energy and Combustion Science, 25, 5, 437-562

Chapter 6: The Impact of Ethanol and Iso-butanol Blends on Gaseous and Particulate Emissions from Passenger Cars Equipped with Gasoline Direct Injection and Flex-Fuel Vehicles

6.1. Introduction

The proportion of gasoline vehicles operating with spark ignition (SI) direct injection (DI) fueling systems is steadily increasing in both the European and the United States (U.S.) markets. In the U.S. alone, half of all light-duty vehicle certifications for the 2012 model year included GDI engines, reaching approximately 24% of the market, up from virtually 0% in 2007 (MECA, 2013). The widespread penetration of GDI vehicles is due to their improved fuel economy over conventional throttled SI port fuel injection (PFI) engines, which increases thermodynamic efficiency and improves fueling control, and ultimately leads to carbon dioxide (CO_2) reductions (Alkidas 2007).

Currently, the vast majority of GDI engines employ wall-guided designs in which the fuel spray is directed from a side-mounted fuel injector towards a contoured piston and then upward toward the spark plug (Zhao et al. 1999). While wall-guided GDI (WG-GDI) engines offer advantages over their PFI counterparts, there can be issues relating to fuel preparation including fuel in contact with the cylinder wall surfaces during combustion, which will likely form soot or other semi-volatile compounds because the wall quenches the flame and prevents the complete combustion of the fuel. In addition to soot formation, an increase in total hydrocarbon (THC) emissions is expected due to incomplete evaporation and mixing with air and of adsorption and subsequent desorption of the fuel that, after being trapped in the piston top land crevice, is dissolved in lubricant

oil with consequent dilution and lose of lubricant properties (Alkidas 2007; Zhao et al. 1999; Stevens and Steeper 2001).

Currently, there is a trend for stoichiometric homogeneous WG-SIDI engines, which are dynamically penetrating the vehicle market. Alternative designs to WG-SIDI engines use either homogeneous or stratified-charge spray-guided (SG) GDI engines (Giglio et al. 2013). While SG-GDI engines can be operated in a homogeneous charge mode only, the greatest fuel economy benefit is achieved with unthrottled lean stratified operation (Park et al. 2012). Advanced SG-SIDI engines are mostly available in Europe, but not in the U.S. because their lean operation requires nitrogen oxides (NO_x) emissions control (Oh and Bae 2013). For the SG-GDI configuration, the fuel injector and spark plug electrodes are closely spaced in the center of the chamber. The fuel injector confines the fuel spray such that it does not contact the cylinder walls, thus reducing the incidence of fuel wall wetting, improving mixing and reducing soot formation (Giglio et al. 2013; Oh and Bae 2013; Dahms et al. 2011).

While GDI engines are offering important fuel economy and CO_2 reduction benefits compared to their PFI counterparts, additional changes are ongoing in the fuel industry to further reduce greenhouse gas emissions and to secure renewable fuel supply. In the U.S., the passage of the Energy Independence and Security Act (EISA 2007) along with the Renewable Fuel Standard (RFS), which was initiated in 2005 and expanded in 2007, mandates the use of 36 billion gallons of renewable fuels in the transportation fuel pool by 2022 (EPA, 2007). Analogous to the U.S., the European Union (EU) also promotes the use of renewable fuels with the implementation of the EU Renewable Energy

Directive (2009/28/EC), which sets an objective of 10% market share of biomass fuels by 2020 (EURO, 2009). Currently, ethanol produced both from corn and other cellulosic feedstocks is considered to be the most promising biofuel in the U.S. (Gardebroek and Hernandez 2013). More than 95% of gasoline sold in the U.S. contains 10% ethanol (E10), and the U.S. Environmental Protection Agency (EPA) has granted a partial waiver for the use of E15 blends in model year 2000 and newer vehicles. However, there are several drawbacks with the use of ethanol as gasoline extender. These include ethanol's lower energy content compared to gasoline, the increase in Reid vapor pressure (RVP), and the inability to transport it through pipelines due to risk of water-induced phase separation (Anderson et al. 2012; Yan et al. 2013). Ethanol is very corrosive and at large concentrations can harm pipelines and existing infrastructure.

Conventional vehicle technologies are not able to incorporate large volumes of ethanol into the operation of the vehicle. In fact, concentrations higher than E15 are not recommended in conventional vehicles because higher concentrations of ethanol will corrode vehicle components (DOE, 2013). In addition, long-term compliance of vehicles ,in terms of criteria pollutant emissions, isn't known in conventional vehicles with up to 20% ethanol fuel use (Cadle et al. 2009). Flex Fuel Vehicles (FFVs) allow for vehicles to use ethanol fuel mixtures up to E85. FFV use is very popular in Brazil where approximately 85% of vehicles driven are equipped with FFV technology (Delgado et al. 2007). However, the use of E85 fuel blends have resulted in a estimated decrease in fuel economy up to 25% due to ethanol having lower energy content compared to gasoline (Roberts 2008).

Recently, higher alcohols, such as butanol, have been the subject of increased interest as potential fuels in SI engines (Irimescu 2012). Iso-butanol is a higher chain alcohol with a four carbon structure that has different isomers based on the location of the hydroxyl group (1-butanol, n-butanol, 2-butanol, tertiary-butanol, and iso-butanol) (Jin et al. 2011). While n-butanol could be an attractive candidate for ethanol replacement because it can be produced via the mature and well-known acetone-butanol-ethanol (ABE) fermentation process, the dramatic energy demand, high water use, and unfavorable process economics have led research towards to iso-butanol (Tao et al. 2014). Similar to ethanol, iso-butanol can be produced from biochemical pathways via fermentation using biomass-derived feedstocks, including corn, sugarcane, and cellulosic biomass (Tao et al. 2014; Xue et al. 2013). Compared to ethanol, iso-butanol exhibits a higher energy density, which is close to that of gasoline. In addition, iso-butanol has a lower latent heat of vaporization, is less soluble to water, and less corrosive than ethanol. The motor octane number of iso-butanol is lower than ethanol. However, both iso-butanol and ethanol improve the octane ratings of gasoline when they are added (Jin et al. 2011).

The use of ethanol has been widely investigated for SI engines and vehicles, while data on emissions from iso-butanol blends is relatively sparse. While most studies on the effects of ethanol on tailpipe emissions have been focused on PFI engines and vehicles, there are some studies available on GDI engines/vehicles (Karavalakis et al. 2012; Durbin et al. 2007). Storey et al. 2010 analyzed the effect of E10 and E20 blends on a 2007 model year GDI vehicle and found that NO_x, carbon monoxide (CO), formaldehyde, and benzaldehyde emissions decreased with higher ethanol blends, while

acetaldehyde emissions showed increases. They also showed reduced PM mass and particle number emissions with ethanol blends. Maricq et al. 2012 showed small benefits in PM mass and particle number emissions as the ethanol level in gasoline increased from 0 to 20% when they tested a GDI turbocharged vehicle with two engine calibrations over the Federal Test Procedure (FTP), while particle size was unaffected by ethanol level. Chen et al. 2012 investigated the effect of ethanol blending on the characteristics of PM and particle number emissions from a SG-GDI engine. They found increases in particulate emissions as the ethanol content increases. Clairotte et al. 2013 showed that a flex fuel vehicle fitted with GDI engine reduced CO, CO_2, and NO_x emissions with higher ethanol blends. Higher THC emissions with higher ethanol blends were also seen in other studies employing SG-GDI engines (Price et al. 2007). In addition, Graham et al. 2008 showed lower CO and non-methane organic gases (NMOG) emissions from a GDI vehicle with E10 and E20 blends relative to gasoline. Most chassis dynamometer studies on iso- butanol blends have been conducted on PFI-fueled vehicles (Schulz et al. 2011; Ratcliff et al. 2013). Recent engine investigations on butanol blends on WG-GDI engines have shown that NO_x, CO, and THC emissions were lower with increasing butanol content in gasoline, while some increases were seen for formaldehyde and acetaldehyde emissions when they utilized n-butanol and iso-butanol as blending agents with gasoline (Wallner and Frazee 2010). In another study, the same group of authors showed lower volumetric fuel consumption and lower NO_x emissions for butanol compared to ethanol blends (Wallner et al. 2009). Karavalakis et al. 2014 studied the gaseous and particulate emission effects of different ethanol and iso-butanol blends from a fleet of PFI and WG-

GDI vehicles over the FTP and Unified Cycle (UC). Their results did not show strong differences between fuels for THC, CO, and NO_x emissions for both cycles. They showed higher PM mass, particle number, and black carbon emissions for the GDI vehicles compared to their PFI counterparts. They also showed reductions in PM mass, particle number, and black carbon emissions with increasing alcohol content.

Studies have shown that lower THC, NMTHC, and NO_X emissions are associated with E85 fuel blend (Karavalakis et al. 2012; Graham et al. 2008; He et al. 2003). Graham et al. 2008 found that a 45% and 48% decrease in NO_x and NMTHC, respectively, with the use of the E85 fuel blend compared to pure gasoline. In addition, et al. found that CO emissions were reduced by 22% with the E85 fuel blend compared to gasoline (Zhai et al. 2009). However, a 12% increase in THC was found for this study perhaps due to the larger matrix of vehicles tested for this study (Zhai et al. 2009). E55 blend also shows decreased NO_x emissions by 50% but no difference in NO_x emissions was seen between the E85 and E55 fuel blends (Hubbard et al. 2014). Particulate emissions associated with the use of E85 is very limited. Lee et al. 2009 showed that total PN emissions using the Particulate Measurement Programme (PMP) decreased by 37% for the E85 fuel blend compared to pure gasoline.

In this study, the impacts of varying ethanol and iso-butanol blend concentrations on the tailpipe emissions from two passenger cars equipped with SG-GDI and WG-GDI fueling systems, respectively, are evaluated. Emissions and fuel economy testing was conducted over the FTP and the Unified Cycle (UC) test cycles that include both cold-starts and transient operation. A major goal of this study was to investigate the influence

of fuel type and engine technology on particle emissions, including PM mass, particle number, and soot.

6.2. Experimental

6.2.1. Test fuels and vehicles

A total of nine fuels were employed in this study. The fuel test matrix included an E10 fuel (10% ethanol and 90% gasoline), which served as the reference fuel for this study for all four vehicles. The SG-GDI and WG-GDI vehicles were tested on two more ethanol blends, namely E15 and E20. Iso-butanol, which is a branched isomer of butanol with the OH group at the terminal carbon, was blended with gasoline at proportions of 16% (Bu16), 24% (Bu24), and 32% (Bu32) by volume, which is the equivalent of E10, E15, and E20, respectively, based on the oxygen content. The FFVs were tested on ethanol fuel blends of E51 and E83 in addition to an iso-butanol blend of B55. All fuels were custom blended to match the oxygen contents, maintain the Reid vapor pressure (RVP) within certain limits (6.4-7.2 psi), and match the fuel volatility properties. The main fuel parameters of the alcohol blends can be found in Appendix Table C-1 and D-1.

This study utilized two 2012, one 2013, and one 2014 model year gasoline passenger vehicles fitted with three-way catalysts (TWC) and operated stoichiometrically. The first vehicle (WG-SIDI) was a 2.0L I4, California LEVII, SULEV certified passenger car, having a rated horsepower of 148 hp at 6500 rpm, and equipped with a wall-guided direct injection SI engine. The second vehicle (SG-SIDI) was a 3.5L V6 , California LEVII, SULEV certified passenger car, having a rated horsepower of 302 hp at 6500 rpm, and

equipped with a spray-guided direct injection SI engine. The third was a 2013 Light-Duty FFV equipped with a 3.7L V6 PFI engine and was a California LEVII, ULEV certified vehicle. The fourth vehicle was a 2014 Light-Duty FFV with a 5.3L V8 GDI engine and was a California LEVII, ULEV certified vehicle. The four vehicles had an accumulated mileage of 18,851 for the WG-SIDI, 10,996 for the SG-SIDI, 13,687 for the PFI-FFV, and 2,649 for the GDI-FFV at the beginning of the test campaign.

6.2.2. Driving cycles and measurement protocol

Each vehicle was tested on each fuel over three FTPs and three UC tests. The 9 particular fuel tests were conducted sequentially once the vehicle was changed to operate on that fuel, and the fuel was not changed to another fuel during this time. A fuel change with multiple drain and fills was conducted between the testing on each fuel to condition the vehicle and ensure no carryover effects. Detailed information on the driving cycles employed in this study and the testing protocol can be found elsewhere (Karavalakis et al. 2013).

6.2.3. Emission testing and analysis

All tests were conducted in CE-CERT's Vehicle Emissions Research Laboratory (VERL), which is equipped with a Burke E. Porter 48-inch single-roll electric dynamometer. A Pierburg Positive Displacement Pump-Constant Volume Sampling (PDP-CVS) system was used to obtain certification-quality emissions measurements. For all tests, standard bag measurements were obtained for THC, CO, NO_x, NMHC, and CO_2. NMHC was determined from the combined results from the THC analyzer and a separate

methane (CH_4) analyzer. Bag measurements were made with a Pierburg AMA-4000 bench.

PM measurements were made on both a mass and number basis. PM mass samples were collected cumulatively over the entire FTP and UC cycles, with one sample collected for each test. Total PM mass determinations were collected using 47 mm Teflon® filters and measured with a 1065-compliant microbalance in a temperature and humidity controlled clean chamber. Total particle number was measured using a TSI 3776 ultrafine-Condensation Particle Counter (CPC). This CPC is butanol-based and has the ability to count particles down to 2.5 nm with a total concentration of up to 300,000 ($\#/cm^3$). Hence, the ultrafine CPC was ideal for an accurate total particle number measurement. The instrument operated at a flow rate of 1.5 L/min. An ejector diluter was used to collect samples from the CVS tunnel. The ejector diluter uses THC and particle-free compressed air at a pressure of 20 psi.

Real-time particle size distributions were also obtained for some fuel blends using an Engine Exhaust Particle Sizer (EEPS) spectrometer. The EEPS was used to obtain real time second-by-second size distributions between 5.6 to 560 nm. Particles were sampled at a flow rate of 10 L/min, which is considered to be high enough to minimize diffusional losses. They were then charged with a corona charger and sized based on their electrical mobility in an electrical field. Concentrations were determined through the use of multiple electrometers.

Real-time soot emissions were measured using an AVL Micro-Soot Sensor (MSS). The MSS is an instrument that measures soot mass concentrations on a one-Hertz basis

using a photo acoustic detection technique. The instrument is designed to measure soot concentrations down to ~5µg/m^3 and operates at a flow rate of 2 L/min.

6.3. Results and Discussion

6.3.1. THC Emission Factor

The THC emission results for the Mercedes Benz E350 (SG-GDI) and the Mazda 3 (WG-GDI) vehicles over the FTP and UC test cycles are presented in Fig. 6-1. Overall, THC emissions were found to be at relatively low levels for both vehicles, ranging from 0.008 to 0.016 g/mile for the FTP and 0.008 to 0.022 g/mile for the UC. Generally, the higher ethanol blends exhibited lower THC emissions for the SG-GDI vehicle, while no strong fuel trends were observed for the butanol blends or for the WG-GDI vehicle. The decreases in THC emissions could be ascribed to the fuel bound oxygen (Knoll et al. 2009). For the FTP, statistical analyses for the two vehicle fleet as a whole showed that THC emissions did not show any statistically significant differences for the weighted, hot-running, and hot-start phases of the cycle. For the cold-start phase of the FTP (bag 1), THC emissions showed marginally statistically significant reductions of 31% for E20 compared to Bu24 (p=0.101). Similar to the FTP, the THC emissions did not show any statistically significant differences for the UC with the exception of bag 1 emissions. For the cold-start phase, THC emissions showed statistically significant reductions of 40% for E20 compared to Bu24 (p=0.008).

The FFV are also presented in Fig. 6-1 over the FTP and UC. Overall the THC were found to be at elevated levels compared to the Mercedes Benz E350 (SG-GDI) and

Mazda 3(WG-GDI) vehicles. In addition, significant fuel trends existed for the Chevrolet Silverado (GDI-FFV) where a 28% increase existed for the E85 fuel blend compared to E10. THC values ranged from 0.029 to 0.049 for the FTP and 0.020 to 0.040 for the UC. For the SG-GDI and WG-GDI vehicles, a 70% decrease in THC emissions was shown over the FTP cycle for the E10 fuel when comparing to the FFVs (p=0.03). In addition, no statistical difference was shown over the UC between the SG-GDI and WG-GDI vehicles compared to the FFVs.

The majority of THC emissions were emitted during the first 200-300 seconds of the cold-start phase of the FTP and UC. For the FTP, the average cold-start THC emissions ranged from 0.033 to 0.055 g/mile for the SG-GDI vehicle, 0.029 to 0.040 g/mile for the WG-GDI vehicle, 0.133 to 0.197 g/mile for the Ford F150 (PFI-FFV) vehicle, and 0.126 to 0.217 g/mile for the Chevrolet Silverado (GDI-FFV). For the UC, the average cold-start THC emissions ranged from 0.100 to 0.162 g/mile for the SG-GDI vehicle, 0.082 to 0.122 g/mile for the WG-GDI vehicle, 0.262 to 0.433 g/mile for the PFI-FFV vehicle, and 0.379 to 0.621 g/mile for the GDI-FFV. The higher cold-start THC emissions were due to the less efficient operation of the TWC, when it is below the vehicles light-off operating temperature. THC emissions for the hot-running and hot-start phases were practically eliminated due to the efficient oxidation of hydrocarbon fuel fractions by the TWC. Fuel impingement effects can also significantly influence THC emissions in GDI engines (Zhao et al. 1999), especially during cold-start conditions where a portion of THC emissions could be a result of unburned fuel fractions. It is assumed that increased

cylinder surface temperatures also contribute to lower THC emissions during the hot-running and hot-start phases by aiding better fuel vaporization and minimizing pool fires.

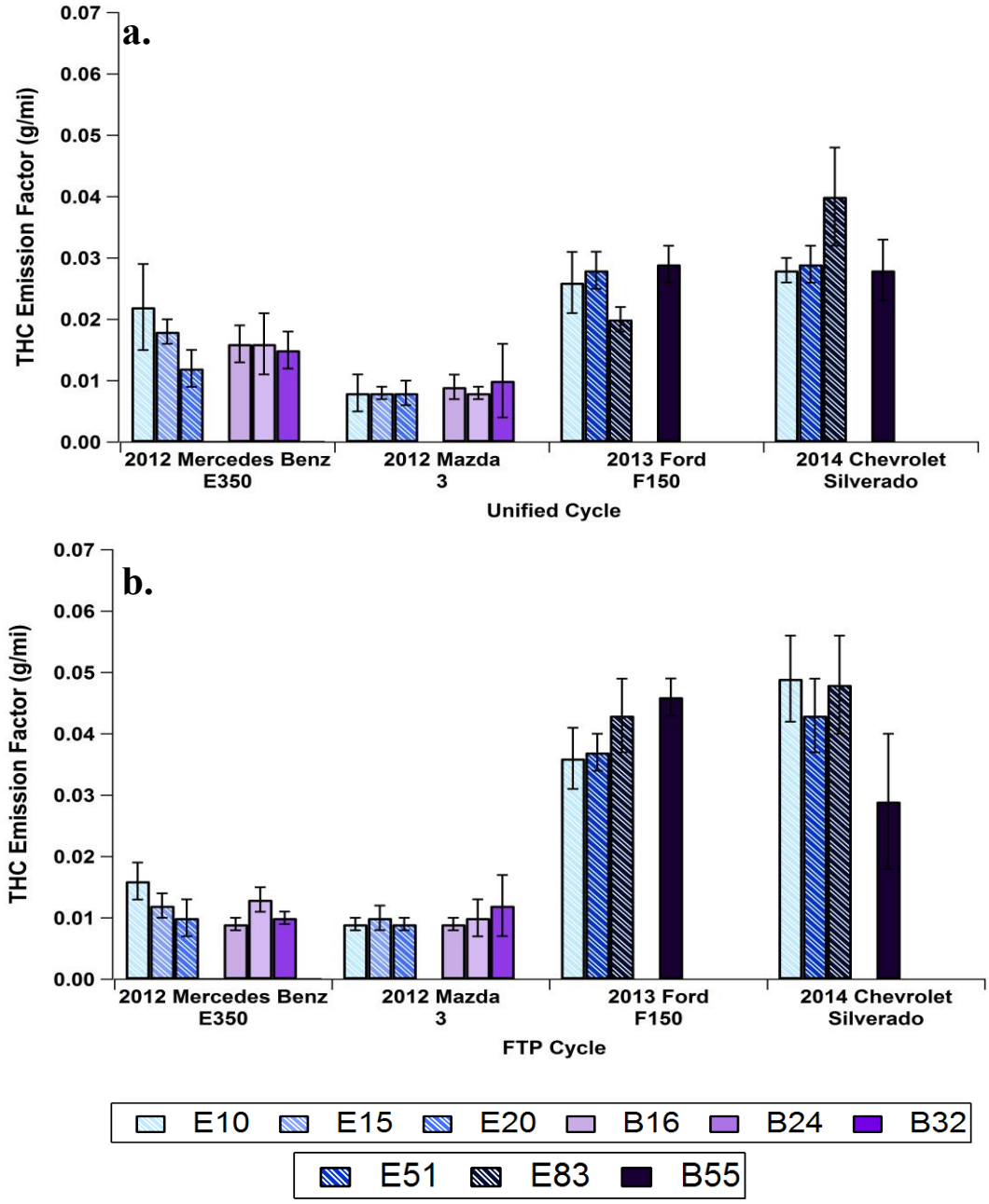

Fig. 6-1 THC Emissions Factors for all four vehicles tested over the UC (a.) and FTP (b.) cycles

6.3.2. NMHC Emissions Factors

NMHC emissions are shown in Fig. 6-2. For the Mercedes Benz E350 (SG-GDI) vehicle, NMHC emissions showed some decreases with increasing ethanol content in the blend over both the FTP and UC. However, these trends were not seen for the iso-butanol blends of the Mazda 3 (WG-GDI) vehicle. Statistical analysis revealed that weighted NMHC emissions for both test cycles did not show any significant differences for the two vehicles combined. NMHC emissions for the cold-start showed statistically significant reductions of 35 (p=0.047) and 42% (p=0.004) for E20 compared to Bu24 for the FTP and UC, respectively. For the FTP, NMHC emissions for the hot-running phase (bag 2) showed marginally statistically significant increases of about 600% for E10 relative to E20 (p=0.097) and marginally statistically significant decreases of 600% for E20 relative to Bu24 (p=0.097).

For the two FFVs, increasing ethanol concentration reduced NMHC over both the FTP and UC. Significant increases in NMHC were shown during the cold start or phase 1 of both cycles for both FFVs. Statistically no differences existed between the weighted NMHC for both cycles. Decreases of 50% and 17% existed between the E20 fuel compared to E10 for the Ford F150 (PFI-FFV) over the UC and FTP, respectively. In addition, a 29% decrease was shown between the E20 fuel compared to the E10 fuel for the Chevrolet Silverado (GDI-FFV) over the FTP cycle. No statistical decrease was shown over the UC for the GDI-FFV. Generally, the B55 fuel blend had a weighted NMHC emission factor lower than the E10 fuel blend except for the PFI-FFV over the FTP which showed a 33% increase compared to the E10 fuel blend.

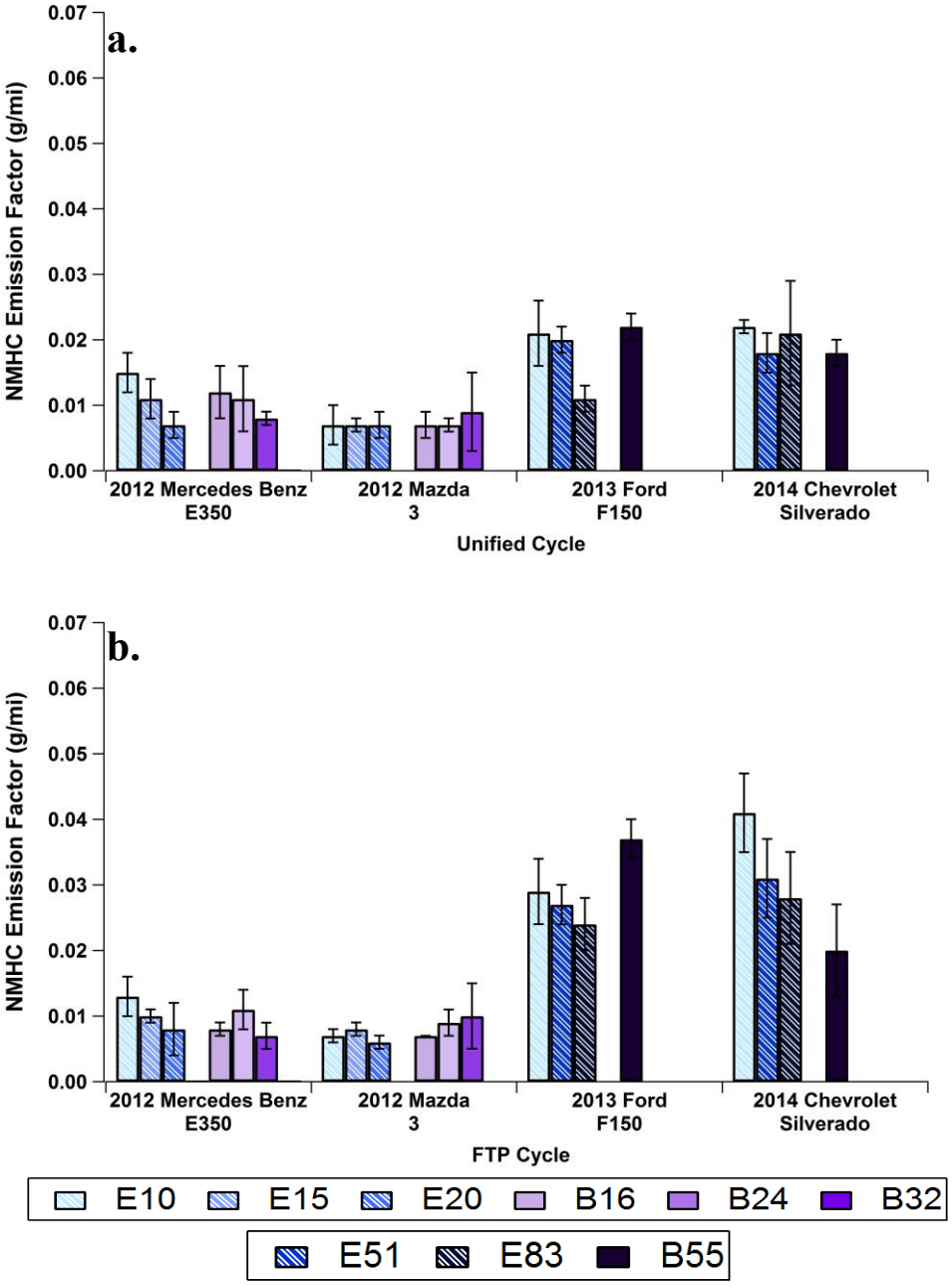

Fig. 6-2. NMHC Emissions Factors for all four vehicles tested over the UC (a.) and FTP (b.) cycles

6.3.3. CH_4 and CO_2 Emission Factor

Although the emissions of CH_4 can contribute significantly to total CO_2-equivalent greenhouse gas (GHG) emissions, CH_4 emissions from mobile sources are not regulated in the U.S., as opposed to the EU. Emissions of CH_4 are a function of the type of fuel used, the design and tuning of the engine, the type of emission control system, the age of the vehicle, as well as other factors. Generally, CH_4 emissions from gasoline are relatively small in terms of global warming potential. As shown in Fig. 6-3 for the Mercedes Benz E350 (SG-GDI) and Mazda 3 (WG-GDI) vehicles, CH_4 emissions were found at very low levels ranging from 0.002 to 0.004 g/mile for the FTP and 0.001 to 0.008 g/mile for the UC, with the SG-GDI vehicle having higher CH_4 emissions compared to the WG-GDI vehicle over both cycles. For the SG-GDI vehicle, some trends towards lower CH_4 emissions with E15 and E20 blends relative to E10 and higher CH_4 emissions with Bu24 relative to Bu16 and Bu32 were seen for both cycles. On the other hand, the WG-GDI vehicle did not show consistent fuel trends. In general, the precursors of CH_4 formation are CH_3 and C_8H_{18}, which suggests that the addition of either ethanol or butanol to gasoline could inhibit the path via C_8H_{18} decomposition to produce CH_4 (Broustail et al. 2012). The cold-start CH_4 emissions for the FTP showed statistically significant differences between fuels, with E10 showing increases of 48, 65, 49, and 50%, respectively, compared to E20 (p=0.040), Bu16 (p=0.001), Bu24 (p=0.031), and Bu32 (p=0.026). For the FTP, further statistically significant increases of 49% for E20 compared to Bu24 (p=0.043) were seen over the hot-start phase. No statistically significant differences between the fuels were observed for the UC. It should be noted

that cold-start CH_4 emissions were found to be somewhat higher compared to hot-running and hot-start phases for both cycles, but the differences in emission levels weren't as pronounced as observed with THC and NMHC emissions. This was probably due to the fact that CH_4 is considered to be an inert gas in terms of its oxidation activity in the TWC.

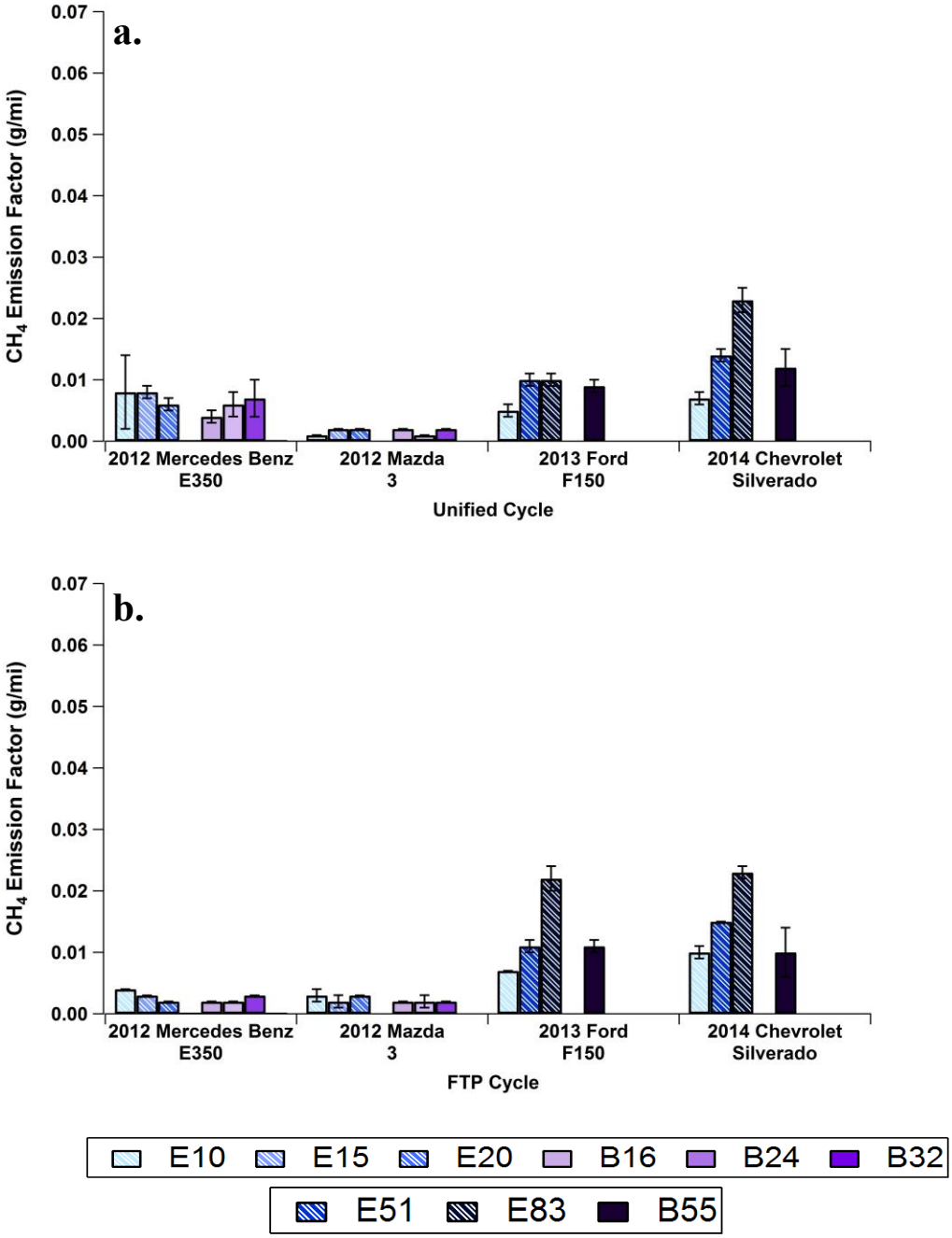

Fig. 6-3. CH_4 Emissions Factors for all four vehicles tested over the UC (a.) and FTP (b.) cycles

More pronounced fuel trends of CH_4 weighted emissions were shown for the FFVs compared to the Mercedes Benz E350 (SG-GDI) and Mazda 3 (WG-GDI) with increasing ethanol concentration (Fig. 6.3). In addition, the Ford F150 (PFI-FFV) showed statistical differences in the E83 fuel between both cycle with a 100% increase in the CH_4 emission factor for the FTP compared to the UC (p=0.008). For the PFI-FFV over the UC, a 100% increase in the CH_4 emission factor was shown from the E10 to E83 fuel blend (p=0.008). The Chevrolet Silverado (GDI-FFV) over the UC, showed a 229% increase in the CH_4 emission factor was shown from the E10 to E83 fuel blend (p=0.003). Over the FTP cycle, a 214% and 130% increase in the CH_4 emissions factor from the E10 to E83 fuel blend was shown for the PFI-FFV and GDI-FFV, respectively (p=0.001). For the cold start emissions (phase 1) over the UC, a 189% increase in the CH_4 emissions was should for the E83 fuel compared to the E10 fuel blend (p=0.018). In addition, the cold start emissions over the FTP cycle showed a increase in CH_4 emissions of 174% for the E83 compared to the E10 fuel blend (p=0.169). No statistical difference was shown for the other cycle phases. All CH_4 emissions were shown to by during the cold start as with the WG-GDI and SG-GDI vehicles with the lower decreases to the warm phases being less profound.

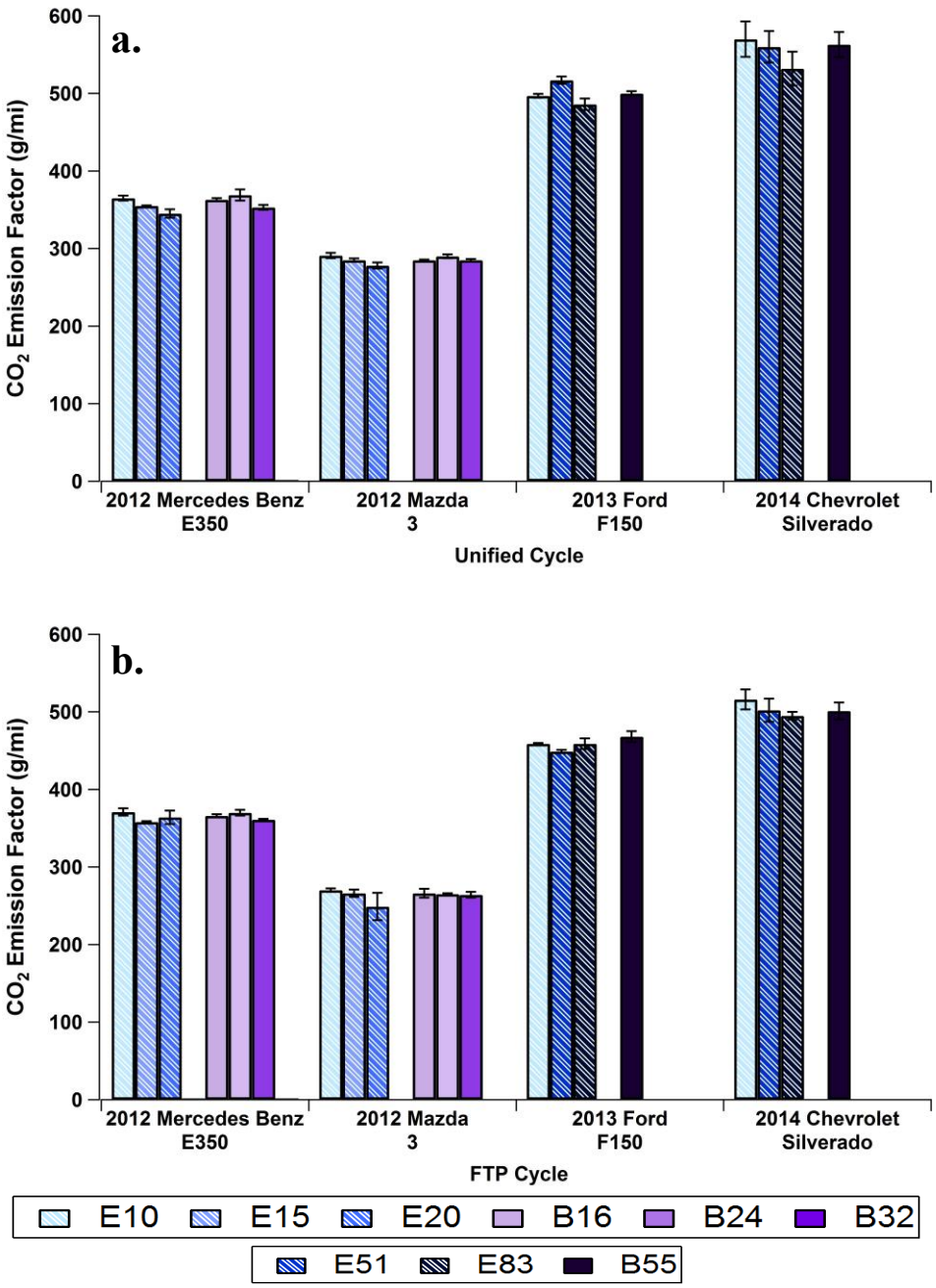

Fig. 6-4. CO_2 Emissions Factors for all four vehicles tested over the UC (a.) and FTP (b.) cycles

Fig. 6-4 shows the effect of alcohol fuel formulation on the CO_2 emissions over the FTP and UC for all four vehicles. From a theoretical standpoint, it might be expected that

CO_2 emissions would trend with the carbon/hydrogen ratio in the fuel. Carbon/hydrogen ratio decreases in the following order E10/Bu16, E15/Bu24, and E20/Bu32. Significant CO_2 emission trends for the Mercedes Benz E350 (SG-GDI) and Mazda 3 (WG-GDI) are shown below. Although some differences are seen between different fuels for different vehicles/cycles, there is not a general trend of CO_2 increases seen with that fuel order for these two different vehicles. Over the FTP for the Mercedes Benz E250 (SG-GDI) and Mazda 3 (WG-GDI) vehicles, the weighted CO_2 emissions showed statistically significant reductions of 8% for E20 compared to Bu24 (p=0.006). Over the UC for the SG-GDI and WG-GDI vehicles, the differences between the fuels were more pronounced with E20 and Bu24 producing statistically significant increases of 4 and 3%, respectively, compared to E10 (p=0.003) and Bu32 (p=0.039). Overall for the SG-GDI and WG-GDI, Bu24 showed the highest weighted CO_2 emissions, with E15 (p=0.008) and E20 (p=0.00003) showing statistically significant reductions of 4 and 5%, respectively, compared to the Bu24 blend, while marginally statistically significant reductions of 3% with B16 compared to Bu24 was also seen (p=0.097). For both test cycles, cold-start CO_2 emissions showed statistically significant reductions of 9% for both the FTP (p=0.023) and the UC (p=0.0008) with E20 compared to Bu24. For the FTP hot-running CO_2 emissions, the lowest emissions were seen for E20, which showed statistically significant or marginally statistically significant reductions of 4 to 6% relative to the Bu24, Bu32, and E10 blends. For the UC hot-running CO_2 emissions, Bu24 showed the highest emissions with E10, E20, and Bu16 showing statistically significantly or marginally statistically significant reductions of 3 to 5% compared to Bu24 blend. E10 also showed

an increase of 4% compared to E20 at a statistically significant level (p=0.002). During the hot-start CO_2 emissions for the FTP, E20 showed a statistically significant decrease of 10% relative to Bu24 (p=0.019), whereas no statistical differences were seen between the fuels for the UC. Overall, it appeared that the influence of ethanol use was more beneficial than iso-butanol in terms of GHG emissions for these vehicles, when considering both CO_2 and CH_4, although this trend would need to be examined over a larger set of vehicles.

Slightly elevated levels of CO_2 emissions were shown for the FFVs compared to the GDI vehicles Fig. 6-4. No significant fuel trends were shown for the Ford F150 (PFI-FFV) over both the FTP and UC. Slight decreases in CO_2 emissions factor with increasing ethanol concentration were shown for the Chevrolet Silverado (GDI-FFV) over both cycles. A 7% decrease in the CO_2 emissions factor was shown over the UC for the GDI-FFV from the E10 to E83 fuel blend (p=0.032). In addition, a 4% decrease in the CO_2 emissions factor was shown over the FTP from the E10 to E83 fuel blend (p=0.059). No statistical differences were shown for the cold start CO_2 emissions factors for both FFVs. However, there were statistical differences between the FTP and UC for the FFVs. For the E10 fuel, a 9% decrease from the UC to FTP cycle was shown for the CO_2 emissions factors (p=0.056). When comparing the averaged CO_2 emissions factors of the cold start phase of the FTP and UC, a 40% decrease was shown from the UC to FTP cycles (p=0.025). This was due to more profound levels of CO_2 emissions during the cold start phase of the UC compared to the FTP which had similar CO_2 emissions compared to

the warm and stabilized phases. The differences in driving conditions during phase 1 of the UC could have increase the efficiency of the TWC.

6.3.4. Fuel Economy

Fuel economy for each vehicle/fuel combination is presented in Fig. 6-5. Fuel economy was calculated based on the carbon balance method and the unique properties for each different test fuel and not according to the standard EPA equation. The carbon balance equation more directly accounts for the differences in energy content between different fuels, which are somewhat normalized out in the standard EPA equation. There were some trends of fuel economy reductions with increasing alcohol content/energy content, but not in all cases. The butanol fuels showed the most significant fuel economy differences for the Mercedes Benz E350 (SG-GDI) and Mazda 3 (WG-GDI). Results below show statistical comparisons between the WG-GDI and SG-GDI results. For the FTP, weighted fuel economy results showed statistically significant increases of 7% for Bu16 compared to Bu24 (p=0.032) and Bu32 (p=0.018), respectively. Statistically significant increases with Bu16 of 5% (p=0.021) and 6% (p=0.003) for the hot-running phase and 9% (p=0.054) and 8% (p=0.082) for the hot-start phase compared to Bu24 and Bu32, respectively, were also observed. For the UC, weighted fuel economy showed statistically significant increases of 5 and 4% for Bu16 relative to Bu24 (p=0.0001) and Bu32 (p=0.005), respectively. There were not statistically significant differences between the fuel economies for the different ethanol fuels, on the other hand. The ethanol fuels did show some statistically significant differences compared to the some of the butanol fuels and generally showed higher fuel economies than the Bu24 and Bu32 fuels.

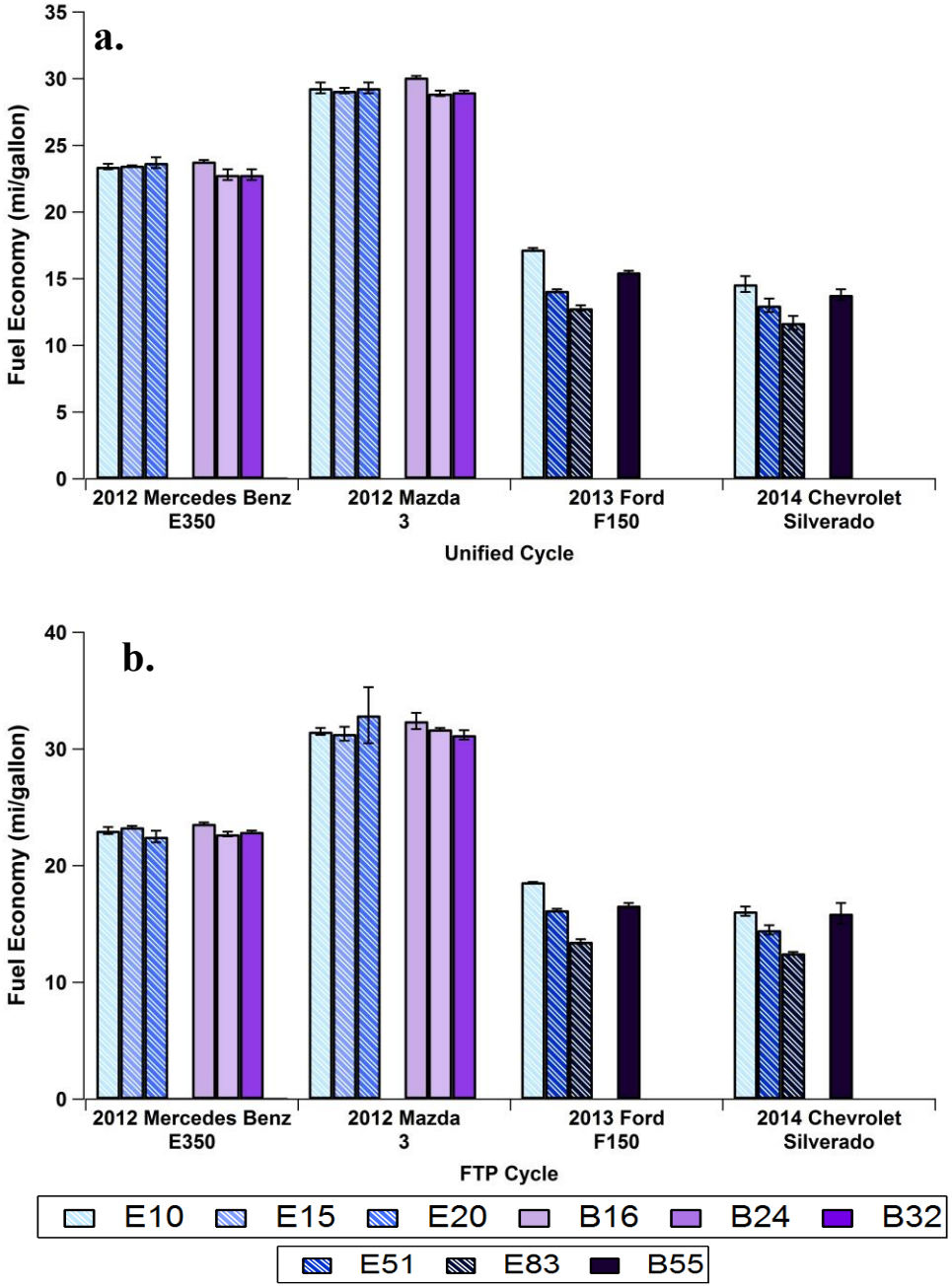

Fig. 6- 5. Fuel Economy results based on the Carbon Balance Method

For the FFVs, decreases in fuel economy were shown with increasing ethanol concentration. No significant differences in fuel economy was shown between the Ford

F150 (PFI-FFV) and Chevrolet Silverado (GDI-FFV). A 25% (p=0.001) and 16% (p=0.004) decrease in fuel economy was should from the E10 to E83 fuel for the PFI-FFV and GDI-FFV, respectively, over the UC. Over the FTP, a 27% (p=0.001) and 23% (p=0.002) decrease in fuel economy was should from the E10 to E83 fuel blend for the PFI-FFV and GDI-FFV, respectively.

6.3.5. CO Emission Factors

CO emissions are shown in Fig. 6-6. CO emissions ranged from 0.134 to 0.527 g/mile for the FTP and 0.168 to 1.080 g/mile for the UC for the Mercedes Benz E350 and Mazda 3, with the Mercedes Benz E350 (SG-GDI) vehicle producing considerably lower CO emissions than the Mazda 3(WG-GDI) vehicle. Statistically significant differences between the WG-GDI and SG-GDI are mentioned below. For the FTP, weighted CO emissions showed statistically significant increases of 37, 33, and 48%, respectively, for E10 compared to E20 (p=0.002), Bu16 (p=0.006), and Bu32 (p=0.00005). Interestingly, the intermediate Bu24 blend also showed emissions that were higher at a statistically significant level than those of E20, Bu16, and Bu32. For the cold-start CO emissions, E10 was statistically significantly higher in the order of 41 and 54%, respectively, compared to E20 (p=0.009) and Bu32 (p=0.0003), and marginally statistically significantly higher in the order of 33% compared to Bu16 (p=0.073). Additionally, Bu24 showed a 37% increase relative to Bu32 at a statistically significant level (p=0.025). For the hot-start phase of the FTP, CO emissions showed statistically significant increases of 44 and 46%, respectively, for E10 (p=0.023) and E15 (p=0.016) compared to Bu32 blend. No strong trends between the test fuels for the weighted CO emissions were seen

for the UC. For the cold-start CO emissions, E10 showed a marginally statistically significant decrease of 41% (p=0.081) and a statistically significant decrease of 45% (p=0.043) compared to B16 and Bu24 blends, respectively. A marginally statistically significant decrease of 39% for was also seen for E20 compared to Bu24 (p=0.093).

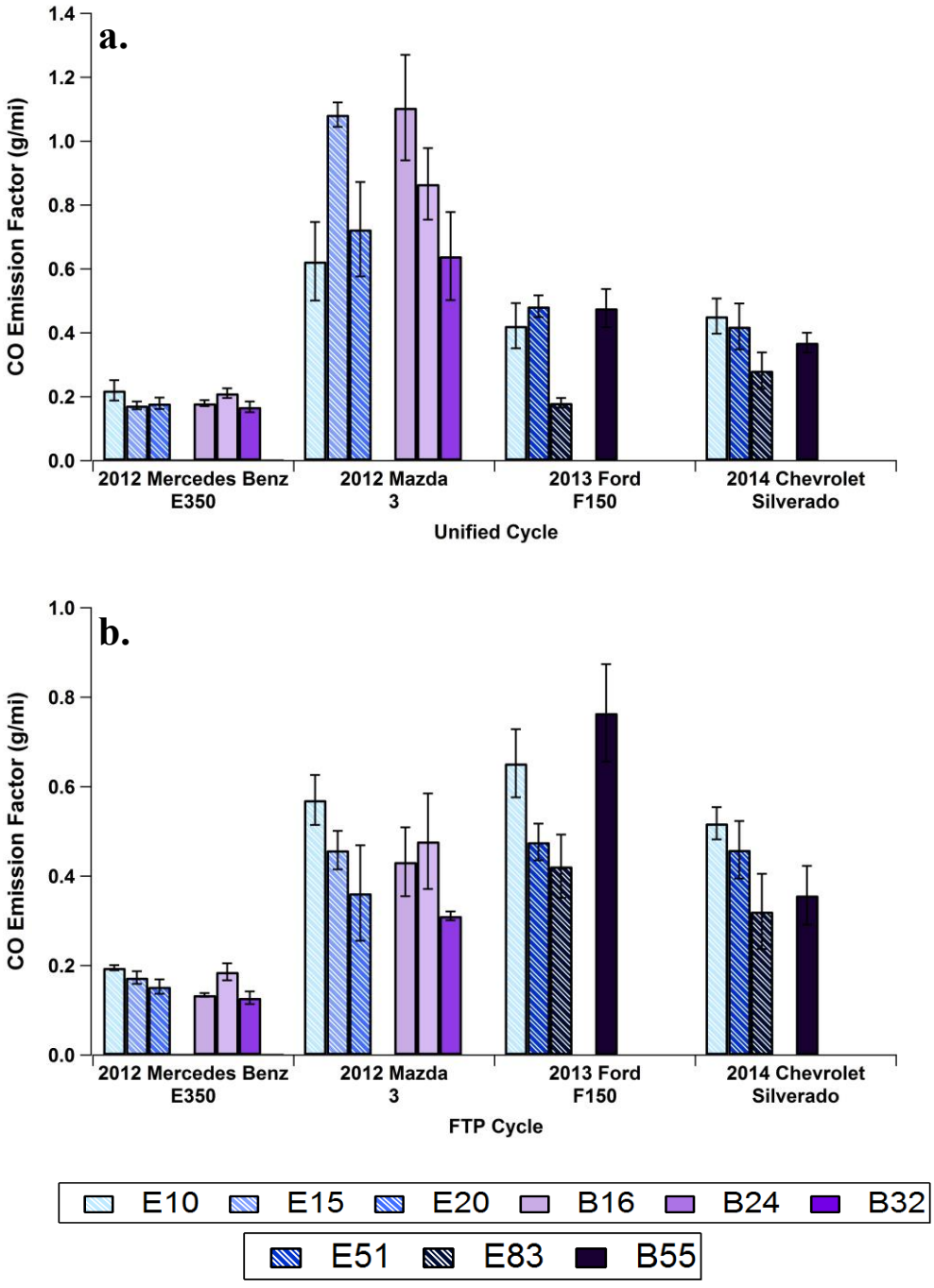

Fig. 6-6. CO Emissions Factors for all four vehicles tested over the UC (a.) and FTP (b.) cycles

For the FFVs, there were strong fuel trends in decreasing CO emission factors with increasing ethanol concentration. In addition, the FTP cycle showed larger CO emission factors for the E10 fuel compared to the UC. The UC decreased the CO emission factor by 35% (p=0.024) and 37% (p=0.031) compared to the FTP cycle for the E10 fuel of the Ford F150 (PFI-FFV) and Chevrolet Silverado (GID-FFV), respectively. Over the UC, a 57% (p=0.019) and 13% (p=0.062) decrease in CO weighted emissions from the E10 fuel to the E83 fuel blend. Over the FTP cycle, a 35% (p=0.055) and 38% (p=0.012) decrease in CO weighted emissions from the E10 fuel to the E83 fuel blend. Both FFVs showed significant decreases in the CO emission factors between the cold start and hot start phase of both cycles, which is due to the TWC not being fully warm thus not to maximum efficiency.

There were trends of lower CO emissions with the higher alcohol fuel blends for both vehicles with some exceptions. This trend was stronger for the ethanol blends, whereas the intermediate Bu24 tended to show the highest emissions for the butanol blends. Previous studies have shown reductions in CO with increasing alcohol content due to improved oxidation of the CO as a result of the oxygen content in the fuel (Karavalakis et al. 2012; Knoll et al. 2009; Schifter et al. 2011). It was observed that the higher CO reductions were achieved with E20 and Bu32 blends relative to E10. While it is hypothesized that the oxygen content was the primary contributing factor for the CO decrease, it might be possible that the CO decreases with E20 could be also a result of the considerably lower 50% distillation temperature (T50) compared to the other blends. This is in agreement with a previous study conducted by Durbin et al. 2007 where they found

reduced CO emissions with lowering T50 in ethanol blends. This is also in agreement with the findings of the EPAct study, which showed that both a combination of fuel-borne oxygen and lower T50 were responsible for lower CO emissions on a fleet of PFI vehicles when running on ethanol blends (EPA 2013). It should be emphasizing that similar to THC/NMHC emissions, CO emissions were dominated by the cold-start portion of the FTP and UC. The significantly higher CO emissions during cold-start compared to hot-running and hot-start emissions suggest that the combustion was rich during the first 200-300 seconds of the test cycles.

6.3.6. NO_X Emission Factor

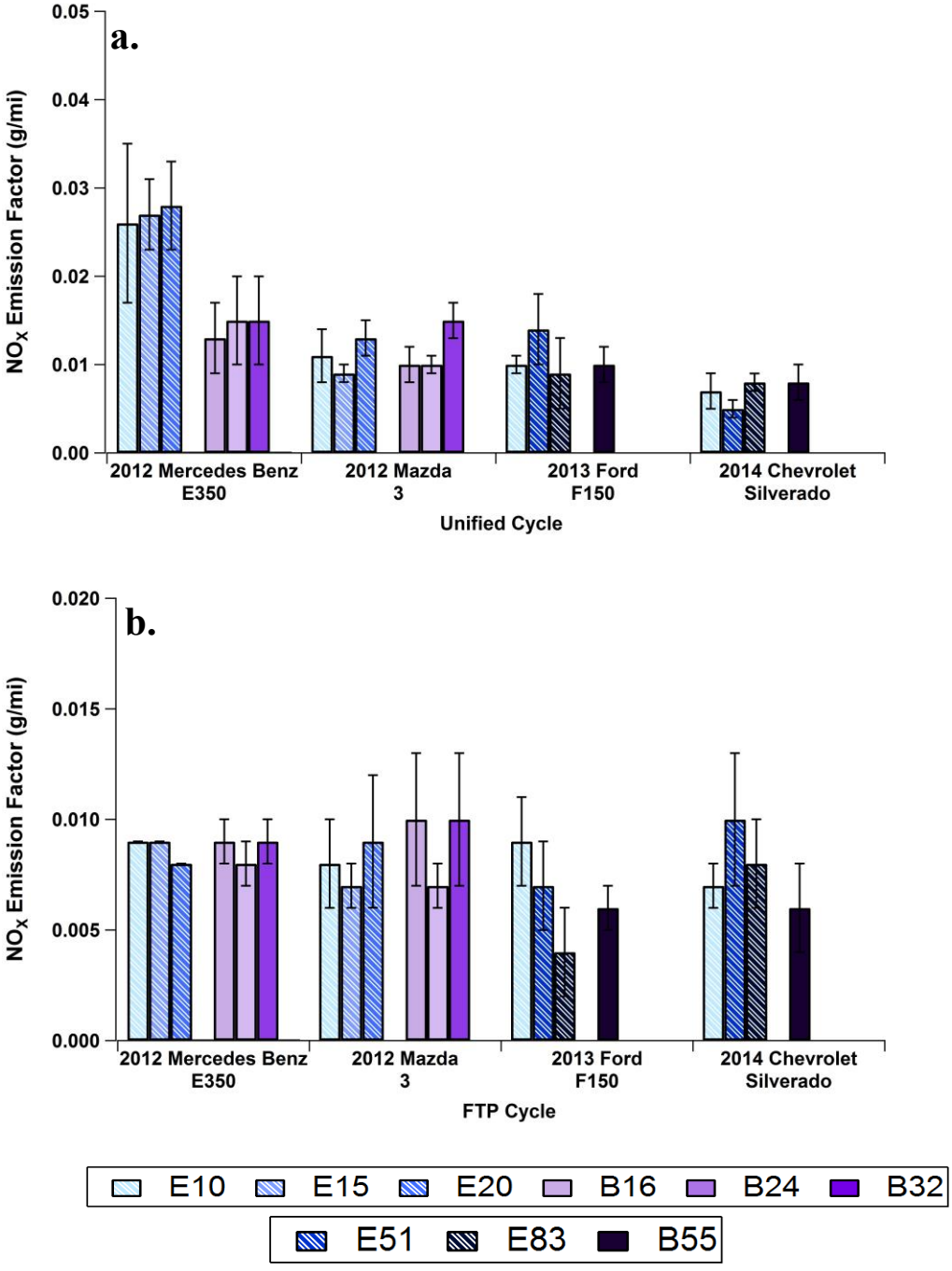

Fig. 6-7. NO_x emissions factors for all four vehicles tested over the UC (a.) and FTP (b.) cycles

NO_x emissions as a function of fuel type are presented in Fig. 6-7. NO_x emissions ranged from 0.004 to 0.010 g/mile for the FTP and from 0.005 to 0.028 g/mile for the UC. The NO_x emissions for the Mazda 3 (WG-GDI) and the Mercedes Benz E350 (SG-GDI) were comparable over the FTP, but lower for the WG-GDI for the ethanol fuels over the UC. Overall for all four vehicles, NO_x emissions did not show any consistent fuel trends or any statistically significant differences between fuels for the FTP and UC. However for the Ford F150 (PFI-FFV), a 54% decrease in NO_X emissions with increasing ethanol content was shown over the FTP (p=0.067). Interestingly, some differences between the fuels were only observed for the hot-start phase of both the FTP and UC cycles for the SG-GDI and WG-GDI vehicles which are mentioned below. For the FTP, E10 and E15 showed statistically significant NO_x decreases of 65% (p=0.049) and 67% (p=0.037), respectively, compared to Bu32. For the UC, NO_x emissions showed statistically significant decreases of 96 and 101%, respectively, for E15 compared to E20 (p=0.010) and Bu32 (p=0.008).

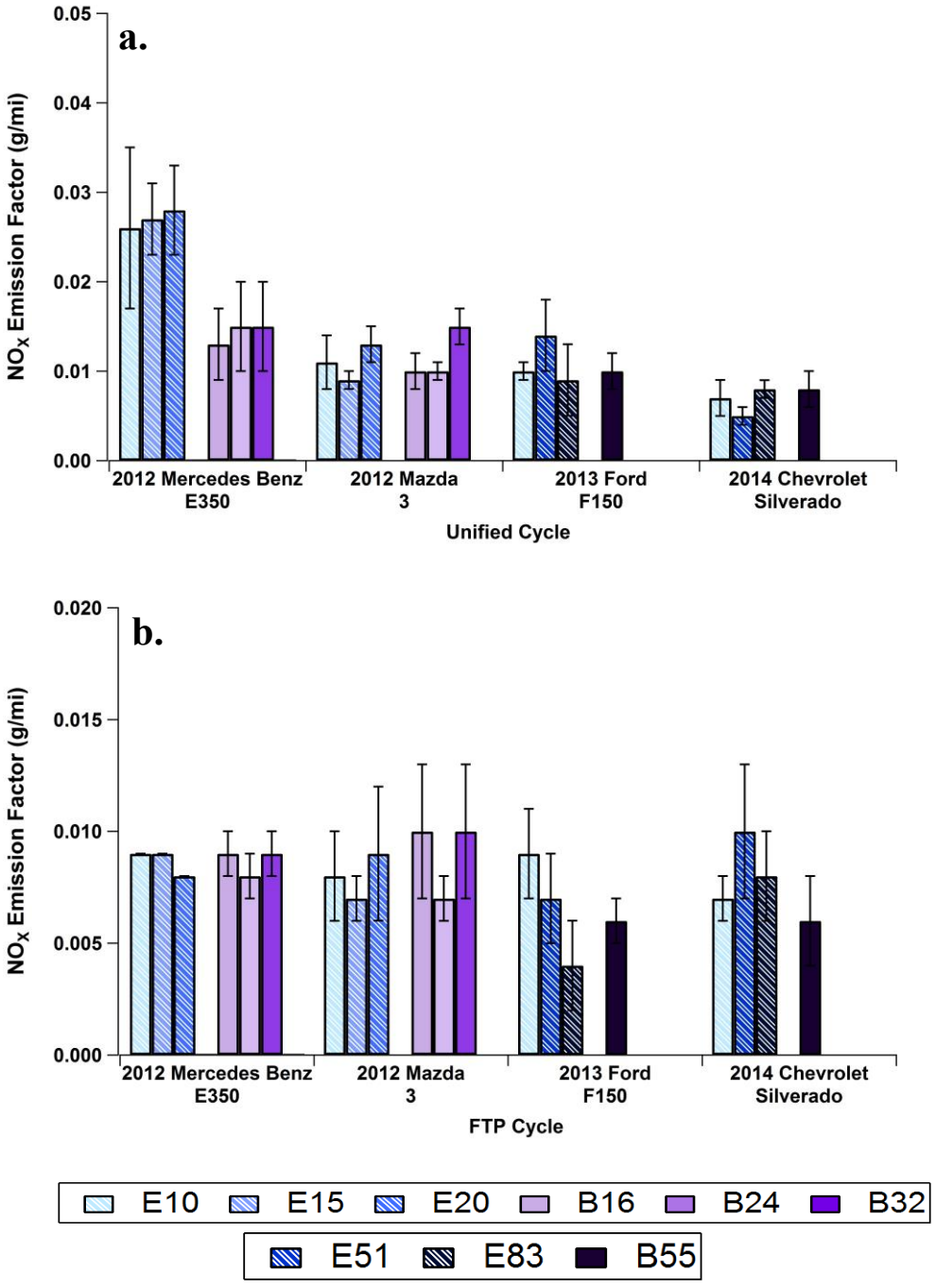

Fig. 6-8. NO_x emissions factors for all four vehicles tested over the UC (a.) and FTP (b.) cycles

6.3.7. PM Mass, Number, and Size Distributions

6.3.7.1. PM Mass Emission Factor

The cycle-based PM mass emissions are shown in Fig. 6-8. PM emissions for the Mazda 3 (WG-GDI) vehicle, Ford F150 (PFI-FFV), and Chevrolet Silverado (GDI-FFV) were considerably higher than those of the Mercedes Benz E350 (SG-GDI) vehicle. For the WG-GDI vehicle, PM emissions ranged from 1.23-2.74 mg/mile for the FTP and from 0.68-2.53 mg/mile for the UC, while for the SG-GDI vehicle PM emissions ranged from 0.09-0.38 mg/mile for the FTP and from 0.17-0.45 mg/mile for the UC. For the PFI-FFV, PM emissions ranged from 0.79 to 3.06 for the FTP and 0.73 and 1.49 for the UC, while the GDI-FFV have PM emissions range from 1.68 to 4.85 for the FTP and 1.15 to 4.83 for the UC. Lower PM emissions have been found in previous chassis dynamometer studies utilizing SG-GDI vehicles compared to WG-GDI vehicles (Zhang and McMahon 2012; Li et al. 2014). This study confirmed that PM emissions from SG-GDI and WG-GDI (both the WG-GDI and GDI-FFV) engines are significantly different. The lower PM emissions from a spray-guided system were due to the fuel injection architecture with an injector located close to the spark plug thereby providing better mixture preparation and more efficient fuel evaporation, and less fuel present on the floor of the piston bowl (Pioch et al. 2011). Our results showed that both GDI vehicles can potentially meet the future California LEV III and Tier 3 standards for PM mass emissions to be implemented by 2017 (3 mg/mile), with the SG-GDI vehicle even complying with the ultra-low PM standard of 1 mg/mile, which is expected in 2025.

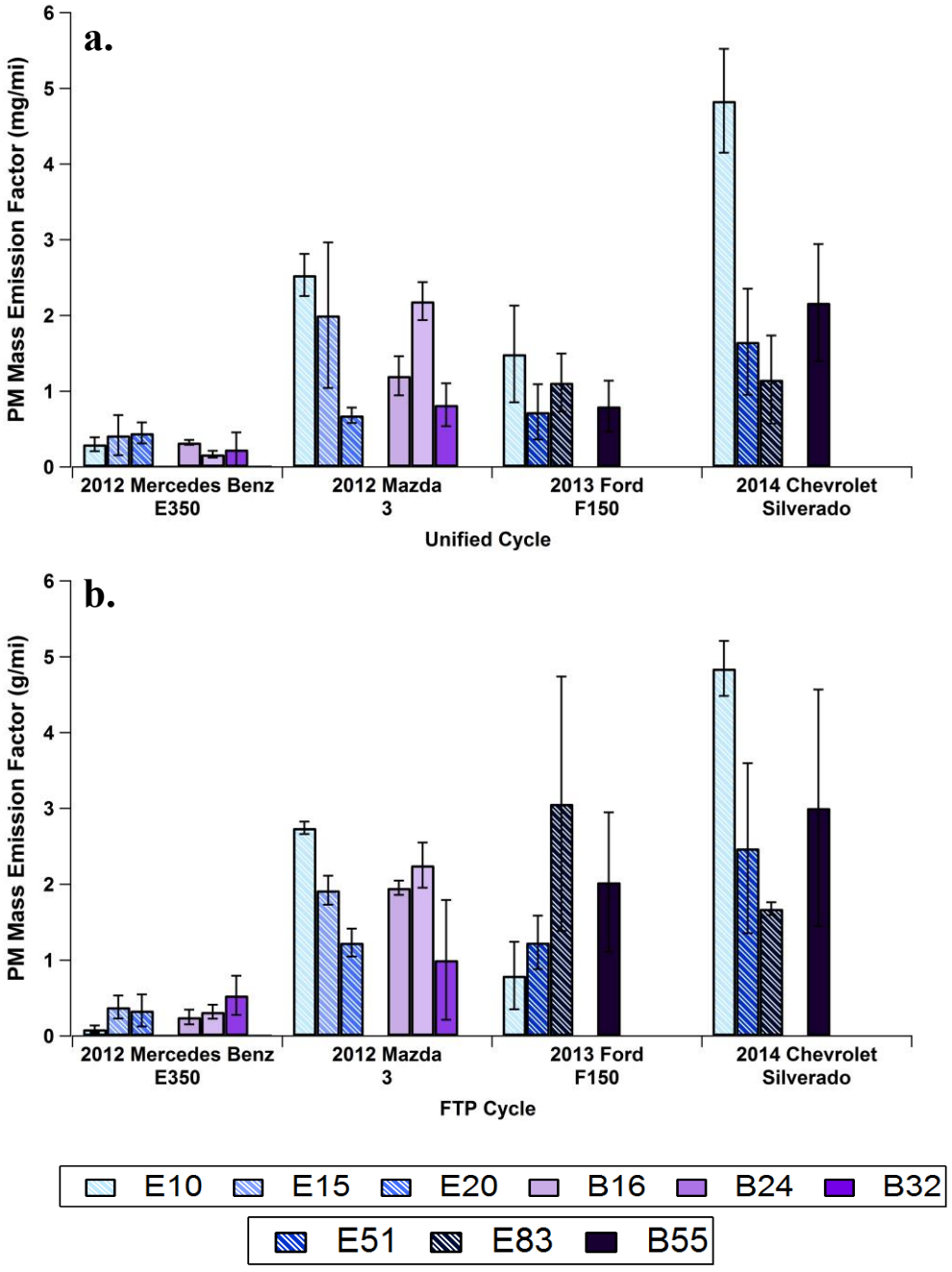

Fig. 6- 9. PM Mass emissions factor for all four vehicles over the UC (a.) and FTP (b.)

Statistical analysis of the results showed that there was no strong fuel effect on the cycle-based PM emissions for neither the FTP nor the UC. This result was probably due to the minor differences between the fuels for the Mercedes Benz E350 (SG-GDI) vehicles for both test cycles, which ultimately influenced the fleet-based statistics. However, the Chevrolet Silverado (GDI-FFV) found a strong fuel trend of decreasing PM mass emissions by 65% (p=0.031) and 76% (p=0.018) for the FTP and UC, respectively. It is worth mentioning that for the SG-GDI vehicle, a trend towards higher PM emissions for E15 and E20 relative to E10 was seen, however. Similar to the results reported here, Chen et al. 2012 showed an increase in PM emissions with increasing ethanol content on a SG-GDI engine. They attributed these phenomena to the higher enthalpy of vaporization and lower energy density of ethanol, and the poor spray atomization performance for the ethanol blends, which will produce a greater mixture in-homogeneity and induce high PM emissions. For the WG-GDI vehicle, the use of increasing alcohol content resulted in lower PM emissions, indicating that the oxygen content was the primary factor for reducing PM. The lower PM emissions with alcohol fuels in context with the influence of the oxygen content have been discussed in previous studies (Storey et al. 2010; Maricq et al. 2012; Costagliola et al. 2013).

6.3.7.2. PN Emission Factor

Particle number (PN) emissions are presented in Fig. 6-9. In general, PN emissions corroborate the PM mass trends, with the Mazda 3 (WG-GDI) vehicle showing higher particle number emissions compared to the Mercedes Benz E350 (SG-GDI) vehicle. The SG-GDI vehicle and the Ford F150 (PFI-FFV) showed similar PN emission factors. The

Chevrolet Silverado (GDI-FFV) showed the largest PN emission factors with ranges from 1.59 $x10^{13}$ to 5.24 $x10^{12}$ #/mi for the FTP and 6.95 $x10^{12}$ to 3.20 $x10^{12}$ #/mi for the UC. For both FFVs, decreasing PN emissions resulted with increasing ethanol concentration. A 54% and 67% decrease in PN emissions for the UC and FTP, respectively, from the E10 to E83 fuel for the GDI-FFV. In addition, a 74% and 62% decrease in PN emissions was shown for the UC and FTP, respectively, from the E10 to E83 fuel blends for the PFI-FFV.

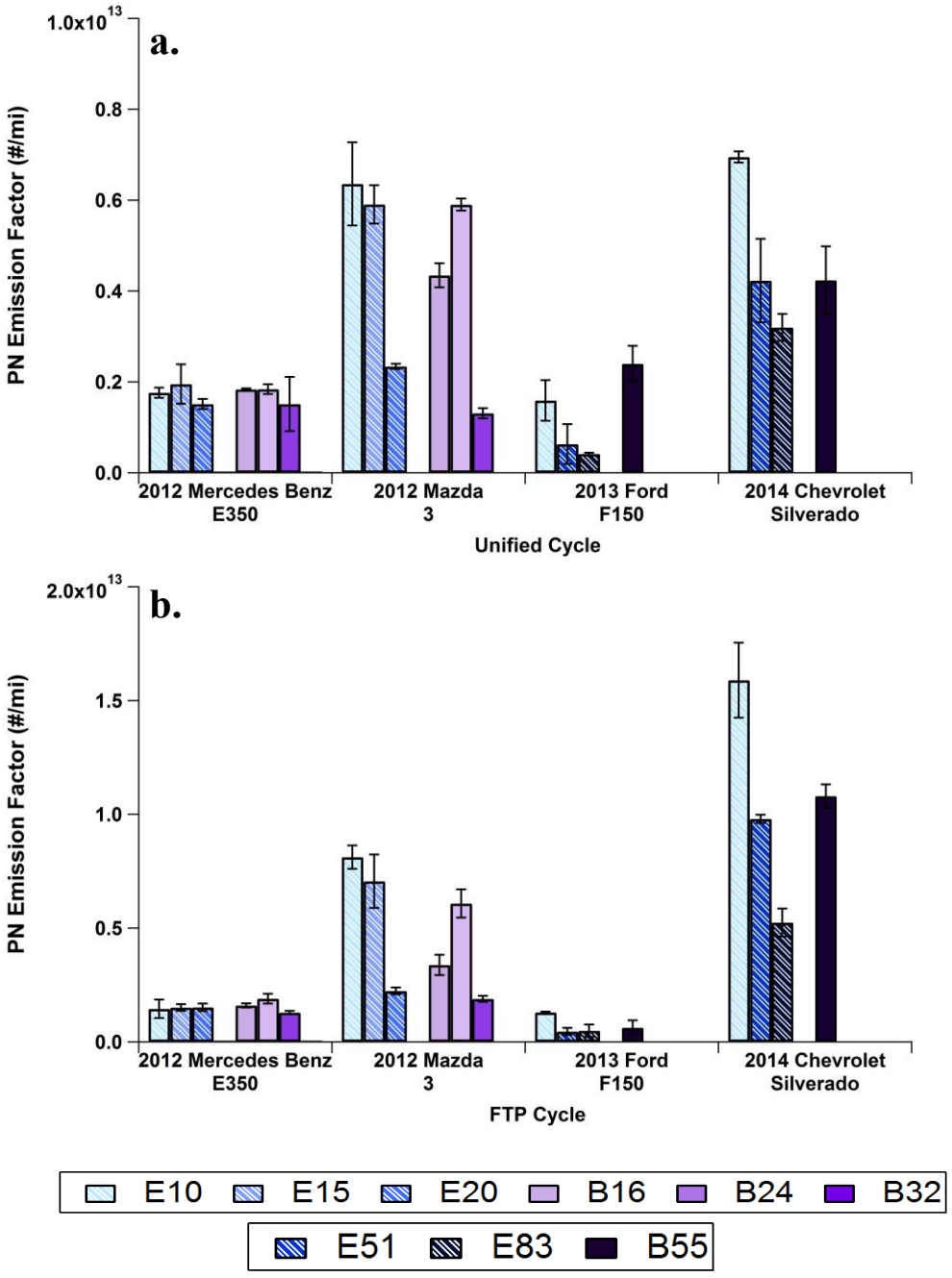

Fig. 6- 10. PN emission factor for all four vehicles over the UC (a.) and FTP (b.)

Further analysis showed that PM mass emissions highly correlated to particle number emissions for the WG-SIDI vehicle, but not for SG-GDI vehicle. The highest correlation

was observed for the UC (R^2 = 0.88), followed by the FTP (R^2 = 0.78). Zhang and McMahon 2012 also reported higher particle number emissions for WG-GDI vehicles compared to SG-GDI vehicles over the FTP cycle. Note, that both vehicles produced higher particle number counts for the higher speed and load UC cycle compared to the FTP. The higher particle number emissions for the WG-GDI vehicle were likely due to the increasing wall wetting by fuel on the piston, valve, and cylinder liner. This may result in liquid fuel that is not totally vaporized at the start of combustion. As a consequence, local fuel-rich combustion or even pool fires can occur near the piston, generating high particle emissions (Maricq et al. 2013; He et al. 2010). For the SG-GDI vehicle, the lower particle number emissions were most likely due to the reduced contact between fuel and combustion chamber surfaces, which was achieved through the higher fuel pressure and therefore better spray atomization and mixture preparation.

6.3.7.3. Particle Size Distributions

The transient particle size distributions for all four vehicles over the FTP and UC cycles are shown in Figs. 10-13, respectively. All three GDI vehicles displayed diesel-like distributions and fit well a bimodal lognormal fit. For the Mercedes Benz E350 (SG-GDI) vehicle for both test cycles, the number-weighted particle size distribution for all fuels was decidedly bimodal. While the accumulation mode peak is dominating the particle size distribution, there is also a nucleation mode present as well. For the SG-GDI vehicle, the accumulation mode geometric mean particle diameter centered around 35 to 50 nm for the FTP and 40 to 50 nm for the UC. The peak particle size of the nucleation

mode for the SG-SIDI was about 11 nm in diameter for both cycles. The Mazda 3 (WG-SIDI) and Chevrolet Silverado (GDI-FFV) vehicle emitted considerably higher concentrations of accumulation mode particles over both test cycles compared to the SG-SIDI vehicle. This can be attributed to the fact that there will be more localized fuel-rich zones in the charge cloud due to the reduced mixture preparation time associated with wall-guided engine architectures. The accumulation mode geometric mean particle diameter ranged from 55 to 70 for the FTP and from 50 to 60 nm for the UC for the WG-GDI. Whereas, the GDI-FFV accumulation mode geometric mean particle diameter ranged from 70-90nm for the UC and 80 to 100nm for the FTP. Similar to the SG-SIDI vehicle, a nucleation mode distribution with peak particle size at around 11 nm was seen for the WG-GDI and GDI-FFV vehicles over both cycles. A lack of an accumulation mode exists for the Ford F150 (PFI-FFV) for both the UC and FTP cycles. However, the E10 fuel has the only accumulation mode peak of 90-100nm for the UC and 50-60nm for the FTP. Most particles were emitted in the nucleation mode (~10nm) during both the FTP and UC for the PFI-FFV.

Fuel properties and type seemed to play an essential role in shaping the nature of particle size distributions from GDI vehicles. For both vehicles, the high oxygen content and high aromatics content fuels resulted in higher number concentration of accumulation mode particles, with this phenomenon being more pronounced for the WG-GDI vehicle. The lower oxygen/aromatic content B32 and E20 blends systematically showed lower number concentration of accumulation mode particles and in most cases a smaller size in

geometric mean diameter compared to the other blends. B32 generally shifted towards smaller particle diameters than E20 for both vehicles over both test cycles.

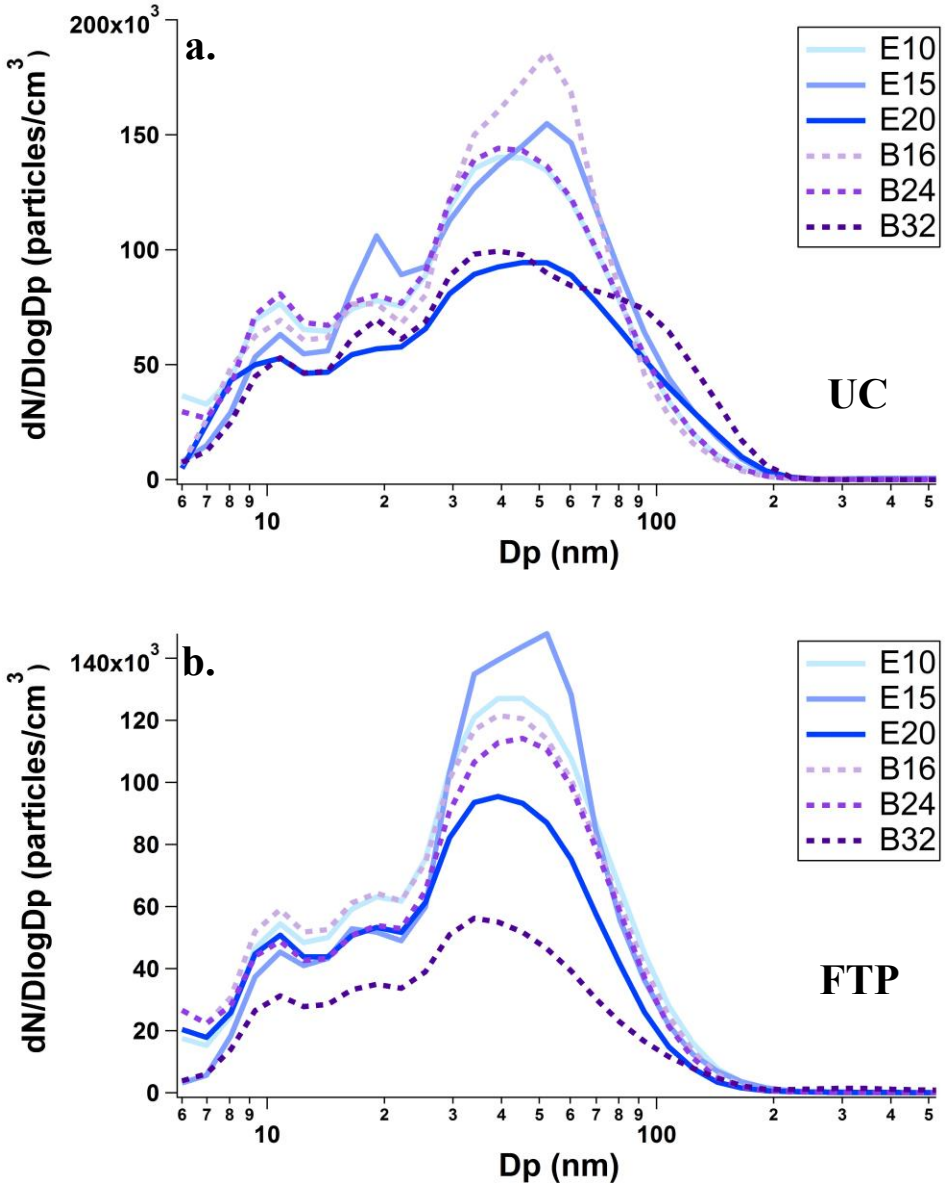

Fig. 6- 11. Mercedes Benz E350 particle size distributions over the UC (a.) and FTP (b.)

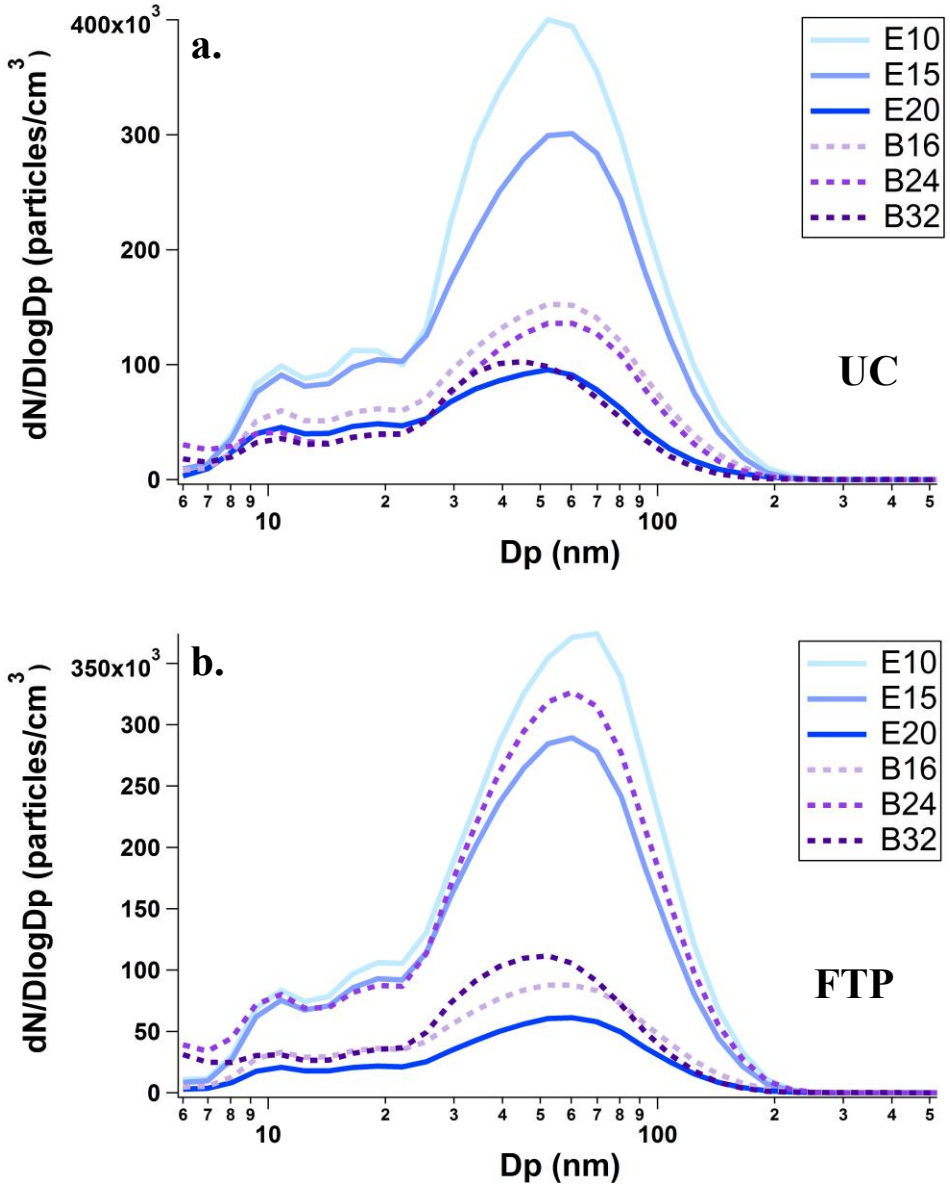

Fig. 6- 12. Mazda 3 particle size distributions over the UC (a.) and FTP (b.)

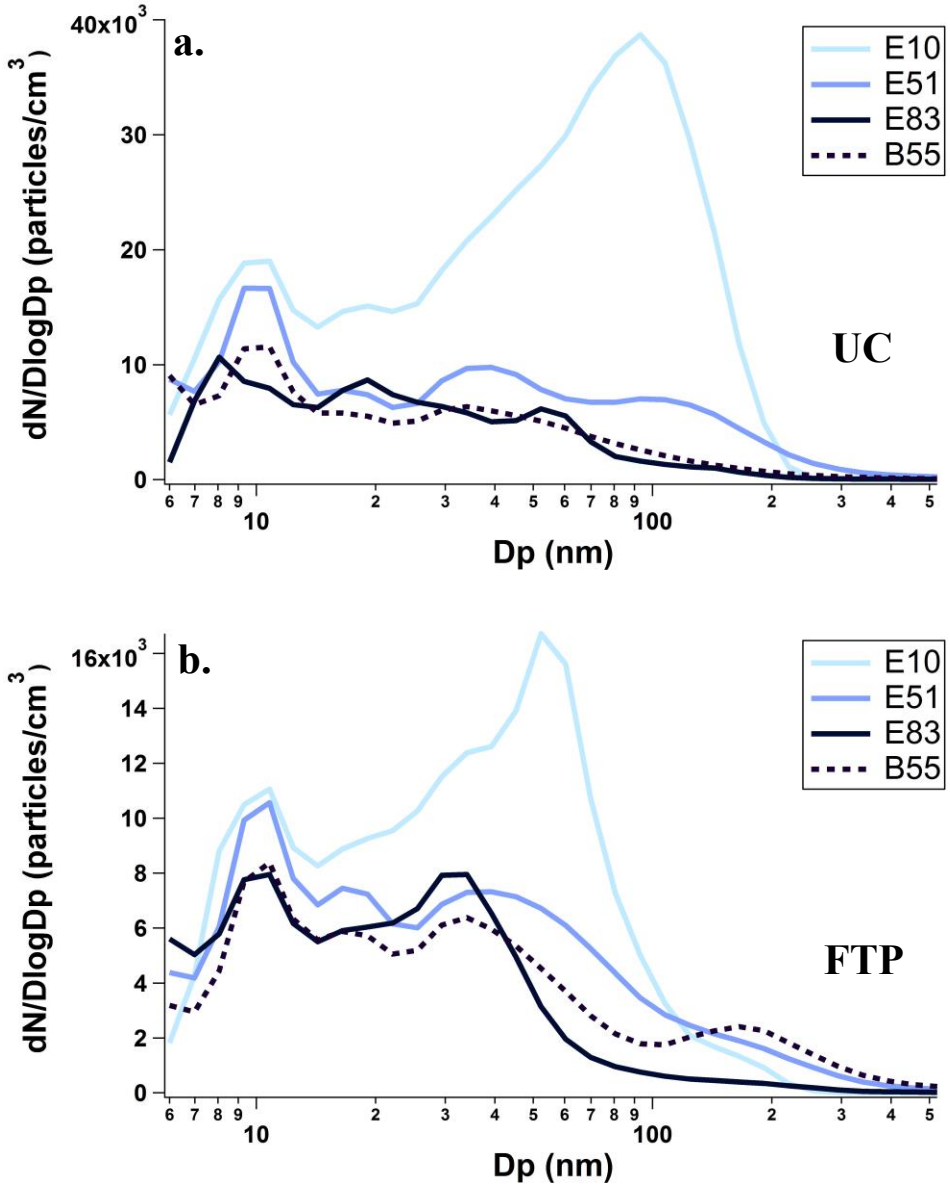

Fig. 6-13. Ford F150 particle size distributions over the UC (a.) and FTP (b.)

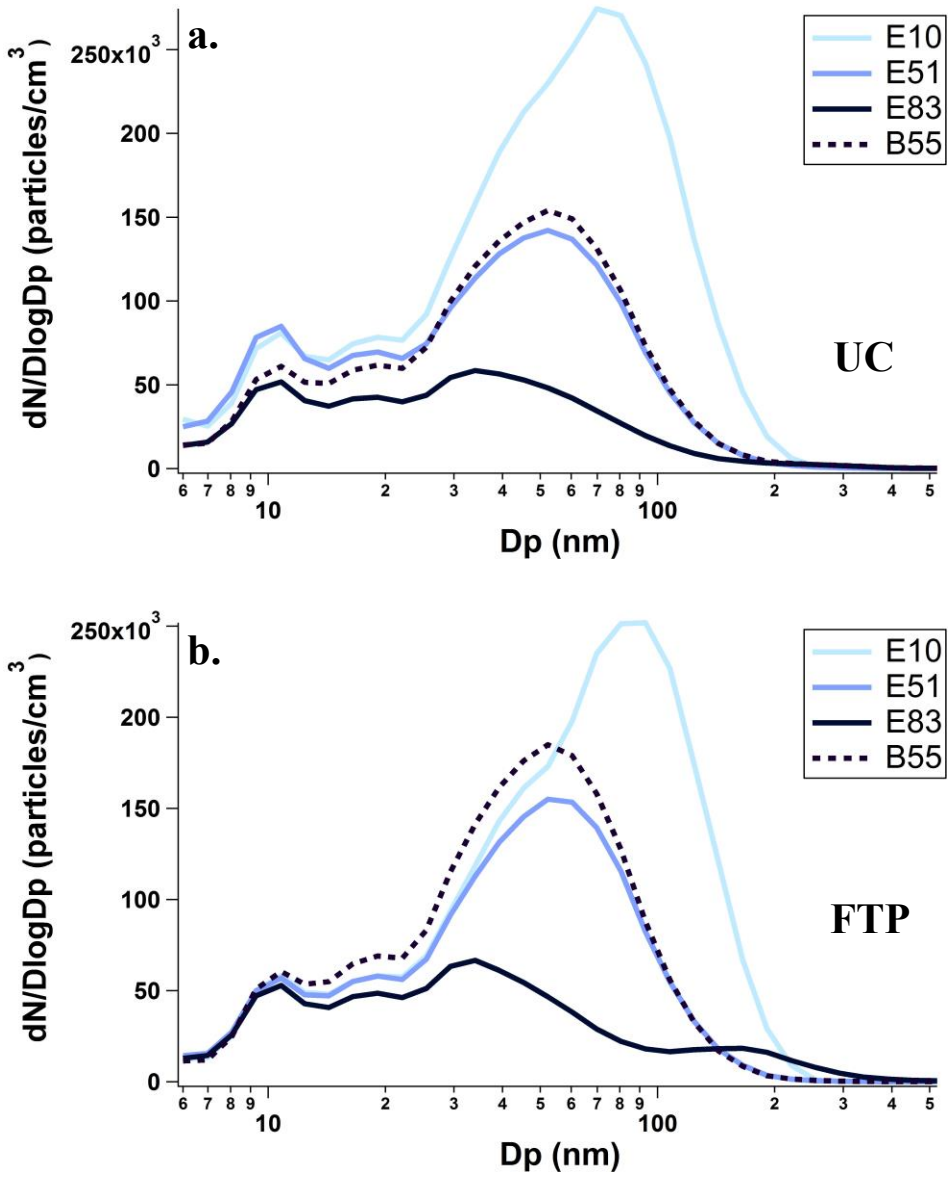

Fig. 6-14. Chevrolet Silverado particle size distributions over the UC (a.) and FTP (b.)

6.4. Conclusions

This study examined the gaseous and particulate emissions impacts of ethanol and iso-butanol blends on a fleet which include a PFI, SG-GDI , WG-GDI, and WG-FFV over the FTP and UC driving cycles using a light-duty chassis dynamometer. Our results

showed some reductions in THC and NMHC emissions with increasing alcohol content in the fuel and an indication that these pollutants were largely dominated by the cold-start driving conditions. In addition, the Mercedes Benz E350 (SG-GDI) and Mazda 3 (WG-GDI) emitted less THC compared to the two FFVs. Emissions of CH_4 and CO_2 also showed reductions with the higher ethanol and butanol blends relative to E10, with some differences being statistically significant for the SG-GDI, WG-GDI, and the Chevrolet Silverado (GDI-FFV). The GDI-FFV and Ford F150 (PFI-FFV) showed statistically significant reductions in CH_4 emissions with increasing ethanol. CO emissions generally decreased with higher ethanol and iso-butanol blends, with some of these differences for the weighted and cold-start CO emissions being statistically significant for all vehicles. For the SG-GDI and WG-GDI vehicles, the highest reductions in CO emissions were observed for E20 and Bu32 blends relative to E10 and could be ascribed to the fuel-bound oxygen and the lower T50 of these fuels. For the weighted NO_x emissions, there was no strong fuel trend in either driving cycle for any of the test vehicles. With the exception of the Ford F150 over the FTP, which showed decreased NO_x emissions with increasing ethanol fuel content.

By increasing the ethanol and iso-butanol blend level, the average PM mass and particle number emissions generally decreased over the FTP and UC cycles, respectively. This may be explained by the higher oxygen content and the lower aromatics in higher ethanol and butanol blends relative to E10. Our results also showed that important particulate reductions can be achieved with low-, mid-, and high-level alcohol blends from GDI vehicles and can potentially meet the future LEV III emission standards. For

both vehicles, the particles were dominated with accumulation mode size distributions having mean diameters between 35 to 50 nm for the FTP and 40 to 50 nm for the SG-SIDI vehicle, and 55 to 70 for the FTP and from 50 to 60 nm for the UC for the WG-SIDI vehicle. The GDI-FFV mean particle diameter ranged from 70-90nm for the UC and 80 to 100nm for the FTP. The higher oxygen content/lower aromatics content blends lowered the accumulation mode particle concentrations. The PFI-FFV had a large mean accumulation mode diameter for the E10 fuel and a nucleation mode for all fuels at a particle diameter of 10nm. The penetration of GDI vehicles into the U.S. market is expected to continue in the future, and the results of this study suggest that high concentrations of alcohol in fuels may prove beneficial in reducing most harmful emissions, especially particulates, while spray-guided DI engine and port fuel injection designs can substantially lower PM mass and number emissions compared to WG-GDI technology.

6.5. Acknowledgements

This study was supported by the California Energy Commission (CEC) under contract 500-09-051. D. Short was supported under University of California Transportation Center (UCTC). The authors thank Mr. Kurt Bumiller, Mark Villela, Kevin Castillo, Michelle Ta, and Danny Gomez of the University of California, Riverside for their contribution in conducting the emissions testing for this program.

6.6. References

Alkidas A.C., 2007. Combustion advancements in gasoline engines. Energy Conversion and Management, 48,2751-2761.

Alternative Fuels Data Center (AFDC), Department of Energy, 2013, http:// http://www.afdc.energy.gov/fuels/ethanol_blends.html

Anderson, J.E., DiCicco, D.M., Ginder, J.M., Kramer, U., Leone, T.G., Raney-Pablo, H.E., Wallington, T.J. 2012. High octane number ethanol-gasoline blends: Quantifying the potential benefits in the United States. Fuel, 97:585-594.

Broustail G, Halter F, Seers P., Moreac G, Mounaim-Rousselle C. Comparison of regulated and non-regulated pollutants with iso-octane/butanol and iso-octane/ethanol blends in a port-fuel injection spark-ignition engine. Fuel 2012;94:251-261.

Cadle , S.H., Ayala, A., Black, K., Graze, R.R., Koupal, J., Minassian, F., Murray, H.B., Natarajan, M., Tennant, C.J., Lawson, D.R. 2009. Real World Vehicle Emissions: A Summary of the 18th Coordinating Research Council On-Road Vehicle Emissions Workshop, Journal of Air and Waste Management Association, 59, 130-138.

Clairotte, M., Adam, T.W., Zardini, A.A., Manfredi, U., Martini, G., Krasenbrink, A., Vicet, A., Tournie, E., Astorga, C. 2013. Effects of low temperature on the cold start gaseous emissions from light duty vehicles fuelled by ethanol-blended gasoline. Applied Energy, 102, 44-54.

Chen, L., Stone, R., Richardson, D. 2012. A study of mixture preparation and PM emissions using a direct injection engine with stoichiometric gasoline/ethanol blends. Fuel, 96, 120-130.

Costagliola MA, De Simio L, Iannaccone S, Prati MV. 2013. Combustion efficiency and engine out emissions of a S.I. engine fueled with alcohol/gasoline blends. Applied Energy, 111, 1162-1171.

Dahms R.N., Drake M.C., Fansler, T.D., Kuo, T.W., Peters, N. 2011. Understanding ignition processes in spray-guided gasoline engines using high-speed imaging and the extended spark-ignition model SparkCIMM. Part A: Spark channel processes and the turbulent flame front propagation. Combustion and Flame, 158, 2229-2244.

Delgado, R.C.O.B., Araujo, A.S., Fernandes, V.J. 2007, Properties of Brazilian Gasoline Mixed with Hydrated Ethanol for Flex Fuel Technology, Fuel Processing Technology, 88(4), 365-368

Durbin, T.D., Miller, J.W., Younglove, T., Huai, T., Cocker, K. 2007. Effects of Fuel Ethanol Content and Volatility on Regulated and Unregulated Exhaust Emissions for the Latest Technology Gasoline Vehicles. Environmental Science Technology, 41,4059-4064.

European Commission. Directive 2009/30/EC of the European parliament and the council of 23 April 2009 on the promotion of the use of energy from renewable sources and amending and subsequently repealing directives 2001/77/EC and 2003/30/EC. Off J Eur communities L140/16; 2009.

Gardebroek, C., Hernandez, M.A. 2013. Do energy prices stimulate food price volatility? Examining volatility transmission between US oil, ethanol and corn markets. Energy Economics, 40, 119-129.

Giglio V, Fiengo G, di Gaeta A, Palladino A., 2013. Common rail system for GDI engines. SpringerBriefs in Control, Automation and Robotics.

Graham, L.A., Belisle, S.L., Baas, C.L. 2008. Emissions from Light-Duty Gasoline Vehicles Operating of Low Blend Ethanol Gasoline and E85, Atomospheric Environment, 42(19), 4498-4516

Schulz M, Clark S. Vehicle emissions and fuel economy effects of 16% butanol and various ethanol blended fuels (E10, E20, and E85). Journal of ASTM International 2011;8:1-19.

He, B.Q., Wang, J.X., Hao, J.J., Yan, X.G., Xiao, J.H. 2003. A study on emission characteristics of an EFI engine with ethanol blended gasoline fuels, Atmospheric Environment, 37, 949–957

He X, Ireland JC, Zigler BT, Ratcliff MA, Knoll KE, Alleman TL, Tester JT. 2010. The impacts of mid-level biofuel content in gasoline on SIDI engine-out and tailpipe particulate matter emissions. SAE Technical Paper 2010-01-2125.

Hubbard, C.P., Anderson, J. E., Wallington, T.J. 2014. Ethanol and Air Quality: Influence of Fuel Ethanol Content on Emissions and Fuel Economy of Flexible Fuel Vehicles, Environmental Science and Technology, 48(1), 861-867.

Irimescu, A. 2012. Performance and fuel conversion efficiency of a spark ignition engine fueled with iso-butanol. Applied Energy, 96, 477-483.

Jin, C., Yao, M., Liu, H., Lee, C.F.F, Ji, J. 2011. Progress in the production and application of n-butanol as a biofuel. Renewable and Sustainable Energy Reviews, 15, 4080-4106.

Karavalakis, G., Durbin, T.D., Shrivistava, M., Zheng, Z., Villela, M., Jung, H. 2012. Impacts of ethanol fuel level on emissions of regulated and unregulated pollutants on a fleet of gasoline light-duty vehicles, Fuel, 93, 549-558

Karavalakis, G., Short, D., Hajbabaei, M., Vu, D., Villela, M., Russell, R., Durbin, T., Asa-Awuku, A. 2013. Criteria Emissions, Particle Number Emissions, Size Distributions, and Black Carbon Measurements from PFI Gasoline Vehicles Fuelled with Different Ethanol and Butanol Blends. SAE Technical Paper 2013-01-1147.

Karavalakis, G., Short, D., Vu, D., Villela, M., Asa-Awuku, A., Durbin, T. 2014. Evaluating the regulated emissions, air toxics, ultrafine particles, and black carbon from SI-PFI and SI-DI vehicles operating on different ethanol and iso-butanol blends. Fuel, 128, 410-421.

Knoll K, West B, Huff S, Thomas J. Effects of mid-level ethanol blends on conventional vehicle emissions. SAE Technical Paper 2009-01-2723, 2009.

Lee, H., Myung, C.-L., Park, S., 2009. Time resolved particle emissions and size distribution characteristics during dynamic engine operation conditions with ethanol-blended fuels, Fuel, 88(9), 1680-1686.

Li Y., Xue J., Johnson K., Durbin T., Villela M, Pham L., Hosseini S., Short D., Karavalakis G., Asa-Awuku A., Jung H. 2014. Determination of Suspended Exhaust PM Mass for Light Duty Vehicles Using IPSD Method. SAE Technical Paper 2014-01-1594.

Maricq, M.M., Szente, J.J., Jahr, K. 2012. The impact of ethanol fuel blends on PM emissions from a light-duty GDI vehicle. Aerosol Science and Technology, 46, 576-583.

Maricq MM, Szente JJ, Adams J, Tennison P, Rumpsa T. 2013. Influence of mileage accumulation on the particle mass and number emissions of two gasoline direct injection vehicles. Environ. Sci. Technol., 47, 11890-11896.

Oh, H., Bae, C. 2013. Effects on the injection timing on spray and combustion characteristics in a spray-guided DISI engine under lean-stratified operation. Fuel, 107,225-235.

Park C., Kim S, Kim H., Moriyoshi Y., 2012. Stratified lean combustion characteristics of a spray-guided combustion system in a gasoline direct injection engine. Energy, 41, 401-407.

Piock W, Hoffmann G, Berndorfer A, Salemi P, Fusshoeller B. 2011. Strategies towards meeting future particulate matter emission requirements in homogeneous gasoline direct injection engines. SAE Int. J. Engines, 4, 1455-1468.

Price, P., Twiney, B., Stone, R., Kar, K., Walmsley, H. 2007. Particulate and hydrocarbon emissions from a spray guided direct injection spark ignition engine with oxygenated fuel blends. SAE Technical Paper 2007-01-0472.

Ratcliff, M.A., Luecke, J., Williams, A., Christensen, E.D., Yanowitz, J., Reek, A., McCormick, R.L. 2013. Impact of higher alcohols blended in gasoline on light-duty vehicle exhaust emissions. Environ. Sci. Technology, 47, 13865-13872.

Roberts, M.C. 2008. E85 and Fuel Efficiency: An Empirical Analysis of E85 of 2007 EPA Test Data, Energy Data, 36(3), 1233-1235

Schifter I, Diaz L, Rodriguez R, Salazar L. Oxygenated transportation fuels. Evaluation of properties and emission performance in light-duty vehicles in Mexico. Fuel 2011;90:779-788.

Schulz, M., Clark, S. 2011. Vehicle emissions and fuel economy effects of 16% butanol and various ethanol blended fuels (E10, E20, and E85). Journal of ASTM International, 8, 1-19.

Stevens, E., Steeper, R. 2001. Piston wetting in an optical DISI Engine: fuel films, poolfires, and soot generation. SAE Int J Engines, 110, 1287-1294.

Storey, J.M., Barone, T., Norman, K., Lewis, S. 2010. Ethanol blend effects on direct injection spark-ignition gasoline vehicle particulate matter emissions. SAE International Journal Fuels Lubricants, 3, 650-659.

Tao, L., Tan, E.C.D., McCormick, R.L., Zhang, M., Aden, A., He, X., Zigler, B.T. 2014. Techno-economic analysis and life-cycle assessment of cellulosic iso-butanol and comparison with cellulosic ethanol and n-butanol. Biofuels, Bioproducts, and Biorefining, 8, 30-48.

Ultrafine particulate matter and the benefits of reducing particle numbers in the United States. A report to the Manufacturers of Emission Controls Association (MECA). Prepared by Gladstein, Neandross & Associates. July 2013; http://www.meca.org/resources/MECA_UFP_White_Paper_0713_Final.pdf

U.S. Environmental Protection Agency. Fuels and Fuel Additives, Renewable Fuel Standard; http://www.epa.gov/otaq/fuels/renewablefuels

U.S. Environmental Protection Agency. Assessing the effect of five gasoline properties on exhaust emissions from light-duty vehicles certified to Tier 2 standards: Analysis of data from EPAct phase 3 (EPAct/V2/E-89). Final Report. EPA-420-R-13-002, April, 2013, http://www.epa.gov/otaq/models/moves/epact.htm

Wallner, T., Frazee, R. 2010. Study of regulated and non-regulated emissions from combustion of gasoline, alcohol fuels and their blends in a DI-SI engine. SAE Technical Paper 2010-01-1571.

Wallner, T., Miers, S.A., McConnell, S., 2009. A comparison of ethanol and butanol as oxygenates using a direct-injection, spark-ignition engine. Journal of Engineering for Gas Turbines and Power, 131, 1-9.

Xue, C., Zhao, X.Q., Liu, C.G., Chen, L.J., Bai, F.W. 2013. Prospective and development of butanol as an advanced biofuel. Biotechnology Advances, 31, 1575-1584.

Yan, X., Inderwildi, O.R., King, D.A., Boies, A.M. 2013. Effects of ethanol on vehicle energy efficiency and implications on ethanol life-cycle greenhouse gas analysis. Environmental Science Technology, 47, 5535-5544.

Zhai, H., Frey, H.C., Rouphail, N.M., Gonclaves, G.A., Farias, T.L. 2009. Comparison of Flexible Fuel Vehicle and Life Cycle Fuel Composition and Emissions of Selected Pollutants and Greenhouse Gases for Ethanol 85 versus Gasoline, Journal of Air and Waste Management Association, 59(8), 912-924

Zhang S, McMahon W. 2012. Particulate emissions for LEV II light-duty gasoline direct injection vehicles. SAE Int. J. Fuels Lubr., 5, 637-646.

Zhao F., Lai M.C., Harrington, D. 1999. Automotive spark-ignited direct-injection gasoline engines. Prog. Energy Combust. Science, 25, 437–562.

Chapter 7: Particle Speciation from the Use of Ethanol and Iso-butanol Fuels in Spray and Wall Guided Gasoline Direct Injection and Flex Fuel Vehicles

7.1. Introduction

In recent years, research into light-duty vehicles and fuels has expanded due to the Renewable Fuels Standard (RFS) and a need to reduce global dependence on crude oil (RFS, 2007). Automotive manufacturers are continually developing new technologies to reduce emissions and improve fuel economy to meet U.S. federal regulations. Some of these technologies include Gasoline Direct Injection (GDI) and Flex Fuel Vehicles (FFVs), which both have shown increased production in the U.S. market (Zhao et al. 1999). In addition, alternative non-petroleum based fuels, such as ethanol, have gained popularity because they are not petroleum based. However, the impacts of different combinations of these fuels and vehicle technologies on emissions is still not fully understood.

The production of GDI vehicles has increased since 2007 because of the increases in fuel economy obtained with the GDI technology (Zhao et al. 1999; Alkidas 2007). Predictions show that by 2025 approximately 93% of the light-duty passenger vehicle market will consist of GDI engines (EPA, 2013). There are two prominent types of GDI engines which include: Wall-Guided (WG-GDI) and Spray-Guided (SG-GDI) (Solomon et al. 2000; Drake et al. 2005: Alkidas 2007). WG-GDI engines have a fuel injector mounted on the side of the combustion chamber that sprays fuel towards the piston bowl surface. SG-GDI engines have a fuel injector located at the top of the combustion

chamber with the spark plug located directly next to the injector; providing an ideal coupling of the fuel injector and spark plug (Drake et al. 2005; Alkidas 2007). This technology, SG-GDI, offers the potential to improve fuel economy and reduce PM associated with GDI engines. However, the cost associated with manufacturing SG-GDI vehicles has limited the use of the spray-guided technology.

There is also a class of vehicles called Flex Fuel Vehicles (FFVs) that are fitted with material to withstand the higher ethanol content fuels with up to 85% ethanol. FFVs can have either a PFI or GDI engine, and this study looks into the particle composition differences of both. Conventional vehicles are not equipped to handle the corrosive higher ethanol concentrations such as E85. Fuel sensors are also used to detect the use of ethanol in the fuel up to E85 to optimize engine performance by taking into account the lower energy content E85 fuel. A few drawbacks on the mainstream use of FFVs include the current fuel distribution infrastructure in the U.S. (pipelines, underground storage tanks, transportation vehicles, etc.) which would have to be retrofitted to incorporate larger use of E85 fuel blends. It has been suggested that large concentrations of ethanol, such as E85, in gasoline can lead to an enhanced ozone health risk (Jacobson 2007). Salvo and Geiger (2014) has shown that heavy ethanol use in Sao Paulo, Brazil has led to reductions in ground level ozone. The current debate on the environmental impact of large uses of ethanol is still ongoing.

The use of renewable fuels has been increasing in gasoline every year since 2007 due to the RFS requirements, which requires 15.21 billion gallons of renewable fuel to be blended in 2014 (RFS, 2014). Iso-butanol alcohol, a renewable fuel other than ethanol,

has been attracting attention because it's less corrosive and exhibits a higher energy density than ethanol, so it can be used without any engine modifications (Wallner and Frazee 2010). Iso-butanol is produced similarly to the production of ethanol; from bio-mass feedstocks using biochemical pathways via fermentation. The primary method for the production of iso-butanol is the Acetone-Butanol-Ethanol (ABE) process (Jin et al. 2011; Nigam and Singh 2011). However, this method has been shown to have low yields of iso-butanol, making it difficult to produce iso-butanol compared to ethanol (Jin et al. 2011; Nigam and Singh 2011). Ways of improving the ABE method to increase the butanol yield to make it more economically feasible as a fuel are under investigation, however.

Vehicle fuels and technology changes can lead to changes in particle composition, which can have impacts on climate, air quality, and human health. Particles below 2.5 μm can be inhaled into the lungs and have been linked to reactive oxygen species (ROS) production (Tao et al. 2003). ROS generation has also been linked to particular PM compositions, such as Water-Soluble Organic Mass (WSOM) and Water-Insoluble Organic Mass (WIOM) (Verma et al. 2012). Long term exposure to WSOM can also effect DNA (Guetterrez- Castillo et al. 2006), and can act as Cloud Condensation Nuclei (CCN), thus impacting climate (Ervens et al. 2005). Despite these potential impacts, the literature is limited in studies of particle composition for fuels with high (>50%) alcohol content in gasoline. Recently, Dutcher et al. (2011) showed that BC emissions decreased over 50% with increasing ethanol concentration (E0 to E85).

This study will discuss the particle composition differences in emissions between WG-GDI, SG-GDI, and FFVs using varying gasoline blends of ethanol and iso-butanol. Soot, Water-Insoluble Mass (WIM) fractions, and Water-Soluble Organic Carbon (WSOC) and Organic Mass (OM) analysis are all preformed to provide a detailed particle composition investigation. The soot and WIM fractions are measured in real-time during transient and steady-state driving conditions. The WSOC and OM analysis are done using integrated filter measurements that are processed in the laboratory. The coupling of the real-time and integrated filter measurements provides important information that can provide a unique understanding of the different contributions to the total PM mass.

7.2. Experimental Method

7.2.1. Test Vehicles

The test vehicles and their specifications and mileages are listed in Table 7- 1. The vehicles included two FFVs and two conventional vehicles. Both FFVs are light-duty pickup trucks with one vehicle being equipped with a Port Fuel Injection (PFI) engine and the other a wall-guided Gasoline Direct Injection (WG-GDI) engine. The other two vehicles are light-duty passenger cars, but with different GDI technology engines. The first is equipped with a spray-guided GDI (SG-GDI) engine and the other is equipped with a WG-GDI engine. All vehicles were certified to LEV II, ULEV, or SULEV emission standards.

Vehicle Make and Model Year	Engine Displacement and Configuration	Injection System	Emission Control Regulations	Mileage
2012 Mercedes Benz E350	3.6L V6	Spray-guided GDI	LEVII, SULEV	10,996
2012 Mazda 3	2.0L I4	Wall-guided GDI	LEVII, SULEV	18,851
2013 Ford F150	3.7 V6	PFI	LEVII, ULEV	13,687
2014 Chevrolet Silverado	5.3L V8	GDI	LEVII, ULEV	2,649

Table 7- 1. Test Vehicle Specifications

7.2.2. Fuel Specification

All vehicles were tested on E10 (10% ethanol and 90% gasoline), and this served as the base fuel. The SG-GDI (Mercedes- Benz E350) and WG-GDI (Mazda 3) were both tested with 6 custom blended ethanol and iso-butanol gasoline fuels. This included E15 and E20. In addition, these vehicles were tested on blends of 16%, 24% and 32% iso-butanol, repectively, denoted as B16, B24, and B32. It should be noted that B16 is the oxygenated equivalent to E10. The PFI-FFV (Ford F150) and GDI-FFV (Chevrolet Silverado) were tested on four custom blended ethanol and iso-butanol fuels (including E10). The other two higher ethanol fuels include E51 and E83. The higher iso-butanol

blended fuel was a 55% iso-butanol fuel (B55). These fuels were custom made to control Reid Vapor Pressure (RVP), oxygen content, and fuel volatility among other properties. Specific fuel properties can be found in the Appendix Table C-1 and D-1.

7.2.3. Experimental Protocol

Vehicles were tested at CE-CERT's Vehicle Emissions Research Laboratory (VERL). VERL is equipped with a Burke E. Porter 48" barrel light-duty chassis dynamometer. The facility is also equipped with a Constant Volume Sampler (CVS) for emissions sampling. All vehicles were tested on both the Federal Test Procedure (FTP) and the Unified Cycle (UC). The FTP is the primary certification test cycle developed by the U.S. EPA. The UC test cycle was developed by the California Air Resources Board (CARB) as a improved and more representative driving cycle compared to the FTP cycle. In addition, each vehicle (except the Chevrolet Silverado) was tested over three steady-state speeds of 30, 50, and 70 miles per hour (mph).

The FTP and UC each consist of three different types of driving simulations or phases. A speed versus time trace for each is shown is Appendix Fig. C-1. The first phase is known as the "Cold Start" phase. The vehicle's engine and catalyst have been cooled for at least 8 hours before the start of the first phase, simulating conditions when the vehicle is first started for the day. The second phase is the stabilized phase; the vehicle's engine and catalyst are now warm, so driving conditions represent normal driving after the vehicle is warmed up. After phase 2, a "hot soak" of the vehicle is performed where the vehicle is turned off for exactly 10 minutes. Phase 3 proceeds directly after the "hot soak". Phase three is a "hot start" where driving conditions are identical to phase 1,

however, the vehicle now has a warm engine and catalyst. This usually results in lower emissions compared to phase 1. After a FTP or UC, the steady-state testing for the vehicle was performed. Each steady-state speed is run for exactly 10 minutes after a warm up period and after operation was stabilized.

7.2.4. Instrumentation and Analysis

This study included a number of particle and gaseous measurements, as listed in Fig. S2, although the focus of this paper is on the particle measurements. Appendix Fig. D-1 shows the inlet connections of the instruments and the instrument flow rates, and the experimental set-up. The measurements for this paper include both filter particle measurements and real-time particle measurements. The following describes the instrumentation used in the particle analysis for this study.

Organic Mass (OM) was measured for both the Ford F150 and Chevrolet Silverado (FFVs), but only over the FTP cycle. Quartz filters were used for this analysis and the OM concentration was reported for the whole particle over all particle diameters. The Organic Carbon (OC) was measured using a Sunset Laboratory Elemental Carbon (EC)/OC Lab analyzer utilizing the National Institutes of Safety and Health (NIOSH) 5040 protocol. The measurement is a thermal-optical method where the sample was thermally desorbed from the filter with helium gas and then oxidized using controlled heating increases. The sample in analyzed using a Flame Ionization Detector (FID). OC values were multiplied by a factor of 1.55 to take into account the non-carbonaceous organic matter, giving the Organic Mass (Turpin and Lim 2001).

For each transient test, Teflon filters were sampled to quantify Water-Soluble Organic Carbon (WSOC) and Water-Soluble Organic Mass (WSOM) was determined for the whole particle over all particle diameters. Particles were first extracted from the Teflon filter into an aqueous solution. Filters were placed in a clean 60 mL amber vial, and 60 mL of Millipore© water (TOC~70 ppb) was added. Vials were then sonicated for approximately 90 minutes at room temperature. After sonication, the sample was then syringed out of the vial with a Whatman© 25 mm syringe filter (to extract any large water-insoluble material from the sample). A pendant drop tensiometer (Attension Theta 200) was used for the surface tension analysis. The WSOC analysis was performed with a GE Seivers 900 TOC Analyzer. The WSOC concentration is multiplied by a factor of 1.6 to convert to the water-soluble organic mass (WSOM) (Turpin and Lim 2001). This factor accounts for all non-carbonaceous organic mass measured that is water-soluble. The Water-Insoluble Organic Carbon (WIOC) is the WSOC subtracted from the OC values, giving the Water-Insoluble Organic Carbon value. This value was multiplied by 1.4, which accounts for all non-carbonaceous mass that is water-insoluble, to give the Water-Insoluble Organic Mass (WIOM) value. Theoretically, the sum of the WIOM and WSOM should be equivalent to the OM. The correlation between the sum of the WIOM and WSOM with the OM from the OC analysis is plotted in Appendix Fig. D-2. The best fit linear line with a forced y-axis intercept of 0 gives a slope of .954 and a R^2 value of .989. This correlation proves the assumption that the sum of the WIOM and WSOM is equivalent to the OM in this study.

The Water-Insoluble Mass (WIM) fraction was estimated using a technique described in Short et al. 2014, which is based on real-time size distributions for particle diameters below 40 nm. The size distributions were measured using a Scanning Mobility Particle Sizer (SMPS), which consists of an electrostatic classifier (TSI 3080) used in tandem with an Butanol Condensation Particle Counter (B-CPC; TSI 3772) and a Water Condensation Particle Counter (W-CPC; TSI 3785). The CPCs use a different working fluid of either water or butanol. Each particle diameter is measured with two distinct particle concentrations from the B-CPC and W-CPC separately measure the particle concentration for that particle diameter. The differences between the two particle concentrations determine the WIM fraction. The particle concentrations for each particle diameter selected during the sampling period (i.e., cycle phase or overall cycle) is summed over each cycle or phase. This method was performed for both the W-CPC and B-CPC measurements; the ratio of the W-CPC by the B-CPC gives an overall ratio of the difference in W-CPC to B-CPC particle counts. This ratio was then used to determine an overall hygroscopicity value, κ, and the overall WIM fraction.

Soot concentrations were measured in real-time using the AVL Micro Soot Sensor (MSS). It measures the soot concentration based on the whole particle, or over all particle diameter sizes from the particle stream (Schindler et al. 2004). The MSS is a photoacustic instrument that has a lower detection limit of 5 $\mu g\ m^{-3}$. An infrared (IR) light beam at 808 nm isa aimed at the soot particles. Once the light beam is absorbed through the particle, sounds waves are produced and measured using a microphone. The GDI vehicles

emission streams were diluted 5 to 1 for the soot emission measurements to keep the analyzer from over ranging, since the emissions are higher than those of the PFI vehicle.

7.3. Results

7.3.1.1 WSOM Emission Factors

The WSOM EFs were measured cumulatively on filters over both the UC and FTP and are shown in Fig. 7-1. The majority of the WSOM EFs are below 1 mg/mi for all 4 vehicles over both cycles. For the FTP cycle, increasing alcohol content increases the WSOM EFs for the WG-GDI and PFI-FFV vehicles. For the UC, the WSOM EFs remain relatively consistent with increasing alcohol content showing that for a more aggressive and high speed cycle WSOM EFs are relatively insensitive to alcohol content. The PFI-FFV showed a 150% increase in the WSOM EF with increasing ethanol content from the E10 to E83 fuels over the FTP cycle, but consistent WSOM EFs at 0.8 mg/mi for the same fuels over the UC. WG-GDI showed a 100% increase in the WSOM EF from the E10 to E20 fuels over the FTP cycle. The SG-GDI showed a small increase in the WSOM EF with increasing ethanol concentration, but a 185% increase from the B16 to B32 fuels. In addition, a 67% decrease in the WSOM EFs was shown from the B16 to B32 fuels over the UC for the SG-GDI. The GDI-FFV over the FTP, on the other hand, showed the opposite trend with a 63% decrease in the WSOM EF with increasing ethanol content from the E10 to E83 fuels over the FTP and a 40% decrease over the UC.

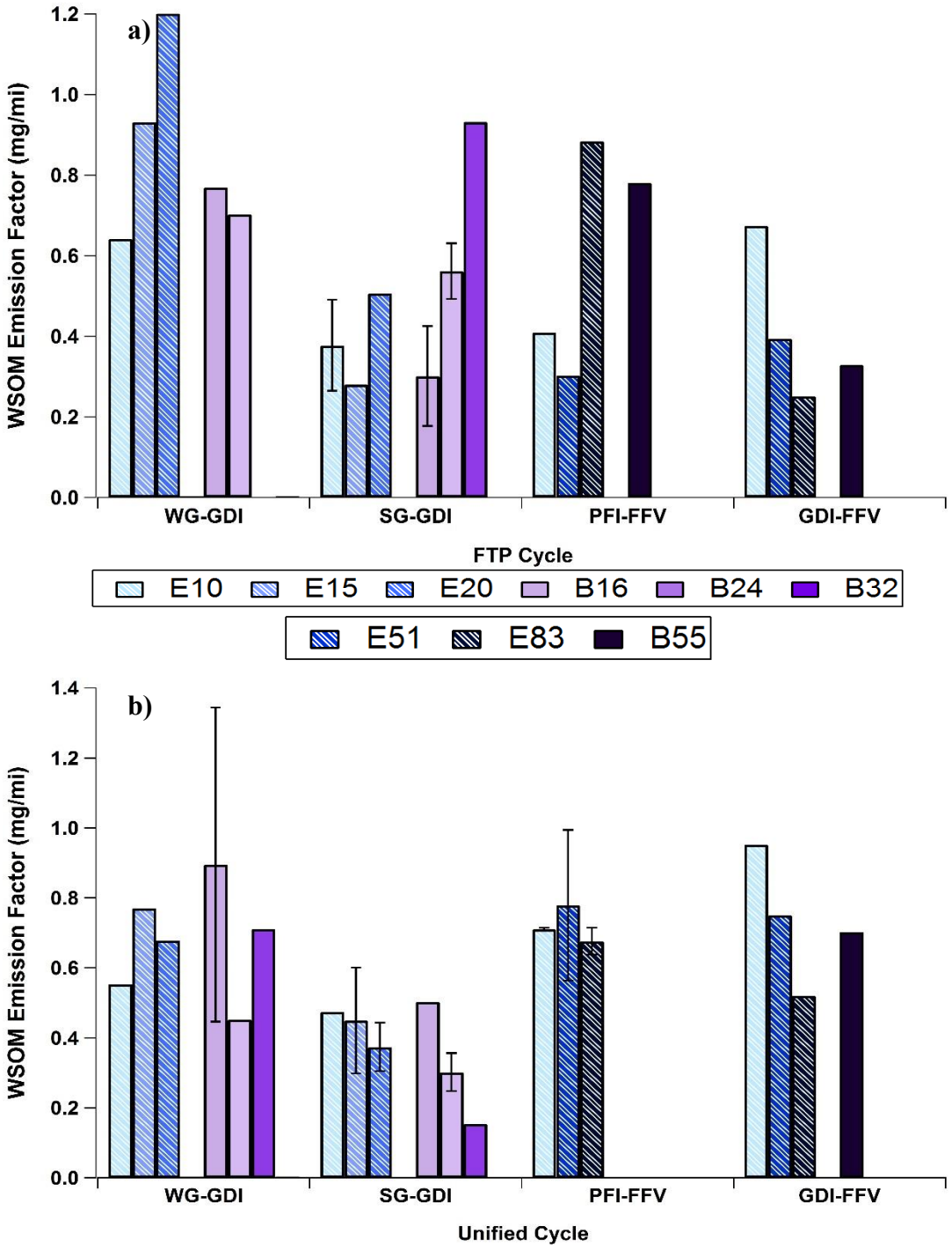

Fig. 7- 1. The WSOM Emission Factors over both the FTP (a.) and Unified (b.) cycles for the WG-GDI, SG-GDI, PFI-FFV, and GDI-FFV

7.3.1.2 WSOM and WIOM Contributions to OM

The determination of the WIOM and OM EFs are described in Section 2.3. The OM EFs are shown in Fig. S3. The EFs of the WSOM, WIOM, and PM mass are shown in Fig 7-2a for the FFVs over the FTP. It should be noted that only one WSOM EF was measured for the FFVs over the FTP cycle, for which a corresponding WIOM and PM EF were reported. The WIOM EFs did not show strong fuels trends for either vehicle, but the E51 fuel had the highest WIOM EF for each FFV. The WSOM EFs showed increases with increasing ethanol content for the PFI-FFV and decreases with increasing ethanol content for the GDI-FFV, as shown in section 3.1.1. The PM mass for the PFI-FFV increased with increasing ethanol content over the FTP. However, the GDI-FFV shows an opposite trend of a decreasing PM mass EF with increasing ethanol content.

The WIOM and WSOM fractions of the total PM mass over the FTP cycle are shown in a stacked bar chart in Fig. 7-2b. The combined WIOM and WSOM (or OM) fractions ranged from about 43% to 72% of the total PM mass for the PFI-FFV, as shown in Fig. 2b. Due to the increase in the PM mass emissions, the fraction of WIOM and WSOM both decreased for E83 for the PFI-FFV. The PFI-FFV shows the majority of the OM emissions for the E10 and E83 fuels were WSOM, and the WSOM/PM mass fraction ranged from 0.48 to 0.37 from the E10 to E83 fuels. The B55 blend showed the highest WSOM emissions for the PFI-FFV, which was 60% of the total PM. For the GDI-FFV, the WIOM PM mass fractions increased with increasing ethanol concentration from 0.18 for the E10 fuel to 0.42 for the E83 fuel. Note that the increases in WIOM fractions are due in part to the decreases in total PM mass for the GDI-FFV with increasing ethanol

content The WSOM fraction, for the GDI-FFV remained constant (~0.14) with all four fuels.

Fig. 7-2b shows the combination of the WSOM and WIOM in relationship to the total PM mass, with the sum of the WSOM and WIOM equalling the total OM of the particles. Effectively, Fig. 7-2b shows the OM to PM mass fractions for both FFVs over the FTP cycle. The OM/PM mass fraction varies greatly for the PFI-FFV, but there is a consistent fuel trend of increasing OM/PM mass fractions with increased ethanol content for the GDI-FFV. As stated above, the WIOM/PM mass also increases with increased ethanol content. Both trends for the GDI-FFV are due more to the decreasing total PM mass with increasing alcohol content that changes with the particle composition. The differences in OM/PM mass trends between the vehicles might be attributed to their engine technologies with the increased ethanol content. Specifically, because the fueling for the GDI vehicles is not as well mixed as for the PFI vehicle, the oxygen in the higher alcohol appears to have a bigger impact in reducing PM in rich zones for the GDI vehicles than during the combustion for the PFI.

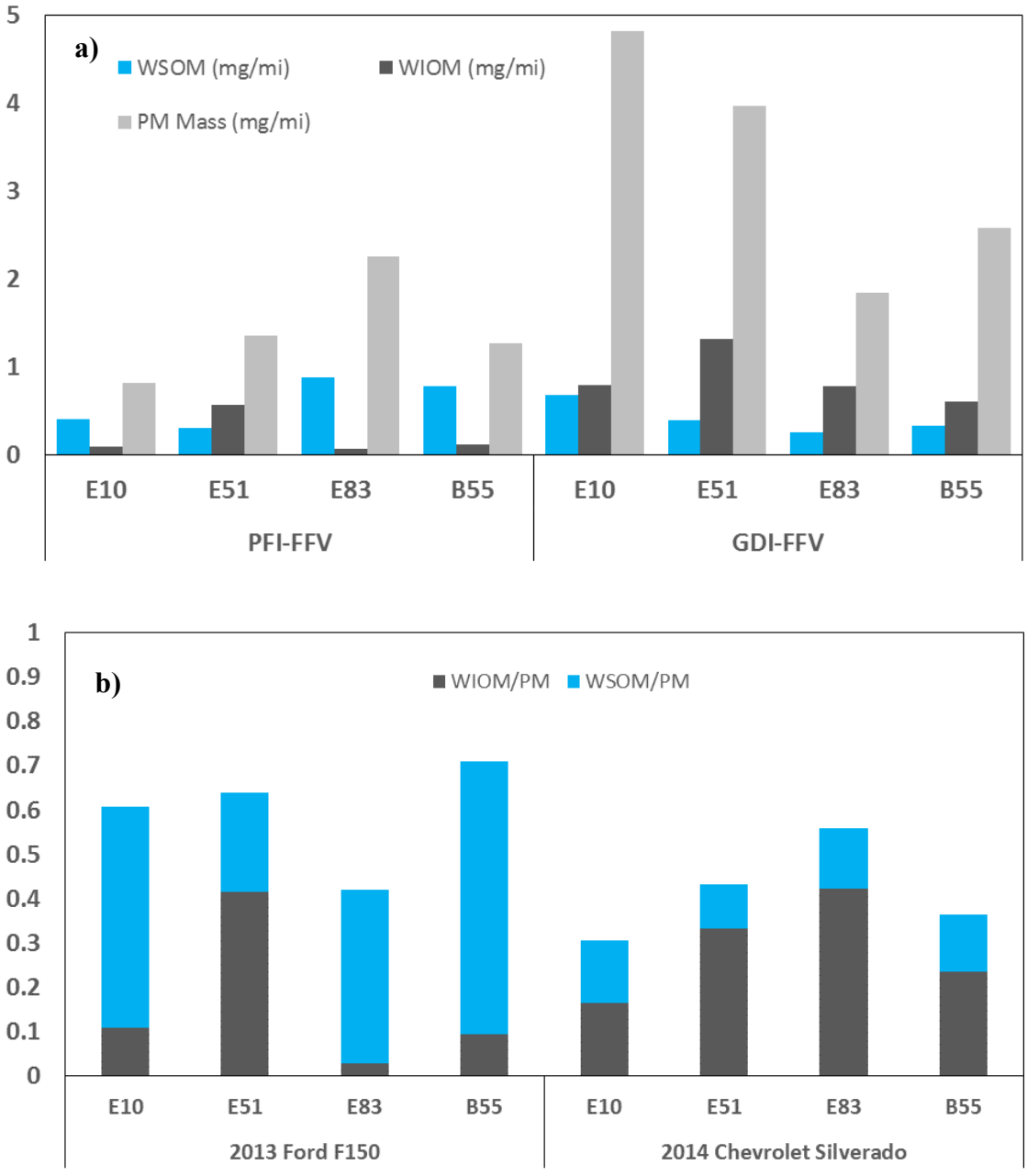

Fig. 7- 2. The WSOM, WIOM, and PM mass Emission Factors for both the PFI-FFV and GDI-FFV (a.). The WSOM and WIOM PM mass fractions in a stacked bar graph (b.) over the FTP cycle for the PFI-FFV and GDI-FFV. Both the addition of the WSOM and WIOM represent the OM/PM mass fraction.

7.3.2. Estimated Water-Insoluble Mass Fraction by Phase

Using our real-time technique described in Section 2.4, the WIM fractions were estimated over both cycles for all four vehicles. These fractions are representative of particles below 40 nm in diameter. The overall cumulative WIM Fractions are shown in Fig. 7- 3. Generally, the WIM fractions are high (above 0.75) for all vehicles and fuels over both cycles, with some differences between the vehicle technologies. The SG-GDI and WG-GDI vehicles both showed consistent WIM fractions, above 0.75, over both cycles and all fuel blends. The FFVs show differences between the PFI and GDI engine technology. The GDI-FFV had WIM fractions above 0.8 for all fuels over the FTP cycle. The PFI-FFV shows a wider range in WIM fractions with low overall WIM fractions for some fuels over both cycles. The GDI-FFV and PFI-FFV have more resembling WIM fractions over the UC, with the GDI-FFV having low overall WIM fractions for some fuels.

Over both cycles, the PFI-FFV showed largely water-insoluble particle emissions with the E10 fuel, but low amounts of water-insoluble particle emissions with the E83 fuel. The decrease from the E10 to E83 fuel was 75% for the FTP cycle and 50% for the UC. The GDI-FFV showed mostly water-insoluble emissions over the FTP cycle. However, the UC showed a 33% decrease in the WIM fraction from the E10 to the E83 fuel blend. The E51 and B55 fuel blend WIM fractions (~0.85) were significantly higher compared to the other WIM fractions.

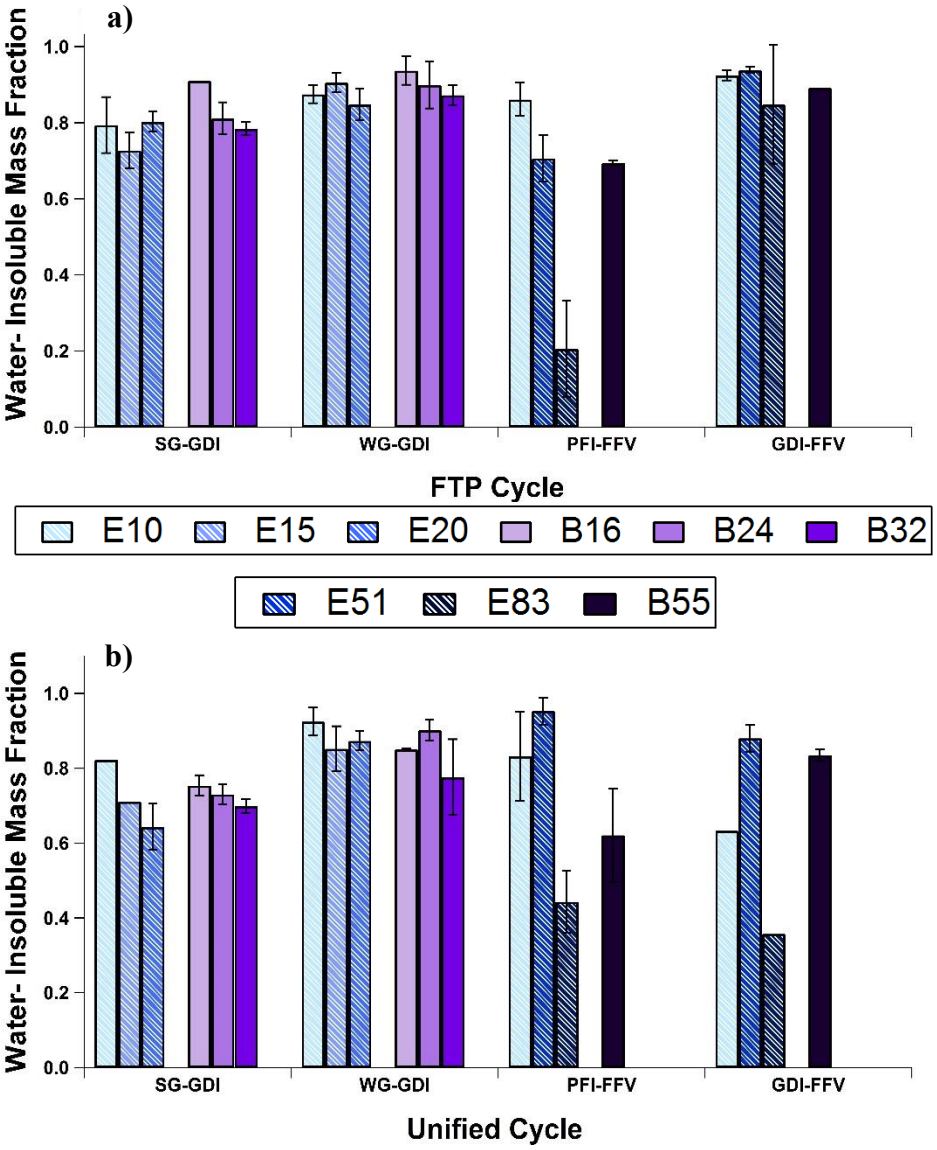

Fig. 7- 3. The estimated water-insoluble mass fraction over both the FTP (a.) and Unified (b.) cycles for the WG-GDI, SG-GDI, PFI-FFV, and GDI-FFV

WIM fractions were also estimated for each phase of the FTP and UC for all four vehicles. Fig. 7- 4 shows the FTP and UC WIM fractions by phase for all four vehicles. The SG-GDI and WG-GDI vehicles showed generally consistent WIM fractions between

all three phases for both cycles, although some variability existed for the SG-GDI with some fuel blends. The FFVs showed more variable WIM fractions between the 3 phases over both cycles. Generally, the E10 and E51 fuel blends had higher WIM fractions between both vehicles and cycles.

The SG-GDI and WG-GDI vehicles had mostly water-insoluble particle emissions by phase. The SG-GDI shows low WIM fractions for the E10 fuel over phase 2 of the FTP cycle, but the E20 fuel has a high WIM fraction. Thus the increase in ethanol content in the fuel increased the WIM fraction for phase 2 of the FTP for that vehicle. The iso-butanol fuel blends show a large decrease in the WIM fraction, 48% for the FTP and 67% for the UC, with increasing iso-butanol concentration over both cycles for the SG-GDI. The WG-GDI vehicle also shows very hygroscopic particle emissions for all three phases over both cycles. The iso-butanol fuels show decreasing WIM fractions with increasing alcohol concentration over both cycles, but these decreases are roughly 20% or just above the method uncertainty of 15% (Short et al. 2014).

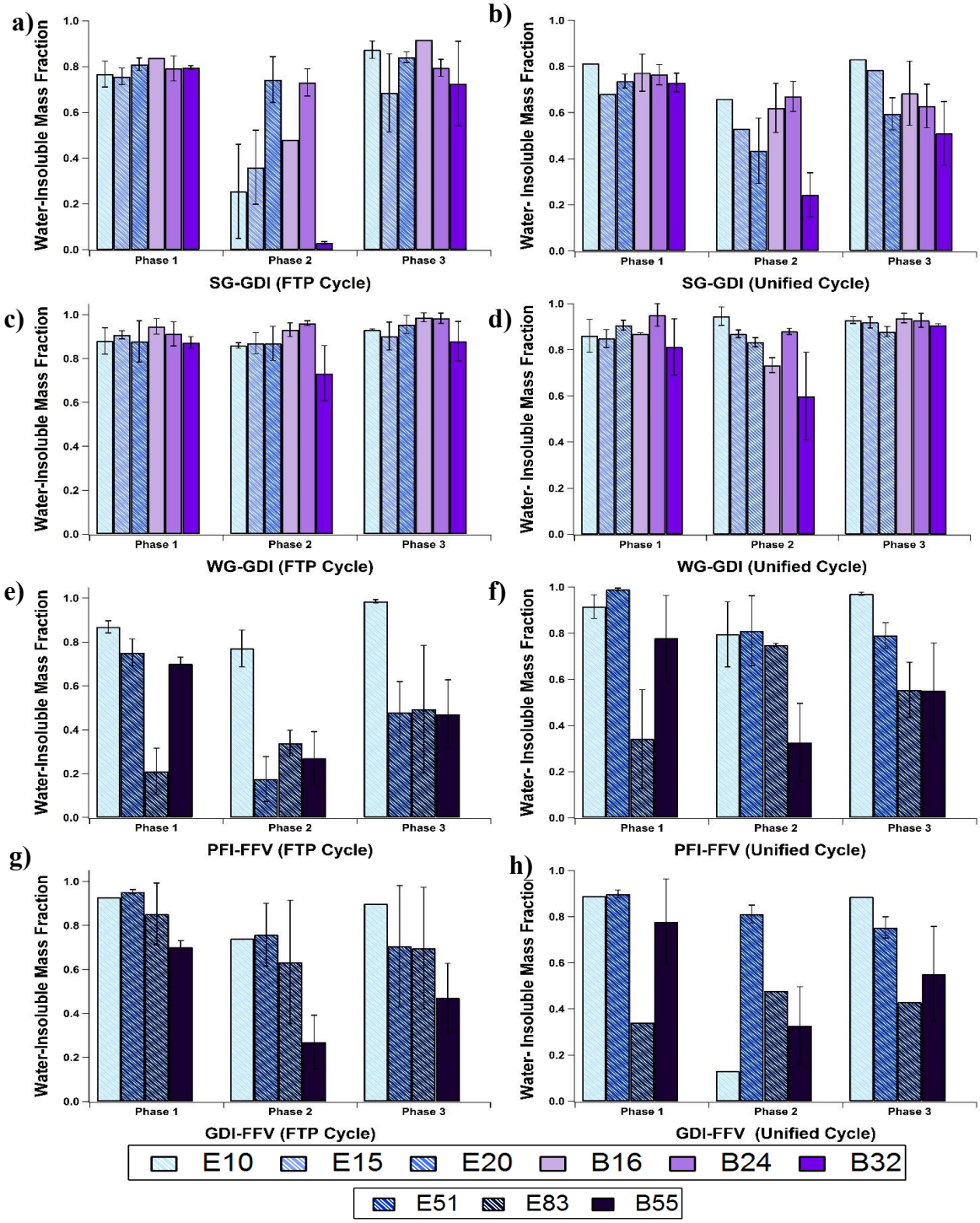

Fig. 7- 4. The estimated water-insoluble mass fraction over both cycles for the SG-GDI{FTP(a.) and UC (b.)}, WG-GDI {FTP(c.) and UC (d.)}, PFI-FFV {FTP(e.) and UC (f.)}, and the GDI-FFV {FTP(g.) and UC (h.)}.

The FFVs had large decreases in the WIM fraction with higher alcohol content. For the PFI-FFV, large WIM fraction decreases were found with higher alcohol content over the FTP cycle for all three phases. Phase 1 had a 76% decrease, Phase 2 had a 56% decrease, and Phase 3 had a 50% decrease in the WIM fraction from the E10 to E83 fuel blend. The UC also showed large decreases from the E10 to E83 fuel blend, but only for phase 1 and 3, which showed decreases of 63% and 43%, respectively. For the GDI-FFV, the ethanol fuel blends had similar WIM fractions over the FTP cycle. The B55 blend had fractions that were lower than the E10 fuel blend for all three phases, with a minimum WIM fraction of 0.6 (Phase 2). The UC has decreasing WIM fractions, from the E10 to E83 fuel blend, by 61% (Phase 1) and 54% (Phase 3). Phase 2 showed a 243% increase in the WIM fraction from the E10 to E83 fuel blend.

7.3.3. Steady-State κ-Values and Soot Concentration

The SG-GDI, WG-GDI, and the PFI-FFV were run for 10 minutes over each of the three steady-state speeds. The κ values and soot concentrations average for each speed and fuel are reported in Fig. 7-5. All three vehicles show a κ value similar to the κ value for sulfuric acid (κ=0.9). The κ are shown here to illustrate how the particle hygroscopicity changes with vehicle speed. The κ values were used for reporting during the steady-state speeds, instead of the WIM fractions, because κ values approach or become greater than the κ value for sulfuric acid (κ=0.9), WIM fractions become negative. In these cases, κ provides a clearer understanding of the particle water-insolubility. If the particle hygroscopicity is high than the particles are more water-soluble, and the opposite for low particle hygroscopicity values. The SG-GDI vehicle

shows κ values that were above 0.5, or were more hygroscopic. Whereas, the WG- GDI vehicle has high κ values, or very hygroscopic particles for the 70 MPH speed, but at the 30 MPH speed the κ values are low, or the particles were less hygroscopic. The PFI-FFV also has high κ values for the 70 MPH speed, but at the 30 MPH speed for the E51 and E83 fuel blends the particles become less hygroscopic, with values of 0.18 and 0.38, respectively. The κ values for the B32 fuel blend for the SG-GDI were low for all three speeds, but for the B32 fuel for the WG- GDI the particles κ was high for all three speeds. For all three vehicles, there was decreasing soot concentration with decreasing vehicle speed. The WG- GDI vehicle showed the highest soot concentration of all three vehicles of 87 mg m^{-3}. These results show that vehicle speed directly impacts the particle hygroscopicity and water-insoluble particle concentrations of the emissions from light-duty vehicles.

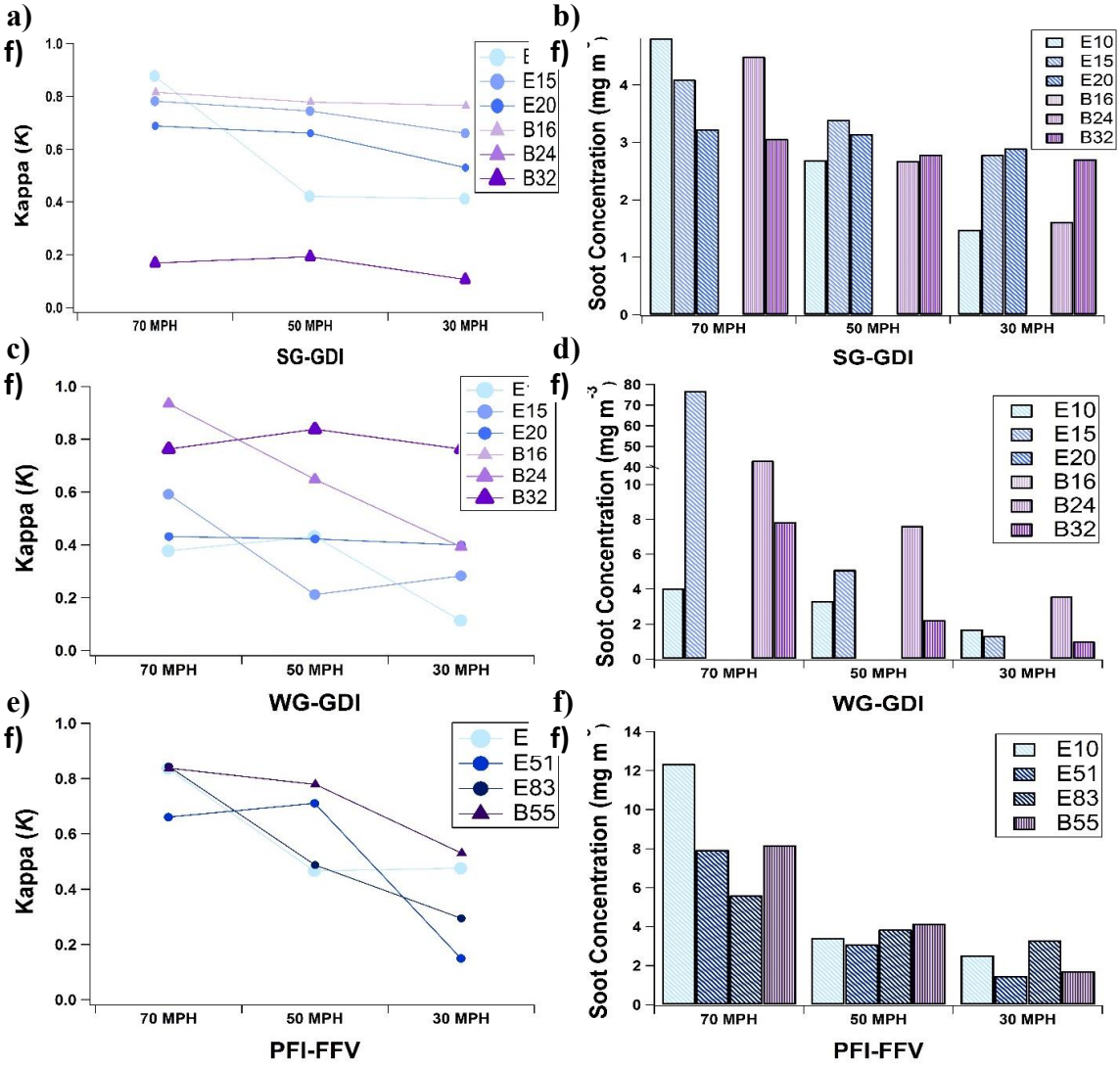

Fig. 7- 5. The estimated water-insoluble mass fraction over 70 MPH, 50 MPH, and 30 MPH steady state speeds for the SG-GDI {κ(a.) and Soot(b.)}, WG-GDI { κ(c.) and Soot(d.)}, and PFI-FFV {κ(e.) and Soot(f.)}

7.3.4. Soot Emissions Factors and Soot/PM Fraction

The soot EFs were measured in real-time using the MSS instrument over both the UC and FTP cycles. The soot emissions presented are divided by the total PM mass to give the overall soot contribution to the PM mass discussed in this section. This fraction will then be compared to the overall WIM fraction and WIOM/PM mass fractions.

Fig. 7-6 shows the soot EFs over both the FTP and UC for all four vehicles tested. Over the FTP and UC, the WG-GDI and GDI-FFV vehicles show higher amounts of soot emitted compared to the SG-GDI and PFI-FFV tested. The soot EF fuel differences between the SG-GDI and PFI-FFV were not significant compared to the WG-GDI and GDI-FFV. The E10 EF for both the SG-GDI and PFI-FFV vehicles was ~0.15 mg mi^{-1} over the FTP, and ~0.3 mg mi^{-1} for the SG-GDI and ~0.19 mg mi^{-1} for the PFI-FFV over the UC. The WG-GDI had a soot EF range of 2.18 to 0.42 mg mi^{-1} between the E10 to E20 fuels, respectively, over the FTP and 1.73 to 0.3 mg mi^{-1} between the E10 to E20 fuels, respectively, over the UC. The GDI-FFV had a soot EF range of 2.88 to 0.22 mg mi^{-1} between the E10 to E83 fuels, respectively, over the FTP and 1.95 to 0.49 mg mi^{-1} between the E10 to E51 fuels, respectively, over the UC. Comparing the SG-GDI and WG-GDI vehicles, the E10 fuel blend showed an 85% difference between the soot EFs. The FFVs tested showed a ~90% difference in the soot EFs when comparing the GDI-FFV to the PFI-FFV for the E10 fuel.

Both the WG-GDI and GDI-FFV showed significant decreases in the soot emission factors with increased ethanol concentration. The WG-GDI vehicle showed a decrease of 81% for soot EFs from the E10 to E20 fuel blend over the FTP and an 83% decrease over the UC from the E10 to E20 fuel blend. The GDI-FFV showed a 93% decrease in the soot EFs from the E10 to E83 fuel blend over the FTP, and a 71% decrease from the E10 to E51 fuel blend over the UC.

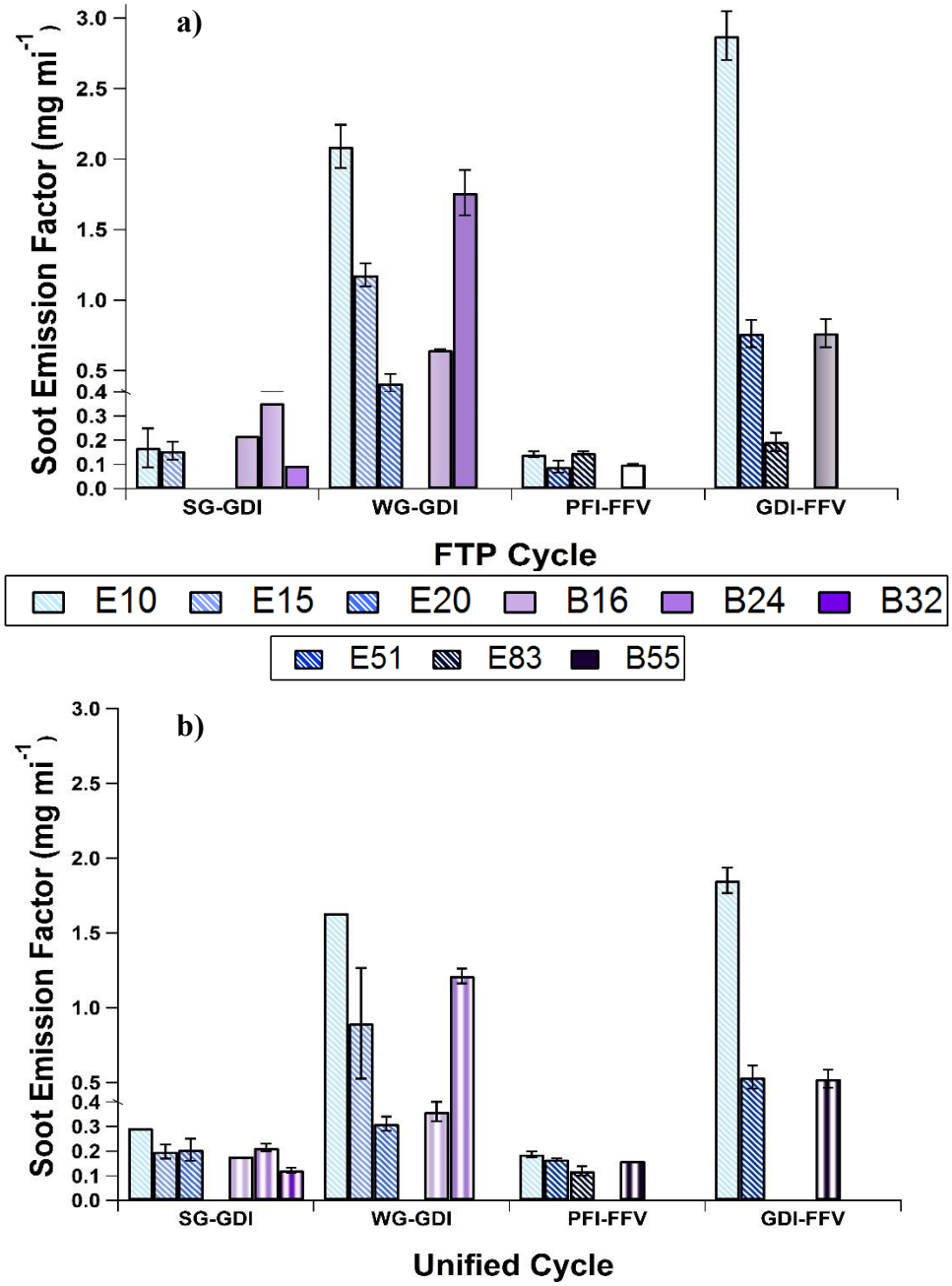

Fig. 7- 6. The Soot Emission Factors over both the FTP (a.) and Unified (b.) cycles for the WG-GDI, SG-GDI, PFI-FFV, and GDI-FFV

The total amount of soot for both the FTP and UC for all four vehicles was divided by the total amount of PM mass, shown in Fig. 7-7. The total PM mass EFs are shown in a companion paper to this study (Karavalakis et al. 2014). The fraction ranges from 0 to 1 and is highly variable. The soot/PM mass EFs show that for the WG-GDI vehicle, on the E10 fuel, ~80% of the PM emissions were soot over the FTP cycle. This is equivalent to values reported by Mariqc at al. (2013), which showed for a WG-GDI vehicle tested about ~80% of the PM emissions were soot. Thus, showing that the measurements in this study were equivalent to other published studies. On average, the SG-GDI and WG-GDI vehicles have large soot/PM mass fractions compared to the FFV vehicles for both the FTP and UC. In addition, increased alcohol concentration in the fuel decreases the soot/PM mass fraction over both cycles. A 60% and 37% decrease in the soot/PM mass fraction was reported from the E10 to the E15 fuel blend for the SG- GDI vehicle over the FTP and UC, respectively. For the WG-GDI vehicle, a 59% and 47% decrease in the soot/PM mass fraction is shown from the E10 to E20 fuel blend over the FTP and UC, respectively. For the PFI-FFV and GDI-FFV vehicles, a 68% and 75% decrease in the soot/PM mass fraction, respectively, was shown from the E10 to E83 fuel blends over the FTP. Over the UC, the FFVs tested didn't show a difference in the soot/PM mass fraction with increasing ethanol concentration.

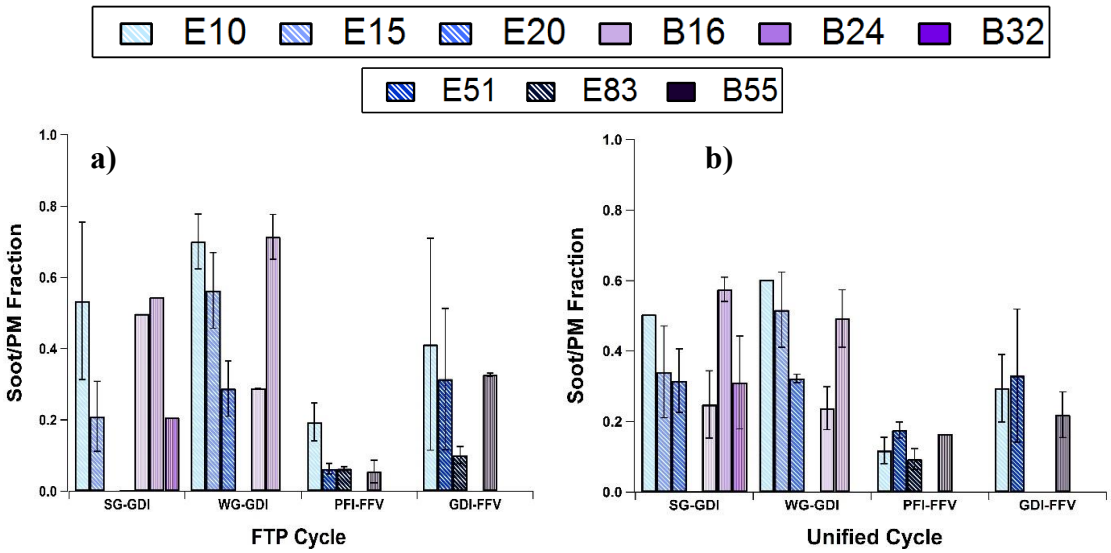

Fig. 7- 7. The Soot/PM Mass fraction over both the FTP (a.) and Unified (b.) cycles for the WG-GDI, SG-GDI, PFI-FFV, and GDI-FFV

The overall cumulative WIM fractions showed a similar trend with the soot/PM mass fraction, in that as the alcohol concentration increases the WIM fraction decreases for particle diameters below 40 nm. The addition of the soot and WIOM contributions to the total PM mass gives a fraction similar to, but below, those of the WIM fraction. This provides a good correlation between the different measurements presented, especially given that the overall cumulative WIM fractions only represent particle water-insolubility below 40 nm and not bulk composition, whereas the OM and soot emissions are determined for all particle diameters.

Soot EFs show that vehicle technology and fuels can have an impact on the soot emissions, thus effecting the total amount of Black Carbon (BC) emitted. GDI technology is expected to be the primary vehicle technology for new model year vehicles in 2025.

The WG-GDI vehicle shows 6 times more soot emissions compared the SG-GDI vehicle. The GDI-FFV also shows about 8 times more soot emissions compared to the PFI-FFV. The SG-GDI vehicle has soot emissions that were comparable to the PFI-FFV. SG-GDI vehicle is a potential technology in terms of soot emissions comparable to PFI vehicle technology. In addition, increased ethanol concentrations were shown to reduce soot emissions for the FFVs and the GDI vehicles.

7.4. Conclusions and Implications

WSOM, WIM, and soot/BC are all important components of the total PM mass, making up 70- 100% of the total PM mass. The WSOM/PM mass and WIM fractions appear to correlate well in that low WSOM fractions (<15%) were shown with high (<75%) WIM fractions. In relation to the vehicle technologies tested, numerous findings were shown. The PFI-FFV had much larger WSOM/PM mass fractions than the GDI-FFV, which the GDI-FFV had larger WIOM/PM mass emissions. All vehicles had high (<0.75) WIM fractions except the PFI-FFV which showed decreasing WIM fractions with increasing alcohol content. Vehicle speed was shown to have a correlation with the particle hygroscopicity value, κ, where increased vehicle speed increase the particle hygroscopicity or decreased the amount of water-insoluble particles. The EFs of WSOM and soot appear to follow the total PM mass fuel trend. However, the composition in terms of total PM shifts with the alcohol content in the fuel. As with the WIOM/PM mass fraction, where increased alcohol concentration increased the WIOM/PM mass fraction due to the decrease in the total PM mass. This also correlates with the soot/PM mass

fraction where the trend of decreasing soot/PM mass was shown with increasing alcohol content.

As the RFS mandate increases ethanol concentration, a reduction in soot or BC emissions could be a result. A combination of SG-GDI technology and higher ethanol concentration could provide a solution to the maximum reduction in BC emissions from light-duty vehicles while providing increased fuel efficiency. More BC emissions could have an impact on climate due to BCs ability to absorb solar radiation. Thus WG-GDI or GDI-FFV technology would increase the overall BC emissions in the atmosphere with the possible increased production in this vehicle technology. Although GDI-FFVs operating on E83 would show comparable soot EFs to the PFI-FFV and SG-GDI vehicles thus limiting the impact of BC on the environment.

Vehicle speed has an effect on particle water-insolubility can needs to be considered when defining new regulations. These particle emissions will be more prevalent near major roadways were increased speeds of 70 MPH prevail. Communities near these roadways could be particularly vulnerable to water-soluble particle composition thus possibly impacting residents overall health. In addition, changes in water-soluble particle emissions can have an impact on CCN activity thus impacting climate patterns. Overall particle composition allows for a better determination on climate effects from changes in vehicle and fuel technology.

7.5. Acknowledgements

The authors would like to thank Tyler Berte, Hans Phang, Chun Liang, and Wartini Ng for their contributions to this work. In addition, the authors thank Kurt Bumiller and Mark Villela for their technical support of the dynamometer test cell. This study was substantially supported by the California Energy Commission Grant Number 500-09-051. Also, D.S. would like to acknowledge the funding support from the University of California Transportation Center (UCTC) Graduate Fellowship. Funding for BC measurements were made possible by the U.S. Environmental Protection Agency (EPA) grant number 83504001. Its contents are solely the responsibility of the grantee and do not necessarily represent the official views of the EPA. Further, the EPA does not endorse the purchase of any commercial products or services mentioned in the publication.

7.6. References

Alkidas, A.C. 2007. Combustion Advancements in Gasoline Engines, Energy Conversion and Management, 48(11), 2751-2761.

Drake, M.C., Fansler, T.D., and Lippert A.M. 2005. Stratified-charge combustion: modeling and imaging of a spray-guided direct-injection spark-ignition engine, Proceedings of the Combustion Institute, 30(2), 2683-2691.

Dutcher, D.D., Stolzenburg, M.R., Thompson, S.L., Medrano, J.M., Gross, D. S., Kittelson, D.B., McMurry, P.H. (2011) Emissions from ethanol-gasoline blends: a single particle perspective, Atmosphere, 2, 182-200; DOI: 10.3390/atmos2020182

Ervens, B., Feingold G., and Kreidenweis, S.M., 2005. Influence of water-soluble organic carbon on cloud drop number concentration, Journal of Geophysical Research,110, D18211

Gutiérrez-Castillo, M, Roubicek, D A, Cebrián-Garcia, M E, De Vizcaya-Ruiz, A, Sordo-Cedeòo, M and Ostrosky-Wegman, P. 2006. Effect of chemical composition on the induction of DNA damage by urban airborne particulate matter. Environmental and Molecular Mutagenesis, 47: 199–211.

Hackney J. and Neufville R. 2001. Life Cycle Model of Alternative Fuel Vehicles: Emissions, Energy, and Cost Trade-offs, Transportation Research Part A: Policy and Practice, 35, 243-266

Jacobson, M.Z. 2007. Effects of Ethanol (E85) Versus Gasoline Vehicles on Cancer and Mortality in the United States, Environmental Science and Technology, 41(3), 4150-4157

Jin, C., Tao, M., Liu, H., Lee, C and Ji, J. 2011. Progress in the Production and Application of n-Butanol as a Biofuel, Renewable and Sustainable Energy Reviews, 15, 4080-4106

RFA- Renewable Fuels Association, 2007. Federal Regulations: Renewable Fuels Standard. Washington, 2006.

Maricq, M.M., Szente, J.J., Adams, J., Tennison, P., Tumpsa, T. 2013. Influence of mileage accumulation on the paticle mass and number emissions of two gasoline direct injection vehicles, Environmental Science and Technology, 47(20), 11890-11896, DOI: 10.1021/es402686z

Nigam, P.S. and Singh, A. 2011. Production of Liquid Biofuels from Renewable Resources, Progress in Energy and Combustion Science, 37, 52-68

Petzold, A. and Schönlinner, M. 2004.The Multi-angle absorption photometer – A new method for the measurement of aerosol light absorption and atmospheric black carbon. Journal of Aerosol Science, 35, 421-441

Schindler, W., Haisch, C., Back, H.A., Niessner, R., Jacob, E., and Rothe, D., 2004. A Photoacoustic Sensor System for Time Resolved Quantification of Diesel Soot Emissions. SAE 2004-01-0968

Short, D., Giordano, M., Zhu, Y., Fine. P., Polidori, A., Asa-Awuku, A., (2014). A Unique On-line method to infer black carbon contributions to water-insoluble contributions, Aerosol Science and Technology

Solomon A.S., Anderson, R.W., Najt, P.M., and Zhao, F. 2000. Direct Fuel Injection for Gasoline Engines, SAE PT-80.

Tao, F., Gonzalez-Flecha, B., Kobzik, L., 2003. Reactive oxygen species in pulmonary inflammation by ambient particulates, Free Radical Biology and Medicine, 35(4), 327-340.

Transportation and Climate Divison March 2013, Light- Duty Automotive Technology, Carbon Dioxide Emissions, and Fuel Economy Trends: 1975 Through 2012, U.S. EPA Office of Transportation and Air Quality, Report EPA-420-R-13-001

Turpin, B.J., Lim, H., 2001. Species Contributions to PM 2.5 Mass Concentrations: Revisiting Common Assumptions for Estimating Organic Mass, Aerosol Science and Technology, 35(1) 602-610

Verma, V., Rico-Martinez, R., Kotra, N., King, L., Liu, J., Snell, T.W., Weber, R.J. 2013. Contribution of Water-Soluble and Insoluble Components and Their Hydrophobic Subfractions to the Reactive Oxygen Species-Generating Potential of Fine Ambient Aerosols, Environmental Science and Technology, 46, 11384-11392

Yang, B., Obwald, P., Li, Y., Wang, J., Wei, L., Tian, Z., Qi, F., Kohsa-Höinghaus, K. 2006. Identification of Combustion Intermediates in Isomeric Fuel-Rich Premixed Butanol-Oxygen Flames at Low Pressure, Combustion and Flame, 148,198-209.

Yanowitz, J., Knoll, K., Kemper, J., Luecke, J., McCormick, R. 2013. Impact of Adaptation on Flex-Fuel Vehicle Emissions When Fueled with E40, Environmental Science and Technology, 47, 2990-2997.

Wallner, T. and Frazee, R. 2010. Study of Regulated and Non-Regulated Emissions from Combustion of Gasoline, Alcohol Fuels and Their Blends In a DI-SI Engine, SAE Technical Paper, 2010-01-1571

Zhao F., Lai, M.-C., and Harrington D.L. 1999. Automotive spark-ignited direct-injection gasoline engines. Progress in Energy and Combustion Science, 25, 437-562.

Chapter 8: Conclusions

8.1 Dissertation Summary

The objectives of this dissertation were to investigate the PM and gaseous emissions from a variety of emerging and conventional light-duty vehicles from various biofuels. High vehicular speeds were shown to decrease the amount of water-insoluble particles and increase particle hygroscopicity. As it was shown, passenger vehicles make up a large amount of the light-duty vehicle fleet and a factor in the selection of vehicles for this dissertation. GDI vehicle technologies, although increase fuel economy, show significant differences in PM emissions compared to conventional vehicles. Ethanol in gasoline has become common in the U.S. and increased concentrations result in differences in emissions. Iso-butanol is a viable fuel source and shows that emission levels are not significantly different when comparing to ethanol at equivalent oxygen levels. High levels of alcohol concentration decreased PN and PM emissions.

Chapter 2 developed a real-time method for determining the water-insoluble particle emissions from near-roadway sources off of the I-710 freeway in Long Beach, CA. The method used two electrostatic classifiers with either a butanol or water based CPC. Results showed that fresh vehicular emissions contained the most BC in terms of its contribution to the water-insoluble particle mass. However, during the weekend the water-insoluble particle mass was two times that of the BC concentration. Thus concluding that the method is accurate for determining the water-insoluble mass below 40 nm particle diameter and its use in determining the BC contribution to the water-insoluble mass.

Chapter 3 investigated the particle speciation of emissions from a variety of GDI, PFI, and hybrid vehicles on varying aromatic and octane rating fuels. The results showed increased vehicles speeds reduce the amount of water-insoluble particles and increase particle hygroscopicity. In addition, increasing aromatic concentration increased PM mass, BC, and WSOM emission factors. In addition, increased iso-paraffin concentration, contained in the 15% aromatic fuel, increased the WSOM/PM mass fraction to be ~50% of the total PM mass. The 35% aromatic fuel in the GDI vehicles showed significantly high emission factors of BC compared to the PFI vehicle, which could have potential climate impacts. High octane fuels from the increased concentration of ethanol could reduce PM emissions.

Chapter 4 discusses the criteria and PM emissions from 5 vehicles, which included 3 PFI and 2 GDI vehicles. These vehicles were driven on varying blends of ethanol and iso-butanol in gasoline. The criteria pollutants lacks strong fuel trends which indicate significant advancements in catalyst technology and/or the air to fuel ratio. PM mass and PN was significantly lower for the PFI vehicles compared to the GDI vehicles. In general, PN decreased with decreasing alcohol concentration. PM mass showed reductions with the highest alcohol concentration or oxygen levels.

Chapter 5 analyzed the differences in particle composition emissions from 3 PFI and 2 GDI vehicles. These vehicles were on various ethanol and iso-butanol blended fuels. The results showed that higher vehicle speeds increased particle hygroscopicity and decrease the water insoluble mass fraction. About 30% of the PM mass consisted of WSOM. The Toyota Camry and both GDI vehicles showed that the PM mass was 5 times

the total amount of BC mass. The oxygen content in the fuels tested in this chapter doesn't have an effect on the BC emission factors.

Chapter 6 evaluates the criteria and PM emissions from 4 vehicles, which include a SG-GDI, WG-GDI, PFI-FFV, and GDI-FFV. The vehicles were running on varying amounts of ethanol and iso-butanol in gasoline. The results showed significant reduction in CH_4 emissions with the E83 fuel compared to E10 for both FFVs. The SG-GDI, WG-GDI, and GDI-FFV showed reductions in CO_2 emissions with higher ethanol concentration. In general, no strong fuel trends in NO_x emissions were shown for any of the vehicles tested. PM mass was significantly reduced with increasing ethanol concentration for the FFVs. In addition, the particle mode diameter was reduced from the E10 to the E83 fuel blend for both FFVs. The study concluded that significant reductions in PM emissions were shown with the SG-GDI vehicle compared to the WG-GDI and that higher ethanol concentration also reduce PM emissions.

Chapter 7 discussed the particle composition emissions from a SG-GDI, WG-GDI, PFI-FFV, and GDI-FFV on varying ethanol and iso-butanol concentrations. The results showed the increased vehicles speed decreases the amount of water-insoluble mass fraction and increases particle hygroscopicity. The SG-GDI vehicle emitted 6 times less soot compared to the WG-GDI vehicle tested. In addition, the PFI-FFV emitted 8 times less soot compared to the GDI-FFV. For the GDI-FFV, increasing ethanol concentration also increased the OM/PM mass fraction. WSOM/PM mass fraction remain consistent with increasing ethanol concentration, but WIOM/PM mass increased with increasing ethanol concentration.

Chapter 9: Future Work

This dissertation determined that different driving conditions effect the particle water-insoluble emissions. The continuation in studying vehicle driving conditions on water-insoluble particle emissions should be implemented. It is not known the fraction of BC to PM mass emissions during steady-state driving conditions. In addition, the composition of the particle coatings is not known. Both of these would lead to a better understanding of why the high speed driving conditions produce the higher hygroscopic and low water-insoluble mass fractions. Additional work is also needed on the WIOM and OM emissions from conventional and emerging light-duty vehicles. Little information is known about the WIOM and OM emissions from PFI vehicles. To the author's knowledge, no information is available on OM and WIOM emissions from GDI and FFVs. This dissertation determined the WIOM and OM emissions from the FFVs. However, more research should be studied on these emissions from GDI vehicles to see changes in the WIOM and WSOM fractions of the total PM mass. These collectively could help better understand the particle composition of emissions from emerging vehicle technologies as well as during various vehicle driving conditions, which impact human health and climate.

Appendix A.

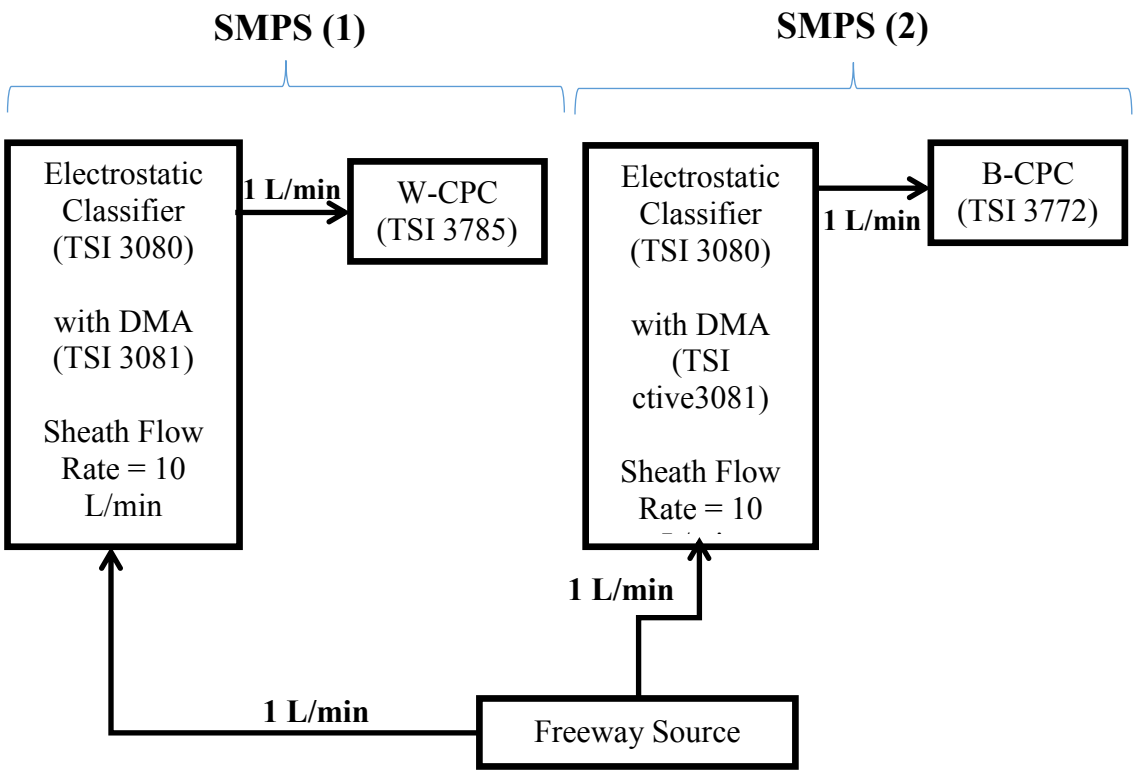

Fig. A- 1. Experimental setup for the method to determine the water-insoluble mass fraction. Two difference SMPS systems were used.

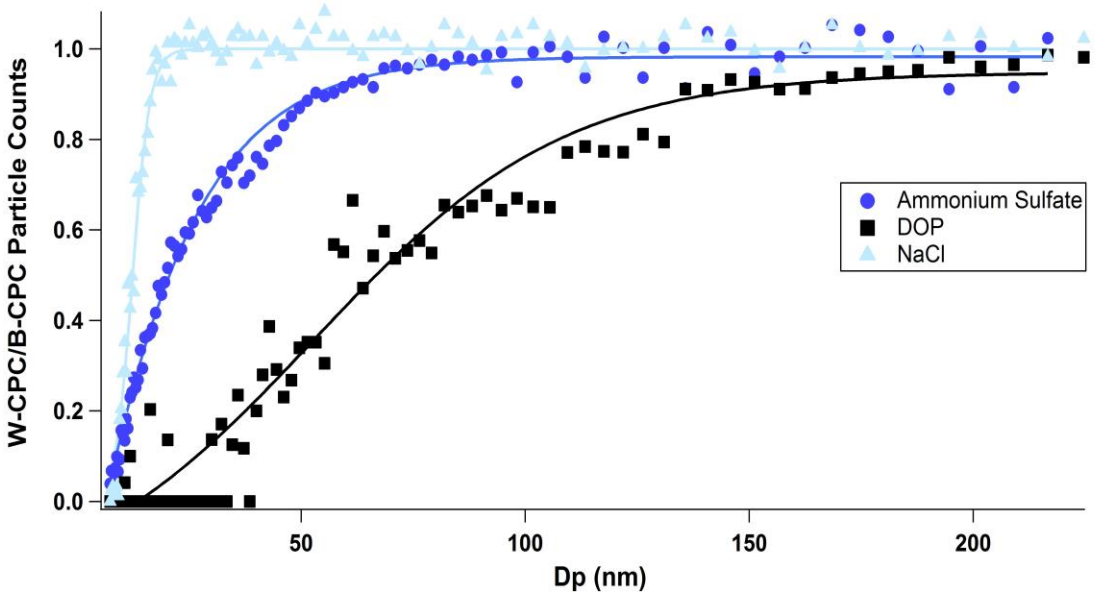

Fig. A- 2. Calibration curves for sodium chloride (light blue), ammonium sulfate (dark blue line), and DOP (black line). The dotted line shows the activation diameter when the ratio of W-CPC/B-CPC particle counts equals 0.5. The activation diameter is 12.9 nm for sodium chloride, 16.9nm ammonium sulfate- 71.3 nm for DOP at 2% instrument supersaturation.

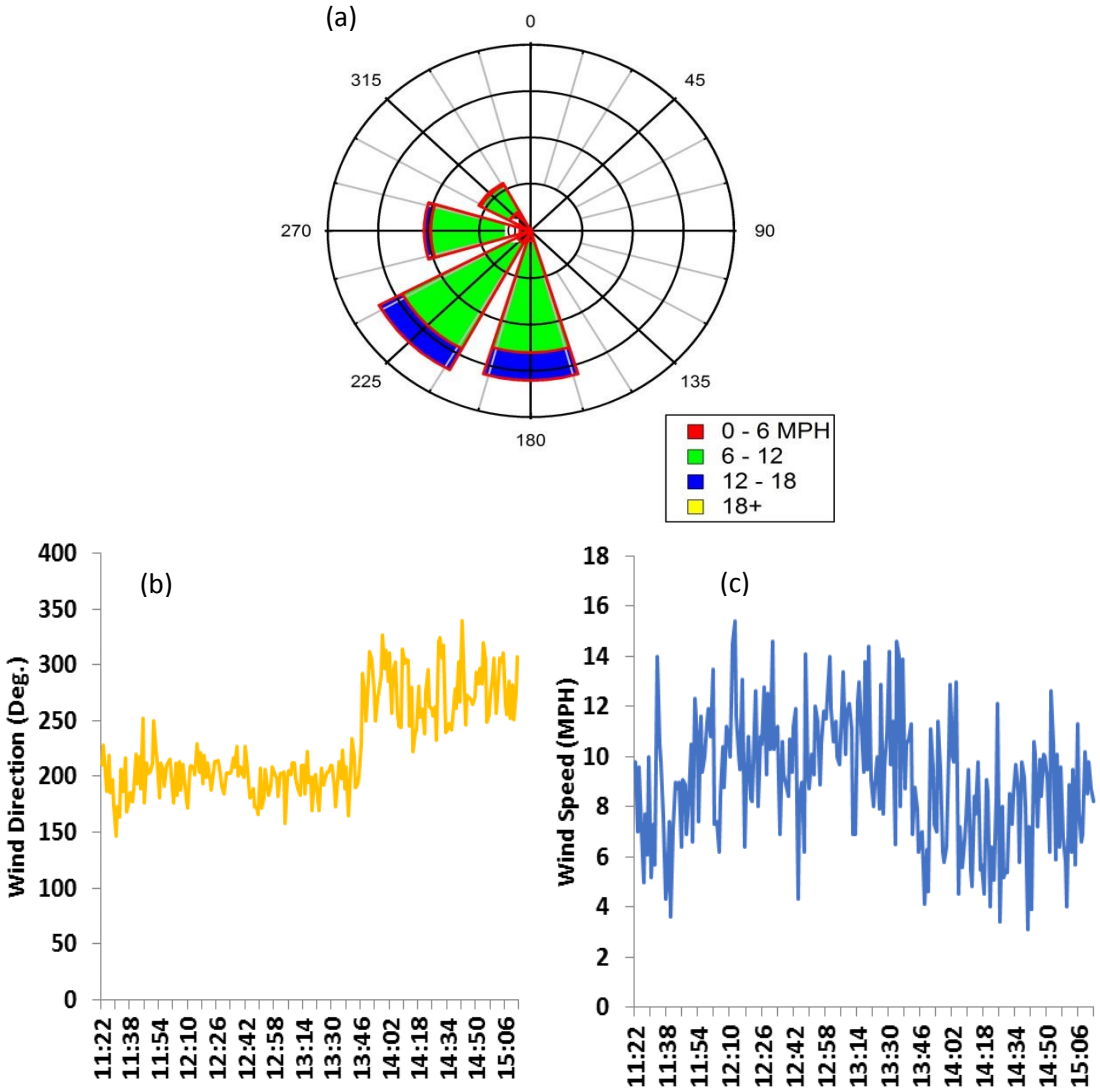

Fig. A- 3. Wind Rose Plot (a.). Wind Direction (b.) and speed (c.) are also plotted. Note the direction change in wind direction around 14:00.

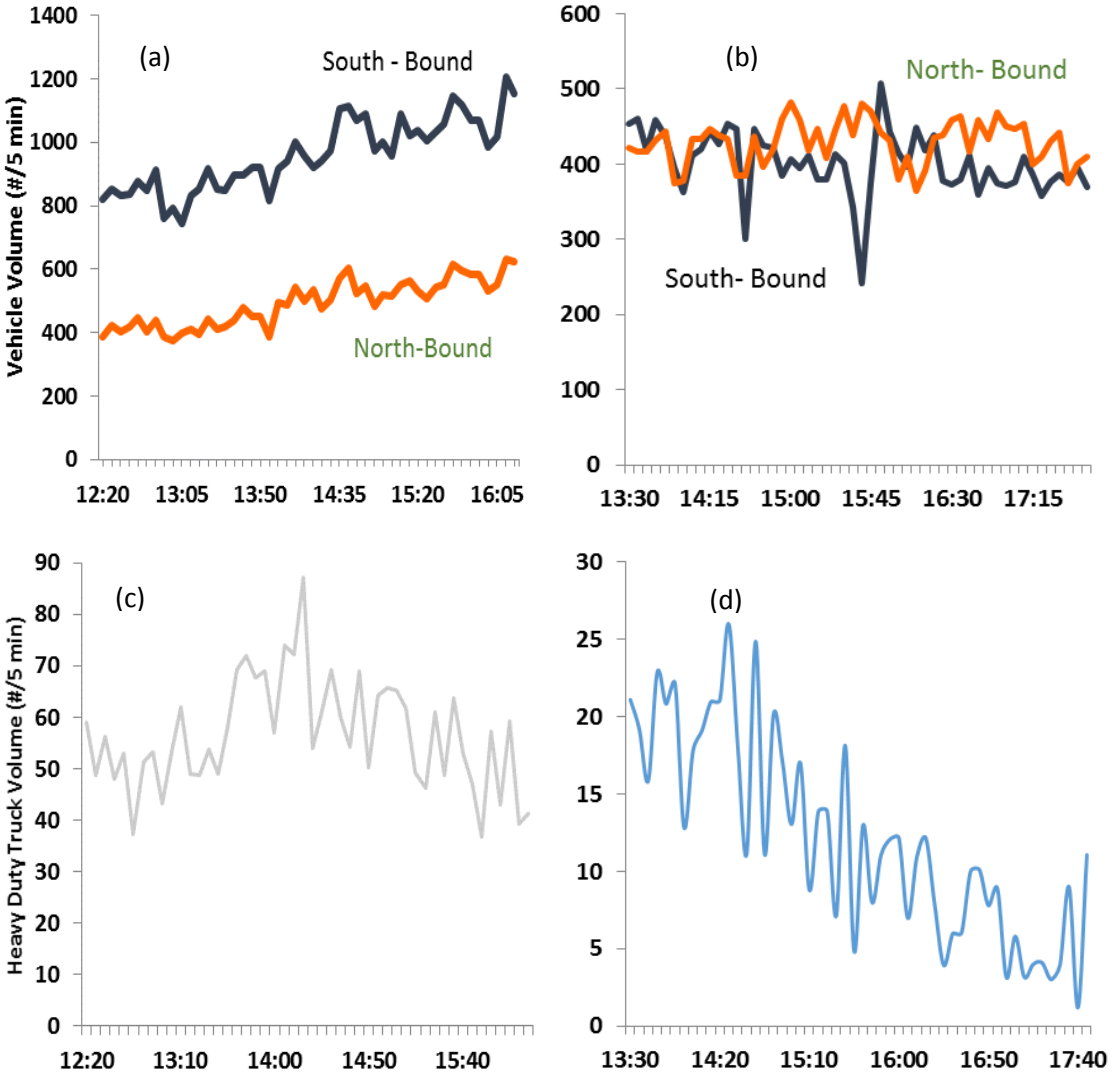

Fig. A- 4. Light-Duty vehicular traffic for the weekday (a.) and weekend (b.). The dark blue line represents the south bound lane where the orange light color represents the North bound lane. Heavy Duty traffic for both lanes is also shown for the weekday (c.) and weekend (d.).

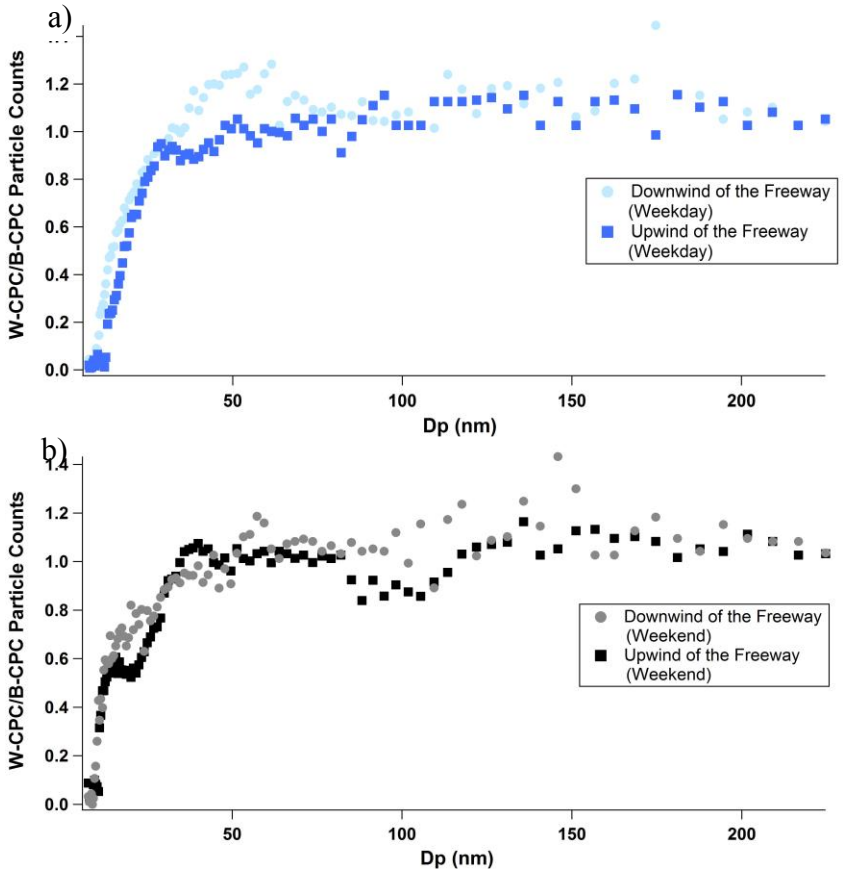

Fig. A- 5. Activation curves for weekday (a) and weekend (b). For the weekday, the activation diameter was 15.93 nm (light blue markers) downwind of the freeway and 18.3 nm (dark blue markers) upwind of the freeway. The weekend had a activation diameter of 15.686 nm (grey markers) downwind of the freeway. The black markers, over the weekend, had a double activation diameter of 16.102 nm and 21.5 nm to give an overall activation diameter of 18.801 nm upwind of the freeway

Appendix B.

B.1 Experimental Details

B.1.1 Driving Procedure

The UC was developed by the California Air Resources Board (CARB) and is more representative of real world driving than the U.S. Environmental Protection Agency (EPA) driving cycle, Federal Test Procedure (FTP) (Gammariello et al. 1996, Austin et al. 1993, and Gammariello and Long, 1993). The cycle consists of 3 phases with a "hot soak" period between phase 2 and 3, shown in Supplemental Fig. 1. Each vehicle was tested as a cold start, which the car was not started for at least 8 hours. The cold start allows for a cooled engine and three way catalyst (TWC) at the start of the cycle. Phase 1 and 3 are identical except phase 3 starts after the hot soak period which the engine and TWC are now warmed. During the hot soak period the engine was turned off for 10 minutes. The start of phase 3 occurs with re-ignition of the engine. Phase 2 has higher speeds compared to the other phases with a maxiumum speed of 65 MPH. The average speed during the UC? cycle is 24.6 MPH. The UC is more aggressive than the FTP with a higher average speed of 24.6 MPH compared to 21.2 MPH for the FTP. Steady-state testing occurs after the transient cycles while the engine and three way catalyst are still warm.

B.1.2 Emission Rate

BC and WSOM concentrations were reported in this study as $\mu g\ mi^{-1}$, or the emission factor (EF) of BC. The average BC concentration ($\mu g\ m^{-3}$) is multiplied for each

phase by the total volume of air through the CVS during each cycle phase (m^3). The total BC mass for each phase, (in the units of μg). The EF of BC is calculated as follows:

$$ER(BC) = .43\frac{BC_1 + BC_2}{x_1 + x_2} + .57\frac{BC_2 + BC_3}{x_2 + x_3}$$

The numerator in these fractions was the total BC mass for each phase. For example, the total BC mass for phase 1 is BC_1. The denominator, x , was the total mileage traveled for each phase, For example, x_1, was the total mileage for phase 1. The constant values 0.43 and 0.57 are weighing factors used to give an unbiased emission factor.

B.2 Real-Time Water-Insoluble Mass Fraction Estimation

A full description of the method is provided in Short et al. (2014). A condensation particle counter (CPC) exposes particles to a high relative humidy or super-saturation region (S_c) generated by a particular working fluid. Saturation, S, is defined as the ratio of the partial pressure, P_v, to the saturation vapor pressure, P_{sat}, of its particular working fluid. This is further described in Equation 1. P_{sat} is lower for butanol than it is for water at the same temperature. Butanol is also more volatile than water. Thus, these saturation conditions are more easily achieved when using butanol as a working fluid. A butanol-based CPC (B-CPC) exposes particles to a warmed growth tube that is used to condense the working fluid, butanol, onto the particle surface (Stoltzenberg and McMurry, 1991). In a water-based CPC (W-CPC), a cooled growth tube is employed, followed by a warm saturation tube to condense water onto dry particles (Hering et al. 2005). Heterogenous condensation of a bulk fluid into the particulate phase can be describe using Köhler Theory (Köhler 1936).

$$S = \frac{P_v}{P_{sat}(T)} = a_b \, exp\left(\frac{4M_b\sigma_b}{\rho_b RTD}\right) \qquad (1)$$

Where, R is the universal gas constant, T is the temperature at activation, D is the wet droplet diameter, ρ_b is the density of the bulk fluid condensing onto the particle (water or butanol), M_b is the molecular weight of the bulk fluid, and σ_b is the surface tension at the droplet vapor/liquid interface, and a_b is the activity of the solute in the bulk fluid. Assuming a_b is equivalent to 1, Equation 1 can be reduced to just the kelvin effect. This effectively creates a maximum critical supersaturation, s_c, which is the minimal conditions required for water to condenseonto a dry particle. s_c is greater than one so to simplify S_c-1, or s_c, is used in its place.

Assuming a_b is equivalent to the mole fraction of water in droplet solution, s_c can be described using Equation E-2, which is a variation of Equation 1.

$$\ln s_c{}^2 = \frac{4A^3\rho_b M_s}{27\nu\rho_s M_b d_s{}^3}, \; A = \frac{4M_b\sigma_b}{\rho_b RT} \qquad (2)$$

Where d_s is the particle diameter at which 50% of total particles have formed droplets and ν is the ion dissociation of the particle in water.

Köhler theory can be rewritten in terms of a single solute parameter known as κ- Köhler theory (Petters and Kreidenweis 2007). This single solute parameter, κ, can range from 0 to above 1 and characterizes the effects of solute composition for droplet growth. When κ is 0, the particle is considered to be water-insoluble but wettable, whereas when κ is 1 the particle is water-soluble and easily wettable. This term can be described using d_s and s_c parameters in Equation 3.

$$\kappa = \frac{4A^3}{27{d_s}^3 \ln(s_c)^2} \quad (3)$$

Equation 3 is very similar to Equation 2, except Equation 3 assumes the σ_b properties of the droplet are those of the pure fluid. For particles that have larger diameters, greater than 40 nm (s_c= 2%), the particles will experience uncontrolled particle growth. The changes of the κ term for an unknown composition can be approximated using a two component model solute. This model will consist of both a soluble solute, sulfuric acid (SA), and an insoluble solute, dioctyl phthalate (DOP). SA has been extensively measured in diesel exhaust and is highly soluble atκ_{sa}= 0.9 (Tobias 2001; Arnold et al 2006; Arnold et al. 2012). Vehicle lubrication oil has been shown to represent 95% of particulate emission making DOP a suitable choice for an insoluble but wettable, $\kappa_{DOP} \approx$ 0.01, vehicle exhaust aerosol substitute (Asa-Awuku et al. 2009). By using these κ parameters for the two component mixture, we can assume the water-insoluble mass (WIM) fraction, χ, to be defined as in equation 4.

$$\kappa_{am} = \kappa_{sa}(1-\chi) + \kappa_{DOP}(\chi) \quad (4)$$

Where κ_{am} is the unknown composition found using equation 3 from parameters determined during experimentation. Equation 3 consists of all known constants needed to calculate κ_{am} with the exception of d_s. The WIM fraction method is helpful in determining real-time particle composition without the use of filters. The value d_s is calculated from the ratio of W-CPC to B-CPC particle counts. The method has been

tested and applied to nearby roadway sources and has been shown to capture quick changes in hygroscopic aerosol composition (Short et al. 2014).

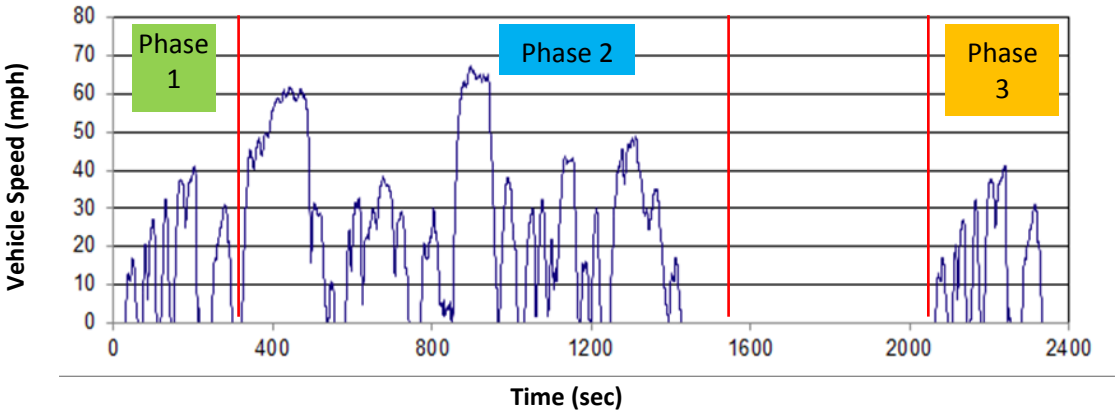

Fig. B- 1. UC cycle speed trace

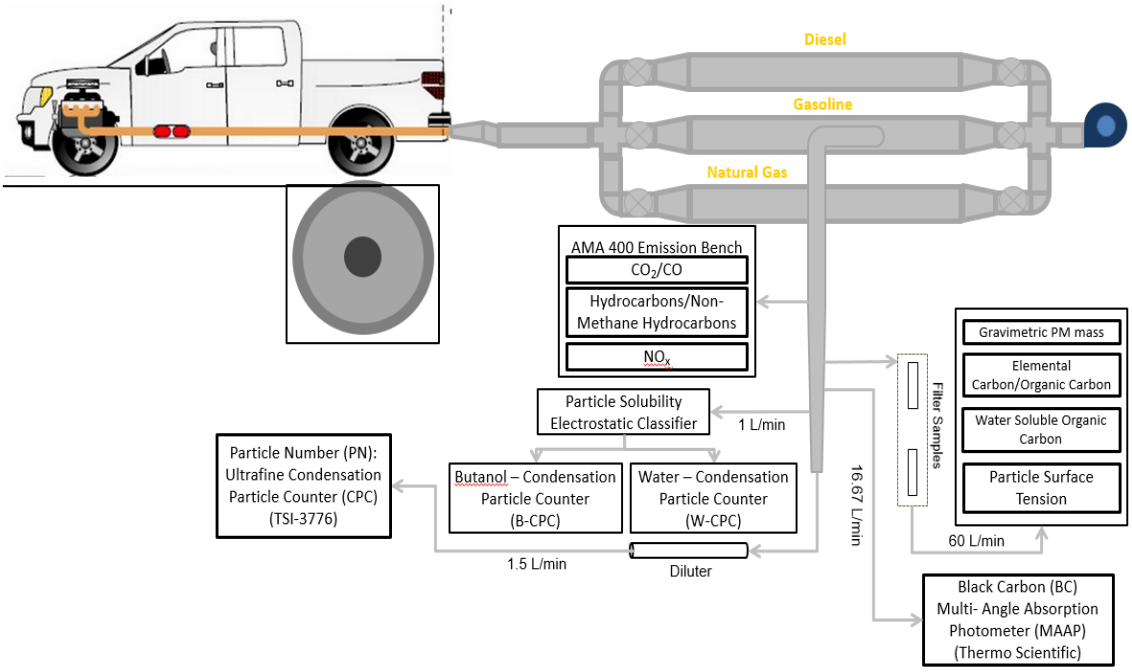

Fig. B- 2. UC cycle speed trace

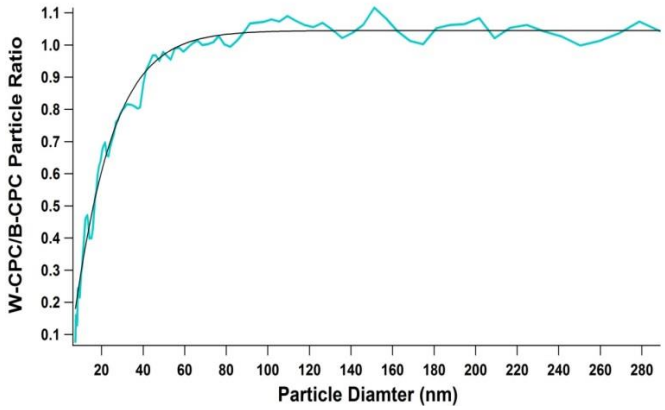

Fig. B- 3. W-CPC/B-CPC Particle Ratio for the Kia Optima on Fuel Containing 35% Aromatics and High Octane

Property	Test Method		15% Arom.	25% Arom.	35% Arom.	35% Arom. With HO
Aromatics	ASTM D1319	Vol. %	14.7	25.4	34.7	34.7
Specific Gravity	ASTM D4052	API	0.7309	0.7490	0.7631	0.7597
API Gravity	ASTM D4052	API	62.1	57.4	53.8	54.8
RVP	ASTM D5191	psi	7.88	7.88	7.50	7.85
T_{10}	ASTM D86	°F	133.7	133.0	133.2	131.2
T_{50}	ASTM D86	°F	194.7	198.7	205.3	196.2
T_{90}	ASTM D86	°F	315.9	329.4	329.7	323.1
FBP	ASTM D86	°F	378.1	380.7	381.6	372.6
RON	ASTM D2699	RON	90.4	92.0	91.4	96.6
MON	ASTM D2700	MON	84.5	83.6	82.8	85.7
(R+M)/2			87.5	87.8	87.1	91.2
Benzene	ASTM D5580 or D3606	Vol. %	0.69	0.62	0.65	0.67
Saturates	ASTM D1319	Vol. %	68.5	58.6	49.5	48.9
Olefins	ASTM D1319	Vol. %	7.2	6.4	6.3	6.8
Sulfur	ASTM D5453	ppm	26.1	26.1	27.9	26.6
Ethanol	ASTM D4815	Vol. %	9.64	9.63	9.50	9.63
Carbon		Wt.%	82.08	82.88	83.59	83.43
Hydrogen		Wt.%	14.33	13.46	12.9	12.94
Gross Heating Value	ASTM D4809	BTU/gal.	118,207	119,417	120,469	119,628
Carbon content per unit of energy		lbs. carbon/ BTU	4.23×10^{-5}	4.33×10^{-5}	4.41×10^{-5}	4.42×10^{-5}

Table B- 1. Main Physicochemical Properties of the Test Fuels

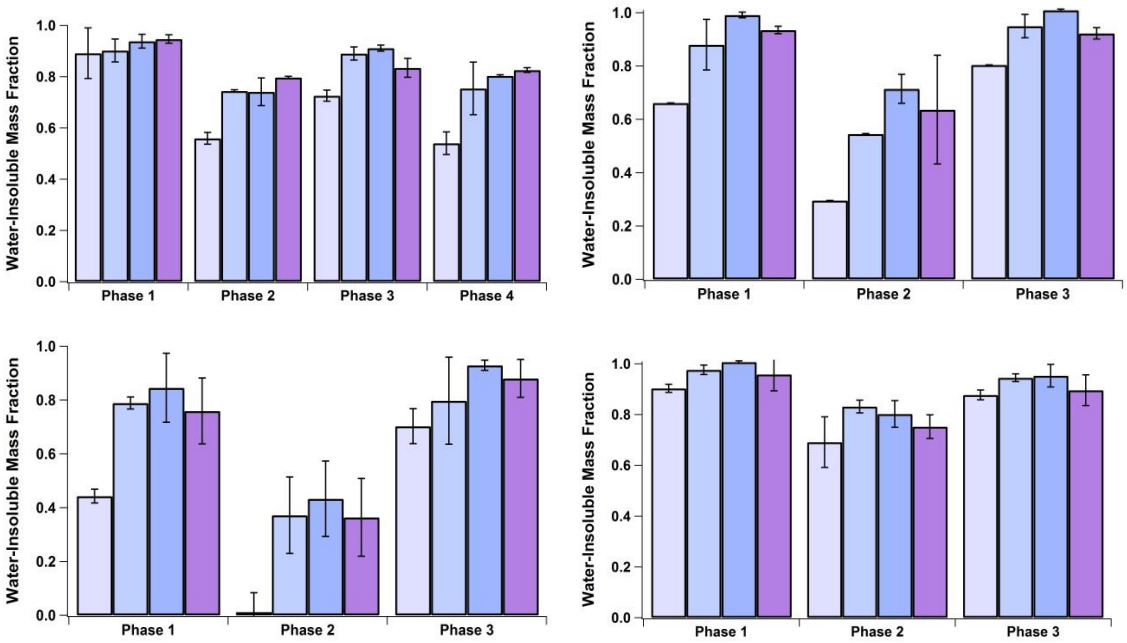

Fig. B- 4. The water-insoluble mass fraction by phase for the Honda Civic Hybrid (a.), Ford F-150 (b.), GMC Terrain (c.), and the Mazda 3 (d.)

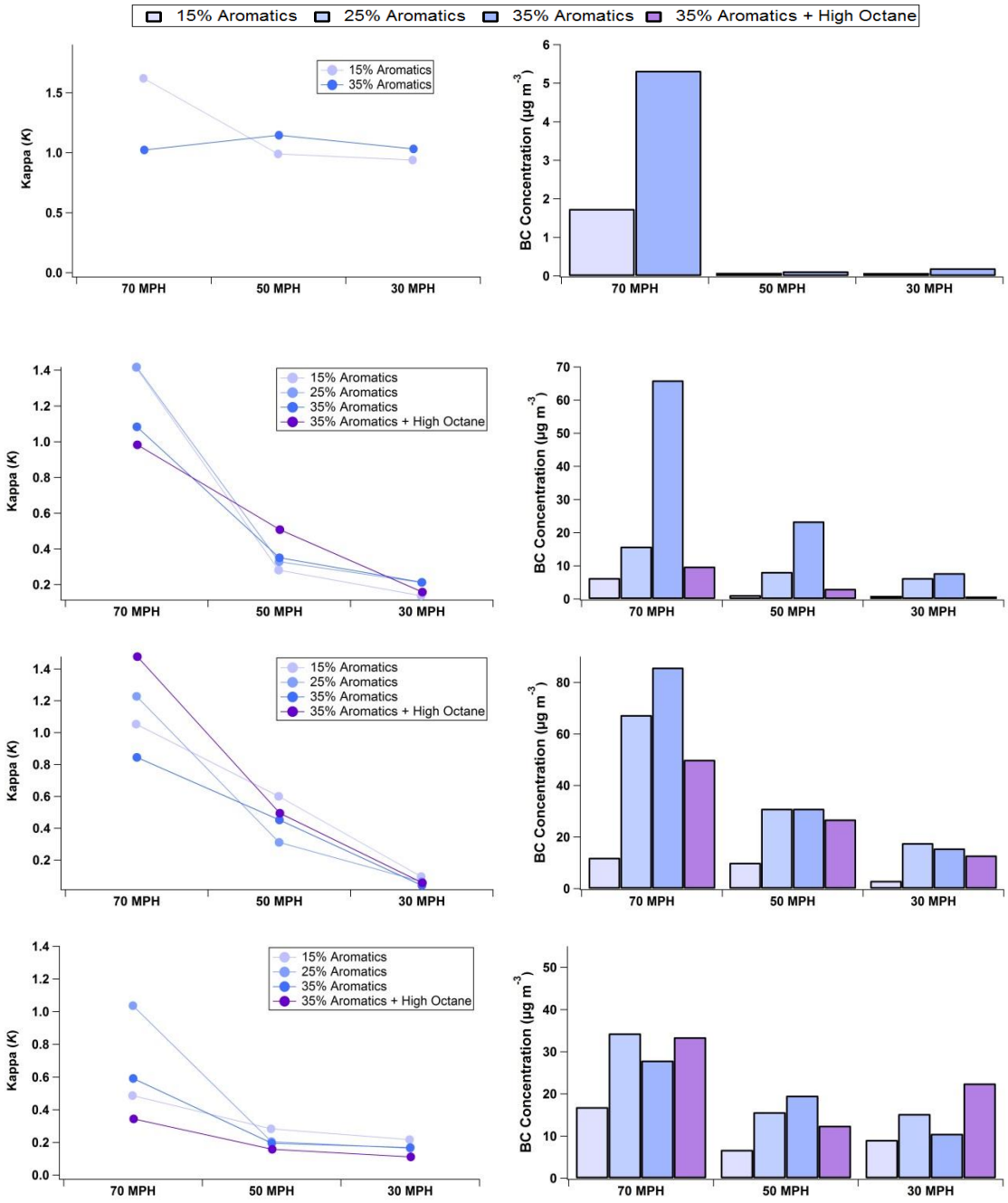

Fig. B- 5. The κ values for each steady-state speed for the Honda Civic Hybrid (a.), Ford F-150 (c.), GMC Terrain (e.), and the Mazda 3 (g.) and the BC concentration for each steady state speed for the Honda Civic Hybrid (b.), Ford F-150 (d.), GMC Terrain (f.), and the Mazda 3 (h.). Note: two steady-state fuels were tested for the Honda Civic Hybrid which are the 15% and 35% aromatic fuels

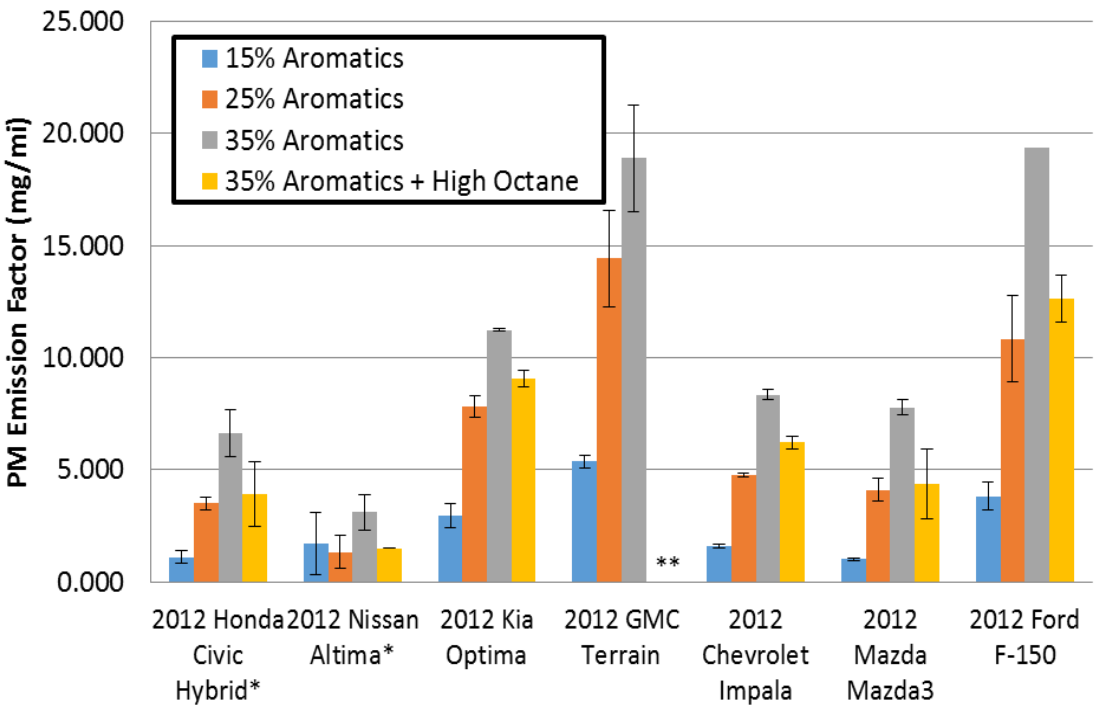

Fig. B- 6. The PM Mass Emissions Factors for all seven vehicles tested.
*Represents Emission Factors multiplied by 5
** Represents unreported data values

Appendix C.

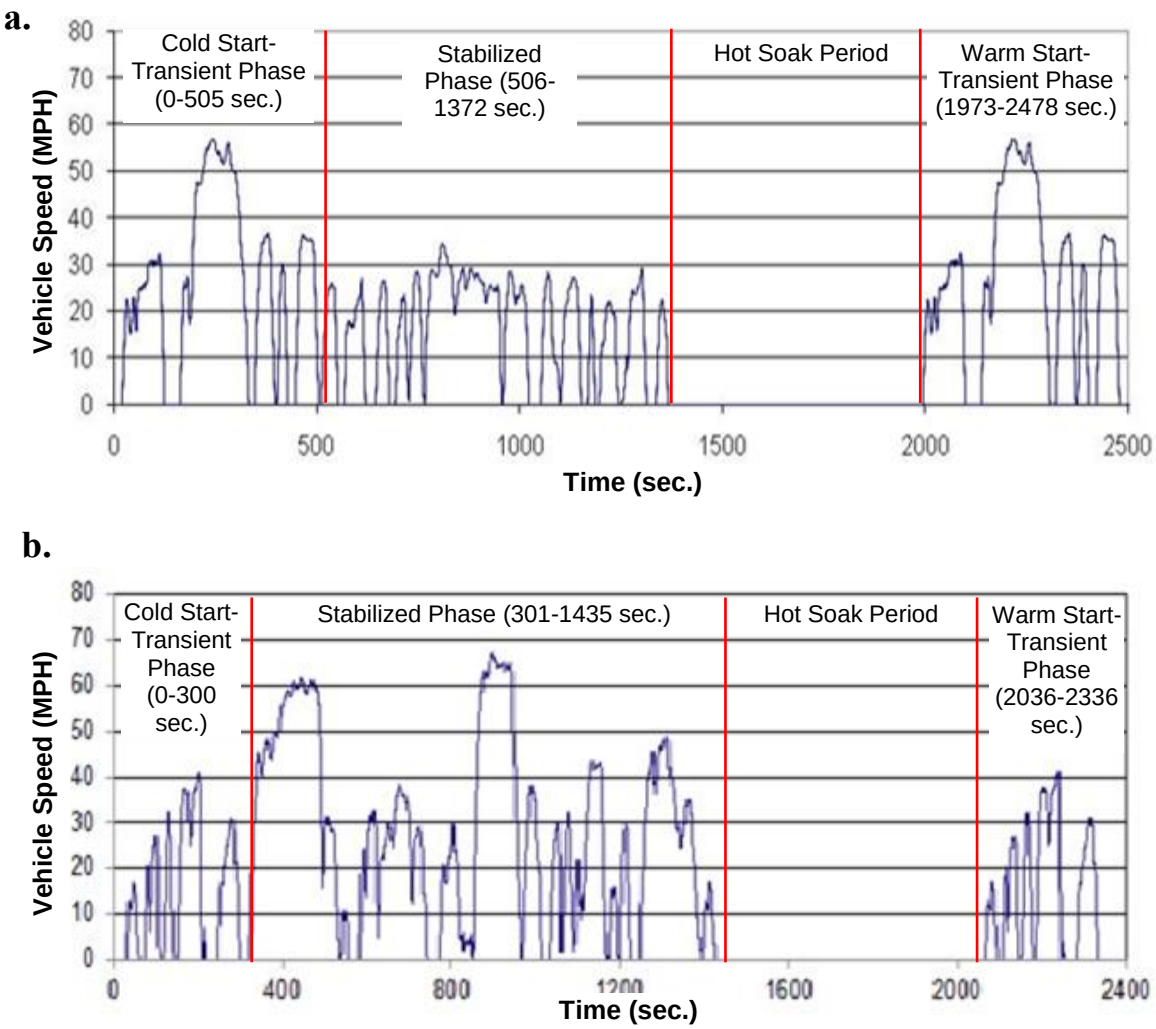

Fig. C- 1. FTP (a.) and UC (b.) speed trace

Property	Test Method		E10	E15	E20	B16	B24	B32
Aromatics	ASTM D5580	Vol. %	21.8	19.4	19.4	22.8	20.4	17.8
API Gravity	ASTM D4052	API	57.8	57.8	57.6	56.3	56.7	55.9
RVP	ASTM D5191	psi	7.0	6.91	7.2	7.1	6.9	7.1
T_{10}	ASTM D86	°F	137	144	143	148	145	142
T_{50}	ASTM D86	°F	206	215	163	203	209	207
T_{90}	ASTM D86	°F	313	309	291	313	317	232
FBP	ASTM D86	°F	344	350	356	341	379	339
RON	ASTM D2699	RON	92.9	94.6	94.5	93.0	96.9	97.0
MON	ASTM D2700	MON	84.7	86.1	85.0	84.0	86.2	86.6
(R+M)/2	ASTM 2699/2700		88.8	90.4	89.8	88.5	91.6	91.8
Olefins	ASTM D6550	Vol. %	5.1	4.5	4.5	5.6	5.1	3.6
Sulfur	ASTM D5353	ppm	10	9	7.56	9	8	7
Oxygenates	ASTM D4815	Vol. %	9.96	15.08	20.10	15.79	24.01	31.86
Carbon	ASTM D5291	Wt.%	82.54	80.70	78.89	82.79	80.95	79.09
Hydrogen	ASTM D5291	Wt.%	13.85	13.96	13.70	13.65	13.66	13.56
Gross Heating Value	ASTM D240	BTU/lb.	18056	17515	17029	17637	17648	17339

Table C- 1. Main Physicochemical Properties of the Test Fuels

	Honda Civic	Dodge Ram	Toyota Camry	Kia Optima	Chevrolet Impala
MY	2007	2007	2012	2012	2012
Configuration	Inline, 4 cylinders	V8	Inline, 4 cylinders	Inline, 4 cylinders	V6
Displacement, L	1.8	5.7	2.5	2.4	3.6
Horsepower	140@3600 rpm	345@5400 rpm	178@6000 rpm	200@6300 rpm	300@6500 rpm
Compression Ratio	10.5:1	9.6:1	10.4:1	11.3:1	11.5:1
Bore x Stroke, mm	81 x 87.3	99.6 x 91	90 x 98	88 x 97	94 x 85.6
Emission Control Systems	TWC/AF/H0$_2$S/EGR/ OBD II	2TWC/2H0$_2$S/EGR/SFI, OBD II	WU-TWC/H0$_2$S/TWC	DFI/H0$_2$S (2)/WU-TWC/TWC, OBD II	DGI/H0$_2$S/TWC/AIR, OBD II
Emissions Certification	U.S. Tier 2 Bin 5/ULEV II	U.S. Tier 2 Bin 4/LEV II	U.S. Tier 2 Bin 5/PZEV	Federal Tier 2, Bin 2	LEV II, SULEV

TWC: three-way catalyst; AF: air-fuel ratio sensor; HO_2S: heated oxygen sensor; EGR: exhaust gas recirculation; OBD: on-board diagnostic; SFI: sequential fuel injection; WU-TWC: warm-up three-way catalyst; DFI; direct fuel injection; DGI; direct gasoline injection; AIR: secondary air injection

Table C- 2. Technical specifications of the test vehicles

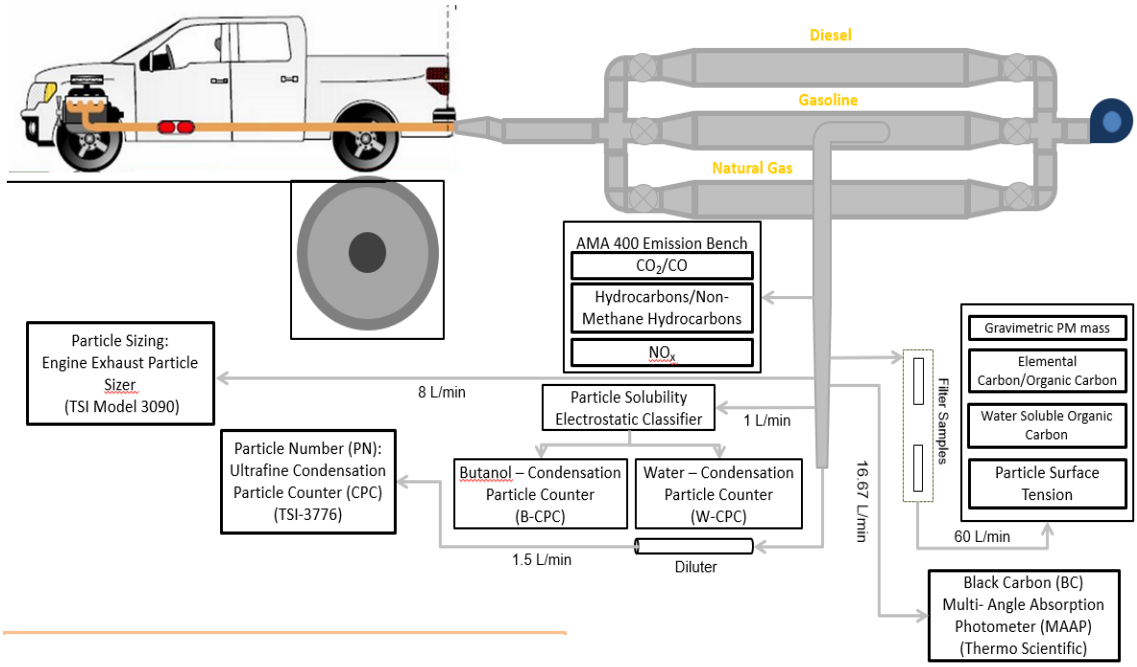

Fig. C- 2. Experimental Setup of the study

C-2: Driving cycles and measurement protocol

The FTP-75 is the primary emission certification driving cycle of light-duty vehicles in the U.S. The FTP-75 cycle consists of three segments or bags representing a cold-start transient phase, a stabilized phase, and a hot-start transient phase. The cycle covers a total distance of 11.04 miles with an average speed of 21.2 mi/hr. The vehicle is turned off for a period of 10 minutes at the conclusion of the stabilized phase and prior to starting the hot-start transient phase. The California Unified Cycle (UC) is a dynamometer driving schedule for light-duty vehicles developed by the California Air Resources Board (CARB). The UC test has a three-bag structure similar to the FTP, with bags representing a cold-start transient phase, a stabilized phase, and a hot-start transient phase, but is a more aggressive driving cycle. It has a higher average speed, higher acceleration rates, fewer stops per mile, and less idle time. The UC test also has a ten minute hot soak, between Bags 2 and 3.

Prior to testing any particular vehicle, an extensive preconditioning procedure was followed for oil and fuel changes. Prior to beginning testing on a vehicle, its lubricant oil was changed. Following the oil change, the vehicle was conditioned on the oil over two US06 cycles, followed by an LA4 and a US06 cycle sequence repeated twice (i.e., a total of 4 US06 cycles and 2 LA4s). The vehicle fuel preconditioning procedure incorporated multiple fuel drains and fills to ensure complete changeover of the fuel and to minimize or eliminate carryover effects between test fuels. The preconditioning procedure was similar to that specified in the Code of Federal Regulations (40 CFR 86.132-96). This

drain and fill sequence included two drain and 40% fills and one drain and 3 gallon fill. After the drain and 3 gallon fill, and the first drain and 40% fill, the vehicle was then conditioned either on the road or on the dynamometer over the Urban Dynamometer Driving Schedule (UDDS)/LA4, or the first two bags of the FTP. The on-road course was designed to simulate the LA4 portion of the FTP in terms of typical speeds as well as number of stops. In between drain and fill and preconditioning cycles, the vehicle was idled one or two times for two minutes with the vehicle being rocked back and forth. Following the first LA4, a sequence of engine off and idles was performed along with a drain and 40% fill. After this sequence, the vehicle was given its final preconditioning LA4 on the dynamometer, and then placed into cold soak overnight prior to performing the FTP or UC test.

Appendix D.

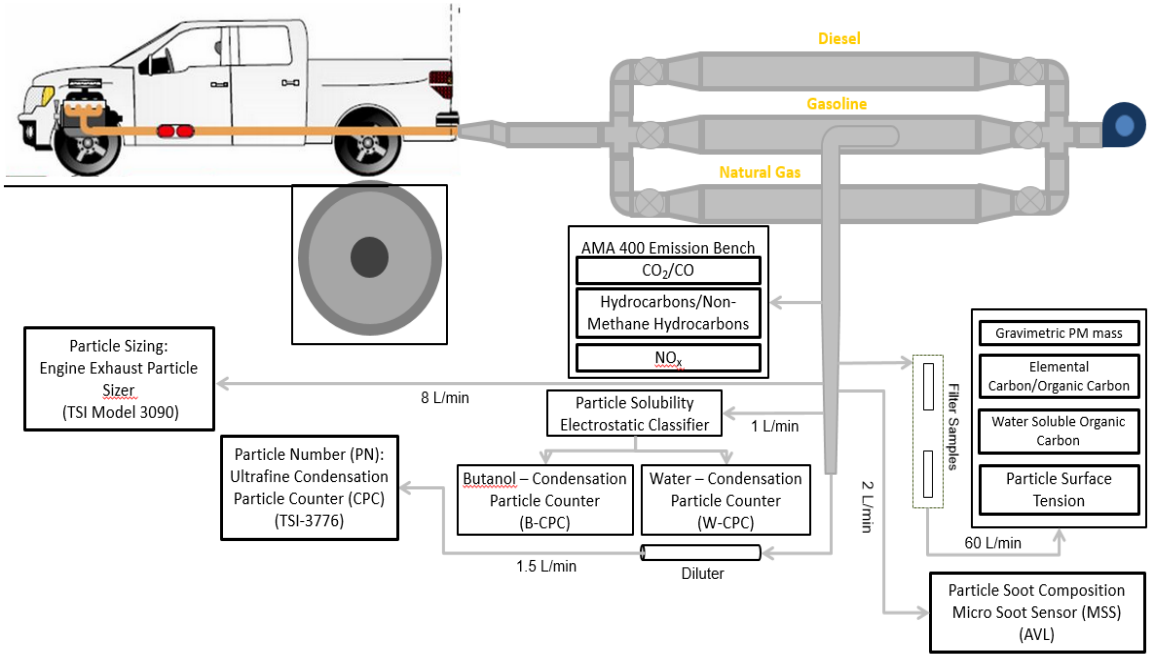

Fig. D- 1. Experimental Setup of the study

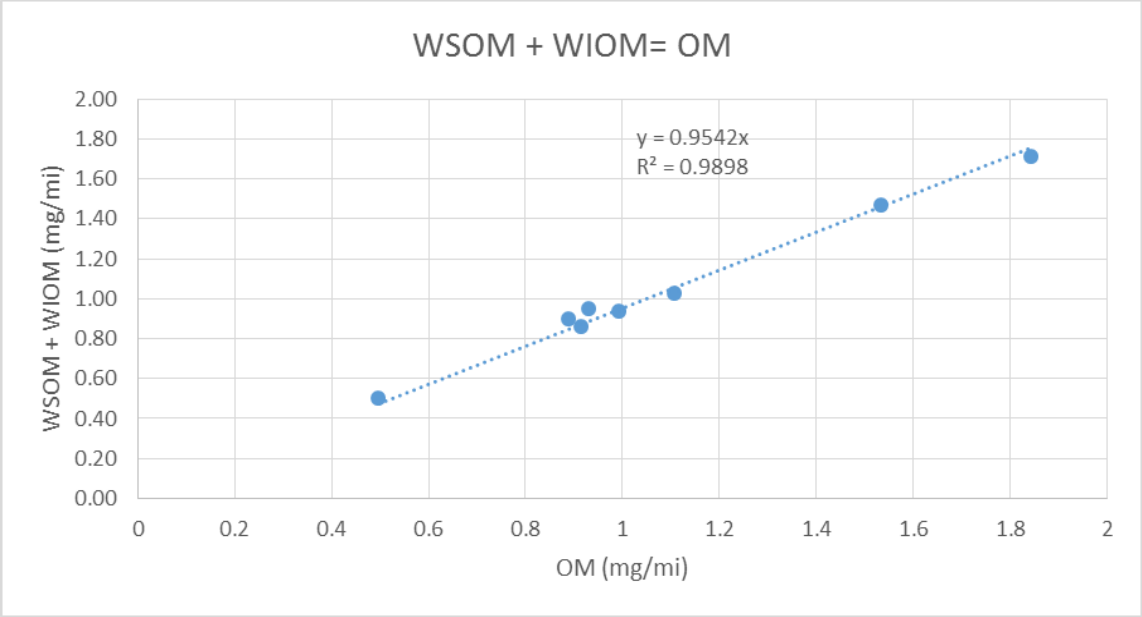

Fig. D- 2 Correlation plot of OM with the sum of WIOM and WSOM.

Property	Test Method		E10	E51	E83	B55
Aromatics	ASTM D5580	Vol. %	21.8	12.7	3.8	
API Gravity	ASTM D4052	API	57.8	52.4	48.9	53.7
RVP	ASTM D5191	psi	7.0	7.1	6.15	7.0
T_{10}	ASTM D86	°F	137	147	162.5	148.9
T_{50}	ASTM D86	°F	206	169	172.2	211.6
T_{90}	ASTM D86	°F	313	224	173.7	225.8
FBP	ASTM D86	°F	344	353	188.6	232.0
RON	ASTM D2699	RON	92.9	105	106	99.6
MON	ASTM D2700	MON	84.7	89	90.5	87.5
(R+M)/2	ASTM 2699/2700		88.8	97	98.3	93.6
Olefins	ASTM D6550	Vol. %	5.1	2.3	1.0	1.1
Sulfur	ASTM D5353	ppm	10	7	3	1
Oxygenates	ASTM D4815	Vol. %	9.96	50.89	83.24	53.46
Carbon	ASTM D5291	Wt.%	82.54	68.28	0.571	73.61
Hydrogen	ASTM D5291	Wt.%	13.85	13.43	0.133	14.23
Gross Heating Value	ASTM D240	BTU/lb.	18056	14992	11540	16313

Table D- 1 Main Physicochemical Properties of the Test Fuels